Investigation into human macrophage phenotype transcriptome and importance of CALHM6

Kajus Baidžajevas

A thesis submitted in partial fulfilment of the requirements for the degree of Doctor of Philosophy

The University of Sheffield
Faculty of Medicine, Dentistry & Health
Department of Infection, Immunity & Cardiovascular Disease

First submission: September 2019

Thesis format

This thesis is structured into chapters as follows:

1. Introduction – introduce the topics relevant to the whole thesis;
2. Materials and methods – combined for all results chapters;
3. Transcriptome, protein expression and lipid handling;
4. Glycolysis and cytokine secretion;
5. CALHM6 in macrophages;
6. Bioinformatics on CALHM6 and its family;
7. Discussion – overview of the results, limitations and future work;
8. References – combined for the thesis;
9. Abbreviations – combined for the thesis.

Furthermore, the results chapters (3 – 6) are structured as follows and **Chapters 3** and **5** each include a manuscript that has been or is intended to be submitted to a peer–reviewed journal:

- Further introductory section to provide with more specialised background;
- Hypotheses and aims for my own work in each chapter;
- Contributions, including work done by others with indications where work was or will be submitted in a different thesis;
- Results (in **Chapters 3** and **5** included in the manuscript);
- Discussion (in **Chapters 3** and **5** included in the manuscript).

Acknowledgements

I would like to thank my supervisors Heather L Wilson, Siew Cheng Wong and Endre Kiss–Tóth for their help, support and patience every step of this degree. All of the friends and great people (below and more) I met in the UK and Singapore. Éva Hadadi for all of the hard work and support. Bernett Lee for the bioinformatics work. Jessica Johnston, Zabran Ilyas, Klaudia Kocsy, George Pickering, Bezaleel Mambwe, Sin Yee Gun, Siew Min Ong for all of the chats we had about macrophages, immunology, metabolism and everything else. All of the collaborators during my time in Sheffield and Singapore. Jack Green, Rehab Alqurashi, Taghreed Shamrani, Laura Martínez Campesino, Taewoo Kim, Chiara Niespolo, Yang Li, Favour Felix, Ahmed Bukhari, Sharon Lee, Jie Lin Seow, Thomas Loy, Hweixian Leong Penny, Wei Hseun Yeap for being great lab mates. David Rutherford and Dovydas Lukauskas for being hardworking and persistent in their projects. All of the technicians for their help with any query or problem. All of the blood and tissue donors for their donations.

Didžiausias AČIŪ Tau, MAMA! Be tavo meilės ir pagalbos aš nebūčiau tiek pasiekęs!

(The largest THANK YOU to You, MUM! Without your love and help I would not have been able to achieve this!)

Abstract

Atherosclerosis and related cardiovascular diseases are the leading cause or mortality. Stimuli polarise macrophages into phenotypes with different functions in atherosclerosis. Some phenotypes have been studied more than others, therefore a systematic assessment of their transcriptome in relation to protein expression, lipid handling and other functions is needed. Also, due to macrophage phenotype complexity *in vivo* some phenotype markers may not be as useful and new more robust markers are needed.

The aims of this study were to (1) characterise the transcriptomes of human macrophage phenotypes with roles in atherosclerosis development and relate the transcriptomes to protein expression and lipid handling, (2) explore phenotype glycolysis and pro-inflammatory cytokine secretion, (3) confirm the specificity of a novel pro-inflammatory macrophage marker and investigate associated signalling and function, (4) along with using bioinformatics resources.

Healthy volunteer monocytes were differentiated into macrophages before polarisation. Polarised cells were assessed for gene, protein expression and functional properties. Alternatively, knockdowns of genes were performed before polarisation to determine signalling pathway components that participate in activating gene expression and to investigate potential functions of selected genes and proteins.

Upon polarisation human macrophage phenotypes underwent profound changes in their transcriptomes that were reflected in their protein expression and lipid handling capacities. Glycolytic capacity and possibly pro-inflammatory cytokine expression may have also been affected. Calcium homeostasis modulator family member 6 (CALHM6) was confirmed as a novel *in vitro* marker for pro-inflammatory macrophages that is induced by non-canonical Toll–like receptor 4 and interferon γ signalling. Macrophage CALHM6 may also participate in controlling chemokine expression and immune cell activation. Also, bioinformatics approaches further hinted towards importance of CALHM6 in the immune system.

Current efforts are aimed at investigating the role of CALHM6 in interferon signalling and in collaborations with other researchers in immune cell activation, infection, human and animal model atherosclerosis.

Associated publications

The publications below are associated with the work presented in this thesis through one or more authors.

BAIDŽAJEVAS, K., HADADI, É., LEE, B., LUM, J., SHIHUI, F., SUDBERY, I., KISS-TÓTH, E., WONG, S. C., WILSON, H. L. 2019. Macrophage polarisation associated with atherosclerosis differentially affects their capacity to handle lipid. *Atherosclerosis,* in submission. (Original research)

BAIDZAJEVAS, K., HADADI, E., LEE, B., LUM, J., SUDBERY, I., LAI, S., WONG, S. C., KISS-TOTH, E., WILSON, H. 2017. Human oxidised phospholipid macrophages have high lipoprotein handling capabilities without readily forming unwanted foam cells. *Heart,* 103, A136-A136. (Meeting abstract)

HADADI, É. 2015. Contribution of macrophage phenotypes and their precursors in inflammatory function and the development of cardiovascular disease. *University of Sheffield*. (PhD thesis)

HADADI, E., KISS-TOTH, E., WILSON, H. L., WONG, S. C. 2015. Investigation of human monocyte derived macrophage phenotypes for their functional role in atherosclerosis. *Heart,* 101**,** A101-A102. (Meeting abstract)

HADADI, E., KISS-TOTH, E., WILSON, H. L., WONG, S. C. 2014. Functional characterisation of monocyte derived macrophage phenotypes for their role in atherosclerosis. *Heart,* A117-A117. (Meeting abstract)

Other publications

The publications below include my contributions, but not work presented in this thesis.

JOHNSTON, J. M., ANGYAL, A., BAUER, R. C., HAMBY, S., SUVARNA, S. K., **BAIDŽAJEVAS, K.**, HEGEDUS, Z., DEAR, N. T., TURNER, M., THE CARDIOGENICS CONSORTIUM, WILSON, H. L., GOODALL, A. H., RADER, D. J., SHOULDERS, C. C., FRANCIS, S. E. KISS-TOTH, E. 2019. Myeloid Tribbles 1 induces early atherosclerosis via enhanced foam cell expansion. *Science Advances,* 5, eaax9183. (Original research)

JOHNSTON, J. M., ANGYAL, A., BAUER, R. C., HAMBY, S. E., SUVARNA, S. K., **BAIDŽAJEVAS, K.**, HEGEDUS, Z., DEAR, N. T., TURNER, M., THE CARDIOGENICS CONSORTIUM, WILSON, H. L., GOODALL, A. H., RADER, D. J., SHOULDERS, C. C., FRANCIS, S. E. KISS-TOTH, E. 2019. Myeloid trib1 promotes experimental atherosclerosis. *Cardiovascular Research*, 114, S4-S4. (Meeting abstract)

KOCSY, K., ALQURASHI, R., JOHNSTON, J. M., **BAIDZAJEVAS, K.**, MAJID, A., WILSON, H. L., KISS-TOTH, E., REDGRAVE, J., FRANCIS, S. E. 2018. Human macrophage subsets in the pathogenesis of carotid atherosclerosis. *Cardiovascular Research,* 114, S5-S5. (Meeting abstract)

HADADI, E., ZHANG, B. Y., BAIDZAJEVAS, K., YUSOF, N., PUAN, K. J., ONG, S. M., YEAP, W. H., ROTZSCHKE, O., KISS-TOTH, E., WILSON, H., WONG, S. C. 2016. Differential IL-1 beta Secretion by monocyte subsets is regulated by Hsp27 through modulating mRNA stability. *Scientific Reports,* 6, 3905. (Original research)

List of contents

List of figures

List of tables

1. Introduction

1.1. Atherosclerosis

Cardiovascular diseases (CVDs) are the leading cause of death world–wide, accounting for an estimated 17.86 million (31.4%) deaths in 2016, which is 3.57 million (4.1%) more than in 2000 (WHO, 2018). A common feature of most cardiovascular diseases is the formation of fat and immune cell rich atherosclerotic plaques (atheromas) within the artery wall (Frostegard, 2013).

Physiological lipid metabolism is a complex process that involves multiple organs, cell types and carriers (**Figure 1.1.**) (Goodman, 2010, Ramasamy, 2014, Kwan et al., 2007, Ferro et al., 2018). Dietary fat is mainly digested in the stomach/small intestine by enzyme–containing bile and pancreatic secretions, which emulsify and then break down lipids into their constituents (Goodman, 2010). Common dietary lipids such as triglycerides are converted into monoglycerides and free fatty acids, which are then absorbed by epithelial cells lining the intestine (Goodman, 2010). In these cells the triglycerides are reformed, aggregated and coated with apoliproteins (Apo) and phospholipids to form chylomicron particles, which enter the lymphatic system and eventually the blood (Goodman, 2010). In the bloodstream excess chylomicron triglycerides are hydrolysed by lipases to generate chylomicron remnants and free fatty acids, the former is taken up by the liver, while the latter is used in muscle or stored in adipose tissue (Ramasamy, 2014). The liver modifies chylomicron remnants into very low density lipoprotein (VLDL) (Kwan et al., 2007), which is released back into circulation and further processed by lipases to gradually release more fatty acids and yield lower density particles such as intermediate and low density lipoproteins (ILDL and LDL respectively), which contain increasingly more cholesterol than triglycerides (Ramasamy, 2014, Ferro et al., 2018). LDL particles can deliver lipid to tissues or back to the liver by interacting with the LDL receptor (LDLR), scavenger receptor class B member 1 (SCARB1) and other receptors (Ramasamy, 2014, Ferro et al., 2018). Excess lipid is removed via high density lipoprotein (HDL), the discoidal form of which is formed by an Apo–AI and ATP–binding cassette subfamily A member 1 (ABCA1) interaction, subsequently the mature spherical HDL is formed by the lecithin–cholesterol acyltransferase (LCAT) esterifying free cholesterol in HDL (Brewer, 2004). Mature spherical HDL can interact with other lipid efflux receptors, such as ATP–binding cassette subfamily G member 1 (ABCG1) and SCARB1 to acquire more lipid (Brewer, 2004). In the bloodstream and HDL interacts with chylomicron remnants and VLDL, donating cholesterol esters while receiving triglycerides (via cholesteryl ester transfer protein, CETP) thereby increasing its own triglyceride and its interactors' cholesterol ester content (Kwan et al., 2007). HDL can be taken up by cholesterol–requiring tissues for further metabolism or by the liver for lipid removal from the body (Brewer, 2004, Kwan et al., 2007).

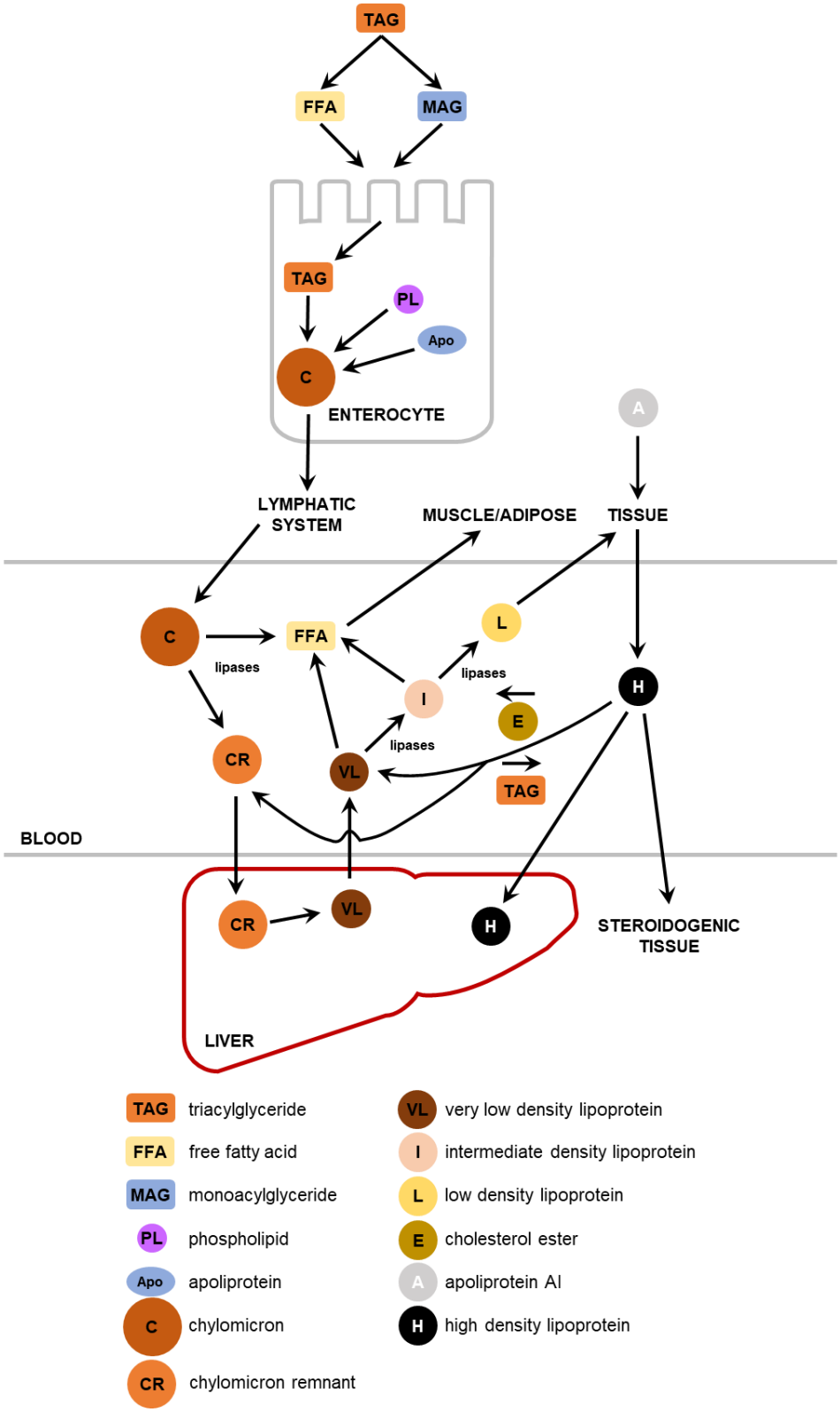

Figure 1.1.: Physiological lipid trafficking.

Simplified schematic of dietary lipid absorption in gut epithelial cells (enterocytes), trafficking in blood, modifications in the liver and blood, use in the body (steroidogenic tissue) and efflux via the liver (high density lipoprotein). Based on (Goodman, 2010, Ramasamy, 2014, Kwan et al., 2007).

Increased lipid retention may be the result of genetic disorders such as Tangier disease, which arises due to mutations in the *ABCA1* gene rendering the protein unable to transfer lipids to forming HDL particles, leading to excess lipid accumulation in the cells and reduced circulating HDL concentration (Nofer and Remaley, 2005). However, individuals without known genetic predisposition for CVD can still develop atherosclerosis. Prominent risk factors include blood lipid imbalance (high LDL and low HDL), personal habits (fat, sugar and sodium–rich diet, smoking, physical inactivity, high alcohol intake), pre-existing conditions (hypertension, diabetes, insulin resistance, inflammation), age, stress, sex and family history (NIH, 2019).

Progression of atherosclerosis is a multifactorial process, which is stratified into histologically–defined steps (**Figure 1.2.**) (Yahagi et al., 2016). In due to dyslipidaemia, inflammation or hypertensive conditions the inner artery wall endothelium can become disturbed, especially in regions of artery wall exposed to disturbed blood flow, allowing increased retention of excess lipoprotein, such as LDL, and recruitment/capture of leukocytes (Steffensen et al., 2015, Libby et al., 2011). Modifications of LDL, such as oxidation due to reactive oxygen species abundance in inflammation, can be endocytosed by monocyte–derived macrophages (MDMs) (Libby et al., 2011). Macrophages are able to process lipid for adenosine triphosphate (ATP) production or efflux, however in atherosclerosis macrophages are eventually overwhelmed with lipid and become lipid–laden foam cells with large deposits of intracellular lipid (Yahagi et al., 2016). Presence of macrophage foam cells is characteristic of all stages of atherosclerosis, including the initial ones, such as fatty streak appearance on the artery wall (Yahagi et al., 2016). As the plaque grows continuous thickening of the intima and bulging of the artery wall are observed, which is promoted by lipid retention and leukocyte infiltration (Yahagi et al., 2016, Libby et al., 2011). The next stage in atherosclerosis progression is characterised by migration and proliferation of smooth muscle cells (SMCs) from the media into the intima. The human intima normally contains some SMCs, unlike that of most animal models (Libby et al., 2011), but due to long–term atherosclerosis the SMCs form a protective cap filled with collagen and other extracellular matrix proteins to strengthen the plaque against mechanical damage (Libby et al., 2011). Also, continuing inflammation and excessive lipid deposition (observable lipid pool) cause cell apoptosis and cholesterol crystallisation in the tissue (Libby et al., 2011). Hypoxia(–like) conditions are common due to the bulged tissue being deprived of oxygen and inflammatory signalling, therefore, local neovascularisation occurs (Libby et al., 2011). In late stage atherosclerosis the plaque occludes a large proportion of the artery lumen, severely restricting blood flow and in over 75% luminal area occlusions, raising the risk of angina, congestive heart failure and sudden death (Yahagi et al., 2016). The lipid pool evolves into a necrotic core, while matrix metalloproteinases (MMPs)

secreted by macrophages and other leukocytes breakdown the collagen in the protective cap which may cause it to rupture, especially at mechanically weaker areas, such as the plaque shoulders (Yahagi et al., 2016, Libby et al., 2011, Stoger et al., 2012). During rupture the plaque contents are released into the bloodstream, causing thrombosis (Libby et al., 2011). Smaller ruptures may heal with scar tissue formation and calcification of the site, however, in larger ruptures the thrombosis may be substantial enough to cause complete occlusion of the artery with the plaque, or a connected narrower artery (Yahagi et al., 2016). Depending on the size and location of the thrombus, it may cause unstable angina, myocardial infarction, stroke and other potentially serious complications (Yahagi et al., 2016). It has been widely recognised that the immune system, especially differentially activated (polarised) macrophage phenotypes play a large role in the progression of atherosclerosis (Chinetti-Gbaguidi et al., 2015).

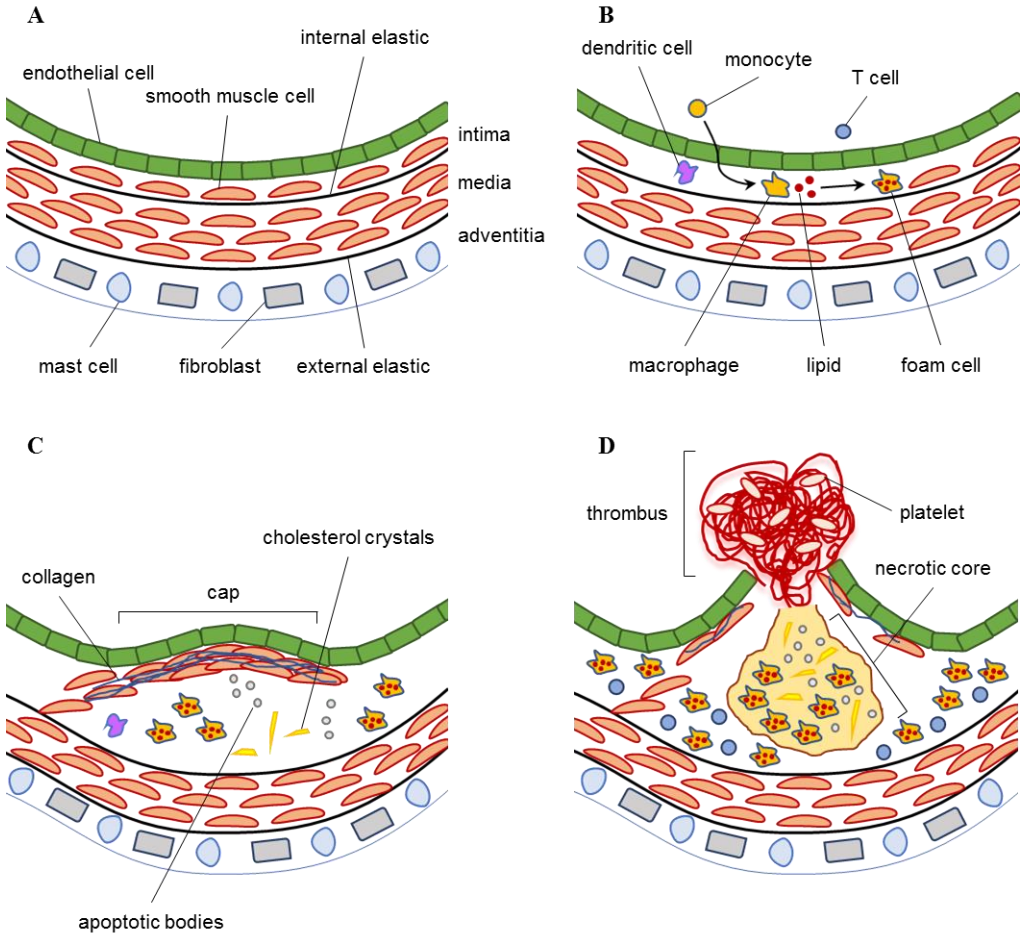

Figure 1.2.: Arterial atherosclerosis development.

Schematic representations of distinct stages of atherosclerosis indicating the major structures and cell types present. Cross–section of (**A**) healthy human artery, note the presence of smooth muscle cells in the intima, unlike in most model species, (**B**) early atherosclerosis, characterised by intimal thickening, leukocyte infiltration and foam cell formation, (**C**) progressive atheroma with significant artery wall bulging, lipid accumulation and cap formation (smooth muscle cells and collagen underneath the endothelium) and (**D**) late/end stage disease, particularly, plaque rupture, due to cap weakening, and release of the necrotic core into the artery, causing thrombosis. Adapted from (Libby et al., 2011).

1.2. Mouse models in atherosclerosis research

Mice are commonly used to perform *in vivo* atherosclerosis research due to their low cost, maintenance required, quick generation and tool availability for effective genetic manipulation (Veseli et al., 2017). However, mice differ in their cardiovascular anatomy and physiology, lack CETP (in humans involved in transferring cholesterol from HDL to VLDL and acylglycerides from VLDL to HDL) therefore, most cholesterol is transported by HDL, which makes it difficult to induce atherosclerosis of similar location and severity in wild–type mice even if they are fed a toxically high cholesterol diet (up to 30% fat, 5% cholesterol, 2% cholic acid), which induces acute inflammation, weight loss and heightened risk of infections (Oppi et al., 2019, Gargiulo et al., 2016). Several mouse models have been developed to overcome these issues (Veseli et al., 2017, Oppi et al., 2019, Gargiulo et al., 2016).

Apoe knockout mice are less able to clear chylomicrons and VLDL remnants, resulting in increased plasma VLDL, making such mice prone to develop atherosclerosis even on a normal diet, because in mice the APOE protein is part of most lipoproteins, playing an essential role in their metabolism (Veseli et al., 2017, Oppi et al., 2019). However, the lipid profile of *Apoe* knockout mice is different from human atherosclerosis, because in the latter plasma LDL and not VLDL is elevated (Oppi et al., 2019). Furthermore, *Apoe* is also involved in inflammatory responses, making this model less appropriate to study the roles of inflammatory regulators and effectors (Veseli et al., 2017, Oppi et al., 2019).

Ldlr knockout mice were developed to have a lipid profile more similar to human atherosclerosis in order to study aspects of lipid metabolism: loss of functional LDLR results in plasma LDL accumulation, because LDLR mediates clearance of LDL via receptor–mediated endocytosis (Veseli et al., 2017, Oppi et al., 2019). Also, the inflammatory profile of these mice is not affected by absence of functional *Apoe*, making this model more suitable for studying inflammatory processes (Veseli et al., 2017, Oppi et al., 2019). However, unlike the *Apoe* knockout mice, this model requires a modified cholesterol–rich diet to develop atherosclerosis (Veseli et al., 2017). *Apoe* and *Ldlr* double knockout mice have also been produced to combine the features of its two parent models and to study the effects of treatments even on a normal diet (Veseli et al., 2017).

The Apoe3–Leiden model was created to elevate plasma lipoprotein concentration without affecting *Apoe*, achieved by injecting mice with a gene fragment containing a partially duplicated *Apoe3* allele, *Apoc1* and regulatory elements from a familial dysbetalipoproteinemia patient (van den Maagdenberg et al., 1993). These mice are used to study *Apoe* metabolism and remodelling of venous grafts, which are commonly used in heart surgery to bypass coronary arteries blocked

by atherosclerotic plaques (Veseli et al., 2017). This model can also include expression of the human *CETP* to further match the human lipid profile (Oppi et al., 2019).

Atherosclerosis in mice can also be induced without genetic modifications, but via injection of adeno–associated virus carrying gain–of–function mutated proprotein convertase subtilisin/kexin type 9 (PCSK9), which increases degradation of LDL receptors, therefore lowering cellular lipid uptake and promoting lipid accumulation in the plasma (Veseli et al., 2017). Also, the expression of the mutant PCSK9 is reportedly highly stable as well as the virus infection has little to no inflammatory effect on the mice, which under a cholesterol–rich diet makes this model convenient for studying atherosclerosis (Veseli et al., 2017, Oppi et al., 2019).

The mentioned models are mainly used to study plaque progression and in late stages develop plaques with necrotic cores and fibrous caps (Veseli et al., 2017). However, these models are not always suitable to study plaque vulnerability to rupture and induce severe complications seen in human atherosclerosis, such as thrombus formation (Veseli et al., 2017). Some suggest that the PCSK9 and Apoe3–Leiden models can be used to study aspects of plaque vulnerability, although mechanical manipulation of the vessels has been in wider use (Veseli et al., 2017, Oppi et al., 2019, Gargiulo et al., 2016). A cuff/collar is placed and/or single/tandem ligations are performed on the carotid vessels to produce vulnerable plaques in *Apoe* knockout mice (Gargiulo et al., 2016). Angiotensin II has also been administered to *Apoe* knockout mice to induce vulnerable atheroma (Gargiulo et al., 2016). Also, a genetic approach has recently been developed to study vulnerable plaques in mice by crossing *Apoe* knockout mice with fibrillin 1 heterozygous C1039G mice (Veseli et al., 2017, Oppi et al., 2019, Gargiulo et al., 2016). The mice have a phenotype similar to that observed in humans with Marfan syndrome due to fragmentation of elastic fibres (Veseli et al., 2017, Oppi et al., 2019, Gargiulo et al., 2016). In combination with an *Apoe* background and a cholesterol–rich diet, these mice develop large vulnerable plaques prone to rupture due to lower matrix protein content and heightened inflammation (Veseli et al., 2017, Gargiulo et al., 2016).

While convenient to use and maintain it is important to remember that laboratory mice are only a model of human atherosclerosis (Veseli et al., 2017). This is particularly highlighted by differences in lipid metabolism, sites of plaque development and course of the disease between the two species (Veseli et al., 2017, Oppi et al., 2019). Ultimately, if possible, mouse model experimental data should be verified by observations in human cells and/or investigations that involve patients.

1.3. Monocyte subsets

Monocytes are mostly circulating leucocytes that given specific stimuli can differentiate into macrophages (Kapellos et al., 2019). Human monocytes have been commonly broadly classified into subsets based on their cell–surface protein expression of cluster of differentiation (CD) 14 and CD16 (Kapellos et al., 2019). In humans the classical monocytes highly express CD14, but not CD16 (here referred to as $CD14^{++}CD16^{-}$ as in (Wong et al., 2011)), constitute the majority of blood monocytes (Kapellos et al., 2019). Intermediate and non-classical monocytes (here referred to as $CD14^{++}CD16^{+}$ and $CD14^{+}CD16^{++}$ respectively as in (Wong et al., 2011)) express more CD16 protein on their surface, while the non-classical monocytes also express less cell–surface CD14 protein (Kapellos et al., 2019). It is suggested by observations of monocyte repopulation in haematopoietic stem cell transplantation patients and such experiments as measurements of maturation–associated gene transcription, proliferation marker expression and telomere length that the first subset to develop is the classical monocytes, followed by the intermediate monocytes as a transitionary subset into the non-classical monocytes (Rogacev et al., 2015, Wong et al., 2011, Ong et al., 2018). Functions and roles of these subsets are not entirely clear and it is difficult to determine if the current classification needs to be revised or if differences in study designs have more impact on the observed outcomes. The latter reason involving study designs is particularly of interest discussing subset response to lipopolysaccharide (LPS) by secretion of cytokines. In some subset purification by cell sorting the M5E2 anti-CD14 antibody clone has been used, which had been previously described as a neutralising antibody in experiments on neutrophils, possibly affecting the function of CD14 as a coreceptor for LPS (Power et al., 2004).

Classical monocytes follow chemokine gradients, supported by increased expression of chemokine receptors, and can produce reactive oxygen species, secrete inflammatory cytokines (Kapellos et al., 2019, Idzkowska et al., 2015). These cells also express anti-microbial proteins and are phagocitically active, suggesting they are important in combating pathogens (Idzkowska et al., 2015). Some studies have also suggested that classical monocytes are important in tissue repair, including wound healing, due to observed gene expression patterns (Wong et al., 2011), although other sources have attributed the latter role in particular more to non-classical monocytes (Kapellos et al., 2019). Also, given their high inflammatory potential, it is surprising that this subset has the highest cell–surface expression of the modified lipoprotein scavenger receptor CD36 (Nozaki et al., 1995) among the three subsets (Wong et al., 2011), especially considering that its gene expression is lower in pro-inflammatory than unstimulated macrophages (Xue et al., 2014).

Intermediate monocytes have high expression of CX3CR1 (CX3C receptor 1), CCR (C–C chemokine receptor) 5 and molecules involved in antigen presentation (Idzkowska et al., 2015,

Kapellos et al., 2019). Intermediate monocytes also have pronounced production of reactive oxygen species (although reports disagree if this or the classical subset are the primary producers, (Cros et al., 2010, Zawada et al., 2011)) and upon LPS stimulation secretion of pro-inflammatory cytokines, such as interleukin (IL) –1β (reports disagree if intermediate or non-classical monocytes are the most responsive (Cros et al., 2010, Wong et al., 2011)). Interestingly, these cells have also been noted for their anti-inflammatory IL–10 production and intermediate cell–surface expression of CD36 relative to other subsets (Wong et al., 2011). Therefore, intermediate monocytes may be a more heterogenous population than previously thought and/or have multiple differing roles in the immune response.

Non-classical monocytes have been shown to highly express CX3CR1 (Idzkowska et al., 2015). Upon stimulation with LPS non-classical monocytes have been reported to have both high and low secretion of pro-inflammatory cytokines (Idzkowska et al., 2015, Cros et al., 2010, Wong et al., 2011). These cells have also been observed to have lower levels of cell–surface CD36 expression than the other two subsets (Wong et al., 2011) and suggested to function in opposing processes: wound healing and anti-viral responses (Kapellos et al., 2019).

Several studies have been carried out to determine if the abundance of any monocyte subsets correlated with occurrence of cardiovascular events. In the PHAMOS trial hospitalised coronary artery disease patients that experienced severe cardiovascular and related complications had higher numbers only of the classical monocytes compared to those who did not (Hopfner et al., 2019). Another study measuring numbers of thawed monocytes in individuals from the general public split into control and cardiovascular disease cases showed that higher levels of classical monocytes predicted cardiovascular events (Berg et al., 2012). Conversely, it had previously been reported by the HOME SWEET HOMe study of patients assessed with elective coronary angiography that numbers of intermediate subset monocytes were higher in cardiovascular event cases compared with individuals who did not have such an event (Rogacev et al., 2012). Also, Schlitt et al. reported that intermediate monocytes were more abundant in patients with stable angina or acute coronary syndrome than the control group, which consisted of patients with no angiogram evidence of coronary stenosis and healthy individuals (Schlitt et al., 2004). In addition, a study focused on individuals undergoing dialysis also found that cardiovascular events in such patients were related to increased numbers of intermediate monocytes (Heine et al., 2008).

Differences in study designs, especially population selection as well as technical differences in experimental and data analysis protocols make it difficult to draw conclusions on monocyte subset functions and roles in predicting cardiovascular events across studies. It is also difficult to determine if the classical, intermediate and non-classical subsets directly relate to any particular

macrophage phenotypes due to conflicting conclusions from published reports. Additionally, it is possible that human monocytes may be an even more heterogenous population. Either way, further rigorous experimentation is needed to clarify the functions and relations of monocyte subsets in cardiovascular disease.

1.4. Macrophage phenotypes

Human macrophages are tissue leukocytes that are thought to initially originate from the foetal yolk sac and liver (tissue resident macrophages), supported by mouse model experiments (Ginhoux et al., 2016) and patients with *GATA2* (involved in haematopoietic and endocrine cell development and proliferation) deficiency having few circulating monocytes, dendritic (DC), B and natural killer (NK) cells, but retaining resident macrophage populations (Bigley et al., 2011, Dickinson et al., 2014). Circulating blood monocytes can be recruited into tissue and differentiated to macrophages (Coillard and Segura, 2019). In contact with local stimuli naïve macrophages can become activated (polarised) to a phenotype, displaying different gene and protein expression patterns, inflammatory potential, metabolism, protein secretion, efferocytosis, repolarisation and other capacities (Chinetti-Gbaguidi et al., 2015) (see **Chapter 3** for further discussion on macrophage lipid handling, associated gene and protein expression as well as **Chapter 4** for glucose metabolism and cytokine secretion).

Early descriptions of macrophage phenotypes were based on T helper cell dichotomy, giving rise to the M1 and M2 classification (Murray et al., 2014). M1 or classically–activated pro-inflammatory macrophages are generated *in vitro* by exposure to such inflammatory stimuli as, interferons (IFNs), LPS, tumour necrosis factor (TNF), (Martinez et al., 2006). Macrophage treatment with IFNγ and/or LPS appears to have a wide–ranging effect on their transcriptome: expression of inflammation, cytokine signalling, cell death, antigen processing and selected glycolysis genes is up–regulated, while, this phenotype displays down–regulated expression of genes in transcription, deoxyribonucleic acid (DNA) repair, electron transport chain (ETC)/cellular respiration, protein metabolism pathways and certain lipid uptake genes (Healy et al., 2018, Derlindati et al., 2015, Martinez et al., 2006, Xue et al., 2014). The functional properties of pro-inflammatory macrophages correlate directly with their transcriptome: low lipid uptake capacity (Geng and Hansson, 1992), high pro-inflammatory cytokine secretion and as observed in mouse cells active aerobic glycolysis, generation of ATP in the mitochondria is sacrificed for the production of reactive oxygen species (Van den Bossche et al., 2016, Tarique et al., 2015) to further raise the anti-microbial potential of these cells.

The M2 alternatively–activated or anti-inflammatory macrophages are described as having properties largely different from M1 (Martinez et al., 2006). Anti-inflammatory human macrophages are produced *in vitro* by exposure to IL–4 or less frequently IL–13 (M2a macrophages), immune complexes (opsonised antigen such as LPS, M2b macrophages), IL–10 (M2c macrophages); these M2 subtypes have usually been assumed to have properties very close to those of IL–4 macrophages (Martinez et al., 2006). The transcriptome of IL–4 macrophages is

at the other extreme end of the *in vitro* phenotype spectrum from IFNγ+LPS macrophages (Derlindati et al., 2015, Martinez et al., 2006, Healy et al., 2018, Xue et al., 2014). The IL–4 macrophages up–regulate expression of genes in the tricarboxylic acid (TCA) cycle, ETC, oxidative phosphorylation, protein translation pathways as well as genes involved in lipid uptake, while down–regulating genes involved in inflammatory cytokine and chemokine signalling, apoptosis, cell cycle regulation, glycolysis (Derlindati et al., 2015, Martinez et al., 2006). IL–4 macrophages secrete little or no pro-inflammatory cytokines and as observed in mouse cells have a significantly higher fatty acid uptake than pro-inflammatory macrophages, mostly rely on fatty acid oxidation (FAO), the TCA cycle and oxidative phosphorylation instead of glycolysis for energy production (Huang et al., 2014, Van den Bossche et al., 2016, Vats et al., 2006, Tarique et al., 2015). Interestingly, C56BL/6 wild–type and *Apoe*$^{-/-}$ 6–10 week–old mouse bone marrow–derived macrophage (BMDM) repolarisation was performed from pro- to anti-inflammatory and vice versa by culturing the cells with each of the appropriate stimuli for 10 h (Khallou-Laschet et al., 2010). However, in a more recent study only the anti- to pro-inflammatory repolarisation was achieved, when lower concentrations of the stimuli were used for 24 h on C57BL/6J(c) and B6.SJL-Ptprca Pepcb/BoyJ CD45.1^{+} 8–16 week–old mouse macrophages *in vitro* and *ex vivo/in vivo* and on human macrophages *in vitro* (Van den Bossche et al., 2016). The differences between these two reports highlight two of the main challenges in the field of macrophage biology: differences in the origin of the cells as well as polarising agent concentration and exposure time can lead to notably different observations.

Recent research has expanded our understanding of macrophage functions and the number of recognised phenotypes. Therefore, the nomenclature used to denote phenotypes has been revised to indicate this (Murray et al., 2014). $M^{INFγ+LPS}$ (M1) and $M^{IL–4}$ (M2a) are recognised as the most prominent and different *in vitro* phenotypes (Murray, 2017). However, $M^{IL–10}$ (M2c), M^{oxPAPC} (Mox, oxidised phospholipid: 1-palmitoyl-2-arachidonyl-sn-glycero-3-phosphorylcholine), M^{CXCL4} (M4, C-X-C motif chemokine ligand [CXCL] 4) and M^{Hb} (Mhem) have also been described in atherosclerosis: these phenotypes are thought to be more similar to $M^{IL–4}$ than $M^{IFNγ+LPS}$, notably in their inflammatory potential upon polarisation and cellular metabolism, however, transcriptionally and functionally some key differences are emerging (Xue et al., 2014, Kadl et al., 2010, Gleissner et al., 2010, Boyle et al., 2012). The overall mRNA transcription patterns of $M^{IL–10}$ and mouse M^{oxPAPC} are noticeably different from M^{un} (unpolarised macrophages), $M^{IFNγ+LPS}$ and $M^{IL–4}$ of the appropriate species (Xue et al., 2014, Kadl et al., 2010). Monocyte (macrophage precursor) stimulation with haeme was distinct from oxidised phospholipid, pro- and anti-inflammatory macrophages (Boyle et al., 2012). Surprisingly though,

monocytes exposed to CXCL4 for 6 days to differentiate into macrophages and polarise at the same time differentially expressed less than 2% of the genes tested than cells treated with M–CSF, although the former up–regulated some genes associated with inflammation (*CD86*) and antigen processing (*HLA*), while the latter up–regulated expression of lipid uptake receptors (macrophage scavenger receptor 1 [*MSR1*] and *CD36*) (Gleissner et al., 2010).

IL–10 is thought to have an immunosuppressive effect on macrophages (Grutz, 2005), however, murine pro-inflammatory macrophage repolarisation with IL–10 has been recognised to maintain transcriptional up–regulation of inflammatory and down–regulation of mitochondrion and oxidative phosphorylation genes as well as restore macrophage sensitivity to LPS (expression of *IL1B*, *IL6*, *IL8*, *CXCL1*, *CXCL2*) upon repeated challenge (Gharib et al., 2019). IL–10 macrophages are also competent at efferocytosis (Proto et al., 2018). Macrophage response to oxidised phospholipids appears to vary both *in vitro* and *in vivo*, largely depending on the length and kind of phospholipid (Serbulea et al., 2018b, Serbulea et al., 2018a). M^{Hb} were initially thought be atheroprotective due activating transcription factor 1 (ATF1), haeme oxygenase 1 (HMOX1) and nuclear receptor subfamily 1 group H member 3 (NR1H3, liver X receptor alpha [LXRA]) signalling in reducing foam cell formation capacity and lowering oxidative stress at sites of intraplaque haemorrhage (Boyle et al., 2012), but more recent research has suggested that these macrophages may contribute to weakening of the plaque by secreting increased levels of vascular endothelial growth factor A (VEGFA) due to hypoxia–inducible factor 1 alpha (HIF1A) signalling, increasing angiogenesis, vascular permeability, neovascularisation, monocyte and lymphocyte infiltration (Guo et al., 2018).

Macrophages have key roles at every stage of atherosclerosis and are therefore an important focus of current research (Chinetti-Gbaguidi et al., 2015). Here, the main focus is on macrophage phenotypes with known/predicted roles in the development of atherosclerosis: M^{un}, $M^{IFN\gamma+LPS}$, M^{IL-4}, M^{IL-10}, M^{oxPAPC} and M^{CXCL4} (Chinetti-Gbaguidi et al., 2015). As part of the innate immune system macrophages react to and release cytokines and chemokines (discussed with glycolysis in **Chapter 4**), which regulate inflammation and leukocyte recruitment to the artery wall (Chinetti-Gbaguidi et al., 2015). Also, macrophages handle lipid and form foam cells (discussed in **Chapter 3**), which are important in plaque development (Yahagi et al., 2016, Tabas and Bornfeldt, 2016). In addition, macrophage secretion of MMPs and their inhibitors contributes to modulating the stability of the plaque cap, therefore, influencing the likelihood of rupture and potentially deadly complications (Newby, 2016). Given the multitude of functions macrophage phenotypes carry out and the influence they have in plaque, it is crucial to know the presence and localisation of different phenotypes at each stage of atherosclerosis.

1.5. Presence of macrophage phenotypes in atherosclerosis and use of phenotype–specific markers

A common way to relate *in vitro* findings on macrophage lipid handling and other functions to *in vivo* research and treatment is by utilizing phenotype–specific markers to identify *in vitro* phenotype–like cells in tissue and imply their functional characteristics. Numerous proteins have been used to identify *in vitro*–like macrophage populations in tissue (several examples given): human leukocyte antigen (HLA), CD86, IL–1β and macrophage receptor with collagenous structure (MARCO) for pro-inflammatory, mannose receptor C-type 1 (MRC1) and CD163 for anti-inflammatory (also for haemoglobin/haptoglobin macrophages as listed below), S100 calcium binding protein A8 (S100A8) and MMP7 for CXCL4, CD163, HMOX1, MRC1 and iron staining for haemoglobin macrophages (Chinetti-Gbaguidi et al., 2015, Stoger et al., 2012, Thornton et al., 2019, Erbel et al., 2015) in human atherosclerosis as well as HMOX1, sulfiredoxin 1 (SRXN1) and thioredoxin reductase 1 (TXNRD1) staining for oxidised phospholipid in mouse atherosclerosis (Kadl et al., 2010).

Presence of *in vitro*–like pro- and anti-inflammatory macrophages has been implied by staining sections of different stages of human plaques for specific marker proteins as well as the pan-macrophage marker CD68 (Stoger et al., 2012). The authors compared early, advanced and haemorrhaged plaques and reported that presence of both implied pro- and anti-inflammatory macrophages increased with disease progression. The plaque shoulders mainly contained pro-inflammatory macrophage staining, these cells possibly contributing to inflammation and extracellular matrix protein breakdown and as a result increasing the risk of plaque rupture (Stoger et al., 2012). Interestingly, the authors also reported negligible macrophage co-staining for inducible nitric oxide synthase (NOS2) and MRC1 in these areas, but also did not examine or show possible colocalisation of staining for other markers of the two different groups of macrophages (Stoger et al., 2012). The cap regions did not predominantly contain either one of the implied macrophage phenotypes, while the adventitia contained mostly anti-inflammatory macrophage staining (Stoger et al., 2012). In addition, the authors reported varied staining of implied pro- and inti-inflammatory macrophage markers in macrophages that appeared like foam cells (Stoger et al., 2012). However, the results of this study should be interpreted with caution, because lipid–specific staining was not performed and also there are multiple problems associated with using the currently available markers (see the rest of this section).

Beyond the commonly examined pro- and anti-inflammatory dichotomy CD163 has been shown to be a specific marker for *in vitro* IL–10, but not IL–4 macrophages (Thornton et al., 2019). Use of this gene/protein may help to further split the M2 group, but more markers are needed if this is to be achieved, because CD163 is an uptake receptor for haemoglobin/haptoglobin complexes and

is found at sites of plaque haemorrhage as well as macrophages activated with haemoglobin/haptoglobin complexes (Finn et al., 2012). Oxidised phospholipid macrophages were shown to be distinct from pro- and anti-inflammatory macrophages in mouse atherosclerosis (Kadl et al., 2010), while CXCL4 macrophages have been stained for in human carotid plaque sections (Erbel et al., 2015).

However, recent advances in single cell ribonucleic acid (RNA) sequencing (RNA–seq), cytometry by time of flight (CyTOF) and cellular indexing of transcriptomes and epitopes by sequencing (CITE–seq) technologies have allowed a deeper interrogation of plaque leukocyte composition and individual cell phenotype. It was demonstrated that an atherosclerotic artery wall is populated by many different types of $CD45^+$ cells (Cochain et al., 2018, Winkels et al., 2018, Kim et al., 2018). Female *Apoe*$^{-/-}$ mice fed a western diet for 12 weeks developed plaques with, compared to the chow diet controls, increasing numbers of leukocytes (except decreased monocyte and T helper 2 and also unchanged $CD8^+$ T and NK cell counts) (Winkels et al., 2018). The authors also interrogated another data set to show that macrophages were the largest leukocyte population (around 50%) in the lesion area, while 25 – 30% of the muscle and outer artery wall layer leukocytes were macrophages.

Cochain et al. performed aligned single cell transcriptome profiles of $CD45^+$ cells from male *Ldlr*$^{-/-}$ mice fed a high fat or chow diet for 11 weeks (the former presented as a model of "intermediate stage of lesion development") and identified 11 distinct leukocyte clusters. Within the high fat diet group analysis 28.9% of the cells had enriched macrophage–specific marker expression and the authors broadly categorised these macrophages into inflammatory, resident–like and $TREM2^{high}$ (triggering receptor expressed on myeloid cells 2) macrophages (Cochain et al., 2018).

Another study used a near identical approach (viable $CD45^+$ cells of male *Ldlr*$^{-/-}$ mice fed a western diet for 12 weeks isolated and sequenced), but obtained more diverse macrophage clusters in their analysis (Kim et al., 2018). These included groups enriched for endocytosis, nuclear factor κ–light–chain–enhancer of activated B cells (NF–κB) signalling, DNA replication and ribosomes, cholesterol metabolism with oxidative phosphorylation and peroxisome proliferator activated receptor alpha (PPAR) signalling, inflammatory cytokine and chemokine pathways, interferon response, cell cycle genes.

Crucially, it was observed that several of the *in vitro* macrophage phenotype–specific genes were up–regulated in multiple clusters. *Mrc1* of M^{IL-4} overlapped into the pro-inflammatory macrophage and interferon response clusters (Cochain et al., 2018, Kim et al., 2018) and *Nfe2l2* (nuclear factor, erythroid 2 like 2) was shared among pro-inflammatory, resident–like and

TREM2^{high} macrophage clusters (Cochain et al., 2018). Also, it was observed in an *Ldlr*$^{-/-}$ mouse model of atherosclerosis progression (prolonged western diet) that macrophage cluster diversity was notably higher than in the regression model (chow diet and anti-ApoB therapy for the last two weeks), which also lacked M^{IL-4}–like cells (Lin et al., 2019). Fernandez et al. have recently conducted single–cell omics experiments of human plaques and, similarly to the mouse model experiments, in their CITE–seq experiment, using cells from a plaque of one patient that had a cardiovascular event within 6 months before their surgery, identified two distinct macrophage populations, both positive for two pro-inflammatory markers, but clearly separated by levels of MRC1 (Fernandez et al., 2019). These observations show that mixed macrophage phenotypes exist *in vivo* and that when possible *in vitro*–specific markers should be used to infer a level of specific functional capability instead of an absolute set of *in vitro* phenotype–associated properties.

However, phenotype gene/protein markers should still be considered as useful tools. Single cell–based approaches are expensive and time consuming, which may not always be a hurdle for research, but can hinder widespread patient diagnosis and treatment. Also, *in vitro* models are easier to manipulate, which allows a much greater control of gene and protein expression, protein interaction and other molecular event, to investigate biological processes. Therefore, single cell–based approaches could be used to identify specific macrophage and other cell populations, which are key to and/or indicative of disease type, advancement/regression, while testing for several markers of such populations may be far cheaper and quicker in diagnostics. Aside from the outdated concept of M1 vs M2, there are more problems associated with the currently available markers:

1. Most markers have been tested for their specificity in cells activated with only a few agents;
2. Some of the markers are secreted proteins, which may be detected in cells other than their cell of origin;
3. Not all markers can be used across species in model organisms as well as humans;
4. Not all markers are up–regulated/retain their specificity at both RNA and protein levels.

Therefore, thorough testing of existing and identification of new markers as well as their function in macrophages would greatly improve the reliability of experimental data and our understanding of disease. Calcium homeostasis modulator family member (CALHM) 6 could become one of such new markers for a subtype of pro-inflammatory macrophages with a possible (further testing needed) function of linking innate to adaptive immunity (focuses of **Chapter 5**). Bioinformatics approaches applied to CALHM6 and other members of its family (focus of **Chapter 6**) may help to guide further research on this protein.

1.6. Initial plan for the PhD and subsequent changes

The initial plan for my PhD was to investigate how the abundance and tissue localisation of macrophage phenotypes changes during the progression of human atherosclerosis. In addition, provided sufficient data were gathered and time was left, these potential variations would have been related to age and statin use through *in vitro* and patient sample experimentation. One of the main techniques to be used to achieve this would have been staining of human atherosclerotic plaque sections for *in vitro*–confirmed macrophage phenotype–specific membrane proteins.

However, at the start of my PhD I needed to perform additional *in vitro* confirmation experiments to supplement the validation of such potential new markers and their specificity. While a number of proteins showed promise for different phenotypes, only CALHM6 appeared to be uniquely up–regulated in one phenotype (see **Chapter 5**). Previous reports demonstrated CALHM6 also had possible involvement in regulating the immune response and was otherwise a relatively little studied gene/protein (see **Chapter 6** for bioinformatics), which also contributed to it becoming one of the main focuses of the research I have carried out in this degree.

In addition, most of the research published before the start of my degree focused on one or several distinct *in vitro* stimulations, animal model gene knockouts and marker stainings in atherosclerotic tissue to draw conclusions about roles of specific macrophages in atherosclerosis. However, during my PhD it became increasingly clear that the stimulatory environment for macrophages in atherosclerotic plaques and therefore macrophage activation were far more complex and heterogeneous than previously thought (see **Sections 1.4.** and **1.5.**). This was particularly highlighted towards the end of my degree by reports of *in vivo* atheroma immune cell assessment using single–cell omics. These reports clearly demonstrated that earlier *in vitro* experimentation while still of value to our understanding of macrophage functions and mechanisms used to achieve them may not be as directly translatable as previously thought.

One such example is the human MDM *in vitro* phenotype RNA–seq presented in this thesis (**Chapter 3**). The experiment clearly fails to replicate the complexity of environmental stimuli and resulting macrophage phenotypes within the plaque. However, the data allow to appreciate how specific stimuli affect the macrophage transcriptome and relate those changes to down–stream properties in macrophage lipid handling. These findings have been and could still be used in future research to explain observations made from *in vivo* omics experiments.

2. Materials and methods

Methods that I did not perform any part of are marked with an asterisk (*).

2.1. Primary human macrophages

Cells were isolated from apheresis cones, buffy coats or whole blood donated by healthy adult donors. Apheresis cones and buffy coats were provided by the Blood Donation Centre, Health Sciences Authority and National University Hospital Transfusion Centre, Singapore, respectively. Ethical approval for all blood sources and processes used in this study were given by either the National University of Singapore Institutional Review Board (NUS-IRB 08-352E, NUS-IRB 09-256, NUS-IRB 10-250) or the University of Sheffield Research Ethics Committee (SMBRER310). All donors gave written informed consent in accordance to the Declaration of Helsinki.

Peripheral blood mononuclear cell (PBMC) isolation was carried out by density centrifugation. Blood was carefully layered upon Ficoll–Hypaque (GE Healthcare) at a 2 to 1 volume ratio and centrifuged at 900 g for 20 min with no/minimal acceleration and breaking. The PBMC layer was gathered using a Pasteur pipette, topped up to at least 50 ml volume with phosphate–buffered saline (PBS) containing 2 mM ethylenediaminetetraacetic acid (EDTA, Thermo Fisher) (PBSE) and centrifuged at 450 g for 5 min. Red blood cells were lysed by resuspending the pellet in 10 ml of 155 mM NH_4Cl, 10 mM $KHCO_3$, 0.1 mM EDTA in H_2O and incubating at room temperature for 5 min. Lysis was stopped with 40 ml of PBSE and the cells were pelleted by centrifugation at 450 g for 5 min. Cells were then resuspended in fresh PBSE and counted using a haemocytometer.

Monocyte ($CD14^+$ PBMC) isolation was carried out by positive magnetic selection. After counting the cells were again pelleted by centrifugation at 450 g for 5 min and resuspended in 9 µl MACS buffer (0.5% (w/v) bovine serum albumin (BSA, Sigma) in PBSE) and 1 µl human CD14 MicroBeads (Miltenyi) for every 10^6 cells counted. The suspension was incubated at 4 °C for 15 min with gentle agitation every 5 min. 2 ml of cold MACS buffer were added and the suspension was centrifuged at 390 g for 5 min. One LS column (Miltenyi) was placed into a magnet and rinsed with 3 ml of cold MACS buffer before resuspending and loading the cells in at least 500 µl of cold MACS buffer. The column was then washed three times with 3 ml of cold MACS buffer each time and the retained cells were flushed out of the column with cold MACS buffer. The cells were counted using a haemocytometer and centrifuged at 450 g for 5 min prior to further use.

Monocytes were cultured in complete media: Roswell Park Memorial Institute (RPMI-1640, Gibco), 10% (v/v) low–endotoxin heat–inactivated foetal bovine serum (FBS, Biowest), 1% (v/v) L–glutamine (Gibco) and 1% (v/v) penicillin/streptomycin (Gibco). Recombinant human (rh) M–CSF (100 ng/ml, Peprotech/Immunotools) was added to differentiate monocytes into MDMs over

7 days. On day 7, the media was replaced with fresh complete media containing the following polarising agents: 20 ng/ml rhIFNγ (Peprotech/Immunotools), 100 ng/ml Toll–like receptor (TLR) grade *E. coli* LPS (Enzo Life Sciences), 20 ng/ml rhIL–4 (Peprotech/Immunotools/Miltenyi), 20 ng/ml rhIL–10 (Peprotech/Immunotools), 25 μg/ml oxPAPC (Invivogen) or 1 μM (7.8 μg/ml) rhCXCL4 (Peprotech/Immunotools/BioLegend), incubated for 24 h. Unpolarised macrophages (M^{un}) were used as internal baseline controls in each experiment. The workflow for polarisation is summarised in **Figure 2.1**.

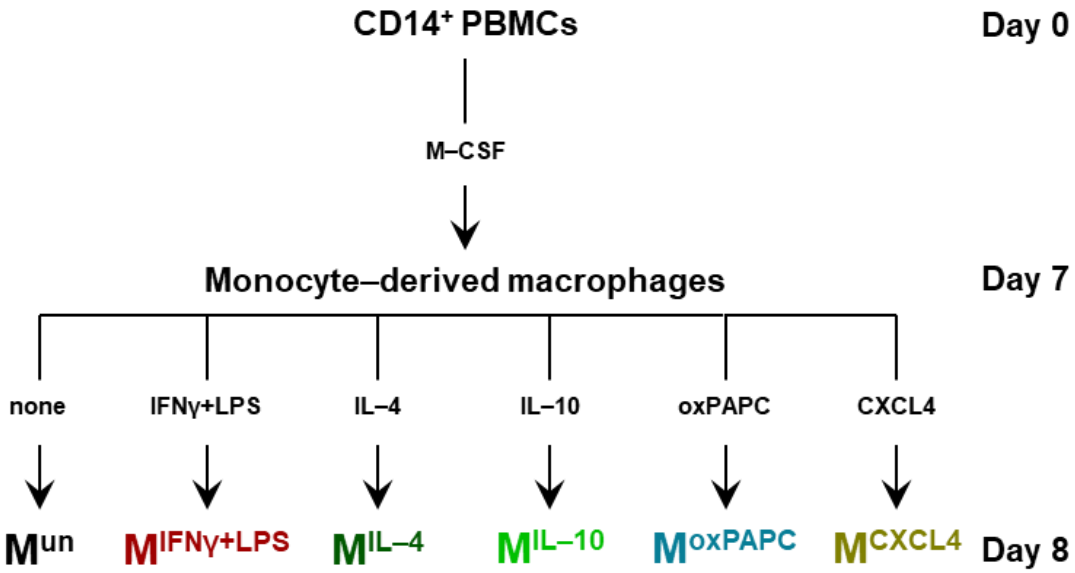

Figure 2.1.: Cell differentiation and polarisation.

Schematic of purified human $CD14^+$ PBMC differentiation into macrophages and subsequent polarisation into specific *in vitro* phenotypes.

2.2. Immunocytochemistry and immunofluorescence microscopy

MDMs cultured on chamberslides (LabTek) were fixed with 4% (w/v) paraformaldehyde (Sigma) in PBS for 30 min, permeabilised with 0.1% (v/v) Triton X–100–PBS (Sigma) for 15 min and blocked with 2% (w/v) BSA–PBS for 45 min. For **Chapter 3** 2 μg/ml mouse anti-human CD68 (Dako) or IgG isotype control (Vector) in 1% BSA–PBS were added and incubated overnight at 4 °C. For **Chapter 5** 1:50 dilution (1 or 4 μg/ml, batch dependant) of anti-human CALHM6 rabbit polyclonal (Novus NBP1–86754 or Sigma–Aldrich HPA017948) or the same concentration of IgG isotype control (Invitrogen 10500C or Vector I–1000) in 1% BSA–PBS were added and incubated overnight at 4 °C. In all experiments all wells were then incubated with 2 μg/ml goat anti–mouse AlexaFluor–488 and 2 μg/ml goat anti–rabbit AlexaFluor–647 (Abcam ab150079) in 1% BSA–PBS in the dark for 1 h. Coverslips were mounted using the ProLong Gold Antifade Mountant with 4′,6-diamidino-2-phenylindole (DAPI, Life Technologies). Images were taken using the Leica AF6000 microscope. Fluorescence signal intensities were adjusted using LAS AF Lite (v 2.6.3, Leica). Integrated densities of regions of interest (cells) were measured in Fiji/ImageJ (v 1.50f).

2.3. Flow cytometry

All antibodies used are listed in **Table 2.1**.

For **Chapter 3** antigen staining was performed in 5% (v/v) FBS–PBS for 15 mins at 4°C in the dark. Measurements were taken using an LSR II cytometer (BD). Dead cells were gated out using live/dead fixable dyes (Molecular Probes) and compensation was performed with anti–mouse IgGκ or negative control compensation particles (BD Biosciences). Isotype antibodies were used as controls for determining positively-stained cell percentages. Data were analysed using FlowJo (v 10).

For **Chapter 5** THP–1s were pelleted and then washed in PBS by centrifugation at 500 g for 5 min. Dead cells were stained with LIVE/DEAD Fixable Aqua Dead Cell stain (Invitrogen) and washed in 2 mM EDTA, 5% (v/v) foetal calf serum , 5% (v/v) human serum, 0.1% (w/v) NaN_3 in PBS by centrifugation at 500 g for 5 min. CytoFix/CytoPerm (BD) was used to permeabilise and wash the cells prior to and during staining with antibodies. Compensation was performed using Arc (Molecular Probes A10346) and UltraComp eBeads (eBioscience 01-2222-42). Measurements were taken using the LSR II cytometer (BD) and analysed in FlowJo (v 10).

Table 2.1.: FACS antibodies.

* Conjugated to their respective fluorochromes using a Lightning–Link conjugation kit (Innova Biosciences). Note: for FLAG detection a λ antibody was used parallel to a κ isotype control.

Test antibody	Dilution	Isotype antibody	Dilution
CD14 APC Cy7 (clone: HCD14, 400 μg/ml, Biolegend)	1:10	**mouse IgG1, κ** APC Cy7 (clone: MOPC-21, 50 μg/ml, Biolegend)	1:50
IFN-γ R1 FITC (clone: 92101, R&D Systems)	1:10	**mouse IgG1, κ** FITC (clone: P3, eBioScience)	1:100
IL-10R PE (clone: 3F9, 400 μg/ml, Biolegend)	1:10	**rat IgG2a, κ** PE (clone: RTK2758, 200 μg/ml, Biolegend)	1:50
LRP-1 APC (clone: 545503, R&D Systems)	1:5	**mouse IgG2b** APC (clone: 133303, R&D Systems)	1:100
CXCR3 PE Cy7 (clone: G025H7, 200 μg/ml, Biolegend)	1:75	**mouse IgG1, κ** PE Cy7 (clone: MOPC-21, 50 μg/ml, Biolegend)	1:100
CD36 FITC (clone: 5-271, Biolegend)	1:5	**mouse IgG2a, κ,** FITC (clone MOPC-173, 200 μg/ml, Biolegend)	1:20
IL-4RA PE (clone: S4-56C9, Beckman Coulter)	1:5	**rat IgG1** PE (clone: eBRG1, 200 μg/ml eBioScience)	1:50
MSR1 APC (clone: 351615, R&D Systems)	1:5	**mouse IgG2b** APC (clone: 133303, R&D Systems)	1:50
TLR4 BV421 (clone: HTA125, Biolegend)	1:5	**mouse IgG2a, κ** BV421 (clone: MOPC-173, 50 μg/ml, Biolegend)	1:5
TLR2 PE (clone:TL2.1, eBioScience)	1:50	**mouse IgG2a, κ** PE (clone: MOPC-173, 50 μg/ml, Biolegend)	1:50
IL-13RA1 APC (clone: 419718, R&D Systems)	1:5	**mouse IgG2b** APC (clone: 133303, R&D Systems)	1:10
ABCA1 * PE (rabbit polyclonal, Novus)	1:100	**anti-rabbit IgG** PE (eBioScience)	1:100
ABCG1 * PE-Texas Red™ (rabbit polyclonal, Thermo Fischer Scientific)	1:100	**anti-rabbit IgG** PE (eBioScience)	1:100
SCARB1 PE (clone m1B9, Biolegend, 100 μg/ml)	1:80	**mouse IgG1a, κ** PE (clone P3.6.2.8.1, eBioScience, 100 μg/ml)	1:80
FLAG APC (Clone L5, rat IgG2a **λ**, Biolegend 637307, 0.17 μg/ml)	1:80	**rat IgG2a, κ** APC (Pharmingen 553932, 0.17 μg/ml)	1:80

2.4. RNA–seq

Polarised MDM from 8 separate donors were lysed in extraction buffer from the ARCTURUS® PicoPure® RNA Isolation Kit (ThermoFisher Scientific) and incubated at 42 °C for 30 min followed by centrifugation at 3,000 g, for 2 min. Supernatants were stored at – 80°C, until total RNA was extracted using the ARCTURUS® PicoPure® RNA Isolation Kit (ThermoFisher Scientific) according to the manufacturer's protocol. Total RNA integrity was assessed using an Agilent Bioanalyzer with RNA Integrity Number (RIN) ≥ 8.5. Complimentary DNA (cDNA) libraries were prepared using 2 ng of total RNA and 1 µl of a 1:50,000 dilution of ERCC RNA Spike in Controls (Ambion) using SMARTSeq v2 protocol (Picelli et al., 2014). The length distribution of the cDNA libraries was determined using a DNA High Sensitivity Reagent Kit on the Perkin Elmer Labchip. All samples were subjected to an indexed pair–end sequencing run of 2 × 51 cycles on Illumina HiSeq 2000 (16 samples/lane).

RNA-Seq data in FASTQ files were obtained and mapped using STAR (Dobin et al., 2013) against build 38 of the human genome. The number of reads per gene was counted using feature Counts (part of Subread package (Liao et al., 2014)) using annotations from GENCODE (v 24). Log_2RPKM (reads per kilobase per million mapped) values were computed using edgeR (Robinson et al., 2010) in R (v 3.1.2) and used for Principle Component Analysis (PCA). Pairwise differential gene expression analyses for each of the cell types were performed using edgeR with unpolarised macrophage samples as the reference. Differentially expressed genes (DEGs) were identified using False Discovery Rate (FDR) of < 5% (Benjamini and Hochberg method (Benjamini and Hochberg, 1995)) and fold change $|\log_2 FC| > \log_2(1.5)$ when compared to unpolarised macrophages. Ingenuity Pathway Analysis (IPA, Qiagen) was used on 13 September, 2018 to perform Canonical Pathway analyses on data from all phenotypes (or excluding M^{CXCL4}) by thresholding for DEGs with or without filtering for human MDM–specific hits. Pathway Heatmaps were generated in R (v 3.5.1) and Microsoft Excel 2016 using reactome.org ENSEMBL annotations to all pathway levels downloaded on 16 October, 2018.

2.5. Quantitative real–time polymerase chain reaction (qRT–PCR)

For the confirmation of RNA–seq (**Chapter 3**) RNA was isolated using the ReliaPrep™ RNA Miniprep Systems kit (Promega) according to the manufacturer's instructions. RNA concentration and purity were assessed using a NanoDrop 1000 spectrophotometer (Thermo Scientific). cDNA was prepared using iScript™ cDNA Synthesis Kit (Bio–Rad) from up to 400 ng of RNA in 25 µl following the manufacturer's protocol.

cDNA (3 ng) was mixed with 0.28 µM of each specific SYBR primer (Sigma) and Precision Plus SYBR Green master mix (PrimerDesign) at a total volume of 10.6 µl/well in triplicate wells on a

384–well plate (Bio–Rad). Measurements were taken using the Bio–Rad CFX384 system. Changes in gene expression were calculated relative to glyceraldehyde 3-phosphate dehydrogenase (*GAPDH*) and unpolarised macrophages, expressed as $\log_2$FC (–ΔΔCt).

For the CALHM6 study (**Chapter 5**) human macrophage RNA was isolated using the Qiagen RNeasy Micro and UCP Micro kits following the manufacturer's protocol (statin pre-treatment experiments) or a modified procedure (all other experiments). Briefly, for the modified procedure 1 ml of macrophage TRIzol/TRI Reagent (Thermo Scientific/Sigma) lysates were mixed with 230 µl of chloroform, shaken for 15 s, allowed to separate for 3 min and centrifuged at 13,400 g, 4 °C for 15 min. The upper phase was collected and mixed with an equal volume of 70% ethanol before following the manufacturer's instructions, except 8,500 and 12,000 g centrifugations were used and the RNA was eluted twice using the same water first applied to each sample. The BMDM RNA was isolated using the ReliaPrep™ RNA Miniprep Systems kit (Promega, following the manufacturer's instructions). RNA concentration and purity were measured using the NanoDrop 1000 spectrophotometer (Thermo Scientific). Human cDNA was prepared using the iScript™ cDNA Synthesis Kit (Bio–Rad) while the mouse cDNA was prepared using the Precision nanoScript2™ Reverse Transcription kit (PrimerDesign) following the manufacturers protocol.

cDNA was loaded with specific SYBR primer pairs (Sigma/IDT,) and KAPA Biosystems SYBR FAST qPCR Master Mix (ABI PrismPrecision) at a total volume of 10 µl/well or Plus SYBR Green master mix (PrimerDesign) at a total volume of 10.6 µl/well in triplicate wells on a 384–well plate (STARLAB). Measurements were taken using the ABI 7900 or the Bio–Rad CFX384 system. Gene expression was calculated relative to *GAPDH* and expressed as $\log_2$FC (–ΔCt). All primer pairs and their sequences are given in **Table 2.2.**

Table 2.2.: qRT–PCR primer pairs.

All sequences are displayed from 5' to 3' ends.

Target	Forward primer	Reverse primer
Human		
ABCA1	TACATCTCCCTTCCCGAGCA	GGGCCAGAGTCCCAAGACTA
ABCG1	GGGAACGAAGCCAAGAAGGT	CCAGTAGTTCAGGTGTTCCCG
CALHM6	GAGGGCTCGCATCCAAAAGA	GTACTGGCCCTTCGGATTGAA
CCL5	CCTCGCTGTCATCCTCATTGC	TAGGCAAAGCAGCAGGGTGT
CD36	TCTGTCCTATTGGGAAAGTCACTG	GAACTGCAATACCTGGCTTTTCTC
CD86	CCCAGACCACATTCCTTGGAT	TCCCTCTCCATTGTGTTGGT
CXCL8	CTCCAAACCTTTCCACCCCAA	ACCCTCTGCACCCAGTTTTC
CXCL9	AGTGCAAGGAACCCCAGTAGT	GTGGATAGTCCCTTGGTTGGTG
CXCL11	GTGTGCTACAGTTGTTCAAGGC	TGCTTTTACCCCAGGGCCTAT
GAPDH	ATTGCCCTCAACGACCACTTT	CCCTGTTGCTGTAGCCAAATTC
MSR1	CGAGGTCCCACTGGAGAAAGT	CAATTGCTCCCCGATCACCTTT
MYD88	TCTTGAACGTGCGGACACAG	TGTGTCTCCAGTTGCCGGAT
NCEH1	TGCATTTCTGGTGACAGTGCT	AGGCTGGCATCTTGAGTAAACTG
STAT1	CTCTGCCCGTTGTGGTGAT	GACAGATTCCTGGGTTCCGC
TICAM1	GCCACCTTCTGCGAGGATTT	CTCAGGCGACAGTCGAAGTT
Mouse		
Calhm6	CAGAAGGTGGAAATGCAGGAGAT	AGCTATCAGAATCCAACCGAAC
Gapdh	TGGCAAAGTGGAGATTGTTGCC	AAGATGGTGATGGGCTTCCCG

2.6. Foam cell formation*

Foam cell formation was induced after polarisation on day 8 by incubating macrophages in complete media supplemented with 25 μg/ml acetylated LDL (acLDL, Molecular Probes) for 24 h. Foam cell formation was assessed by Oil–Red–O (ORO, Sigma) staining and bright–field microscopy (CellSens Software, Olympus IX81 microscope).

Quantification was performed using Image J (v 1.50e). Polygonal selection and area measurement were used to measure quantify the area of lipid (ORO stain) and nucleus. Cells with a total lipid area greater than the area of the nucleus were considered as foam cells. The proportion of foam cells in each condition was calculated as the number of foam cells over total number of cells in each image (3 images/condition). The extent of foam cell formation was expressed as the percentage difference of foam cells between the acLDL and the corresponding control samples.

2.7. acLDL uptake*

Polarised MDM were incubated for 30 min in complete media supplemented with 0.5 μg/ml AlexaFluor–488–conjugated acLDL (Molecular Probes). Internalised fluorescent acLDL was detected by flow cytometry (LSR II, BD). Auto–fluorescence of untreated cells was used to determine positively stained cells. Data were analysed using FlowJo (v 10).

2.8. Cellular cholesterol*

Polarised MDM were incubated for 24 h in complete media with or without 25 μg/ml acLDL. Cellular cholesterol content was measured using the colorimetric Cholesterol Quantitation Kit (Sigma–Aldrich) according to the manufacturer's protocol, except that dried lipids were dissolved in 60 μl instead of 200 μl of cholesterol assay buffer. Sample absorbance was determined at 570 nm using a Tecan Infinite M200 plate reader and analysed using linear regression. Cholesterol ester content was determined by subtracting the free cholesterol from the total cholesterol values. Measurements were normalised to sample protein concentration determined by a colorimetric protein assay (BioRad, performed following the manufacturer's instructions) and expressed as Δ cholesterol, ng / protein, μg (Δ cholesterol = M^x acLDL cholesterol – M^x control cholesterol, where x = polarisation condition).

2.9. Cholesterol efflux*

A fluorescent TopFluor cholesterol (Avanti Polar Lipids Inc.) assay was used to assess cholesterol efflux, and optimised based on previous methods (Low et al., 2012, Sankaranarayanan et al., 2011). Polarised macrophages were plated in 96–well black plates (Nunc) at 2.5×10^4 cells/well. After resting for 1 h, the cells were incubated with 2.5 μM TopFluor cholesterol in serum–free RPMI–1640 for 2 h. The cells were then incubated with 100 μl 0.2% (w/v) BSA in RPMI-1640 with or without the addition of cholesterol acceptors: HDL (kindly provided by Veronique Angeli)

or Apo–AI (Sigma–Aldrich) were used at 50 µg/ml and 20 µg/ml, respectively. The plates were then centrifuged at 450 g for 5 min and supernatants were transferred into clean empty wells. 100 µl of distilled H_2O/well was added to lyse the cells. Plates were covered and placed on a shaker at room temperature for 4 h. Following the incubation, 100 µl of RPMI-1640 or distilled H_2O per well was added to the lysate or supernatant, respectively, to achieve the appropriate dilution for balancing fluorescence intensities. Florescence was measured using a Tecan Infinite M200 plate reader (excitation at 490 nm and emission at 520 nm). The percentage of cholesterol effluxed via HDL or Apo–AI was calculated as follows (where SN denotes supernatant):

$$\text{Efflux} = \frac{\text{SN fluorescence} \times \text{dilution factor}}{\text{lysate fluorescence} \times \text{dilution factor} + \text{SN fluorescence} \times \text{dilution factor}}$$

$$\text{Final efflux} = \text{efflux with acceptor} - \text{background efflux}$$

Total percentage of effluxed cholesterol was calculated by adding the percentages obtained for HDL and Apo–AI–mediated efflux.

2.10. Glycolytic stress assay

Following polarisation, the cells were harvested by replacing the media with 1 ml of warm 2 mM EDTA in PBS and incubating for at least 5 min. The cells were gently scraped and collected before washing the well with 1 ml of fresh culture media (RPMI-1640 media [Gibco] including 10% [v/v] low–endotoxin heat–inactivated FBS [Biowest], 2 mM L–glutamine [Gibco/Lonza], 100 U/ml penicillin and 100 µg/ml streptomycin [Gibco/Sigma]) and combining this media with the collected cell suspension. The harvesting procedure was repeated once or twice without the incubation. The cells were pelleted by centrifugation at 450 g for 5 min. The pellets were carefully resuspended in fresh culture media and the Trypan Blue (Sigma) negative cells were counted to calculate the total number of live cells obtained for each phenotype. The cells were then centrifuged again, carefully resuspended in warm assay media (Seahorse XF Base Medium [Dulbecco's modified eagle media [DMEM]–based without glucose or buffers] supplemented with 2 mM L–glutamine, 100 IU/ml penicillin and 100 µg/ml streptomycin) and plated at 10^5 live cells in 140 µl per well onto a 96 well cell plate (Agilent). The cell plate was briefly centrifuged to settle the cells before visually confirming the confluency and spread of the plating under a microscope and incubating the cells in a CO_2–free incubator for 1 h. Three measurements of extracellular acidification rate (ECAR, mpH/min) and oxygen consumption rate (OCR, pmol/min) were taken as basal using the XFe96 analyser (Agilent) and repeated after exposing the cells to glucose (Agilent, 10 mM in–well at 16.20 min), oligomycin (Sigma, 10 µM in–well at 35.70 min) and 2–

deoxyglucose (2–DG, Sigma, 100 mM in–well at 55.18 min). Any technical replicates not showing an increase in ECAR upon addition of glucose (indication of failed glycolysis) or a drop in OCR upon addition of oligomycin (indication of failed blockade of the ETC), or a drop in ECAR upon addition of 2–DG (indication of failed competitive inhibition of hexokinase catalytic interaction with glucose) were discarded from further analysis, leaving at least 3 technical replicates for each phenotype in each experiment. 3 – 4 media–only wells with plain assay media injections were used as baseline controls to normalise each measurement. In each experiment both ECAR and OCR were normalised to their respective first measurement of M^{un} to counteract variation among different donors. Glycolytic activity was expressed as the difference between the first ECAR measurement after and the last (basal) before adding glucose.

2.11. Enzyme–linked immunosorbent assays (ELISAs)

Cells were differentiated and polarised in 24 well plates at 2×10^5 cells/well. Following polarisation the cells were washed with PBS and 1 ng/ml LPS and/or 25 µg/ml acLDL containing media were added for 24 h. 30 min before the end of this secondary stimulation 100 or 300 µM of BzATP (Sigma, 2′(3′)-O-(4-Benzoylbenzoyl)adenosine triphosphate triethylammonium salt) was added (the final volume per well was 300 – 322.2 µl) to maximise IL–1β secretion. Polarisation and secondary stimulation media were collected, centrifuged at 300 g for 5 min to pellet any insoluble contaminants. The cells were lysed on ice in 100 µl radioimmunoprecipitation (RIPA) buffer (Millipore) with protease inhibitors (Sigma) and additional 0.1% (w/v) sodium dodecyl sulphate (Sigma). Both the supernatants and the lysates were stored at –80 °C until analysis.

IL–1β and IL–8 ELISAs (both from R&D Systems) were performed undiluted or at 1 in 50 dilution respectively, one technical replicate per condition, following the manufacturer's instructions. Optical densities were measured at 450 nm and analysed in GraphPad Prism (v 7.01) using the four–parameter logistic equation. Cytokine concentration in the samples was interpolated from the linear portion of each standard curve, plotted in a $\log_{10}$ graph and any measurements below such part of the standard curve (there were none above) were reported as zero to represent absence or levels below the limit of detection, before adjusting for sample dilution in the assay if necessary. Total protein (as an estimate of total cell number) was measured using the Pierce BCA Protein Assay Kit (Thermo Scientific) in duplicate following the manufacturer's instructions. The total protein content of each sample was divided by that of M^{un} without a secondary stimulation and then the cytokine concentration of the sample was divided by this ratio (performed for all secondary stimulation samples of both donors). Results were further adjusted to account for the final well volume differences between the two donors by multiplying the 300 µM BzATP donor

post-protein normalised cytokine concentrations by the ration between 322.2 and 300 µl (1.074, performed for all secondary stimulation samples of that donor).

2.12. Cytometric bead array (CBA)*

The samples were processed using CBA Flex Sets (BD) for human proteins following the manufacturer's instructions on the Attune Acoustic Focusing cytometer. The data were analysed using the cytometer software.

2.13. Stable isotope labelling with amino acids in cell culture (SILAC) membrane proteomics*

MDMs were washed twice with PBS before 24 h polarisation in media based on lysine and arginine–deprived RPMI (Sigma) with 10% dialysed foetal calf serum (v/v) (Thermo Fischer) and 100 U/ml penicillin and 100 µg/ml streptomycin (Gibco), containing 30 µg/ml Lys+8 Da (15N213C6 lysine, light) and 50 µg/ml Arg+10 Da (15N413C6 arginine, heavy) or 30 µg/ml Lys+4 Da (2H4 lysine, light) and 50 µg/ml Arg+6 Da (13C6 arginine, medium) purchased from Cambridge Isotopes. Each polarisation condition was coupled with a control condition (unpolarised). Polarisation efficiency was confirmed by AlexaFluor 488–acLDL uptake (Molecular Probes) one day before isotopic labelling.

Membrane extracts were prepared following a previously published report (Parker et al., 2011). Equal numbers of cells from all polarisations were lysed in 100 mM sodium carbonate pH 11.0 for 20 min followed by sonication and centrifugation at 100,000 g for 2 h. In–solution digestion with Lys-C (Wako) / trypsin (Promega) was performed before isoelectric focusing technique using OFFgel equipment (Agilent) separation following a modified manufacturer's protocol (Hubner et al., 2008).

Following desalting on STAGEtips (Rappsilber et al., 2003) peptides were separated and analysed by reverse phase liquid chromatography (RP-LC) on Dionex 3000 HPLC system (Thermo) coupled with a Q-Exactive mass spectrometer (Thermo, Germany) in a 140 min gradient of solvent A (0.5% [v/v] CH_3COOH in water) and solvent B (80% [v/v] MeCN and 0.5% [v/v] CH_3COOH in water).

Raw MS/MS spectra were processed using MaxQuant (v 1.4.1.2). Peak lists were searched against Uniprot database version (73000 entries); contaminants were searched using the Andromeda search engine. Parameters used: *Fixed modification, Carbamidomethyl cysteine, Variable modifications: Oxidation on methionine; Acetylated N-terminal protein, phospho STY, deamidation (NQ), SILAC amino acids (Arg+6 Da, Arg+10 Da, Lys+4 Da, Lys+8 Da), 2 missed cleavages, MS accuracy 7 ppm, MS/MS accuracy 20 ppm*. The cut-off rate for identification was

set to a False Discovery Rate of 1%. Unique and common peptides were used for protein ratio quantification with a minimum ratio count of 1.

Samples were generated from 2 different healthy donors. The majority of proteins were identified with at least 2 unique peptides. Raw XIC intensities were Quantile normalized (R software) followed by heavy/light and medium/light ratio estimation. Estimated ratios were used to calculate newly synthesized proteins by taking into account the incorporation of labelled amino acids (threshold: 10%). Proteins were enriched for membrane fraction using gene-ontology (GO-terms). For those missing annotation, manual verification was performed. Statistical analyses were performed on incorporation data to identify proteins with differential/unique expression. All missing values were given a numerical value of 0. Wilcoxon rank sum tests were performed to identify expressed proteins for each macrophage phenotype by comparing the phenotype of interest to all the others. The level of protein induction was calculated by incorporation in polarised macrophage / median of incorporation in all controls.

2.14. Immunohistochemistry*

Atherosclerotic plaques were removed from consented patients (study ethics approval STH18222) undergoing carotid artery endarterectomy surgery. The tissue was placed in 10% (v/v) neutral buffered formalin, decalcified in 0.5 M EDTA pH 8 for 7 days, divided into 3 mm regions and embedded in paraffin.

For immunofluorescence staining sections were dewaxed and rehydrated for treatment with with 3% (v/v) hydrogen peroxide in methanol before antigen retrieval was performed for 10 min in 10 mM heated trisodium citrate buffer. The sections were then treated with 0.1% (v/v) Triton X–100 (Sigma) in PBS for 15 min, followed by blocking in 5% (v/v) donkey serum (Sigma) in PBS for 30 min. Mouse anti-human CD68 (Abcam ab125157, 4 µg/ml), rabbit anti-human CALHM6 (Novus NBP1-86754, 2.5 µg/ml), mouse (Vector Laboratories I-2000, 4 µg/ml) and rabbit (Vector Laboratories I-1000, 2.5 µg/ml) control IgGs were diluted in PBS for a 1 h incubation at room temperature. Donkey anti-mouse NL-493 (R&D Systems NL009, 2.5 µg/ml) and anti-rabbit NL-557 (R&D Systems NL004, 5 µg/ml) secondary antibodies were then incubated with the sections the same way. Coverslips were mounted with ProLong Gold Antifade Mountant with DAPI (Invitrogen) and dried overnight at room temperature before imaging using a Nikon Ti Eclipse microscope. Fluorescence intensities were adjusted in Fiji/ImageJ (v 1.52p) equally across all images according to the isotype antibody staining.

For assessment of atherosclerosis stage and plaque stability sections were cut from each region and counting from the bifurcation as the centre the same number section from each region was stained with haematoxylin and eosin, Elastic Stain Kit (Verhoeff Van Gieson / EVG Stain) (Abcam

ab150667), anti-CD3 and CD68 antibodies. For antibody staining the sections were processed the same as for immunofluorescence staining except for the following: Triton treatment was omitted and blocking was performed using the ImmPRESS Horse Anti-Rabbit /Anti-Mouse IgG Plus Polymer Kit (Vector) for 20 min at room temperature. Sections were incubated with anti-CD3 (Dako A0452, 2 μg/ml) or anti-CD68 (Dako M0814, 1.85 μg/ml) primary antibodies and secondary antibodies from the ImmPRESS Horse Anti-Rabbit /Anti-Mouse IgG Plus Polymer Kit (Vector, 30 min incubation at room temperature). SignalStain® DAB Substrate Kit (Cell Signalling Technologies) was used to visualise the antibody staining before counterstaining with haematoxylin, dehydrating and coverslip mounting.

2.15. Mouse BMDM culture*

Mice were handled in accordance with UK legislation (1986) Animals (Scientific Procedures) Act. Mouse experiments were approved by the University of Sheffield Project Review Committee and carried out under a UK Home Office Project Licence (70/7992). All mice used were congenic on a C57BL/6J background (N17) and were housed in a controlled environment with a 12–hour light/dark cycle, at 22°C in Optimice individually ventilated cages (Animal Care Systems) and given free access to a standard chow diet (#2918; Harlan Teklad) and water. Bone marrow was isolated and BMDMs were cultured for 5 days in DMEM (Gibco), 10% (v/v) low–endotoxin heat–inactivated FBS (Biowest), 100 U/ml penicillin and 100 μg/ml streptomycin (Gibco) and 10% v/v L929 medium. The non-adherent cells were then washed off, while the adherent cells were scraped and plated in fresh media at 2×10^5 cells/ml. The following day the cells were polarised for 24 h with 20 ng/ml recombinant mouse IFNγ (Peprotech) and 100 ng/ml TLR grade *E. coli* LPS (Enzo), 20 ng/ml recombinant mouse IL–4 (Peprotech), 20 ng/ml recombinant mouse IL–10 (Peprotech). Unpolarised cells were used as a baseline control.

2.16. siRNA knockdown

Day 7 MDMs were treated in fresh media for 24 h with 28 nM of small interfering RNA (siRNA, Dharmacon) in Viromer Green (Lipocalyx) following the manufacturer's protocol. The media was then changed again to polarise the cells for another 24 h.

2.17. CALHM6–3×FLAG THP–1s

Codon–optimised human CALHM6 isoform 1 coding sequence (from NM_001010919.3) with a CACC at the 5' end and without the STOP codon at the 3' end was purchased from IDT gBlocks and inserted into a pENTR/D vector (Thermo Fisher) following the manufacturer's protocol using high–competency *E. coli* (NEB). The plasmid was purified using a Miniprep kit (Sigma) and insert size and sequence were confirmed by EcoRV + NotI restriction digest and Sanger sequencing. A 3×FLAG tag was cloned into the vector by PCR amplifying the tag from a previously validated

plasmid, recombined using the In-Fusion HD Cloning kit (Clonetech) and validated by Sanger sequencing. The control plasmid did not contain the CALHM6–3×FLAG construct.

The construct was sub-cloned in into the PE1A plasmid followed by gateway transfer into the lentiviral vector. In brief, HEK293 cells were transfected using Xfect (Clontech) with the viral packaging construct (pMDLg/pRRE, pRSV/REV, pMD2.G/V-SVG). Supernatants containing lentiviral particles were collected every 48 to 72 h after transfection, concentrated by LentiX concentrator (Clontech), tittered by qPCR (determination of number of transducing or infectious units/ml) on HeLa cells. Titres for control and CALHM6–3×FLAG viruses were 6×10^7 TU/ml.

THP–1 cells (ATCC) were adjusted to a concentration of 1×10^6 cells/ml, for gene transduction, duplicate wells of a flat bottom 96-well plate were seeded with 0.1 ml/well of the cell suspension (1×10^6 cells/ml) and virus was added in the presence of 6 μg/ml polybrene (Sigma); multiplicity of infection of 25 was routinely used in most experiments. Cells were then incubated overnight with the virus and the media was replaced with fresh complete media. 3 days post viral infection, cells were selected for in 2 μg/ml puromycin (Gibco)–containing complete media. The transfected cells were maintained for 3–4 weeks between 0.1 and 1×10^6 cells/ml with minimal passaging before testing for FLAG by flow cytometry (passage 6). The cells were then maintained at the same density interval or grown for co-immunoprecipitation experiments by splitting to 0.25 – 0.3×10^6 cells/ml once the density reached or exceeded 1×10^6 cells/ml.

For differentiation into macrophage–like cells, monocytic THP–1s were centrifuged at 1,000 g for 5 min and treated with 0.5 μM phorbol myristate acetate (PMA, Sigma) in fresh culture media for 3 hours at 8×10^6 cells per 75 cm^2 flask. The PMA–containing media was then discarded and replaced with fresh culture media for 21 hours. The cells were then polarised with 20 ng/ml rhIFNγ (Peprotech/Immunotools), 100 ng/ml TLR grade *E. coli* LPS (Enzo Life Sciences) for 24 hours.

2.18. Jurkat cell culture*

Jurkat cells were obtained from ATCC and cultured at the same density as THP–1s, in the same media as THP–1s, but without puromycin. The cells were activated with 100 nM PMA for 20 h followed by centrifugation at 1,200 rpm for 5 min and treatment with 2 μM Ca^{2+} ionophore A23187 (Sigma C7522) for 4 hours, followed by a 20 h resting period in fresh media.

2.19. Co-immunoprecipitation*

Cells were collected and washed in PBS before lysis in 50 mM Hepes–NaOH (pH7.5), 100 mM NaCl, 1 mM EDTA (pH8), 0.5% Triton–X100, 10% glycerol (wash buffer) supplemented with 1% (v/v) Nonidet™ P40 (NP40, Roche), 1 mM dithiothreitol, protease inhibitors (Sigma, 1:100 dilution), 10 μg/ml RNase A. Cells were sheared using a needle and syringe before centrifugation

at maximum speed for 5 min to separate the supernatants. Bradford assays (Bio–Rad) were performed following the manufacturer's protocol to quantify total protein content in the supernatants.

50 µl of FLAG–agarose beads were washed in wash buffer before blocking in wash buffer supplemented with 1% (w/v) BSA (Sigma) for 2 h at 4 °C with agitation before removal of supernatant by centrifugation at 2,500 g for 1 min and washing. Equal amounts of control and CALHM6–3×FLAG protein were loaded onto the beads and the volumes were adjusted with wash buffer, followed by incubation for 2 h at 4 °C with agitation. The unbound fraction was then removed before washing the samples in wash buffer lacking detergent or glycerol. Bound proteins were eluted in 1 M arginine (Sigma) at pH 3.5 followed by neutralisation with 1.5 M Tris–HCl at pH 8.8. Coomassie blue staining, western blotting and mass spectrometry were used to test the samples for presence of specific proteins.

2.20. Co-immunoprecipitation mass spectrometry*

LC MS/MS (liquid chromatography with mass spectrometry) was performed and analysed by nano-flow liquid chromatography (U3000 RSLCnano, Thermo Scientific) coupled to a hybrid quadrupole–orbitrap mass spectrometer (Q Exactive HF, Thermo Scientific). Peptides were separated on an Easy–Spray C18 column (75 µm x 50 cm) using a 2–step gradient from 97% solvent A (0.1% formic acid in water) to 10% solvent B (0.1% formic acid in 80% acetronitrile) over 5 min then 10% to 50% B over 75 min at 300 nL/min. The mass spectrometer was programmed for data dependent acquisition with 10 product ion scans (resolution 30,000, automatic gain control 1×10^5, maximum injection time 60 ms, isolation window 1.2 Th, normalised collision energy 27, intensity threshold 3.3×10^4) per full MS scan (resolution 120,000, automatic gain control 106, maximum injection time 60ms) with a 20 second exclusion time.

MaxQuant (version 1.5.2.8) software was used for database searching with the *.raw MS data file using standard settings. The data for searched against the Homo sapiens Uniprot proteome database (taxa id: 9606, downloaded 25 November 2018, 73101 entries), using the following settings: Digestion type: trypsin; Variable modifications: Acetyl (Protein N–term); Oxidation (M); fixed modifications: carbamidomethyl (C); MS scan type: MS2; PSM FDR 0.01; Protein FDR 0.01; Site FDR 0.01; MS tolerance 0.2 Da; MS/MS tolerance 0.2 Da; min peptide length 7; max peptide length 4600; max mis–cleavages 2; min number of peptides 1.

2.21. Western blotting

Human macrophages were washed with cold PBS and lysed by scraping on ice in RIPA buffer (Sigma) supplemented with protease inhibitor cocktail (Sigma) and PhosSTOP (Roche). The lysates were sonicated with a probe sonicator while on ice for 15 s and centrifuged at 10,000 g, 4

°C for 10 min. Total protein content was determined using the Pierce BCA Protein Assay Kit (Thermo Scientific). Equal amount of protein of each MDM or THP–1 co-immunoprecipitation lysate (for preparation method see **Section 2.19.**) were run on a 4 – 12% Bis–Tris gel (Invitrogen) before transferring to an Immobilon–P polyvinylidene difluoride (PVDF) membrane (Millipore) and blocking for 60 min in 5% (w/v) BSA– or milk–Tris buffered saline with Tween 20 (TBST, 0.1% v/v of Tween 20).

For signal transducer and activator of transcription 1 (STAT1) detection the membrane was incubated with Y701 phosphorylated (Invitrogen 33-3400, 1 μg/ml) and total STAT1 (Cell Signalling Technology 9172, 125 ng/ml) antibodies or a GAPDH antibody (Santa Cruz sc-47724, 40 ng/ml) overnight at 4 °C. Secondary antibodies (LiCor 925-32210 and 925-68071, 83.3 ng/ml) were incubated with the membranes for 60 min at room temperature before imaging on the Odyssey CLx system.

For protein detection THP–1 co-immunoprecipitation samples the membrane was incubated with one of the following primary antibodies: 60 min at room temperature anti-FLAG (Sigma F1804, 66.7 ng/ml), overnight at 4°C anti-LAT (Invitrogen, 14-9967-82, 5 μg/ml), overnight at 4°C anti-dermicidin (DCD) (Invitrogen PA5-13677, 2 μg/ml). Secondary goat anti-mouse–horse radish peroxidase (HRP, Dako P0447, 500 ng/ml) or goat anti-rabbit–HRP (Dako P0448, 125 ng/ml) antibodies were incubated with the membrane for 60 min at room temperature before detection using enhanced chemiluminescence (ECL) reagent (GE Healthcare) and the Gel Doc™ XR+ imager (Bio–Rad).

2.22. Cell interaction assay*

THP–1s and Jurkat cells were stained with PKH26 (Sigma) and PKH67 (Sigma) respectively before treatment with PMA. Both cell types were then differentiated and activated or polarised as described in their culture methods. Macrophage–like IFNγ+LPS control and CALHM6–3×FLAG THP–1s were co-cultured 1:1 with activated Jurkats in culture media without puromycin and imaged using the Leica AF6000 microscope. Fluorescence signal intensities were adjusted using LAS AF Lite (v 2.6.3, Leica). Overlapping or touching cells were considered as attached.

2.23. Publicly available transcriptome data search

The individual human *CALHM* NCBI pages were accessed on 30 July, 2018 and the HPA RNA–seq normal tissues RPKM averages (Fagerberg et al., 2014) were downloaded. The data were then converted to $\log_2$ and plotted in a heatmap (up to 3 significant figures), zero values before the $\log_2$ transformation were left out of the heatmaps. The RNA–seq data were surveyed for *CALHM* (RNA–seq discussed in **Chapter 3**) gene expression in each phenotype and donor. Data on atherosclerotic tissue compared and adjacent macroscopically intact tissue RNA expression was

retrieved from a published microarray dataset (Ayari and Bricca, 2013). Data on monocyte subset transcriptomes (Wong et al., 2011) was obtained by averaging the expression values of the two replicates for each donor (n = 4).

2.24. Alternative transcript isoform expression estimation*

Frequencies of *CALHM6* transcript isoforms in the RNA–seq samples (obtained as detailed in **Chapter 3**) were computed using REM using annotations from GENCODE V24 against the human genome (build GRCh38) and expressed as fragments per kilobase million mapped (FPKM) in $\log_2$, again leaving the zero values out of the $\log_2$ transformation, and isoform percentage (ISOPCT).

2.25. Protein sequence alignment

Protein sequences for entries Q8IU99 (CALHM1), Q9HA72 (CALHM2), Q86XJ0 (CALHM3), Q5JW98 (CALHM4), Q8N5C1 (CALHM5) and Q5R3K3 (CALHM6) were downloaded from UniProt on 29 May, 2019, annotated for transmembrane regions using UniProt data in SeqBuilder (v 14.0.0.88) and aligned using the Clustal Omega algorithm in MegAlign Pro (v 14.0.0).

2.26. Statistical analyses

Unless otherwise stated, statistical tests were performed in GraphPad Prism (v 8.4). Paired two–tailed t tests (for comparing two groups), matched/repeated measures (for comparing more than two groups if data from all conditions and donors were available) or ordinary (for comparing more than two groups when some data were missing) one–way analysis of variance (ANOVA) tests, two–way ANOVAs (data matched by cell donor) were performed. Gaussian distributions and sphericity were assumed in matched/repeated measures tests due to the measurements being performed on full sets of samples generated from cells of the same donor in each experiment. Post tests were carried out to check for statistical significance $\alpha = 0.05$. The n number in each experiment represents the number of individual donors or separate experiments on cell lines of different passages. Standard error of the mean (SEM) shown where noted.

3. Macrophage phenotype transcriptomes and selected protein expression in relation to lipid handling and foam cell formation

3.1. Introduction

Lipid handling by macrophages (**Figure 3.1.**) can regulate atheroma growth (Chinetti-Gbaguidi et al., 2015). Macrophages uptake lipoprotein via cell surface receptors such as CD36 (Park, 2014), MSR1 (Gough et al., 1998) and LDLR. In late endosomes cellular lipases breakdown lipoprotein particles to release their contents, in particular, triglycerides are hydrolysed to glycerol and fatty acids while cholesterol esters are converted into free cholesterol (Fasano et al., 2012, Vinje et al., 2018). Liberated fatty acids can be incorporated into cytoplasmic lipid droplets for storage or used in peroxisomal/mitochondrial oxidation to fuel the Kreb's cycle (Viola et al., 2019). Free cholesterol is removed (effluxed) from the macrophage to Apo–AI and/or HDL (Brewer, 2004) or re-esterified for storage by sterol O-acyltransferase (SOAT1) (Rudel et al., 2001). Cholesterol esters can be converted back into free cholesterol for efflux by neutral cholesterol ester hydrolase 1 (NCEH1) (Igarashi et al., 2010). Macrophages can efflux lipid by passive diffusion through the plasma membrane, SCARB1–facilitated diffusion and active transport (requiring energy input) involving ABCA1 and ABCG1 (Brewer, 2004). As mentioned, ABCA1 is able to load lipid to Apo–AI, initiating HDL formation, while ABCG1, SCARB1 and similar receptors load more lipid into the immature HDL particles to yield mature spherical HDL (Brewer, 2004). All of these processes influence the presence of esterified lipids stored in the cytoplasm (lipid droplets), which at high levels (e.g. total lipid droplet area/volume larger than that of the cell nucleus) result in the formation of a macrophage foam cell (Ghosh et al., 2010).

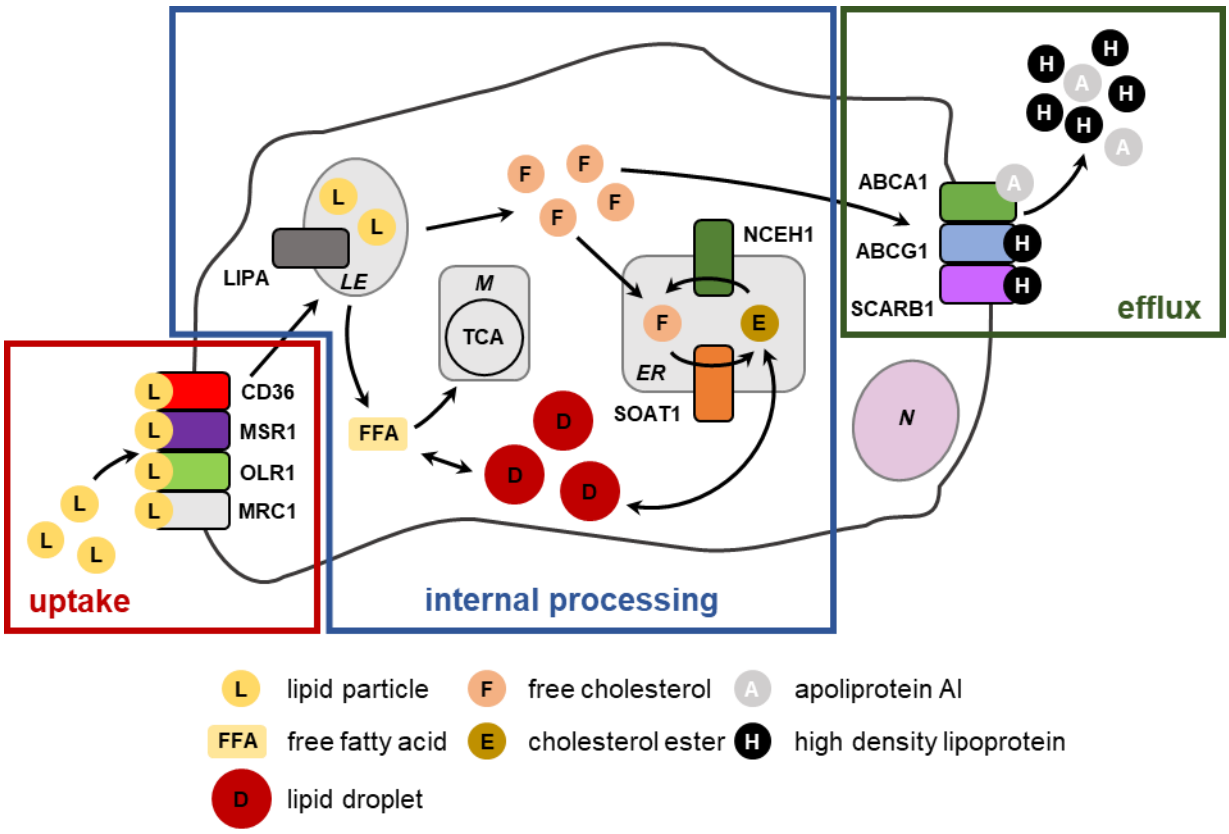

Figure 3.1.: Current model of human macrophage lipid handling.

Simplified schematic of macrophage lipid handling with key stages outlined: uptake, processing and efflux. Excessive accumulation of cytoplasmic lipid droplets is indicative of foam cell formation, a hallmark of atherosclerosis. ABCA1 – ATP–binding cassette subfamily A member 1, ABCG1 – ATP–binding cassette subfamily G member 1, CD36 – cluster of differentiation 36, ER – endoplasmic reticulum, LE – late endosome, LIPA – lipase A, lysosomal acid type, M – mitochondria, MRC1 – mannose receptor C-type 1, MSR1 – macrophage scavenger receptor 1, N – nucleus, NCEH1 – neutral cholesterol ester hydrolase 1, OLR1 – oxidised low density lipoprotein receptor 1, SCARB1 – scavenger receptor class B member 1, SOAT1 – sterol O–acyltransferase 1, TCA – tricarboxylic acid (Kreb's) cycle. Adapted from (Hadadi, 2015).

Macrophage and macrophage–derived foam cell exposure to IFNγ manifests as reduced capacity to uptake, process and efflux lipid, decreasing the effectiveness of macrophages to remove lipid from the artery wall (Geng and Hansson, 1992, Wang et al., 2002, Panousis and Zuckerman, 2000b). In combination with high inflammatory potential, this increases atheroma vulnerability to rupture (Chinetti-Gbaguidi et al., 2015). In the context of atherosclerosis, anti-inflammatory M2 macrophage lipid handling is highly important: relatively high capacity to handle lipid is beneficial in the early stages of atheroma formation, because sufficient tissue lipid efflux to HDL can lead to plaque regression, possibly delaying disease potentially deadly complications, but could also result in foam cell formation due to increased lipid uptake (van Tits et al., 2011, Han et al., 2009). Over time, continued lipid accumulation in the plaque and macrophages can overwhelm the cells, leading to cell death, contributing to atheroma growth (Tabas, 2002, Chinetti-Gbaguidi et al., 2015, Libby et al., 2011).

Despite these descriptions, less is known about the lipid handling and foam cell formation capacities of other human macrophage phenotypes, underestimating their potential contributions. Therefore, it is important to systematically characterise the transcriptional patterns of human macrophage phenotypes relevant to the progression of atherosclerosis ($M^{IFN\gamma+LPS}$, M^{IL-4}, M^{IL-10}, M^{oxPAPC} and M^{CXCL4}) and relate these observations to previously reported protein expression, foam cell formation and lipid handling capacities of macrophage phenotypes.

3.2. Hypothesis and aims

The following hypotheses and aims refer to the original research being submitted as part of the completion of this degree. Work that has been submitted before in a different thesis has been acknowledged as such in the **Contributions** (**Section 3.3.**) for this chapter. Both original and previously submitted work (**Section 3.4.**) were included in the submission for publication in a peer–reviewed journal with overall hypotheses and aims throughout the manuscript.

Hypothesis: Alterations to macrophage transcriptome along with selected protein expression upon polarisation affect down–stream macrophage lipid handling abilities.

Aim 1: Examine the overall and lipid handling pathway gene expression in human macrophage phenotypes.

Aim 2: Gather additional data on lipid efflux protein expression.

Aim 3: Identify the relationships between differential gene, protein expression upon polarisation and down–stream foam cell formation, lipid handling.

3.3. Contributions

My own contributions to the data in this chapter are:

RNA–seq sample generation, RNA–seq data analysis, RNA isolation and qRT–PCR of samples parallel to the RNA–seq, SCARB1 flow cytometry, data analysis and interpretation, manuscript writing.

The following people have also contributed to the data presented in this chapter for completion of their degree and/or publication purposes:

Éva Hadadi (previously submitted work as part of completion of PhD): foam cell formation, acLDL uptake, cholesterol content, cholesterol efflux assays, all flow cytometry, except SCARB1, data analysis and interpretation, manuscript writing (methods) and editing;

Bernett Lee: RNA–seq data analysis, manuscript writing (methods) and editing;

Josephine Lum: RNA isolation and library preparation for RNA–seq, RNA–seq, manuscript writing (methods) and editing;

Foo Shihui: RNA isolation and library preparation for RNA–seq, RNA–seq;

Ian Sudbery: RNA–seq data analysis;

Endre Kiss–Tóth: conception and design, data interpretation, manuscript editing;

Siew Cheng Wong: conception and design, data interpretation, manuscript editing;

Heather L Wilson: conception and design, data interpretation, manuscript writing.

3.4. Manuscript: Macrophage polarisation associated with atherosclerosis differentially affects their capacity to handle lipid

As mentioned in the **Hypothesis and aims** (**Section 3.2.**) for this chapter, the following manuscript has been submitted to a peer–reviewed journal. The **Introduction** (**Section 3.4.2.**) of the manuscript provides additional context for the data introduced, while the **Results** and **Discussion** (**Sections 3.4.4.** and **3.5.5.** respectively) of this manuscript represent their respective sections that would be in place in a traditionally formatted thesis. The **Materials and methods** (**Chapter 2**) and the **References** (**Chapter 8**) of the thesis contains the **Materials and methods** and **References** respectively for this manuscript.

Macrophage polarisation associated with atherosclerosis differentially affects their capacity to handle lipid

Short Title: Macrophage polarisation & lipid handling capacity

Kajus Baidžajevas*[a,b], Éva Hadadi*[a, b, c], Bernett Lee[b], Josephine Lum[b], Foo Shihui[b], Ian Sudbery[d], Endre Kiss-Tóth[a], Siew Cheng Wong[b§], Heather L Wilson[a§].

*These authors contributed equally.

a Department of Infection, Immunity & Cardiovascular Disease, University of Sheffield, Beech Hill Road, Sheffield, S10 2RX, UK.

b Singapore Immunology Network (SIgN), Agency for Science, Technology and Research (A*STAR), Singapore.

c Current address: INSERM U935, Villejuif, France.

d Department of Molecular Biology and Biotechnology, University of Sheffield, Western Bank, Sheffield, S10 2TN, UK.

§Corresponding authors:

Heather Wilson: Department of Infection, Immunity & Cardiovascular Disease, University of Sheffield, Beech Hill Road, Sheffield, S10 2RX, UK. Tel. + 44 114 215 9560. Email: H.L.Wilson@sheffield.ac.uk

Siew Cheng Wong: Singapore Immunology Network (SIgN), Agency for Science, Technology and Research (A*STAR), 8A Biomedical Grove, Immunos, Level 4, Singapore 138648. Tel: +65 6407 0030. Email: wong_siew_cheng@immunol.a-star.edu.sg

Category: Original Research Paper / Basic Research Paper.

Keywords: Inflammation, Atherosclerosis, Macrophage, Innate

3.4.1. Abstract

Background and Aims:

Lipid-rich foam cell macrophages predominate in atherosclerotic plaques impacting inflammation, lipid uptake, lipid deposition and plaque vulnerability. The atheroma environment determines macrophage function and phenotype; anti-inflammatory macrophages improve plaque stability while pro-inflammatory macrophages promote rupture. Current evidence suggests a variety of macrophage phenotypes occur in atherosclerotic plaques with local lipids, cytokines, oxidised phospholipids and pathogenic stimuli altering their phenotype. In this study, we addressed differential functioning of macrophage phenotypes via a systematic analysis of *in vitro* polarised, human monocyte-derived macrophage phenotypes, focussing on molecular events that regulate foam-cell formation.

Methods:

We examined transcriptomes, protein expression and functionally determined lipid handling and foam cell formation capacity in macrophages polarised with IFNγ+LPS, IL–4, IL–10, oxPAPC and CXCL4.

Results:

Total mRNA sequencing of differentially polarised macrophages revealed distinct gene expression changes, with enrichment in atherosclerosis and lipid-associated pathways. Analysis of lipid processing activity showed IL–4 and IL–10 macrophages have higher lipid uptake and foam cell formation activities, while inflammatory and oxPAPC macrophages displayed lower foam cell formation. Inflammatory macrophages showed low lipid uptake, while higher lipid uptake in oxPAPC macrophages was matched by increased lipid efflux capacity.

Conclusions:

Atherosclerosis-associated macrophage polarisation dramatically affects lipid handling capacity underpinned by major transcriptomic changes and altered protein levels in lipid-handling gene expression, leading to phenotype-specific differences in LDL uptake, cellular cholesterol levels and cholesterol efflux. Key molecular differences between inflammatory and oxPAPC polarised macrophages account for their low foam cell formation, informing how the plaque environment influences atherosclerosis progression.

3.4.2. Introduction

Arterial macrophages form disease-associated lipid-rich foam cells in atherosclerotic plaques (Tabas and Bornfeldt, 2016). Progressive atherosclerosis results in cardiovascular diseases, which are a leading cause of death, worldwide (Nascimento et al., 2014). Plaque formation arises from the accumulation of lipid in the artery wall over decades; acute myocardial infarction or stroke can occur following a loss of plaque stability due to cellular changes in the artery wall (Kavurma et al., 2017). Macrophages are a predominant cell type within the artery wall, whose major functions in the plaque are to regulate inflammation, clear apoptotic cells via efferocytosis, regulate plaque stability by secreting MMPs or protease inhibitors and to uptake, process, accumulate and efflux lipid (Moore et al., 2013). The capacity of macrophages to accumulate or process lipid and to regulate proteases and cytokines in their local environment is a critical determinant of plaque development, lipid core formation and plaque stability (de Gaetano et al., 2016).

The local cellular environment determines macrophage function and phenotype (Sica et al., 2015). Traditionally, macrophages have been described as classically activated M1 and alternatively activated M2 macrophages (Sica et al., 2015). Pro-inflammatory M1 macrophages arise from exposure to bacterial LPS and IFNγ (Chistiakov et al., 2015). Cytokines such as IL-4 and IL-13 drive polarisation to M2 macrophages (Gordon and Martinez, 2010). In arterial atherosclerotic plaques, pro-inflammatory macrophages localise to areas of increased vulnerability, such as the shoulder regions (Stoger et al., 2012). In these vulnerable areas, they promote rupture by secreting MMPs and inflammatory cytokines thus weakening the cap structure (Stoger et al., 2012). In contrast, anti-inflammatory macrophages are associated with increased plaque stability, at times with plaque regression and less severe disease (Tabas and Bornfeldt, 2016). The traditional classification of M1 and M2 macrophages is now widely understood to be simplistic where many differently polarised phenotypes exist according to the local environment (Chistiakov et al., 2015). Macrophages expressing markers for both M1 and M2 phenotypes have been labelled within atherosclerotic plaques (Chistiakov et al., 2015). The plaque environment contains oxidised phospholipid (Que et al., 2018), platelet-derived CXCL4 (Gleissner, 2012) and IL-10 (Gordon and Martinez, 2010) as well as haemoglobin (Boyle et al., 2012), which can each influence macrophages to polarise to different functional states.

The same processes that have evolved for macrophages to phagocytose pathogens, also means they are critical regulators of lipid metabolism (Bories and Leitinger, 2017). Macrophages take up lipoproteins from dying cells and also have the capacity to eliminate cholesterol (Remmerie and Scott, 2018). The uptake of LDL, VLDL and oxidised lipoproteins occurs via micropinocytosis, phagocytosis and scavenger receptor mediated mechanisms. Ingested lipids are processed within

lysosomes where they are either converted to free fatty acids for subsequent oxidisation and energy, or converted to free cholesterol which undergoes either efflux at the plasma membrane or re-esterification and storage as lipid droplets within the cytosol, characteristic of foam cells (Remmerie and Scott, 2018). The build-up of cellular cholesterol activates transcription factors RXR (retinoid X receptor), NR1H3, NR1H2 (nuclear receptor subfamily 1 group H member 2), PPARα and PPARγ (Chawla et al., 2001). Heterodimerisation of NRH (LXR) and RXR increases the expression of proteins ABCA1 and ABCG1, which actively transport HDL loaded-cholesterol out of the cell at the plasma membrane (Remmerie and Scott, 2018).

Foam cell formation is altered according to macrophage phenotype (Cochain and Zernecke, 2017). Inflammatory IFNγ macrophages appear to have a lower lipid uptake and foam cell formation capacity (Geng and Hansson, 1992). In contrast, anti-inflammatory macrophages are considered to have high lipid handling and foam cell formation capacities (van Tits et al., 2011). The effect of IL–10, CXCL4 and oxidised phospholipid on human macrophage lipid handling is less well understood.

Compelling evidence shows that a variety of macrophage phenotypes occur in atherosclerotic plaques and that the arterial environment can alter with respect to lipid, cytokine, oxidised phospholipids and pathogenic stimuli (Chinetti-Gbaguidi et al., 2015). In order to address how this variety of plaque macrophage phenotypes differentially handle lipid, we undertook a systematic study to model human macrophages polarised towards the factors relevant to the atherosclerotic plaque environment. We examined whole transcriptomes, protein expression and functionally determined lipid handling and foam cell formation capacity in human macrophages polarised with IFNγ+LPS, IL–4, IL–10, oxPAPC and CXCL4. Our data revealed transcriptionally distinct phenotypes, differential lipid uptake, processing and efflux capacities and functional differences to account for low foam cell formation in differentially polarised inflammatory macrophages.

3.4.3. Materials and methods

Detailed materials and methods for this manuscript are included in the **Materials and methods** (**Chapter 2**) of this thesis. In brief, PBMCs were isolated from whole blood donated by healthy adult donors and monocytes purified by CD14 positive magnetic selection. Monocytes were differentiated into MDMs over 7 days in M–CSF. On day 7, the media was replaced for 24 h with fresh complete media containing the following polarising agents: IFNγ and LPS; IL–4; IL–10; oxPAPC; CXCL4; or unpolarised as controls in each experiment. RNA was extracted from unpolarised and polarised MDM from 8 separate donors for RNA-seq analysis. Differential gene expression was validated by qRT–PCR, and protein by immunofluorescence and flow cytometry. Functional changes in foam cell formation and lipid handling were assessed by ORO staining, acLDL uptake, cholesterol content and efflux determination. Replicate values (n) represent separate human donors.

3.4.4. Results

3.4.4.1. CD14$^+$ monocytes differentiate into CD68$^+$ macrophages expressing polarising factor receptors

In order to determine that polarisation factors would be effective in vitro, human MDMs were tested for the expression of receptors responsive to IFNγ+LPS, IL–4, IL–10, oxPAPC and CXCL4. Flow cytometry staining showed that most naïve (unpolarised) MDMs expressed the following cell–surface receptors required for polarisation: interferon γ receptor (IFNGR) 1, CD14, TLR4, IL–4 receptor α chain (IL4RA), IL–13 receptor α chain (IL13RA), IL–10 receptor (IL10R), MSR1, CD36, low density lipoprotein receptor related protein 1 (LRP1) and CXCR3 (**Table 3.1.**). In addition, immunocytochemistry coupled with immunofluorescence (ICC/IF) imaging confirmed that all day 8 unpolarised macrophages expressed the pan-macrophage marker CD68 (**Figure 3.2.**).

Table 3.1.: Flow cytometry quantification of cell surface receptors positive for polarisation factors in (unpolarised) human MDMs.

Following 7 days of differentiation from monocytes to macrophages cells were assessed and analysed for polarisation factor receptors by flow cytometry (n = 4).

Receptor for	Receptor	Cells positive, %	SEM, %
IFNγ	IFNGR1	25.19	8.02
LPS	CD14	98.98	0.83
	TLR4	97.40	2.20
IL–4	IL4RA	26.46	10.45
	IL13RA	75.73	7.40
IL–10	IL10R	90.28	8.63
oxPAPC	MSR1	48.68	17.31
	CD36	83.10	12.31
	LRP1	16.24	5.69
CXCL4	CXCR3	46.28	16.29

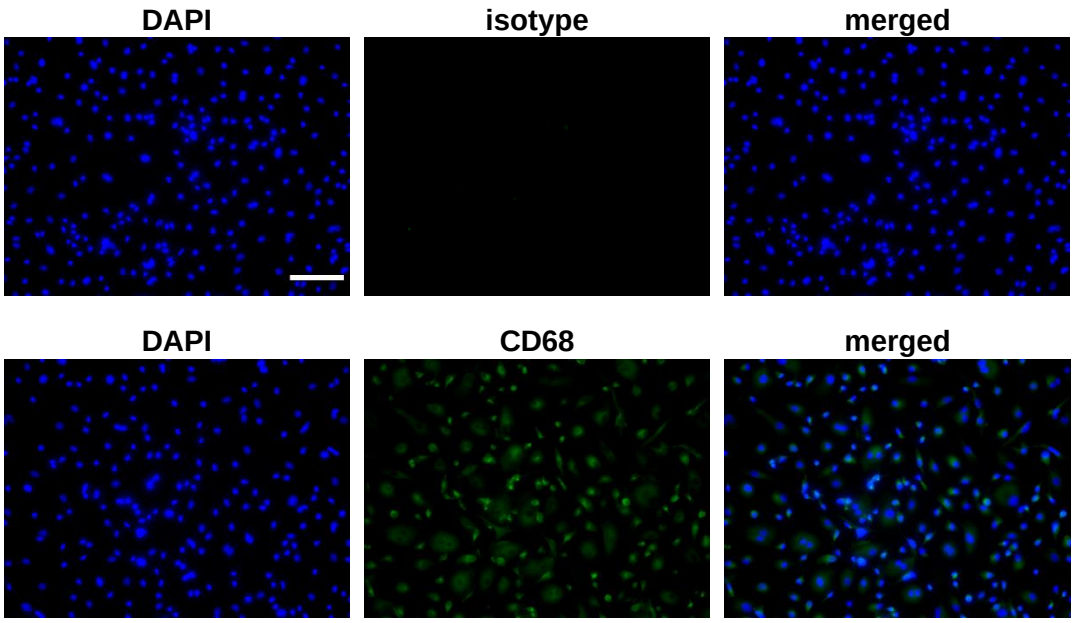

Figure 3.2.: Confirmation of monocyte differentiation into macrophages.

Representative immunocytochemistry fluorescence staining of unpolarised macrophages (M^{un}, day 8) for CD68 (pan macrophage marker); nuclear DAPI and AlexaFluor–488 for isotype/CD68 staining. Scale bar represents 100 μm for all images.

3.4.4.2. Polarisation causes atherosclerosis–related changes in MDM transcriptomes

Differential gene expression for $M^{IFN\gamma+LPS}$ and M^{IL-4} has been well documented (Martinez et al., 2006). We set out to systematically extend this knowledge by assessing gene expression changes specifically in *human* macrophage phenotypes arising from the same donors, treated under a variety of conditions reflecting the arterial plaque environment. Day 7 MDMs were polarised with IFNγ+LPS, IL–4, IL–10, oxPAPC or CXCL4 and examined by RNA–seq for global and specific pathway changes in their transcriptomes that may influence atherosclerosis progression.

PCA clearly showed $M^{IFN\gamma+LPS}$ as the most transcriptionally distinct phenotype (Martinez et al., 2006, Xue et al., 2014) with > 5,500 differentially expressed DEGs compared to unpolarised macrophages and to other phenotypes (**Figure 3.3.**). $M^{IFN\gamma+LPS}$ displayed unique and high upregulation of common pro-inflammatory markers (**Tables 3.2.** and **3.3.**). M^{IL-4} was the next most transcriptionally distinct phenotype as evidenced by the PCA and by *IRF* (interferon regulatory factor) *4* and *MRC1* up–regulation, confirming that $M^{IFN\gamma+LPS}$ and M^{IL-4} represent the extreme ends of the *in vitro* MDM polarisation spectrum. Interestingly, in the PCA M^{IL-10}, M^{oxPAPC} and M^{CXCL4} clustered closely to unpolarised macrophages. M^{IL-10}, M^{oxPAPC} and M^{CXCL4} also showed a mostly M^{IL-4} phenotype with low $M^{IFN\gamma+LPS}$ expression pattern similarity, particularly with respect to cytokine/chemokine expression. These included a notably lower up–regulation of *CXCL8* (IL–8), *CXCL9*, *CXCL11*, *IL1B*, *IL2RA* and *SOCS3* compared to $M^{IFN\gamma+LPS}$, but no changes in *IRF1*, *NFKB1*, *NFKB2*, *RELA* and *RELB* expression (**Table 3.4.**). M^{IL-10} showed consistent *CD163* expression up–regulation, while M^{oxPAPC} was clearly distinguished by increased *HMOX1* and *TXNRD1* expression. M^{CXCL4} were remarkably similar to unpolarised macrophages as indicated by their close clustering in PCA and only 207 DEGs (1.53% of transcripts detected from a total of 13,531 genes) between the two conditions (**Figure 3.3.B**). These results were largely in agreement with transcriptomic data on unpolarised and CXCL4 macrophages from another study (Gleissner et al., 2010), where monocyte differentiation into unpolarised macrophages and M^{CXCL4} with M–CSF or CXCL4 respectively over 6 days resulted in only 460 differentially expressed probes or 375 DEGs (1.77% out of 26,051 probes with signals above the detection limit). Also, previously reported M^{CXCL4} markers *S100A8* and *MMP7* showed expression changes in our study that were highly variable among donors and up–regulated at higher magnitudes in most other phenotypes, especially $M^{IFN\gamma+LPS}$ (**Tables 3.2.** and **3.3.**).

Each MDM phenotype displayed significant enrichment of DEGs in atherosclerosis–related pathways (**Table 3.5.**). In most phenotypes, these pathways included genes clearly involved in macrophage lipid handling, such as *ABCA1*, *ABCG1*, *LIPA* (lipase A, lysosomal acid type) and *MSR1* prompting further investigation into the lipid handling capacity of these phenotypes. M^{CXCL4}

did not have as many lipid–related DEGs: *ABCA3*, *ACOX2*, *ALOX15*, *APOL1*, *CYP1B1*, *ENPP2*, *OLR1* and *SLC25A10*. Given this low difference between M^{CXCL4} and unpolarised macrophages, we omitted M^{CXCL4} from further study. The RNA-sequencing results were validated by qRT–PCR on parallel samples (**Figure 3.4.**), confirming differences in selected atherosclerosis-related genes.

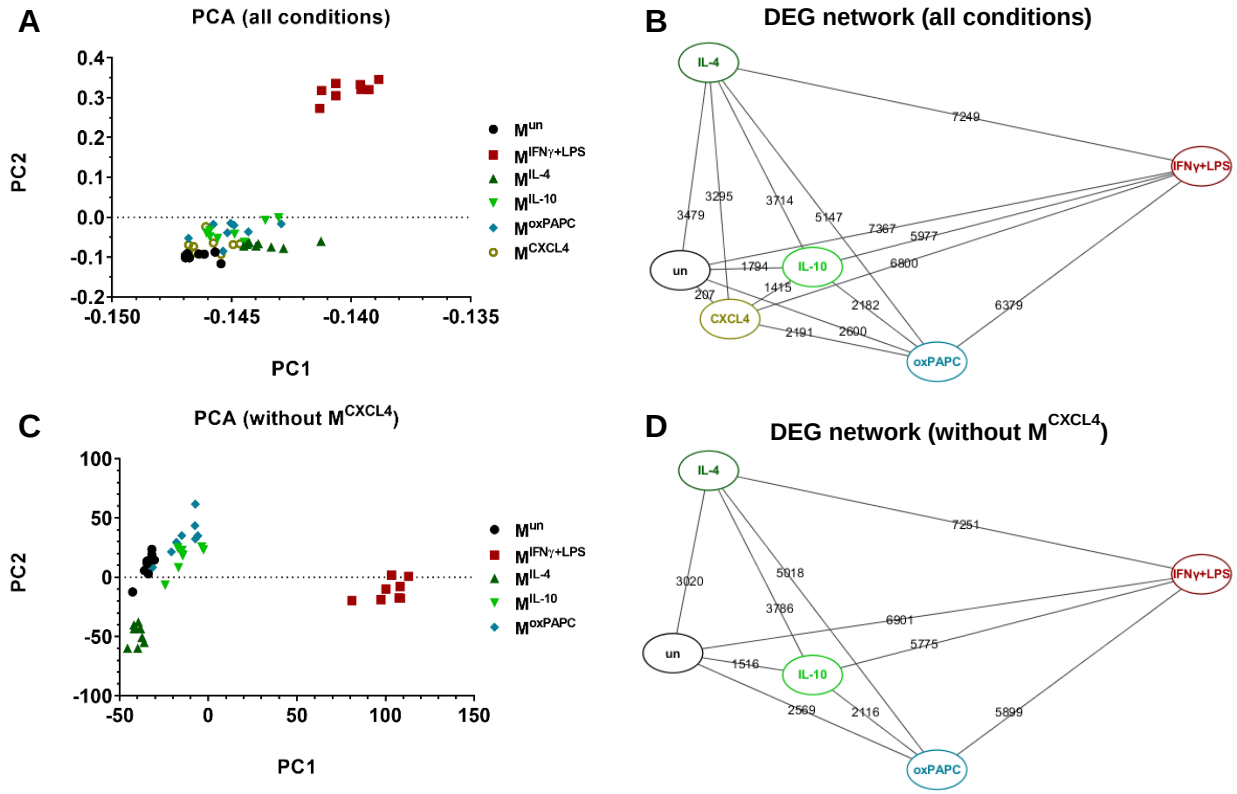

Figure 3.3.: Global analyses of human macrophage phenotype transcriptomes.

(**A**) Principal component analysis (PCA) and (**B**) numbers of differentially expressed genes ($|\log_2 FC| > \log_2(1.5)$ and FDR < 0.05 (Benjamini and Hochberg method)) among all conditions. (**C**) Principal component analysis (PCA) and (**D**) numbers of differentially expressed genes excluding M^{CXCL4}. PC – principal component, DEG – differentially expressed gene.

Table 3.2.: Commonly cited phenotype-specific marker gene expression across donors.

Individual donor log_2FCs of each gene transcript for the indicated macrophage phenotype shown, letters above columns indicate individual donors.

		A	B	C	D	E	F	G	H
IFNγ+LPS	***IFR1***	5.00	5.72	5.36	5.44	5.35	5.13	4.40	5.00
	CXCL9	9.10	15.01	11.17	10.87	9.95	11.70	9.65	11.67
	CXCL8	6.76	5.77	9.12	5.55	5.64	7.34	7.86	8.11
	IL1B	5.67	6.14	8.66	5.47	5.66	7.09	7.74	7.20
IL-4	***IRF4***	4.90	6.86	3.30	3.90	5.81	3.47	4.04	3.11
	MRC1	1.89	2.16	1.69	1.82	1.51	2.03	2.17	1.97
IL-10	***CD163***	2.13	0.75	1.96	1.22	1.74	1.46	1.40	2.29
oxPAPC	***HMOX1***	1.38	0.41	0.61	0.66	1.03	0.56	0.87	0.87
	SRXN1	4.16	1.13	-1.45	0.50	6.66	-0.84	3.74	0.87
	TXNRD1	1.36	2.12	1.33	1.52	1.38	1.42	0.75	1.25
CXCL4	***S100A8***	0.85	1.99	2.87	0.54	5.66	2.53	1.12	2.84
	MMP7	1.21	0.57	1.09	0.90	0.29	0.89	0.33	0.74

-2	0	4	8	12	16

Table 3.3.: Phenotype specificity for up–regulation of commonly cited markers.

Log_2FCs were filtered for FDR < 0.05 and $|log_2FC| > log_2(1.5)$.

Supposed phenotype	Gene	IFNγ+LPS log_2FC	IL-4 log_2FC	IL-10 log_2FC	oxPAPC log_2FC	CXCL4 log_2FC
IFNγ+LPS	***IRF1***	5.17	-0.63			
	CXCL9	11.14		1.47		
	CXCL8	7.02	1.57		3.59	2.13
	IL1B	6.70		1.65	1.70	1.06
IL-4	***IRF4***	2.90	4.42			
	MRC1	-6.02	1.90			
IL-10	***CD163***		-1.32	1.62		
oxPAPC	***HMOX1***	-1.33		0.73	0.80	
	SRXN1					
	TXNRD1				1.39	
CXCL4	***S100A8***	6.05	-2.37	4.10	3.07	2.30
	MMP7	2.09		1.25		0.75

-8	-4	0	4	8	12

Table 3.4.: DEGs in 'Cytokine Signaling in Immune System' and 'Chemokine receptors bind chemokines' pathways.

Log_2FCs were filtered for FDR < 0.05 and $|log_2FC| > log_2(1.5)$.

Cytokine Signaling in Immune System

gene	IFNγ+LPS log_2FC	IL-4 log_2FC	IL-10 log_2FC	oxPAPC log_2FC	CXCL4 log_2FC
AAAS	-1.60		-0.60		
ABCE1	-2.28			-0.95	
ADAM17					
ADAR	0.86				
AGER					
AIP		-0.62			
AKT1	-0.75				
ALOX15	-3.29	11.91	-2.63		-2.53
ALOX5	-1.74	-3.66	0.70		
ANXA1					
ANXA2	-1.43			-0.63	
APP					
ARF1					
ARIH1					
ATF1					
ATF2	0.67				
B2M	1.62				
BATF	1.62		1.21		
BCL2	-0.78		-1.32		
BCL2L1					
BCL6	1.93	0.59			
BIRC2	0.78				
BIRC3	2.32	0.96			
BIRC5	-8.14	-5.77	-1.81	-2.88	
BLNK	-1.08				
BRWD1					
BST2	0.63				
BTRC					
CAMK2A	8.20	-1.20			
CAMK2B	-5.22			-1.57	
CAMK2D	-1.13				
CAMK2G	-1.46	-0.69			
CANX	-0.73				
CAPZA1					
CASP1	0.70	-1.17			
CASP3	1.06				
CBL					
CCL19	12.24				
CCL2	-1.07		1.03		
CCL22	-2.33	2.42			
CCL3	2.13	1.92	0.62	-1.38	
CCL3L3		1.18	0.65	-1.54	
CCL4	3.56	3.73	1.15		
CCL5	5.72		-1.37	-1.47	0.69
CCND1	-1.75			-1.87	
CCR1					
CCR5	0.97	0.63			
CD36	-2.41		0.59		
CD4	-2.09				
CD40	3.63	1.83	0.66		
CD44	2.72	0.66	0.87	0.59	
CD80	6.42	3.08	2.06		

Table 3.4. (continued)

CD86	0.87	1.03		1.02	
CDC42					
CDKN1A	2.26	2.40			
CEBPD					
CFL1	-0.90			-0.76	
CHUK					
CIITA		1.18		1.16	
CISH	0.80	4.09			
CLCF1	2.99			1.41	
CNN2	-0.99	0.68			
CREB1				0.59	
CRK					
CRKL	0.73				
CSF1	-0.79			-1.40	
CSF1R	-1.55				
CSF2RB	3.67		0.80	0.60	
CSF3	8.28			1.35	1.74
CSF3R		-1.49		1.00	
CUL1	2.21				
CXCL1	5.11		2.11	2.05	
CXCL10	6.63				
CXCL2	2.79	-1.79		2.74	
CXCL8	7.02	1.57		3.59	2.13
DDX58	2.09				0.67
DUSP3			0.65		
DUSP4	2.03			0.89	
DUSP6	-1.17	-1.00		-0.61	
DUSP7	-2.41			-1.09	
EBI3	7.38	0.65	1.56	-2.04	
EDA	-4.26	-1.37			
EDA2R		-1.13	-1.89	-2.52	
EGR1	-2.33				
EIF2AK2					
EIF4A1	-0.97				
EIF4A2					
EIF4A3	-0.77				
EIF4E	-1.13			-0.80	
EIF4E2					
EIF4E3					-0.63
EIF4G1	-1.10				
EIF4G2					
EIF4G3					
ELK1	0.74				
F13A1	-7.27	3.11	3.18		
FBXW11					
FCER2		6.71			
FCGR1A	2.28	-4.13	2.17	-0.98	
FCGR1B	2.77	-2.16	2.29	-1.60	
FLNA	-1.33		-0.83		
FLNB	-1.35		-0.86		
FN1	-3.73		-0.99	-0.74	
FOS	-3.07	-1.29		-0.91	
FOXO1		-1.08		0.97	
FOXO3		-1.46			
FPR1	3.71	-2.16	4.17	2.74	
FSCN1				-1.87	
FYN	0.77				
GAB2	1.50			0.62	
GBP1	7.60	0.61			

Table 3.4. (continued)

GBP2	3.70	-0.63			
GBP3	4.45				
GBP4	6.66	-1.78		0.63	
GBP5	8.89	-0.89		1.28	0.75
GRB2					
GSTO1					
HAVCR2					
HCK	1.91		0.83		
HERC5	1.49	-2.11			
HGF	-4.58	-5.08			-0.89
HIF1A	1.97			1.40	
HIST1H3E	0.98			0.89	
HIST1H3H	2.46				
HLA-A	1.77				
HLA-B	1.39				
HLA-C	1.56				
HLA-DPA1		1.22			
HLA-DPB1	-0.87	0.98			-0.69
HLA-DQA1		1.07			
HLA-DQA2		1.11			
HLA-DQB1		1.06		0.67	-0.65
HLA-DQB2	-0.65	1.00		0.61	
HLA-DRA		1.00		0.59	
HLA-DRB1		0.81			
HLA-DRB5		0.82			
HLA-E	1.49				
HLA-F	2.30				
HLA-G	1.36				
HLA-H	1.52				
HMGB1	-0.69			-0.78	
HMOX1	-1.33		0.73	0.80	
HNRNPA2B1				-0.69	
HNRNPDL					
HNRNPF					
HSP90AA1	-0.59				
HSP90B1	-2.04				
HSPA8	-2.18				
HSPA9					
ICAM1	2.92	1.21			
IFI27	6.09			-2.28	1.64
IFI30	1.23			1.38	
IFI35	2.43				
IFI6	0.93	-0.68	-0.65		
IFIT1		-0.87			1.36
IFIT2	1.91	-1.17		0.99	1.20
IFIT3	3.49	-0.67		0.62	1.32
IFITM1	6.43				1.56
IFITM2		-1.32	1.47	-0.63	
IFITM3	2.30	-0.67	1.20		
IFNAR1	1.22				
IFNAR2	0.96				
IFNGR1					
IFNGR2					
IFNLR1				0.66	
IGHE		8.27	0.89		
IKBKB	-0.77				
IKBKG					
IL10				0.77	
IL10RA	1.39			0.68	

Table 3.4. (continued)

IL10RB	1.06				
IL11RA	-1.71	-1.06			
IL12RB1	1.17				
IL12RB2	-4.69	-4.36	2.70	-2.92	
IL13RA1		-0.98		0.60	
IL15	4.11	-0.75		0.82	
IL15RA	4.99	-0.92			
IL16	-3.22				
IL17RA					
IL17RB		2.09			
IL17RC					
IL18	0.81	-1.77		-1.40	
IL18BP	2.46	0.68	-0.69		
IL1A	5.52				
IL1B	6.70		1.65	1.70	1.06
IL1R1	-2.50	1.53	-0.86	1.80	
IL1R2	-4.70	3.39	-2.49		0.81
IL1RAP	0.96	3.00			0.72
IL1RN		1.18		-0.95	
IL20RB					
IL21R	0.80		2.12		
IL23A	3.70				
IL24	-3.30	-1.54	-0.61		
IL27	6.88				
IL27RA	-2.32	1.79			
IL2RA	8.09	-2.89	4.44	1.44	
IL2RB	3.50				
IL2RG			-0.75		
IL31RA	8.57		-1.73	-2.01	
IL32	7.23				
IL36B		1.33			
IL36RN					
IL4R	1.34		0.60		
IL6R	-0.70				
IL6ST					
IL7	4.29		2.37		
IL7R	5.77		2.56		0.99
INPP5D	-2.18				
INPPL1					
IP6K2					
IRAK1	-0.71				
IRAK2	2.80	0.66			
IRAK3	1.26	-1.82			
IRAK4	0.89				
IRF1	5.17	-0.63			
IRF2	1.07	-0.66			
IRF3	0.69				
IRF4	2.90	4.42			
IRF5			-0.87		
IRF6	3.35	-2.54			
IRF7	3.35	-0.78		0.87	0.84
IRF8					
IRF9	1.19			0.77	
IRS2		-2.38		0.84	
ISG15	2.32				1.24
ISG20	6.47			2.40	
ITGAM	-1.96	0.63		-0.59	
ITGAX	-1.38		-0.71		
ITGB1					

Table 3.4. (continued)

ITGB2					
JAK1	1.37				
JAK2	2.46				
JAK3	4.64		4.37		0.75
JUN		1.31		0.59	
JUNB	1.99				
KPNA1					
KPNA2	-0.98	-0.65	-0.91	-1.34	
KPNA3					
KPNA4					
KPNA5	0.83				
KPNB1	0.65				
LBP	7.70				
LCK		-3.08			
LCP1					
LGALS9	-1.91			-0.99	
LIF		-1.60	-1.45	-1.03	
LMNB1		-3.06		-2.51	
LTB					
LTBR					
LYN	1.72		0.73		
MAOA	3.02	5.13			0.68
MAP2K1					
MAP2K3			-0.90		
MAP2K4					
MAP2K6	-2.79	1.32	-1.54	-1.21	
MAP2K7					
MAP3K14	-2.00				
MAP3K3	-0.97				
MAP3K7					
MAP3K8	2.22		1.62	1.11	
MAPK1					
MAPK14					
MAPK3		-1.48			
MAPK7					
MAPK8					
MAPK9	-0.78				
MAPKAPK2					
MAPKAPK3	-1.10				
MCL1	2.15				
MEF2A					
MEF2C	-2.08	-1.11			
MIF					
MMP1	7.34	4.76	3.87	3.13	3.81
MMP2		-2.15			
MMP9	-1.81	-0.93		-0.98	
MSN					
MT2A	5.82	-2.42	0.71	-2.20	1.02
MTAP	-2.60		-0.71	-0.83	
MUC1	7.68				
MX1	2.29	-0.81			1.49
MX2	1.19	-1.14		0.86	1.04
MYC	-4.77			-2.15	
MYD88		-0.79			
NCAM1		-1.66	-1.44		1.27
NDC1	-2.36		-1.02	-1.32	
NDN					
NEDD4					
NFKB1	1.43				

Table 3.4. (continued)

NFKB2	1.44				
NFKBIA	2.09				
NFKBIB	1.00				
NKIRAS1					
NKIRAS2	1.35				
NOD1	1.32				
NOD2	2.73	-1.04			
NUP107					
NUP133	-0.64				
NUP153					
NUP155	-1.26			-0.62	
NUP160	-1.19				
NUP188	-0.85		-0.66		
NUP205	-0.63				
NUP210	-2.65		-1.03	-1.15	
NUP214	-0.71				
NUP35	-1.94			-0.87	
NUP37	-1.52	-0.79			
NUP43				-0.59	
NUP50					
NUP54					
NUP58					
NUP62	0.59				
NUP85	-1.34	-0.64			
NUP88	-1.18		-0.64	-0.71	
NUP93					
NUP98					
NUPL2	-0.60				
OAS1	1.34	-1.16			
OAS2	1.70				1.30
OAS3	1.08		-0.68		1.11
OASL	2.78	-0.76			1.33
OSM	3.74	1.21		2.32	
OSMR	9.05		3.16		
P4HB					
PAK2					
PDCD4	0.61	-1.04			
PDE12	-0.68				
PELI1	1.23	-0.92		0.59	
PELI2		-3.47		1.21	
PELI3				0.81	
PIAS1					
PIK3CA					
PIK3CB		-0.78			
PIK3CD	-1.72				
PIK3R1	-0.66	0.75			
PIK3R3	-1.22	-1.01	-1.09		
PIM1	3.20	-1.48	1.09		
PIN1	-0.68				
PITPNA		0.83			
PLCG1	-1.46				
PML	2.15				
POM121					
POM121C					
POU2F1		-0.63		0.91	
PPIA	-1.61			-0.77	
PPM1B					
PPP2CA					
PPP2CB					

Table 3.4. (continued)

PPP2R1A	-0.84				
PPP2R1B					
PPP2R5D					
PRKACA					
PRKCD					
PRLR		-3.46			
PSMA1					
PSMA2	0.78				
PSMA3					
PSMA4	0.80				
PSMA5					
PSMA6	0.99				
PSMA7	-0.68				
PSMB1					
PSMB10	1.32				
PSMB2					
PSMB3					
PSMB4					
PSMB5					
PSMB6					
PSMB7					
PSMB8	1.30				
PSMB9	3.15				
PSMC1					
PSMC2					
PSMC3	-0.59			-0.67	
PSMC4	-0.85			-0.77	
PSMC5	-0.87				
PSMC6					
PSMD1					
PSMD10					
PSMD11					
PSMD12					
PSMD13	-0.69				
PSMD14	-0.69			-0.61	
PSMD2	-0.71				
PSMD3	-0.87				
PSMD4					
PSMD5					
PSMD6					
PSMD7					
PSMD8					
PSMD9					
PSME1	1.23				
PSME2	2.66			-0.67	
PSME3	-0.74				
PSME4	-0.77				
PSMF1					
PTAFR	1.72			0.85	
PTGS2	7.54				
PTK2B		-1.43	-0.69	0.68	
PTPN1	2.26		0.67		
PTPN11	-0.83				
PTPN12	0.60				
PTPN13	-4.43	-0.99	-2.84	-1.89	
PTPN18					
PTPN2	2.88		1.23		
PTPN23					
PTPN4	-1.17	0.70			

Table 3.4. (continued)

PTPN6	-0.91				
PTPN7	-1.20	0.67			
PTPN9					
RAE1					
RALA	1.57			0.91	
RANBP2	-0.61				
RAP1B	1.37				
RAPGEF1					
RBX1					
RELA	1.82				
RELB	2.53				
RHOU	1.67	-1.42	1.35	0.91	
RIPK2	3.00				
RNASEL	-0.80				
RORA		-1.00			
RPLP0	-1.55		-0.59	-0.89	
RPS27A					
RPS6KA1	-0.74				
RPS6KA2	-1.00	-2.05	-1.10		
RPS6KA3					
RPS6KA5	1.21	-3.66			
RSAD2	6.16				2.02
S100B	-3.27	2.40	1.82		
S1PR1	-3.13	-3.32	1.15		
SAMHD1	-0.82				
SDC1	-4.65				
SEH1L	-0.98			-0.78	
SERPINB2	-1.74	-5.32	-2.22	2.82	
SH2B1	-0.77				
SHC1					
SHFM1					
SIGIRR	-2.39	-0.77			
SKP1					
SMAD3	-3.65	-2.06			
SMARCA4	-0.78				
SNRPA1	-1.00			-0.75	
SOCS1	4.58	5.01			
SOCS2	6.14				
SOCS3	7.26		3.74	1.86	
SOCS5					
SOD1	-1.00				
SOD2	5.30	-1.01	1.91	1.90	0.91
SOS1	0.64				
SOS2					
SP100	0.75	-0.84			
SQSTM1				0.71	
STAT1	3.00				0.92
STAT2	1.64	-0.79			
STAT3	1.81		0.81		
STAT4	4.46	0.68	-0.68	2.26	
STAT5A					
STAT5B					
STAT6					
STX1A		-2.56			
STX3	-0.61				
STX4					
STXBP2					
SUMO1					
SYK	-2.31	-0.68			

Table 3.4. (continued)

TAB1	-0.75				
TAB2					
TAB3	0.92				
TALDO1				0.67	
TBK1	1.76				
TCP1	-1.28			-0.73	
TEC	-0.61			0.83	
TGFB1					
TIMP1			1.11	0.99	
TNF	2.20	1.45		-0.85	
TNFRSF11A	-7.23		-0.69	-2.09	-0.63
TNFRSF12A	-0.69			-1.31	
TNFRSF14					
TNFRSF18			-1.35		
TNFRSF1A			0.77		
TNFRSF1B	1.08				
TNFRSF4		2.27			
TNFRSF8	2.22	-1.64	2.29	2.12	
TNFRSF9		-0.88		-0.82	
TNFSF12	-1.63				
TNFSF13	-2.21		0.73		
TNFSF13B	2.20				
TNFSF14	-1.68		-0.77	-0.97	
TNFSF15		-1.05		-2.06	
TNFSF18	-3.85	5.30	4.46	-2.98	
TNFSF4					
TNFSF8	-3.12				
TNFSF9	1.84				
TNIP2	1.26				
TOLLIP	-0.66				
TP53	-0.89				
TPR					
TRAF2	0.64				
TRAF3					
TRAF6					
TRIM14					
TRIM2		-2.83		1.49	
TRIM21	1.30				
TRIM22	1.40	-1.28			
TRIM25	1.03	-0.66	0.61		
TRIM26	0.83				
TRIM3					
TRIM34					
TRIM35	-0.80				
TRIM38	1.11			0.70	
TRIM46	1.63				
TRIM5		-0.97	-0.61		
TRIM6		-2.19			
TRIM62	0.84				
TRIM68		-0.69			
TRIM8					
TXLNA					
TYK2					
UBA3					
UBA52	-0.79				
UBA7	-0.92				
UBB					
UBC	0.88				
UBE2E1	0.71				

Table 3.4. (continued)

UBE2L6	2.14				
UBE2M	-0.77			-0.90	
UBE2N	-0.62				
UBE2V1					
USP18	0.94		-0.73		0.94
VAMP2		-0.69			
VAV1		-0.97			
VCAM1			-1.34	-4.66	
VEGFA	5.51			1.81	
VIM				-0.72	
VRK3					
XAF1	2.88				0.73
YWHAZ					
ZEB1	-1.32			-1.78	

Chemokine receptors bind chemokines

gene	IFNγ+LPS log_2FC	IL-4 log_2FC	IL-10 log_2FC	oxPAPC log_2FC	CXCL4 log_2FC
ACKR3	5.72				
ACKR4	-3.39	-3.96	-3.16	-3.19	
CCL1	4.97				2.47
CCL13		9.35		1.84	
CCL19	12.24				
CCL5	5.72		-1.37	-1.47	0.69
CCR1					
CCR5	0.97	0.63			
CCR7	8.88	3.09		1.80	
CCRL2	0.59				
CX3CR1	0.63	0.64	4.13	1.81	1.60
CXCL1	5.11		2.11	2.05	
CXCL10	6.63				
CXCL11	5.56				1.66
CXCL12	-2.85	-5.75	0.80	1.50	
CXCL13	13.82		9.23		2.65
CXCL16	1.23	-0.93		1.37	
CXCL2	2.79	-1.79		2.74	
CXCL3	4.32	-1.28	0.83	2.90	
CXCL5	5.54	-5.23		4.04	2.71
CXCL8	7.02	1.57		3.59	2.13
CXCL9	11.14		1.47		
CXCR1	-4.86	2.33			
CXCR2					
CXCR3		-1.71			
CXCR4		-0.74		2.03	
PPBP	-2.99	-2.25		4.15	3.50

Table 3.5.: Atherosclerosis and lipid handling related IPA canonical pathways analyses hits. Filtering and data set used indicated, with only p < 0.05 hits shown.

Table 3.5.A

All cells and tissues, all conditions	
No.	Ingenuity Canonical Pathway
IFNγ+LPS	
1	Superpathway of Cholesterol Biosynthesis
2	Cholesterol Biosynthesis I
3	Cholesterol Biosynthesis II (via 24,25-dihydrolanosterol)
4	Cholesterol Biosynthesis III (via Desmosterol)
5	Fatty Acid β-oxidation I
6	PPAR Signaling
7	Stearate Biosynthesis I (Animals)
8	PPARα/RXRα Activation
IL-4	
1	Atherosclerosis Signaling
2	γ-linolenate Biosynthesis II (Animals)
3	LXR/RXR Activation
4	PPAR Signaling
5	Ceramide Signaling
6	Fatty Acid Activation
IL-10	
1	Atherosclerosis Signaling
2	Stearate Biosynthesis I (Animals)
3	LXR/RXR Activation
oxPAPC	
1	Atherosclerosis Signaling
2	Superpathway of Cholesterol Biosynthesis
CXCL4	
1	Atherosclerosis Signaling
2	LXR/RXR Activation
3	PPARα/RXRα Activation

Table 3.5.B

All cells and tissues, no CXCL4	
No.	Ingenuity Canonical Pathway
IFNγ+LPS	
1	Superpathway of Cholesterol Biosynthesis
2	Cholesterol Biosynthesis I
3	Cholesterol Biosynthesis II (via 24,25-dihydrolanosterol)
4	Cholesterol Biosynthesis III (via Desmosterol)
5	Fatty Acid β-oxidation I
6	PPARα/RXRα Activation
7	Stearate Biosynthesis I (Animals)
8	PPAR Signaling
9	Triacylglycerol Degradation
10	γ-linolenate Biosynthesis II (Animals)
11	Fatty Acid Activation
12	Atherosclerosis Signaling
13	LXR/RXR Activation
14	Ceramide Signaling
IL-4	
1	Atherosclerosis Signaling
2	LXR/RXR Activation
3	PPAR Signaling
4	γ-linolenate Biosynthesis II (Animals)
5	Fatty Acid Activation
6	Stearate Biosynthesis I (Animals)
IL-10	
1	Atherosclerosis Signaling
2	LXR/RXR Activation
oxPAPC	
1	Atherosclerosis Signaling
2	LXR/RXR Activation
3	Superpathway of Cholesterol Biosynthesis

Table 3.5.C

MDMs only, all conditions	
No.	Ingenuity Canonical Pathway
IFNγ+LPS	
1	Cholesterol Biosynthesis I
2	Cholesterol Biosynthesis II (via 24,25-dihydrolanosterol)
3	Cholesterol Biosynthesis III (via Desmosterol)
4	Superpathway of Cholesterol Biosynthesis
5	Triacylglycerol Degradation
IL-4	
1	Atherosclerosis Signaling
2	LXR/RXR Activation
IL-10	
1	Atherosclerosis Signaling
oxPAPC	
1	Atherosclerosis Signaling
2	LXR/RXR Activation
CXCL4	
1	LXR/RXR Activation
2	Atherosclerosis Signaling
3	PPAR Signaling
4	PPARα/RXRα Activation

Table 3.5.D

MDMs only, no CXCL4	
No.	Ingenuity Canonical Pathway
IFNγ+LPS	
1	Triacylglycerol Degradation
2	Cholesterol Biosynthesis I
3	Cholesterol Biosynthesis II (via 24,25-dihydrolanosterol)
4	Cholesterol Biosynthesis III (via Desmosterol)
5	Superpathway of Cholesterol Biosynthesis
6	Fatty Acid β-oxidation I
7	Atherosclerosis Signaling
8	PPARα/RXRα Activation
IL-4	
1	LXR/RXR Activation
2	Atherosclerosis Signaling
3	PPAR Signaling
IL-10	
1	Atherosclerosis Signaling
oxPAPC	
1	LXR/RXR Activation
2	Atherosclerosis Signaling

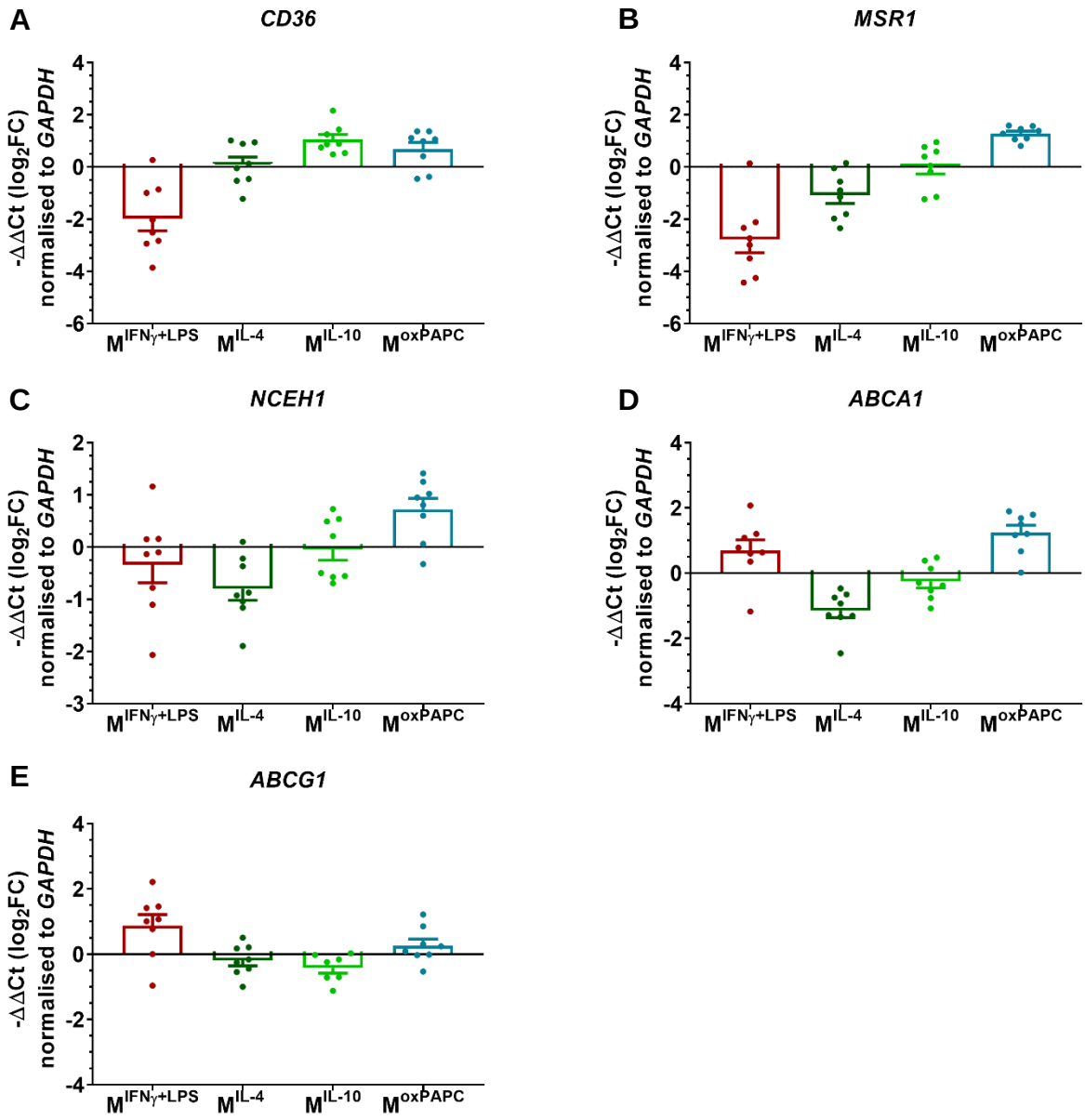

Figure 3.4.: qRT-PCR confirmation of RNA-seq.

Quantification of (**A**) *MSR1*, (**B**) *CD36*, (**C**) *NCEH1*, (**D**) *ABCA1* and (**E**) *ABCG1* gene expression in MDM phenotype samples parallel to the RNA-seq samples. The data were normalised to *GAPDH* and gene of interest M^{un} expression using the -ΔΔCt method and shown here as $\log_2$ fold changes ($\log_2$FCs), mean ± SEM, (**A** – **D**) n = 8, (**E**) n = 7 – 8. Detailed RNA–seq data for expression of these genes is shown in **Figures 3.6. – 3.8**.

3.4.4.3. Reduced foam cell formation capacity in $M^{IFN\gamma+LPS}$ and M^{oxPAPC}

Our transcriptome analyses of macrophage phenotypes revealed key differences in atherosclerosis and lipid handling genes. We therefore sought to assess foam cell formation capacity of the various polarised macrophages since this underlies the pathophysiology of atherosclerosis (Chistiakov et al., 2016). After loading with acLDL, we measured foam cell formation by oil-red-O staining (measured as % control – % acLDL–loaded Area ORO > Area haematoxylin cells) in $M^{IFN\gamma+LPS}$ and M^{oxPAPC}, while M^{IL-4} and M^{IL-10} showed an increase in foam cell formation, similar to that of unpolarised macrophages (**Figure 3.5.**).

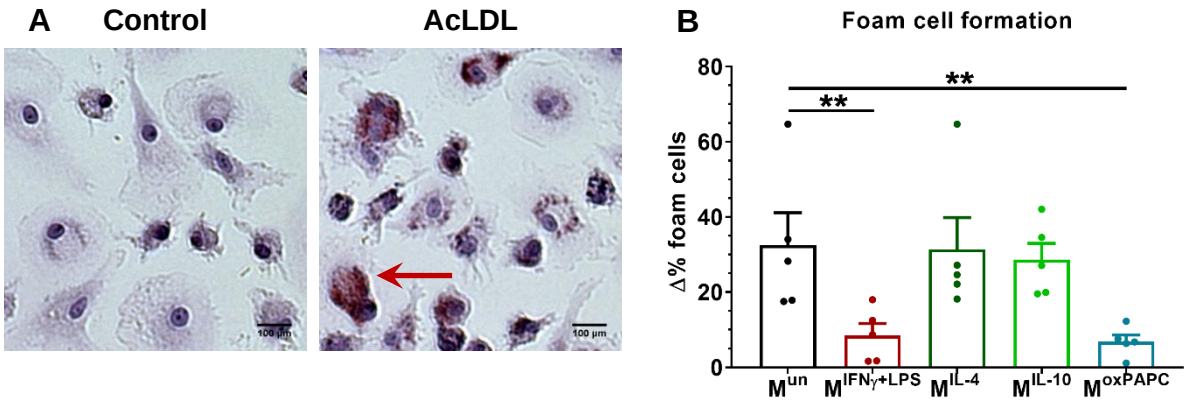

Figure 3.5.: Foam cell formation capacity by macrophage phenotypes.

(**A**) Representative Oil–Red–O staining of control and acLDL–loaded MDMs displaying presence of foam cells (% control – % acLDL–loaded Area $_{ORO}$ > Area $_{haematoxylin}$, red arrow), scale bars = 100 µm. (**B**) Quantification of foam cell formation capacity: Δ% foam cells = control % foam cells – acLDL % foam cells; mean ± SEM, n = 5, one–way ANOVA with Dunnett's post–hoc test, ** $p \leq 0.01$ compared to M^{un}.

3.4.4.4. Reduced LDL uptake in $M^{IFN\gamma+LPS}$

Since $M^{IFN\gamma+LPS}$ and M^{oxPAPC} showed reduced foam cell formation compared to other phenotypes, we assessed lipoprotein uptake, which impacts macrophage lipid handling and resultant foam cell formation (Sorci-Thomas and Thomas, 2016). We therefore measured fluorescently-labelled acLDL uptake in the different MDM phenotypes by flow cytometry. Analysis of MDMs exposed to AlexaFluor–488-conjugated acLDL showed significantly lower uptake in $M^{IFN\gamma+LPS}$. In contrast, M^{IL-4}, M^{IL-10} and M^{oxPAPC} showed intracellular acLDL fluorescence levels similar to unpolarised macrophages (**Figure 3.6.A**). In $M^{IFN\gamma+LPS}$, we detected an overall down–regulation of 'Ligand binding and uptake by scavenger receptors' pathways (**Figure 3.6.B**) and in key lipid uptake genes (**Figure 3.6.C**), such as modified LDL receptors *CD36* and *MSR1* (Kunjathoor et al., 2002, Nozaki et al., 1995). This suggests that differential polarisation influences transcriptional process that affect downstream pathways regulating LDL uptake. In association, a similar expression pattern was detected at the cell surface protein level for both CD36 and MSR1 scavenger receptors (**Figure 3.6.D**), apart from two differences. We detected slightly less *MSR1* mRNA in M^{IL-4} than in M^{un} (**Figure 3.6.B and C**), while the same comparison was not significant in MSR1 protein measurement (**Figure 3.6.D**). In addition, M^{oxPAPC} had significantly less cell–surface CD36 than M^{un}, however, the mRNA levels were not different between the two groups (**Figure 3.6.B and C**).

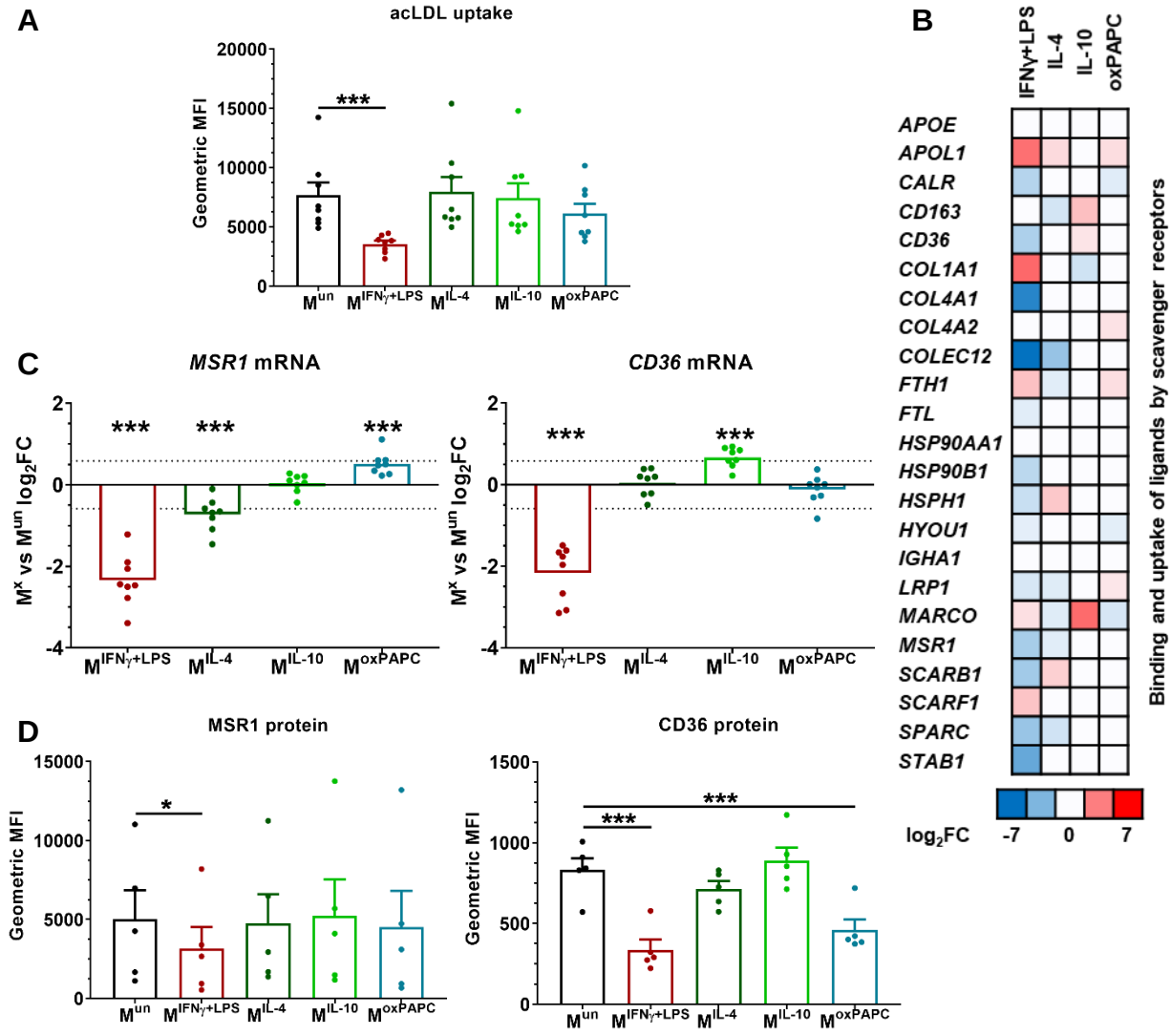

Figure 3.6.: LDL uptake by macrophage phenotypes.

(**A**) Flow cytometry quantification of AlexaFluor–488–acLDL internalisation by MDM phenotypes, n = 8. (**B**) Differentially expressed genes in the 'Binding and uptake of ligands by scavenger receptors' pathway (annotations retrieved from reactome.org on 16 October 2018) in M^{x} compared to M^{un} measured using RNA–seq; n = 8, thresholds for differential gene expression were $|\log_2 FC| > \log_2(1.5)$ and FDR < 0.05 (Benjamini and Hochberg method). RNA–seq. (**C**) *MSR1* and *CD36* gene expression among MDM phenotypes compared to M^{un}; n = 8, dotted lines = $|\log_2(1.5)|$, *** FDR ≤ 0.001. (**D**) Flow cytometry quantification of MSR1 and CD36 cell surface protein expression by MDM phenotypes, n = 5. (**A** and **D**) Mean ± SEM, one–way ANOVA with Dunnett's post-hoc test, * $p < 0.05$, *** $p \leq 0.001$, compared to M^{un}. MFI – geometric mean fluorescence intensity.

3.4.4.5. Cellular cholesterol content in macrophage phenotypes on LDL loading

In addition to lipid uptake, macrophage foam cell formation capacity is influenced by the ability of the cell to regulate its internal lipid content (Ghosh et al., 2010). In the case of lipoprotein, cellular lipases such as LIPA break down the lipoprotein particles that have been taken up, to cholesterol, triglycerides and fatty acids (Huang et al., 2014, Sheriff et al., 1995, Vargas-Alarcon et al., 2013). Cholesterol esters can be stored in lipid droplets, resulting in foam cell formation (Ghosh et al., 2010). NCEH1 can metabolise cholesterol esters into free cholesterol for removal by efflux (Igarashi et al., 2010, Zhao et al., 2007a, Zhao et al., 2007b), while SOAT1 can re-esterify free cholesterol into cholesterol esters for subsequent storage in lipid droplets (Brown et al., 1980, Ghosh, 2011, Yang et al., 2004).

Altering the balance of internal lipid processing and storage may result in changes in total, free and esterified cholesterol content in macrophages (Ghosh et al., 2010). While $M^{IFN\gamma}$ have been shown to contain different levels of free cholesterol and its ester (Panousis and Zuckerman, 2000b), the other phenotypes described in this study have not been assessed in this regard. We therefore measured the abundance of total, free and esterified cholesterol in control and acLDL–loaded cells to determine if intracellular cholesterol processing capacity affected differences in foam cell formation.

Unpolarised macrophages showed a large change in total cholesterol (73.5 ± 19.7 ng cholesterol / ng protein), but it was not significantly different compared to any other phenotype (**Figure 3.7.A**). On average $M^{IFN\gamma+LPS}$ exhibited the lowest change in total cholesterol following loading (**Figure 3.7.A**), but this was not significant when compared to M^{un}. We also calculated the cholesterol ester content, but did not observe statistically significant differences in cholesterol ester by phenotype, when compared to unpolarised macrophages (**Figure 3.7.B**). $M^{IFN\gamma+LPS}$ was the only phenotype to on average have decreased free cholesterol content upon lipid loading, however this was not significant when compared to M^{un} (**Figure 3.7.C**).

We examined the 'LDL clearance' pathway for DEGs according to MDM polarisation, to indicate transcriptional differences in the cholesterol clearance pathways. $M^{IFN\gamma+LPS}$ showed largely down–regulated expression of the entire clearance pathway (**Figure 3.7.D**). Among key genes, *SOAT1* was not differentially expressed in any phenotype, whereas, expression of *NCEH1* was significantly reduced in $M^{IFN\gamma+LPS}$ (**Figure 3.7.E**). In addition, *LIPA* showed decreased expression in $M^{IFN\gamma+LPS}$ and increased in M^{IL-4} (**Figure 3.7.E**).

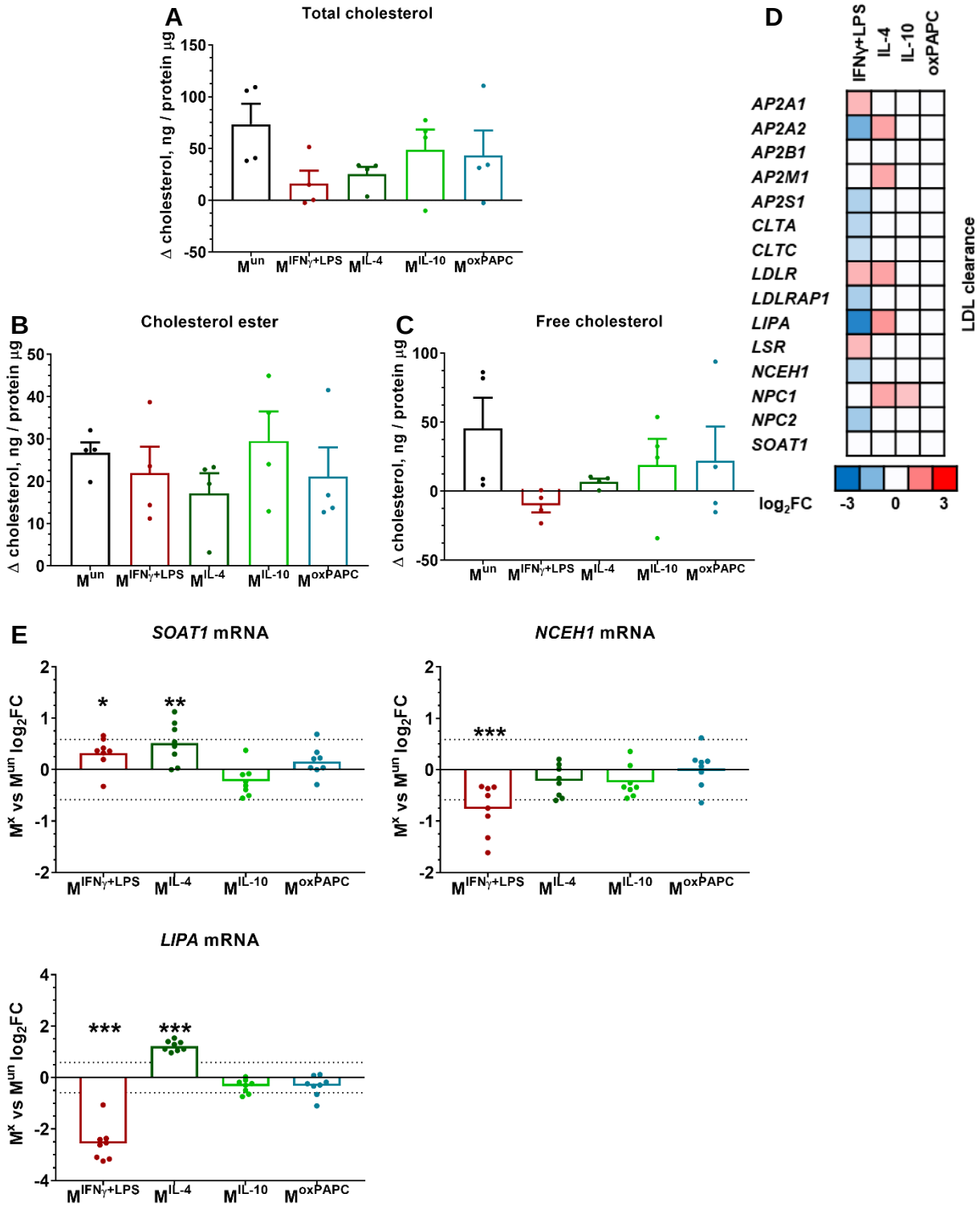

Figure 3.7.: Internal lipid content and lipoprotein processing in macrophage phenotypes.

(continued on the next page)

Figure 3.7.: Internal lipid content and lipoprotein processing in macrophage phenotypes (continued).

Colorimetric quantification of change in (**A**) total cholesterol, (**B**) cholesterol ester and (**C**) free cholesterol; mean ± SEM, n = 4, one–way ANOVA with Dunnett's post–hoc test, compared to M^{un}. (**D**) Differentially expressed genes in the 'LDL clearance' pathway (annotations retrieved from reactome.org on 16 October 2018) of M^{x} compared to M^{un} measured using RNA–seq; n = 8, thresholds for differential gene expression were $|\log_2 FC| > \log_2(1.5)$ and FDR < 0.05 (Benjamini and Hochberg method). (**E**) RNA–seq quantification of *SOAT1*, *NCEH1*, *LIPA* gene expression among MDM phenotypes compared to M^{un}, n = 8, dotted lines = $|\log_2(1.5)|$, * FDR < 0.05, ** FDR ≤ 0.01, *** FDR ≤ 0.001.

3.4.4.6. Reduced cholesterol efflux capacity in $M^{IFN\gamma+LPS}$

In addition to lipid uptake and intracellular processing, lipid and cholesterol content is also influenced by the cellular capacity for cholesterol efflux, pathways of which in macrophages function to remove excess lipid to prevent its accumulation, which can be cytotoxic (Tabas, 2002, Warner et al., 1995, Ghosh et al., 2014). Macrophages mainly unload intracellular lipid to Apo–AI via ABCA1 transporter and HDL is capable of accepting lipid from ABCG1, SCARB1 (Brewer, 2004). Previous reports indicated that pro-inflammatory macrophages had lower cholesterol efflux capacity (Panousis and Zuckerman, 2000a) than anti-inflammatory macrophages (Han et al., 2009). We tested cholesterol efflux via both acceptors to determine the reverse cholesterol transport capacity of each phenotype.

Total TopFluor cholesterol efflux involving both Apo–AI and HDL was significantly reduced in $M^{IFN\gamma+LPS}$ compared to unpolarised macrophages (**Figure 3.8.A**). $M^{IFN\gamma+LPS}$ also showed a significantly lower capacity to efflux cholesterol regardless of either HDL or Apo–AI was used as cholesterol acceptor (**Figure 3.8.B and C**). Surprisingly, upon polarisation expression of key active cholesterol efflux receptors *ABCA1* and *ABCG1* in 'HDL assembly' and 'HDL remodelling' pathways showed a largely opposite pattern (**Figure 3.8.D**) from the down–stream functional data (**Figure 3.8.A–C**). Expression of the major passive cholesterol efflux receptor *SCARB1* (functions via HDL) was significantly lower in $M^{IFN\gamma+LPS}$, but also uniquely increased in M^{IL-4} (**Figure 3.8.E**), suggesting that expression of *SCARB1* and the aforementioned ABC transporters are under different transcriptional regulation. Protein expression of ABCA1 and ABCG1 upon MDM polarisation (**Figure 3.8.F**) was similar to the cholesterol efflux capacities of each of the macrophage phenotypes (**Figure 3.8.A–C**), but noticeably different from their mRNA expression. *ABCA1* mRNA was up–regulated in $M^{IFN\gamma+LPS}$ and down–regulated in M^{IL-4}, while cell–surface protein was not differentially expressed for the former and increased for the latter when compared to M^{un}. Also, M^{IL-10} had more cell–surface ABCA1 than M^{un}, while this was not reflected in the mRNA levels. In addition, *ABCG1* mRNA was up–regulated in $M^{IFN\gamma+LPS}$ and not differentially regulated in M^{IL-4}, while cell–surface protein was not differentially expressed for the former and increased for the latter when compared to M^{un}. Also, M^{IL-10} had more cell–surface ABCG1 than M^{un}, while this was not reflected in the mRNA levels. SCARB1 cell–surface protein was not differentially expressed in $M^{IFN\gamma+LPS}$, while being significantly down–regulated at the transcript level. In contrast, SCARB1 cell–surface protein was uniquely up–regulated in M^{IL-4}, matching our observations at the transcript level and further suggesting differences between regulation of ABCA1/ABCG1 and SCARB1 expression.

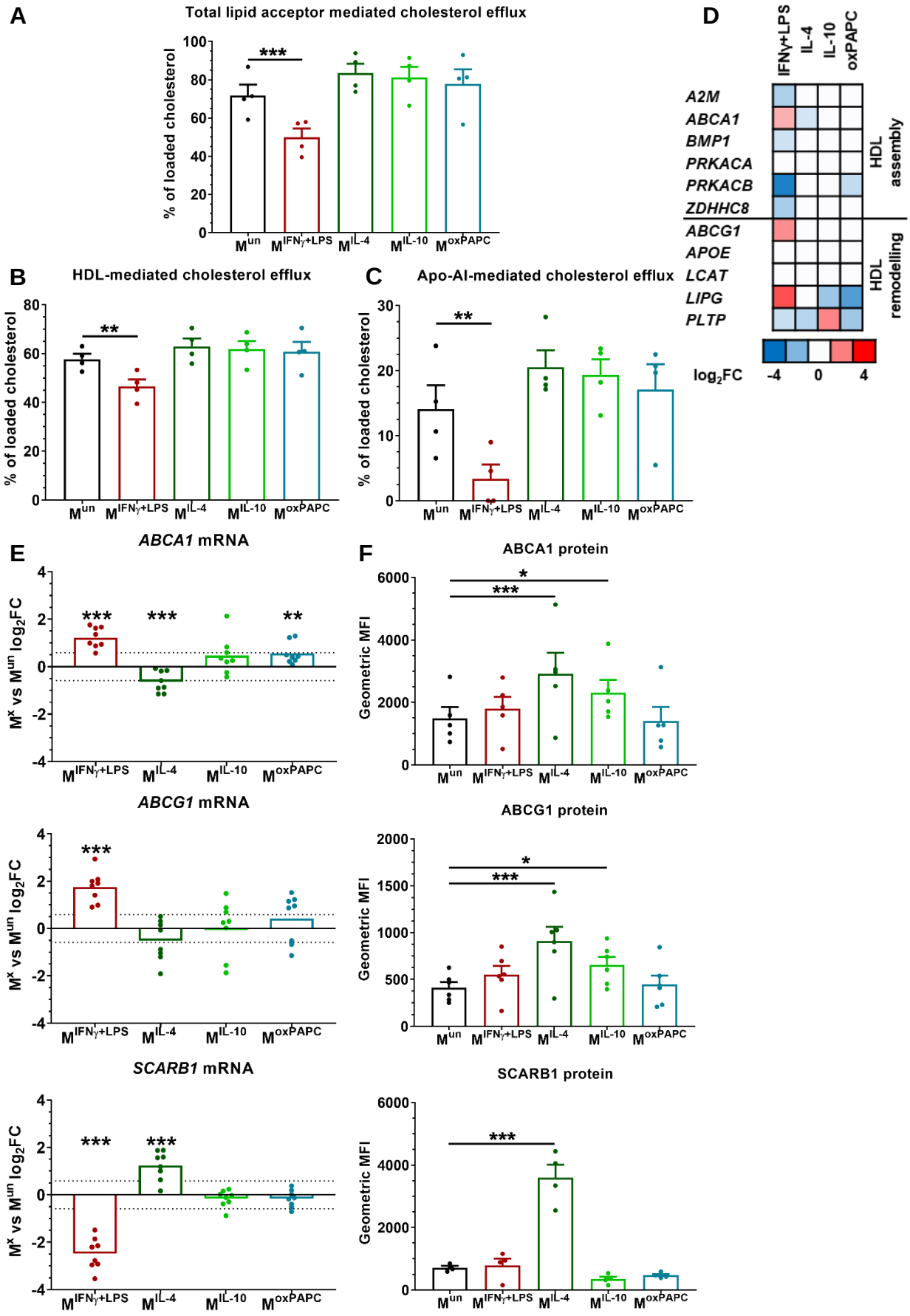

Figure 3.8.: Cholesterol efflux by MDM phenotypes.

(continued on the next page)

Figure 3.8.: Cholesterol efflux by MDM phenotypes (continued).

Fluorescence quantification of MDM cholesterol efflux for total cholesterol (**A**) via both lipid acceptors, HDL (**B**) and Apo–AI (**C**) separately; mean ± SEM, n = 4, one–way ANOVA with Dunnett's post–hoc test, ** $p \leq 0.01$, *** $p \leq 0.001$ compared to M^{un}. (**D**) Differentially expressed genes in the 'HDL assembly' and 'HDL remodelling' pathways (annotations retrieved from reactome.org on 16 October 2018) in M^{x} compared to M^{un} measured using RNA–seq; n = 8, thresholds for differential gene expression were $|\log_2 FC| > \log_2(1.5)$ and FDR < 0.05 (Benjamini and Hochberg method). (**E**) RNA–seq quantification of *ABCA1*, *ABCG1*, *SCARB1* gene expression among MDM phenotypes compared to M^{un}, n = 8, dotted lines = $|\log_2(1.5)|$, ** FDR ≤ 0.01, *** FDR ≤ 0.001. (**F**) Flow cytometry quantification of MDM phenotype for ABCA1 (n = 5), ABCG1 (n = 6) and SCARB1 (n = 4) cell surface protein expression; mean ± SEM, one–way ANOVA with Dunnett's post–hoc test, * $p < 0.05$, *** $p \leq 0.001$, compared to M^{un}.

3.4.5. Discussion

Macrophage polarisation *in vitro* using stimuli found in their tissue environment produces a spectrum of distinct phenotypes (Chinetti-Gbaguidi et al., 2015). In this study we systematically examined the transcriptomes and selected protein expression of multiple human macrophage phenotypes as well as their down–stream ability to form atherogenic foam cells, influenced by different steps in cellular lipid handling.

IFNγ is a multi-functional pro-inflammatory cytokine of the immune system, while LPS is a bacterial product capable of inducing NF–κB and IRF–mediated pro-inflammatory gene expression (Diamond et al., 2015, Majoros et al., 2017, Michalska et al., 2018). On the other hand, IL–4 is an anti-inflammatory cytokine associated with macrophage–mediated wound healing and tissue repair (Dinarello, 2007, Wynn and Vannella, 2016). Consistently with these properties we and others (Martinez et al., 2006, Xue et al., 2014) identified a clear difference in the changes to the unpolarised macrophage transcriptome between *in vitro* polarisation with IFNγ+LPS and IL–4. Notably, in previously published PCA and coregulation analyses M^{IL-4} were more similar to unpolarised macrophages than $M^{IFN\gamma+LPS}$ (Martinez et al., 2006, Xue et al., 2014). Furthermore, Xue et al. in their analysis also showed M^{IL-10} even closer to unpolarised cells than M^{IL-4} (Xue et al., 2014). Previous work on mouse macrophages reported a transcriptionally distinct oxPAPC–activated macrophage phenotype from IFNγ+LPS or IL–4 activated macrophages (Kadl et al., 2010) that we also observed in human MDMs, including consistently specific up–regulation of *HMOX1* and *TXNRD1* expression. As previously observed in monocyte differentiation to macrophages (Gleissner et al., 2010), our naïve MDM stimulation with CXCL4 produced few transcriptional changes relative to other stimulations. Given that less than half of our naïve MDMs expressed the receptor for CXCL4 (CXCR3) (Mueller et al., 2008) on the cell surface, cell sorting approaches could be used to obtain a cell–surface $CXCR3^+$ naïve MDM population for polarisation with CXCL4. This could be followed by gene and protein expression measurements as well as down–stream foam cell formation and lipid handling assays go obtain a clearer description of how CXCL4 affects these processes in macrophages.

Recent advances in single–cell omics techniques have underlined the likely complexity of stimuli macrophages are exposed to *in vivo*. Single–cell RNA–seq data on mouse model atherosclerosis suggest that *in vitro*–like M^{IL-4} may not be present *in vivo*, while distinct signatures of various pro-inflammatory macrophages, such as IFN and NF–κB signalling cells were found (Cochain et al., 2018, Kim et al., 2018). Furthermore, in their CITE–seq experiment on one human plaque Fernandez et al. identified two macrophage populations both expressing pro-inflammatory markers, but distinct in the anti-inflammatory marker MRC1 expression (Fernandez et al., 2019).

Such *in vivo* populations may be the result of simultaneous and/or step–wise stimulations with pro-inflammatory as well as anti-inflammatory molecules, such as IL–4, and may prompt to reconsider and change the currently used *in vitro* models to better reflect the plaque environment. However, such changes would still greatly benefit from increasing our understanding of how macrophages are affected by being exposed to one stimulation at a time, which can be achieved using current *in vitro* culture models.

One such consideration is the ability of macrophages to form atherogenic foam cells. Human plaque macrophages with a foamy appearance have been positively stained for a mixture of some commonly used pro-inflammatory and anti-inflammatory protein markers (Stoger et al., 2012), but not for pro-inflammatory *IL1B* mRNA (Kim et al., 2018), further suggesting presence of more complex stimulatory conditions in the plaque than modelled *in vitro*. In agreement with observations on $M^{IFN\gamma}$ (Geng and Hansson, 1992), we observed that *in vitro* pro-inflammatory polarisation with IFNγ+LPS resulted in lower foam cell formation capacity than in unpolarised cells. This was likely the result of significantly lower acLDL uptake and cholesterol efflux of $M^{IFN\gamma+LPS}$. The only other *in vitro* phenotype with lower foam cell formation capacity was M^{oxPAPC}. Similarly to mouse macrophage experiments performed by Kadl et al. we observed human M^{oxPAPC} low (relative to, but also shared with $M^{IFN\gamma+LPS}$) up–regulation of selected pro-inflammatory gene expression (**Table 3.4.**). However, while mouse oxPAPC macrophages had decreased phagocytic capacity (Kadl et al., 2010), our human M^{oxPAPC} similarly to M^{IL-4} and M^{IL-10} did not significantly differ from M^{un} in acLDL uptake or any other lipid handling assays as opposed to $M^{IFN\gamma+LPS}$. However, these similarities in our measurements of lipid handling capacity did not help to explain why M^{oxPAPC} were able to have a lower foam cell formation capacity than M^{IL-4} and M^{IL-10}.

In most of our data transcriptional and protein expression changes upon polarisation were in agreement with each other and supported observations in down–stream lipid handling. However, mRNA and cell–surface protein expression for M^{IL-4} MSR1 and M^{oxPAPC} CD36 did not display similar patterns. While these differences were small, relative to much larger impact of IFNγ+LPS stimulation on macrophage mRNA and protein expression, they may still indicate differences in mRNA and protein regulation or other factors that were not considered in this study.

We also observed numerous differences in macrophage phenotype ABC transporter gene and protein expression. In our experiments *ABCA1* and *ABCG1* mRNA up–regulation in $M^{IFN\gamma+LPS}$ compared to M^{un} was significant, while both experimental groups had similar levels of cell–surface protein. Interestingly, expression of these ABC transporters' mRNA in M^{IL-4} and M^{IL-10} was similar to M^{un} (except for significantly down–regulated *ABCA1* mRNA in M^{IL-4}), while corresponding cell–surface proteins were up–regulated. These differences may have been the

result of differential regulation of mRNA (a similar RNA expression pattern was observed in a previous study (Xue et al., 2014) although with varying statistical significance and magnitude of change between the two studies) and protein levels, including mechanisms, such as post-translational modifications of proteins. Significant *SCARB1* mRNA down–regulation in $M^{IFN\gamma+LPS}$ compared to M^{un} was not matched by cell–surface protein (similar in $M^{IFN\gamma+LPS}$ to M^{un}), possibly due to regulatory pathways we did not consider in this study. ABC transporters' and SCARB1 levels in M^{IL-4} may at least partially account for the efflux capacity of this phenotype. However, other proteins and mechanisms not assessed here may be involved in macrophage cholesterol efflux, because the cholesterol efflux capacities of other phenotypes, especially M^{oxPAPC}, could not be entirely explained by their ABCA1, ABCG1 and SCARB1 levels. It is also important to note that we only measured the cell–surface expression, but not the activity of each protein, which could be different and affect our results.

Our observations into the effects of selected stimuli on macrophage foam cell formation and lipid handling are largely in support of previous work in the field, while also expanding upon descriptions of less well described human macrophage phenotypes. Research on oxPAPC macrophages in particular may yield interesting outcomes in the future due to the comparatively low foam cell formation and inflammatory capacity of these cells coupled with their efficient lipid handling. In addition, the transcriptome and protein measurements we performed in here could be used beyond this study and cardiovascular disease research.

3.4.6. Funding, acknowledgements, author contributions and conflict of interest

Funding

This work was supported by the Biomedical Research Council (BMRC), Agency for Science, Technology and Research (A*STAR) Research Attachment Programme to HLW, EKT and SCW to support ÉH and KB. BL and JL are part of the SIgN Immunomonitoring platform (supported by a BMRC IAF 311006 grant and BMRC transition funds #H16/99/b0/011).

Acknowledgements

We thank Sarah Lai for data analysis support.

Author contributions:

Conception and design: HLW, SCW, EKT. Performed experiments: KB, ÉH, JL, FS. Experimental analysis: KB, ÉH, BL, IS. Interpretation: KB, ÉH, HLW, EKT, SCW. Wrote manuscript: HLW, KB, ÉH (methods), BL (methods), JL (methods). Edited manuscript: ÉH, BL, JL, EKT, SCW.

Conflict of interest

No conflicts of interest.

3.4.7. References

References for this manuscript are included in the **References** (**Chapter 8**) for the entire thesis.

4. Effect of macrophage phenotype on glucose metabolism and cytokine production

4.1. Introduction

Macrophage phenotypes have greatly varying functions, which require different levels of cellular energy, nutrients and processes (**Figure 4.1.**) to generate it (Verdeguer and Aouadi, 2017). Glucose is used in glycolysis to generate ATP and pyruvate, which can be converted to lactic acid and protons (removed from the cell, causing acidification of the microenvironment) to generate ATP in aerobic glycolysis for rapid energy production or converted to acetyl–coenzyme A (CoA) and gradually broken down in the TCA cycle to feed the ETC (uses oxygen as the terminal electron acceptor, resulting in increased OCR for a slower, but more efficient ATP production (Verdeguer and Aouadi, 2017, Diskin and Palsson-McDermott, 2018, Viola et al., 2019). Fatty acids are oxidised in peroxisomes (longer and branched acids) and in the mitochondria to generate acetyl–CoA for the TCA cycle (Geric et al., 2018, Kunau et al., 1995, Wanders et al., 2010, Lim et al., 2018), while glutamine is converted into glutamate and then into α–ketoglutarate, which is one of the metabolites in the Krebs cycle (Viola et al., 2019).

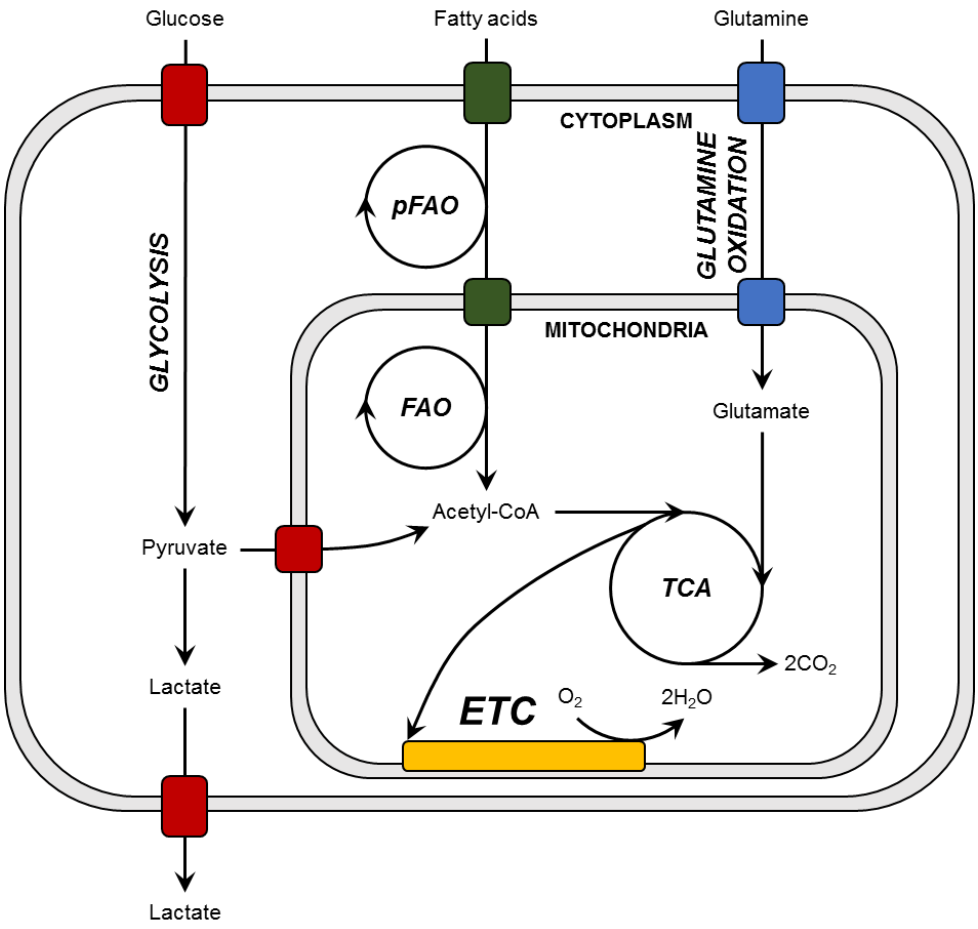

Figure 4.1.: Major cellular energy production pathways

Glucose, fatty acids and glutamine are the primary metabolites for energy production in macrophages. During glycolysis glucose is broken down to pyruvate, which can be converted to acetyl–CoA for use in the TCA (can produce reducing agents for the ETC) or be converted to lactate for rapid ATP production. Very long and branched fatty acids are first processed in peroxisomes and then with the rest of the fatty acids channelled to the mitochondria to complete their oxidation to yield acetyl–CoA for the TCA. Through a series of reactions glutamine is converted into glutamate and further into α-ketoglutarate that can be used in the TCA cycle. ATP and similar molecules can be generated in specific reactions more rapidly outside of the ETC, but this pathway is the most efficient in generating ATP. ETC – electron transport chain, FAO – fatty acid oxidation, pFAO – peroxisomal fatty acid oxidation, TCA – tricarboxylic acid (Kreb's) cycle. Based on and adapted from (Viola et al., 2019, Diskin and Palsson-McDermott, 2018, Kunau et al., 1995).

Among primary metabolite catabolic pathways glycolysis in considered to be important in macrophage function and more rapid than mitochondrial oxidative phosphorylation pathways (Diskin and Palsson-McDermott, 2018). Mouse pro-inflammatory macrophages are known to heavily rely on glycolysis for ATP production instead of the mitochondria, which under some experimental conditions are irreversibly dedicated to reactive oxygen species production promoting inflammation and pathogen killing (Van den Bossche et al., 2016). Meanwhile, mouse IL–4 macrophages were shown to be less glycolytically active and more reliant on the mitochondrial TCA cycle for their energy production, in agreement with their roles in tissue repair (Van den Bossche et al., 2016). Mouse M^{oxPAPC} (depending on the dose of oxidised phospholipid) were observed to behave similarly to M^{IL-4} (Serbulea et al., 2018a), while IL–10 has been reported to dampen LPS–induced mouse macrophage glycolysis and its gene expression (Ip et al., 2017, Minton, 2017) and M^{CXCL4} metabolism is less understood.

Cytokine induced signalling in and their secretion by macrophages also affect the progression of the plaque (Moss and Ramji, 2016, Ramji and Davies, 2015, Chinetti-Gbaguidi et al., 2015). Activation of granulocyte–macrophage colony stimulating factor (GM–CSF) differentiated MDMs separately with IFNγ or LPS alone do not induce secretion of the inflammatory IL–1β, however, the when used together, these stimuli greatly up–regulate IL–β secretion (Tarique et al., 2015). Also, addition of ATP to activate the inflammasome aids induction of IL–1β secretion when M–CSF differentiated MDMs are activated with LPS (Ward et al., 2010). Both IFNγ and LPS are potent inducers of pro-inflammatory IL–12 secretion (Dobashi et al., 2001, Ma et al., 2000), IFNγ stimulation up–regulates its own secretion from MDMs and LPS with and without IFNγ has been shown to induce C–C chemokine ligand (CCL) 5, CXCL10, IL–8 and TNFα secretion (Tarique et al., 2015). Also, LPS is a known IL–6 secretion stimulus (Sarvari et al., 2015). Anti-inflammatory IL–10 secretion is usually not associated with pro-inflammatory macrophages, however, LPS has been shown to induce IL–10 release from GM–CSF–differentiated MDMs (Tarique et al., 2015), highlighting the need for more analysis.

It has been reported that unlike $M^{IFN\gamma+LPS}$, M^{IL-4} secrete no/little pro-inflammatory cytokines (Tarique et al., 2015). M^{IL-4} are also perceived to secrete high levels of anti-inflammatory IL–10, although such behaviour was not observed in GM–CSF–generated MDMs polarised with IL–4 (Tarique et al., 2015). This disagreement could be explained by varying protocols for monocyte differentiation into MDMs (GM–CSF versus M–CSF) and MDM polarisation into phenotypes, however, the effects of these differences on the final polarised macrophage phenotype are still debatable and in need of clarification. CCL17 and 18 were also shown to be secreted by M^{IL-4} (Tarique et al., 2015).

Interestingly, it has recently been shown that following an initial activation with LPS, treatment with IL–10 re-sensitises macrophages to a second stimulation with LPS as evidenced by variably rescued/heightened expression of *IL1B, IL6, CXCL8, CXCL1* and *2* genes (Gharib et al., 2019). Currently, little is known about the secretion of cytokines from M^{oxPAPC}.

The M^{CXCL4} secretome shows elements of pro- and anti-inflammatory macrophage phenotype secretomes (Gleissner et al., 2010). Analyses of M^{un} and M^{CXCL4} culture media indicated that the former secreted higher levels of IL–6, TNFα and CCL18, however, M^{un} secreted more IL–10 and the levels of secreted IL–1β, –8 and –12p70 were similar between the two populations of macrophages (Gleissner et al., 2010).

As evident from the published literature summarised in this thesis, the activity of energy production pathways, including glycolysis, and cytokine secretion can differ widely among different macrophage phenotypes. However, little is known about glucose utilisation in some phenotypes and unfortunately different protocols used to stimulate the cells can make it difficult to compare findings on cytokine secretion from different reports. Therefore, here human M–CSF differentiated macrophages were systematically polarised and assessed for glycolytic capacity and selected cytokine secretion.

4.2. Hypotheses and aims

The following hypotheses and aims refer to the original research being submitted as part of the completion of this degree. Work that has been performed by others is acknowledged as such in the **Contributions** (**Section 4.3.**) for this chapter.

Hypothesis 1: Human macrophage phenotypes differ in their glycolytic capacity.

Hypothesis 2: Human macrophage phenotypes differ in their IL–1β and IL–8 secretion upon polarisation and receiving a subsequent secondary single or combined stimulation of LPS and acLDL.

Aim 1: Measure the glycolytic flux of macrophage phenotypes.

Aim 2: Relate the glycolytic flux results to glycolysis and other energy production pathways.

Aim 3: Measure the concentration of IL–1β and IL–8 in macrophage phenotype media after polarisation and subsequent secondary stimulation.

4.3. Contributions

My own contributions to the data in this chapter are:

Seahorse experiments, IL–1β and IL–8 ELISAs, data analysis and interpretation.

The following people have also contributed to the data presented in this chapter:

Susan Clarke: cytokine bead array and analysis;

Kay Hopkinson: cytokine bead array and analysis.

4.4. Results

4.4.1. Human macrophage phenotypes differ in their glycolytic capacity

In the absence of glucose at basal measurements all phenotypes had similarly low ECAR values (after normalisation, compared to M^{un}), but basal OCR measurements of all phenotypes except for M^{oxPAPC} were significantly higher than M^{un} (**Figure 4.2.,** outcomes of statistical tests are provided in **Tables 4.1.** and **4.3.**). Upon addition of glucose all phenotypes showed a varied increase in ECAR accompanied by a small decrease in OCR in most phenotypes (**Figure 4.2.A and B, Tables 4.2.** and **4.4.**), indicating an increase in glycolysis and a decrease in the Krebs cycle utilisation. Only in $M^{IFN\gamma+LPS}$ and M^{CXCL4} glycolytic activity (expressed as the difference in ECAR between the first measurement after and the last measurement before the addition of glucose) was significantly larger (higher in the former) compared to that of M^{un} (**Figure 4.2.C**). Inhibition of the ETC by oligomycin lead to a large decrease in OCR, but led to only a moderate transient increase in M^{IL-4} ECAR (**Figure 4.2.A and B**), suggesting that the cells were already functioning at their highest glycolytic capacity. Addition of 2–DG successfully inhibited hexokinase activity as indicated by a steep drop in ECAR values for all phenotypes (**Figure 4.2.A)**, which also confirmed that the observed changes in ECAR and OCR occurred due to glycolysis. Differential expression of glycolysis genes in the RNA–seq experiment (**Chapter 3**) supported the functional findings, except for M^{CXCL4} (**Figure 4.2.D**). Also, $M^{IFN\gamma+LPS}$ largely overall down–regulated as well as key gene (*ALDO*, *HK*, *PFKFB*) expression in the other main energy generation pathways (**Figures 4.3.** and **4.4.**). Interestingly, lipase E, hormone sensitive type (*LIPE*, annotated among important genes/enzymes in triglyceride breakdown) expression was not detected in the RNA–seq (**Figure 4.3.**). However, patatin like phospholipase domain containing 4 (*PNPLA4*), monoglyceride lipase (*MGLL*) and other cellular lipases (*LIPA* and *LIPG*) may aid triglyceride digestion. Conversion of pyruvate into lactate or into acetyl–CoA (carried out by lactate dehydrogenase [*LDH*] or pyruvate dehydrogenase complex component X [*PDHX*], respectively) similarly to glycolysis showed opposing (up–/down–regulated) expression of key enzymes (**Figure 4.4.**), especially in $M^{IFN\gamma+LPS}$, however, the overall gene expression patterns were not as clear as in other pathways.

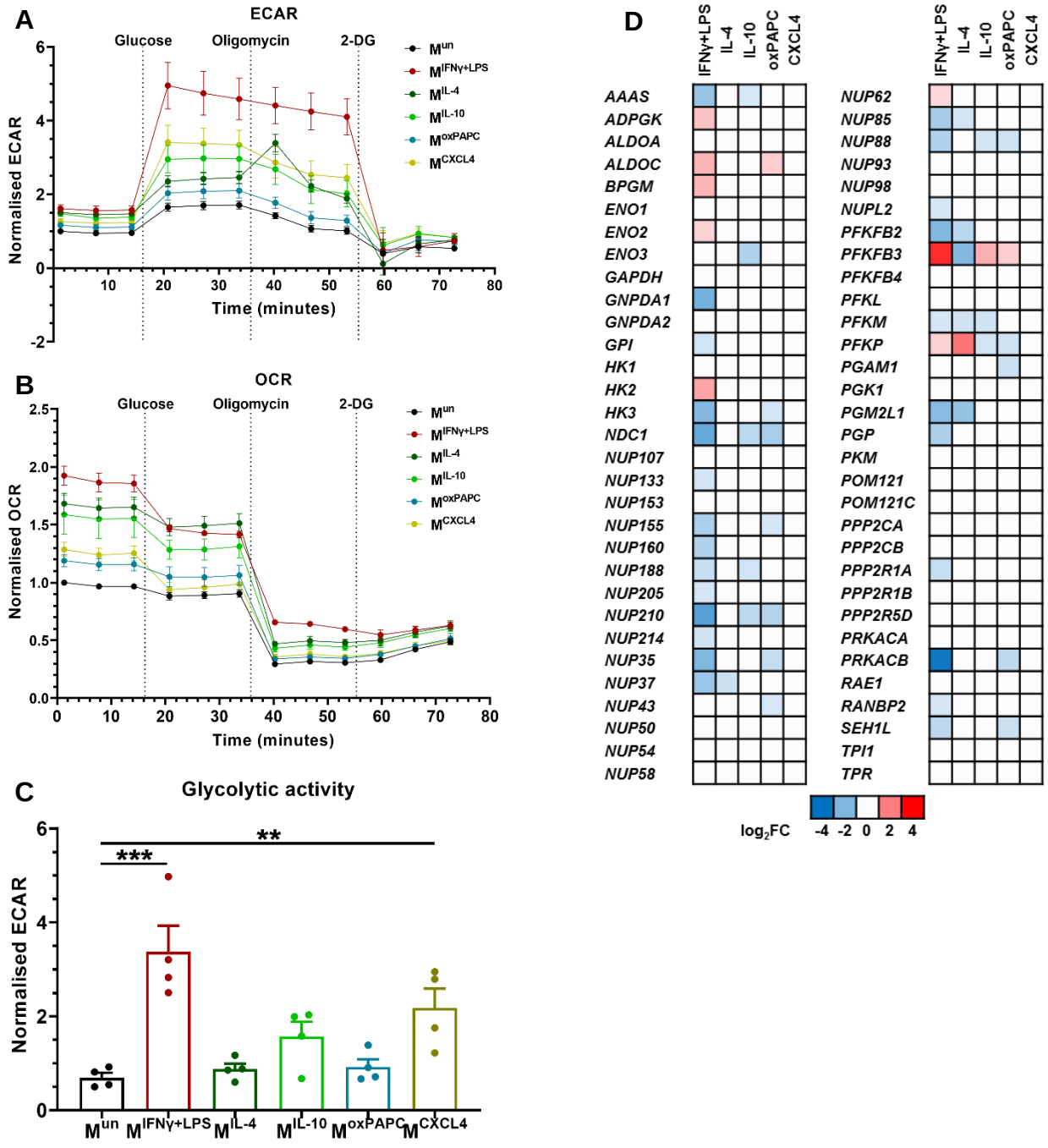

Figure 4.2.: MDM phenotype glycolysis.

Normalised (**A**) ECAR and (**B**) OCR measurements; means ± SEMs, n = 4, outcomes of statistical tests included in **Tables 4.1 – 4.4.** (**C**) Quantification of phenotype glycolytic activity (fourth – third ECAR measurement); means ± SEMs, n = 4, one–way ANOVA with Dunnett's post-hoc test, ** $p \leq 0.01$, ** $p \leq 0.001$ compared to M^{un}. (**D**) Differentially expressed genes in the 'Glycolysis' pathway (annotations retrieved from reactome.org on 16 October 2018) in M^{x} compared to M^{un} measured using RNA–seq; n = 8, thresholds for differential gene expression were $|\log_2 FC| > \log_2(1.5)$ and FDR < 0.05 (Benjamini and Hochberg method). ECAR – extracellular acidification rate, OCR – oxygen consumption rate, 2-DG – 2-deoxyglucose and others added as indicated.

Table 4.1.: Outcomes of Dunnett's for matched/repeated measured two–way ANOVA for normalised ECAR data in Figure 4.2.A (M^{x} vs M^{un} at each measurement, n = 4).

Dunnett's multiple comparisons test	Mean Diff.	95.00% CI of diff.	Significant?	Summary	Adjusted P Value
1.301441 min					
M^{un} vs. $M^{IFN\gamma+LPS}$	-0.612	-1.590 to 0.3658	No	ns	0.37
M^{un} vs. M^{IL-4}	-0.5046	-1.482 to 0.4732	No	ns	0.56
M^{un} vs. M^{IL-10}	-0.4792	-1.457 to 0.4985	No	ns	0.6
M^{un} vs. M^{oxPAPC}	-0.1644	-1.142 to 0.8133	No	ns	>0.99
M^{un} vs. M^{CXCL4}	-0.2549	-1.233 to 0.7228	No	ns	0.95
7.738176 min					
M^{un} vs. $M^{IFN\gamma+LPS}$	-0.615	-1.593 to 0.3627	No	ns	0.37
M^{un} vs. M^{IL-4}	-0.5024	-1.480 to 0.4754	No	ns	0.56
M^{un} vs. M^{IL-10}	-0.4056	-1.383 to 0.5721	No	ns	0.74
M^{un} vs. M^{oxPAPC}	-0.1565	-1.134 to 0.8213	No	ns	>0.99
M^{un} vs. M^{CXCL4}	-0.2766	-1.254 to 0.7011	No	ns	0.93
14.206546 min					
M^{un} vs. $M^{IFN\gamma+LPS}$	-0.6179	-1.596 to 0.3599	No	ns	0.36
M^{un} vs. M^{IL-4}	-0.5162	-1.494 to 0.4615	No	ns	0.53
M^{un} vs. M^{IL-10}	-0.4239	-1.402 to 0.5539	No	ns	0.71
M^{un} vs. M^{oxPAPC}	-0.1579	-1.136 to 0.8199	No	ns	>0.99
M^{un} vs. M^{CXCL4}	-0.2762	-1.254 to 0.7016	No	ns	0.93
20.765388 min	First measurement after addition of glucose				
M^{un} vs. $M^{IFN\gamma+LPS}$	-3.301	-4.278 to -2.323	Yes	***	<0.001
M^{un} vs. M^{IL-4}	-0.6972	-1.675 to 0.2805	No	ns	0.25
M^{un} vs. M^{IL-10}	-1.299	-2.277 to -0.3215	Yes	**	0.004
M^{un} vs. M^{oxPAPC}	-0.3819	-1.360 to 0.5958	No	ns	0.78
M^{un} vs. M^{CXCL4}	-1.76	-2.737 to -0.7818	Yes	***	<0.001
27.212623 min					
M^{un} vs. $M^{IFN\gamma+LPS}$	-3.045	-4.023 to -2.067	Yes	***	<0.001
M^{un} vs. M^{IL-4}	-0.7256	-1.703 to 0.2521	No	ns	0.22
M^{un} vs. M^{IL-10}	-1.282	-2.260 to -0.3042	Yes	**	0.005
M^{un} vs. M^{oxPAPC}	-0.3904	-1.368 to 0.5873	No	ns	0.77
M^{un} vs. M^{CXCL4}	-1.683	-2.660 to -0.7049	Yes	***	<0.001
33.676159 min					
M^{un} vs. $M^{IFN\gamma+LPS}$	-2.875	-3.853 to -1.897	Yes	***	<0.001
M^{un} vs. M^{IL-4}	-0.749	-1.727 to 0.2288	No	ns	0.19
M^{un} vs. M^{IL-10}	-1.252	-2.230 to -0.2743	Yes	**	0.006
M^{un} vs. M^{oxPAPC}	-0.3905	-1.368 to 0.5872	No	ns	0.77
M^{un} vs. M^{CXCL4}	-1.632	-2.610 to -0.6542	Yes	***	<0.001
40.245935 min	First measurement after addition of oligomycin				
M^{un} vs. $M^{IFN\gamma+LPS}$	-2.987	-3.964 to -2.009	Yes	***	<0.001
M^{un} vs. M^{IL-4}	-1.967	-2.944 to -0.9888	Yes	***	<0.001
M^{un} vs. M^{IL-10}	-1.257	-2.235 to -0.2791	Yes	**	0.006
M^{un} vs. M^{oxPAPC}	-0.3456	-1.323 to 0.6321	No	ns	0.84
M^{un} vs. M^{CXCL4}	-1.441	-2.419 to -0.4632	Yes	**	0.001

Table 4.1. (continued)

Dunnett's multiple comparisons test	Mean Diff.	95.00% CI of diff.	Significant?	Summary	Adjusted P Value
46.728973 min					
M^{un} vs. $M^{IFN\gamma+LPS}$	-3.179	-4.157 to -2.202	Yes	***	<0.001
M^{un} vs. M^{IL-4}	-1.158	-2.136 to -0.1800	Yes	*	0.01
M^{un} vs. M^{IL-10}	-1.062	-2.040 to -0.08436	Yes	*	0.03
M^{un} vs. M^{oxPAPC}	-0.2968	-1.275 to 0.6809	No	ns	0.91
M^{un} vs. M^{CXCL4}	-1.464	-2.442 to -0.4863	Yes	***	<0.001
53.206527 min					
M^{un} vs. $M^{IFN\gamma+LPS}$	-3.093	-4.071 to -2.115	Yes	***	<0.001
M^{un} vs. M^{IL-4}	-0.8773	-1.855 to 0.1005	No	ns	0.09
M^{un} vs. M^{IL-10}	-1.005	-1.983 to -0.02733	Yes	*	0.04
M^{un} vs. M^{oxPAPC}	-0.2785	-1.256 to 0.6992	No	ns	0.92
M^{un} vs. M^{CXCL4}	-1.441	-2.419 to -0.4632	Yes	**	0.001
59.748901 min	First measurement after addition of 2-deoxyglucose				
M^{un} vs. $M^{IFN\gamma+LPS}$	-0.08291	-1.061 to 0.8948	No	ns	>0.99
M^{un} vs. M^{IL-4}	0.2792	-0.6986 to 1.257	No	ns	0.92
M^{un} vs. M^{IL-10}	-0.2227	-1.200 to 0.7550	No	ns	0.97
M^{un} vs. M^{oxPAPC}	-0.01097	-0.9887 to 0.9668	No	ns	>0.99
M^{un} vs. M^{CXCL4}	-0.2754	-1.253 to 0.7023	No	ns	0.93
66.20332 min					
M^{un} vs. $M^{IFN\gamma+LPS}$	-0.005875	-0.9836 to 0.9719	No	ns	>0.99
M^{un} vs. M^{IL-4}	-0.08218	-1.060 to 0.8956	No	ns	>0.99
M^{un} vs. M^{IL-10}	-0.3481	-1.326 to 0.6296	No	ns	0.84
M^{un} vs. M^{oxPAPC}	-0.1939	-1.172 to 0.7838	No	ns	0.98
M^{un} vs. M^{CXCL4}	-0.3687	-1.346 to 0.6091	No	ns	0.8
72.66714 min					
M^{un} vs. $M^{IFN\gamma+LPS}$	-0.2059	-1.184 to 0.7719	No	ns	0.98
M^{un} vs. M^{IL-4}	-0.2326	-1.210 to 0.7452	No	ns	0.96
M^{un} vs. M^{IL-10}	-0.2965	-1.274 to 0.6813	No	ns	0.91
M^{un} vs. M^{oxPAPC}	-0.1842	-1.162 to 0.7935	No	ns	0.99
M^{un} vs. M^{CXCL4}	-0.2944	-1.272 to 0.6834	No	ns	0.91

Table 4.2.: Outcomes of Dunnett's for matched/repeated measured two–way ANOVA for normalised ECAR data in Figure 4.2.A (first vs other measurements in minutes, n = 4).

First measurements after addition of: glucose – 20.765388, oligomycin – 40.245935, 2-deoxyglucose – 59.748901.

Dunnett's multiple comparisons test	Mean Diff.	95.00% CI of diff.	Significant?	Summary	Adjusted P Value
M^{un}					
1.301441 vs. 7.738176	0.05405	-0.6288 to 0.7369	No	ns	>0.99
1.301441 vs. 14.206546	0.04369	-0.6392 to 0.7266	No	ns	>0.99
1.301441 vs. 20.765388	-0.6517	-1.335 to 0.03121	No	ns	0.07
1.301441 vs. 27.212623	-0.6957	-1.379 to -0.01283	Yes	*	0.04
1.301441 vs. 33.676159	-0.7106	-1.393 to -0.02772	Yes	*	0.04
1.301441 vs. 40.245935	-0.4242	-1.107 to 0.2587	No	ns	0.46
1.301441 vs. 46.728973	-0.06827	-0.7511 to 0.6146	No	ns	>0.99
1.301441 vs. 53.206527	-0.009229	-0.6921 to 0.6736	No	ns	>0.99
1.301441 vs. 59.748901	0.6033	-0.07958 to 1.286	No	ns	0.11
1.301441 vs. 66.20332	0.4242	-0.2587 to 1.107	No	ns	0.46
1.301441 vs. 72.66714	0.4658	-0.2170 to 1.149	No	ns	0.35
$M^{IFN\gamma+LPS}$					
1.301441 vs. 7.738176	0.05099	-0.6319 to 0.7339	No	ns	>0.99
1.301441 vs. 14.206546	0.03779	-0.6451 to 0.7207	No	ns	>0.99
1.301441 vs. 20.765388	-3.34	-4.023 to -2.658	Yes	***	<0.001
1.301441 vs. 27.212623	-3.129	-3.812 to -2.446	Yes	***	<0.001
1.301441 vs. 33.676159	-2.974	-3.656 to -2.291	Yes	***	<0.001
1.301441 vs. 40.245935	-2.799	-3.482 to -2.116	Yes	***	<0.001
1.301441 vs. 46.728973	-2.636	-3.319 to -1.953	Yes	***	<0.001
1.301441 vs. 53.206527	-2.49	-3.173 to -1.808	Yes	***	<0.001
1.301441 vs. 59.748901	1.132	0.4495 to 1.815	Yes	***	<0.001
1.301441 vs. 66.20332	1.03	0.3474 to 1.713	Yes	***	<0.001
1.301441 vs. 72.66714	0.8719	0.1891 to 1.555	Yes	**	0.005
M^{IL-4}					
1.301441 vs. 7.738176	0.05627	-0.6266 to 0.7391	No	ns	>0.99
1.301441 vs. 14.206546	0.03205	-0.6508 to 0.7149	No	ns	>0.99
1.301441 vs. 20.765388	-0.8443	-1.527 to -0.1614	Yes	**	0.007
1.301441 vs. 27.212623	-0.9167	-1.600 to -0.2339	Yes	**	0.003
1.301441 vs. 33.676159	-0.955	-1.638 to -0.2721	Yes	**	0.001
1.301441 vs. 40.245935	-1.886	-2.569 to -1.203	Yes	***	<0.001
1.301441 vs. 46.728973	-0.7215	-1.404 to -0.03860	Yes	*	0.03
1.301441 vs. 53.206527	-0.3819	-1.065 to 0.3010	No	ns	0.59
1.301441 vs. 59.748901	1.387	0.7042 to 2.070	Yes	***	<0.001
1.301441 vs. 66.20332	0.8466	0.1637 to 1.529	Yes	**	0.007
1.301441 vs. 72.66714	0.7378	0.05497 to 1.421	Yes	*	0.03

Table 4.2. (continued)

Dunnett's multiple comparisons test	Mean Diff.	95.00% CI of diff.	Significant?	Summary	Adjusted P Value
$M^{IL\text{-}10}$					
1.301441 vs. 7.738176	0.1277	-0.5552 to 0.8106	No	ns	>0.99
1.301441 vs. 14.206546	0.09905	-0.5838 to 0.7819	No	ns	>0.99
1.301441 vs. 20.765388	-1.472	-2.155 to -0.7888	Yes	***	<0.001
1.301441 vs. 27.212623	-1.498	-2.181 to -0.8155	Yes	***	<0.001
1.301441 vs. 33.676159	-1.483	-2.166 to -0.8005	Yes	***	<0.001
1.301441 vs. 40.245935	-1.202	-1.885 to -0.5190	Yes	***	<0.001
1.301441 vs. 46.728973	-0.6511	-1.334 to 0.03174	No	ns	0.07
1.301441 vs. 53.206527	-0.5351	-1.218 to 0.1478	No	ns	0.21
1.301441 vs. 59.748901	0.8598	0.1769 to 1.543	Yes	**	0.006
1.301441 vs. 66.20332	0.5553	-0.1276 to 1.238	No	ns	0.17
1.301441 vs. 72.66714	0.6486	-0.03428 to 1.331	No	ns	0.07
M^{oxPAPC}					
1.301441 vs. 7.738176	0.06199	-0.6209 to 0.7449	No	ns	>0.99
1.301441 vs. 14.206546	0.05022	-0.6327 to 0.7331	No	ns	>0.99
1.301441 vs. 20.765388	-0.8691	-1.552 to -0.1863	Yes	**	0.005
1.301441 vs. 27.212623	-0.9217	-1.605 to -0.2389	Yes	**	0.002
1.301441 vs. 33.676159	-0.9367	-1.620 to -0.2538	Yes	**	0.002
1.301441 vs. 40.245935	-0.6054	-1.288 to 0.07742	No	ns	0.11
1.301441 vs. 46.728973	-0.2007	-0.8835 to 0.4822	No	ns	0.99
1.301441 vs. 53.206527	-0.1234	-0.8062 to 0.5595	No	ns	>0.99
1.301441 vs. 59.748901	0.7567	0.07386 to 1.440	Yes	*	0.02
1.301441 vs. 66.20332	0.3947	-0.2882 to 1.078	No	ns	0.55
1.301441 vs. 72.66714	0.446	-0.2369 to 1.129	No	ns	0.4
M^{CXCL4}					
1.301441 vs. 7.738176	0.0324	-0.6505 to 0.7153	No	ns	>0.99
1.301441 vs. 14.206546	0.02248	-0.6604 to 0.7053	No	ns	>0.99
1.301441 vs. 20.765388	-2.156	-2.839 to -1.473	Yes	***	<0.001
1.301441 vs. 27.212623	-2.123	-2.806 to -1.440	Yes	***	<0.001
1.301441 vs. 33.676159	-2.088	-2.770 to -1.405	Yes	***	<0.001
1.301441 vs. 40.245935	-1.61	-2.293 to -0.9274	Yes	***	<0.001
1.301441 vs. 46.728973	-1.277	-1.960 to -0.5944	Yes	***	<0.001
1.301441 vs. 53.206527	-1.195	-1.878 to -0.5124	Yes	***	<0.001
1.301441 vs. 59.748901	0.5828	-0.1001 to 1.266	No	ns	0.14
1.301441 vs. 66.20332	0.3105	-0.3724 to 0.9933	No	ns	0.8
1.301441 vs. 72.66714	0.4264	-0.2565 to 1.109	No	ns	0.45

Table 4.3.: Outcomes of Dunnett's for matched/repeated measured two–way ANOVA for normalised OCR data in Figure 4.2.B (M^{x} vs M^{un} at each measurement, n = 4).

Dunnett's multiple comparisons test	Mean Diff.	95.00% CI of diff.	Significant?	Summary	Adjusted P Value
1.301441 min					
M^{un} vs. $M^{IFN\gamma+LPS}$	-0.925	-1.140 to -0.7104	Yes	***	<0.001
M^{un} vs. M^{IL-4}	-0.6822	-0.8968 to -0.4676	Yes	***	<0.001
M^{un} vs. M^{IL-10}	-0.5886	-0.8032 to -0.3740	Yes	***	<0.001
M^{un} vs. M^{oxPAPC}	-0.1894	-0.4040 to 0.02517	No	ns	0.1
M^{un} vs. M^{CXCL4}	-0.2866	-0.5012 to -0.07203	Yes	**	0.004
7.738176 min					
M^{un} vs. $M^{IFN\gamma+LPS}$	-0.8981	-1.113 to -0.6835	Yes	***	<0.001
M^{un} vs. M^{IL-4}	-0.6774	-0.8921 to -0.4628	Yes	***	<0.001
M^{un} vs. M^{IL-10}	-0.5826	-0.7972 to -0.3680	Yes	***	<0.001
M^{un} vs. M^{oxPAPC}	-0.1882	-0.4028 to 0.02637	No	ns	0.11
M^{un} vs. M^{CXCL4}	-0.2724	-0.4870 to -0.05777	Yes	**	0.007
14.206546 min					
M^{un} vs. $M^{IFN\gamma+LPS}$	-0.8891	-1.104 to -0.6745	Yes	***	<0.001
M^{un} vs. M^{IL-4}	-0.6846	-0.8992 to -0.4700	Yes	***	<0.001
M^{un} vs. M^{IL-10}	-0.5873	-0.8019 to -0.3727	Yes	***	<0.001
M^{un} vs. M^{oxPAPC}	-0.1912	-0.4058 to 0.02339	No	ns	0.1
M^{un} vs. M^{CXCL4}	-0.2861	-0.5007 to -0.07147	Yes	**	0.004
20.765388 min	First measurement after addition of glucose				
M^{un} vs. $M^{IFN\gamma+LPS}$	-0.5848	-0.7994 to -0.3702	Yes	***	<0.001
M^{un} vs. M^{IL-4}	-0.5959	-0.8105 to -0.3812	Yes	***	<0.001
M^{un} vs. M^{IL-10}	-0.4008	-0.6154 to -0.1862	Yes	***	<0.001
M^{un} vs. M^{oxPAPC}	-0.166	-0.3807 to 0.04857	No	ns	0.19
M^{un} vs. M^{CXCL4}	-0.05596	-0.2706 to 0.1587	No	ns	0.95
27.212623 min					
M^{un} vs. $M^{IFN\gamma+LPS}$	-0.5368	-0.7514 to -0.3222	Yes	***	<0.001
M^{un} vs. M^{IL-4}	-0.6014	-0.8160 to -0.3868	Yes	***	<0.001
M^{un} vs. M^{IL-10}	-0.3966	-0.6112 to -0.1820	Yes	***	<0.001
M^{un} vs. M^{oxPAPC}	-0.1565	-0.3711 to 0.05809	No	ns	0.23
M^{un} vs. M^{CXCL4}	-0.06736	-0.2820 to 0.1472	No	ns	0.89
33.676159 min					
M^{un} vs. $M^{IFN\gamma+LPS}$	-0.511	-0.7256 to -0.2964	Yes	***	<0.001
M^{un} vs. M^{IL-4}	-0.6085	-0.8231 to -0.3939	Yes	***	<0.001
M^{un} vs. M^{IL-10}	-0.408	-0.6226 to -0.1934	Yes	***	<0.001
M^{un} vs. M^{oxPAPC}	-0.1583	-0.3729 to 0.05634	No	ns	0.22
M^{un} vs. M^{CXCL4}	-0.08261	-0.2972 to 0.1320	No	ns	0.79
40.245935 min	First measurement after addition of oligomycin				
M^{un} vs. $M^{IFN\gamma+LPS}$	-0.3603	-0.5749 to -0.1457	Yes	***	<0.001
M^{un} vs. M^{IL-4}	-0.1742	-0.3888 to 0.04037	No	ns	0.15
M^{un} vs. M^{IL-10}	-0.1363	-0.3509 to 0.07828	No	ns	0.36
M^{un} vs. M^{oxPAPC}	-0.0443	-0.2589 to 0.1703	No	ns	0.98
M^{un} vs. M^{CXCL4}	-0.05952	-0.2741 to 0.1551	No	ns	0.93

Table 4.3. (continued)

Dunnett's multiple comparisons test	Mean Diff.	95.00% CI of diff.	Significant?	Summary	Adjusted P Value
46.728973 min					
M^{un} vs. $M^{IFN\gamma+LPS}$	-0.3259	-0.5405 to -0.1113	Yes	***	<0.001
M^{un} vs. M^{IL-4}	-0.1789	-0.3935 to 0.03571	No	ns	0.14
M^{un} vs. M^{IL-10}	-0.1422	-0.3568 to 0.07245	No	ns	0.32
M^{un} vs. M^{oxPAPC}	-0.03894	-0.2535 to 0.1757	No	ns	0.99
M^{un} vs. M^{CXCL4}	-0.06447	-0.2791 to 0.1501	No	ns	0.91
53.206527 min					
M^{un} vs. $M^{IFN\gamma+LPS}$	-0.2906	-0.5052 to -0.07602	Yes	**	0.003
M^{un} vs. M^{IL-4}	-0.1751	-0.3897 to 0.03948	No	ns	0.15
M^{un} vs. M^{IL-10}	-0.1343	-0.3489 to 0.08030	No	ns	0.37
M^{un} vs. M^{oxPAPC}	-0.03739	-0.2520 to 0.1772	No	ns	>0.99
M^{un} vs. M^{CXCL4}	-0.05157	-0.2662 to 0.1630	No	ns	0.96
59.748901 min	First measurement after addition of 2-deoxyglucose				
M^{un} vs. $M^{IFN\gamma+LPS}$	-0.2161	-0.4307 to -0.001488	Yes	*	0.05
M^{un} vs. M^{IL-4}	-0.1704	-0.3850 to 0.04419	No	ns	0.17
M^{un} vs. M^{IL-10}	-0.1492	-0.3639 to 0.06537	No	ns	0.27
M^{un} vs. M^{oxPAPC}	-0.04852	-0.2631 to 0.1661	No	ns	0.97
M^{un} vs. M^{CXCL4}	-0.05531	-0.2699 to 0.1593	No	ns	0.95
66.20332 min					
M^{un} vs. $M^{IFN\gamma+LPS}$	-0.1669	-0.3815 to 0.04774	No	ns	0.18
M^{un} vs. M^{IL-4}	-0.1493	-0.3640 to 0.06526	No	ns	0.27
M^{un} vs. M^{IL-10}	-0.1264	-0.3410 to 0.08817	No	ns	0.43
M^{un} vs. M^{oxPAPC}	-0.02924	-0.2439 to 0.1854	No	ns	>0.99
M^{un} vs. M^{CXCL4}	-0.02946	-0.2441 to 0.1851	No	ns	>0.99
72.66714 min					
M^{un} vs. $M^{IFN\gamma+LPS}$	-0.1404	-0.3550 to 0.07418	No	ns	0.33
M^{un} vs. M^{IL-4}	-0.1364	-0.3510 to 0.07822	No	ns	0.36
M^{un} vs. M^{IL-10}	-0.1157	-0.3303 to 0.09891	No	ns	0.51
M^{un} vs. M^{oxPAPC}	-0.02638	-0.2410 to 0.1882	No	ns	>0.99
M^{un} vs. M^{CXCL4}	-0.01107	-0.2257 to 0.2035	No	ns	>0.99

Table 4.4.: Outcomes of Dunnett's for matched/repeated measured two–way ANOVA for normalised OCR data in Figure 4.2.B (first vs other measurements in minutes, n = 4).

First measurements after addition of: glucose – 20.765388, oligomycin – 40.245935, 2-deoxyglucose – 59.748901.

Dunnett's multiple comparisons test	Mean Diff.	95.00% CI of diff.	Significant?	Summary	Adjusted P Value
M^{un}					
1.301441 vs. 7.738176	0.03317	-0.1128 to 0.1791	No	ns	>0.99
1.301441 vs. 14.206546	0.03266	-0.1133 to 0.1786	No	ns	>0.99
1.301441 vs. 20.765388	0.1168	-0.02913 to 0.2628	No	ns	0.19
1.301441 vs. 27.212623	0.1096	-0.03634 to 0.2556	No	ns	0.25
1.301441 vs. 33.676159	0.095	-0.05095 to 0.2409	No	ns	0.4
1.301441 vs. 40.245935	0.7038	0.5579 to 0.8498	Yes	***	<0.001
1.301441 vs. 46.728973	0.6824	0.5365 to 0.8284	Yes	***	<0.001
1.301441 vs. 53.206527	0.6927	0.5467 to 0.8386	Yes	***	<0.001
1.301441 vs. 59.748901	0.6688	0.5228 to 0.8147	Yes	***	<0.001
1.301441 vs. 66.20332	0.5774	0.4314 to 0.7233	Yes	***	<0.001
1.301441 vs. 72.66714	0.5111	0.3652 to 0.6571	Yes	***	<0.001
$M^{IFN\gamma+LPS}$					
1.301441 vs. 7.738176	0.06005	-0.08590 to 0.2060	No	ns	0.88
1.301441 vs. 14.206546	0.0686	-0.07735 to 0.2145	No	ns	0.77
1.301441 vs. 20.765388	0.457	0.3111 to 0.6030	Yes	***	<0.001
1.301441 vs. 27.212623	0.4978	0.3519 to 0.6438	Yes	***	<0.001
1.301441 vs. 33.676159	0.5091	0.3631 to 0.6550	Yes	***	<0.001
1.301441 vs. 40.245935	1.269	1.123 to 1.415	Yes	***	<0.001
1.301441 vs. 46.728973	1.282	1.136 to 1.428	Yes	***	<0.001
1.301441 vs. 53.206527	1.327	1.181 to 1.473	Yes	***	<0.001
1.301441 vs. 59.748901	1.378	1.232 to 1.524	Yes	***	<0.001
1.301441 vs. 66.20332	1.336	1.190 to 1.481	Yes	***	<0.001
1.301441 vs. 72.66714	1.296	1.150 to 1.442	Yes	***	<0.001
$M^{IL\text{-}4}$					
1.301441 vs. 7.738176	0.03788	-0.1081 to 0.1838	No	ns	>0.99
1.301441 vs. 14.206546	0.03022	-0.1157 to 0.1762	No	ns	>0.99
1.301441 vs. 20.765388	0.2031	0.05717 to 0.3491	Yes	**	0.002
1.301441 vs. 27.212623	0.1904	0.04442 to 0.3363	Yes	**	0.004
1.301441 vs. 33.676159	0.1686	0.02270 to 0.3146	Yes	*	0.01
1.301441 vs. 40.245935	1.212	1.066 to 1.358	Yes	***	<0.001
1.301441 vs. 46.728973	1.186	1.040 to 1.332	Yes	***	<0.001
1.301441 vs. 53.206527	1.2	1.054 to 1.346	Yes	***	<0.001
1.301441 vs. 59.748901	1.18	1.035 to 1.326	Yes	***	<0.001
1.301441 vs. 66.20332	1.11	0.9643 to 1.256	Yes	***	<0.001
1.301441 vs. 72.66714	1.057	0.9109 to 1.203	Yes	***	<0.001

Table 4.4. (continued)

Dunnett's multiple comparisons test	Mean Diff.	95.00% CI of diff.	Significant?	Summary	Adjusted P Value
$M^{IL\text{-}10}$					
1.301441 vs. 7.738176	0.03917	-0.1068 to 0.1851	No	ns	>0.99
1.301441 vs. 14.206546	0.03394	-0.1120 to 0.1799	No	ns	>0.99
1.301441 vs. 20.765388	0.3046	0.1587 to 0.4506	Yes	***	<0.001
1.301441 vs. 27.212623	0.3016	0.1556 to 0.4475	Yes	***	<0.001
1.301441 vs. 33.676159	0.2756	0.1296 to 0.4215	Yes	***	<0.001
1.301441 vs. 40.245935	1.156	1.010 to 1.302	Yes	***	<0.001
1.301441 vs. 46.728973	1.129	0.9829 to 1.275	Yes	***	<0.001
1.301441 vs. 53.206527	1.147	1.001 to 1.293	Yes	***	<0.001
1.301441 vs. 59.748901	1.108	0.9622 to 1.254	Yes	***	<0.001
1.301441 vs. 66.20332	1.04	0.8936 to 1.186	Yes	***	<0.001
1.301441 vs. 72.66714	0.984	0.8381 to 1.130	Yes	***	<0.001
M^{oxPAPC}					
1.301441 vs. 7.738176	0.03437	-0.1116 to 0.1803	No	ns	>0.99
1.301441 vs. 14.206546	0.03087	-0.1151 to 0.1768	No	ns	>0.99
1.301441 vs. 20.765388	0.1402	-0.005738 to 0.2862	No	ns	0.07
1.301441 vs. 27.212623	0.1425	-0.003415 to 0.2885	No	ns	0.06
1.301441 vs. 33.676159	0.1262	-0.01977 to 0.2721	No	ns	0.13
1.301441 vs. 40.245935	0.849	0.7030 to 0.9949	Yes	***	<0.001
1.301441 vs. 46.728973	0.8329	0.6870 to 0.9789	Yes	***	<0.001
1.301441 vs. 53.206527	0.8447	0.6988 to 0.9907	Yes	***	<0.001
1.301441 vs. 59.748901	0.8097	0.6637 to 0.9556	Yes	***	<0.001
1.301441 vs. 66.20332	0.7376	0.5916 to 0.8835	Yes	***	<0.001
1.301441 vs. 72.66714	0.6742	0.5282 to 0.8201	Yes	***	<0.001
M^{CXCL4}					
1.301441 vs. 7.738176	0.04743	-0.09852 to 0.1934	No	ns	0.97
1.301441 vs. 14.206546	0.03322	-0.1127 to 0.1792	No	ns	>0.99
1.301441 vs. 20.765388	0.3475	0.2015 to 0.4934	Yes	***	<0.001
1.301441 vs. 27.212623	0.3289	0.1829 to 0.4748	Yes	***	<0.001
1.301441 vs. 33.676159	0.299	0.1531 to 0.4450	Yes	***	<0.001
1.301441 vs. 40.245935	0.9309	0.7850 to 1.077	Yes	***	<0.001
1.301441 vs. 46.728973	0.9046	0.7587 to 1.051	Yes	***	<0.001
1.301441 vs. 53.206527	0.9277	0.7818 to 1.074	Yes	***	<0.001
1.301441 vs. 59.748901	0.9001	0.7541 to 1.046	Yes	***	<0.001
1.301441 vs. 66.20332	0.8346	0.6886 to 0.9805	Yes	***	<0.001
1.301441 vs. 72.66714	0.7867	0.6407 to 0.9326	Yes	***	<0.001

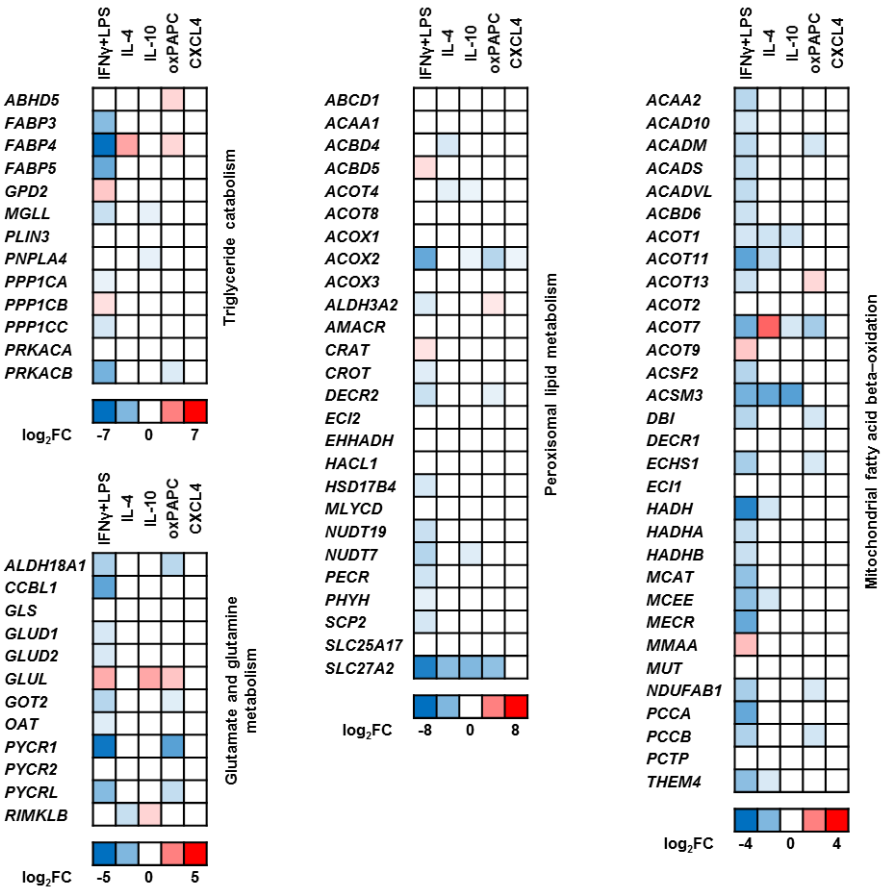

Figure 4.3.: Differentially expressed genes in primary metabolite catabolic pathways.

Triglycerides are broken down in glycerol and fatty acids, the latter are further catabolised in peroxisomes (linear > 18 carbon acids) or mitochondria to generate acetyl–CoA (the mitochondrial oxidation also produces protonated nicotinamide adenine dinucleotide [NADH] and flavin adenine dinucleotide [$FADH_2$]) for the TCA cycle. Glutamine is converted to glutamate, which can then be processed into α–ketoglutarate for the TCA cycle. Differential gene expression for glycolysis, the catabolic pathway for the other primary metabolite, glucose, is shown in **Figure 4.2.** M^x compared to M^{un} measured using RNA–seq; n = 8, annotations retrieved from reactome.org on 16 October 2018, except for Glutamate and glutamine oxidation, which were retrieved on 07 August 2019, thresholds for differential gene expression were $|\log_2 FC| > \log_2(1.5)$ and FDR < 0.05 (Benjamini and Hochberg method).

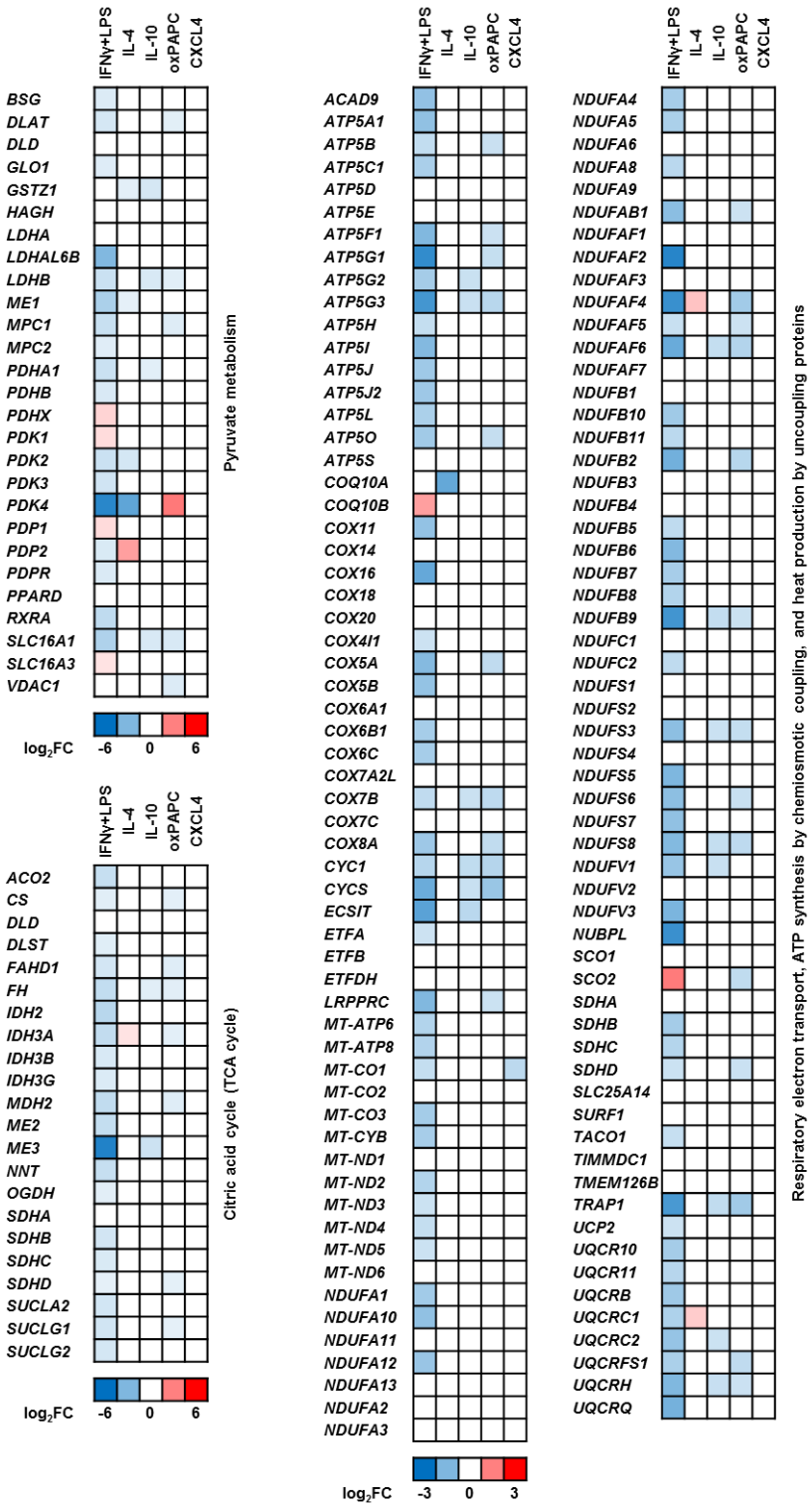

Figure 4.4.: Differentially expressed genes in down–stream metabolic pathways.

Pyruvate from glycolysis is processed into acetyl–CoA or lactate and protons. The TCA cycle uses acetyl–CoA from pyruvate and fatty acid catabolism and α–ketoglutarate from glutamate and glutamine oxidation to generate electron donors for the ETC, which produces a proton gradient for the ATP synthase. M^{x} compared to M^{un} measured using RNA–seq; n = 8, annotations retrieved from reactome.org on 16 October 2018, thresholds for differential gene expression were $|\log_2 FC| > \log_2(1.5)$ and FDR < 0.05 (Benjamini and Hochberg method).

4.4.2. Macrophage phenotype IL–1β and IL–8 secretion may be dependent on cell exposure to pro-inflammatory stimuli, BzATP and acLDL

ELISA measurements were performed on culture medias of differentially activated macrophages to characterise IL–1β and IL–8 secretion and at the same time select the experimental conditions to be tested in CBA assays to detect a much wider spectrum of cytokines. Following polarisation IL–1β was detected only in the $M^{IFN\gamma+LPS}$ media (**Figure 4.5.A**) of cells from both donors. The cells treated with 300 μM BzATP (to provide danger–associate molecular pattern/P2X purinoreceptor 7 caspase–1 IL–1β secretion stimulus) at the end of the secondary stimulation secreted more of both cytokines (**Figure 4.5.B** and **C**), which may have been caused by the higher dose of BzATP or donor differences, but more repeats of the experiments are needed to confirm this. After a secondary stimulation the response of $M^{IFN\gamma+LPS}$ was largely attenuated, except for the secondary LPS stimulation in the 300 μM BzATP–treated cells (**Figure 4.5.B** and **C**). Other phenotypes displayed no IL–1β secretion after polarisation, but upon LPS stimulation secreted IL–1β in some conditions (**Figure 4.5.B** and **C**). Interestingly, secondary stimulation with acLDL did not result in measurable IL–1β secretion, but LPS + acLDL appeared to reduce the amount secreted to in most cases below the limit of reliable quantification (**Figure 4.5.B** and **C**), but more biological repeats are needed to verify this and all other interpretations.

IL–8 was detected at a much higher magnitude (**Figure 4.5.D**) from cells of both donors. It was highly abundant in the $M^{IFN\gamma+LPS}$ post-polarisation media, while M^{CXCL4} displayed lower abundance (magnitude depending on the donor) and other phenotypes showed no/low secretion of IL–8 at this stage (**Figure 4.5.D**). Upon changing the polarisation media to fresh media the cells of both donors receiving no additional stimulants appeared to secrete no or relatively low levels of IL–8, while those receiving acLDL released slightly more of this cytokine (**Figure 4.5.E and F**). An exception to this were the $M^{IFN\gamma+LPS}$ cells of both donors, which appeared to be attenuated in their response to any secondary stimulation, because they secreted IL–8 at similar levels, regardless of the stimulant used (**Figure 4.5.E and F**). Upon secondary stimulation with LPS all phenotypes of both donors, except $M^{IFN\gamma+LPS}$, released large levels of IL–8, which were slightly lower when LPS + acLDL were used for the secondary stimulation (**Figure 4.5.E and F**). As with IL–1β measurements, more biological repeats are needed to confirm these interpretations.

Unfortunately, in the initial run the CBA results appeared to lack consistency, therefore, for the second run controls of fresh media samples were spiked with known concentrations of recombinant human cell culture or ELISA standard cytokines. The results from these samples were qualitatively reasonable, however, more exact cytokine concentration quantification was less reliable and also neither IFNγ nor IL–1β were detected (**Figure 4.6.**), which warrant additional optimisation and validation to be carried out.

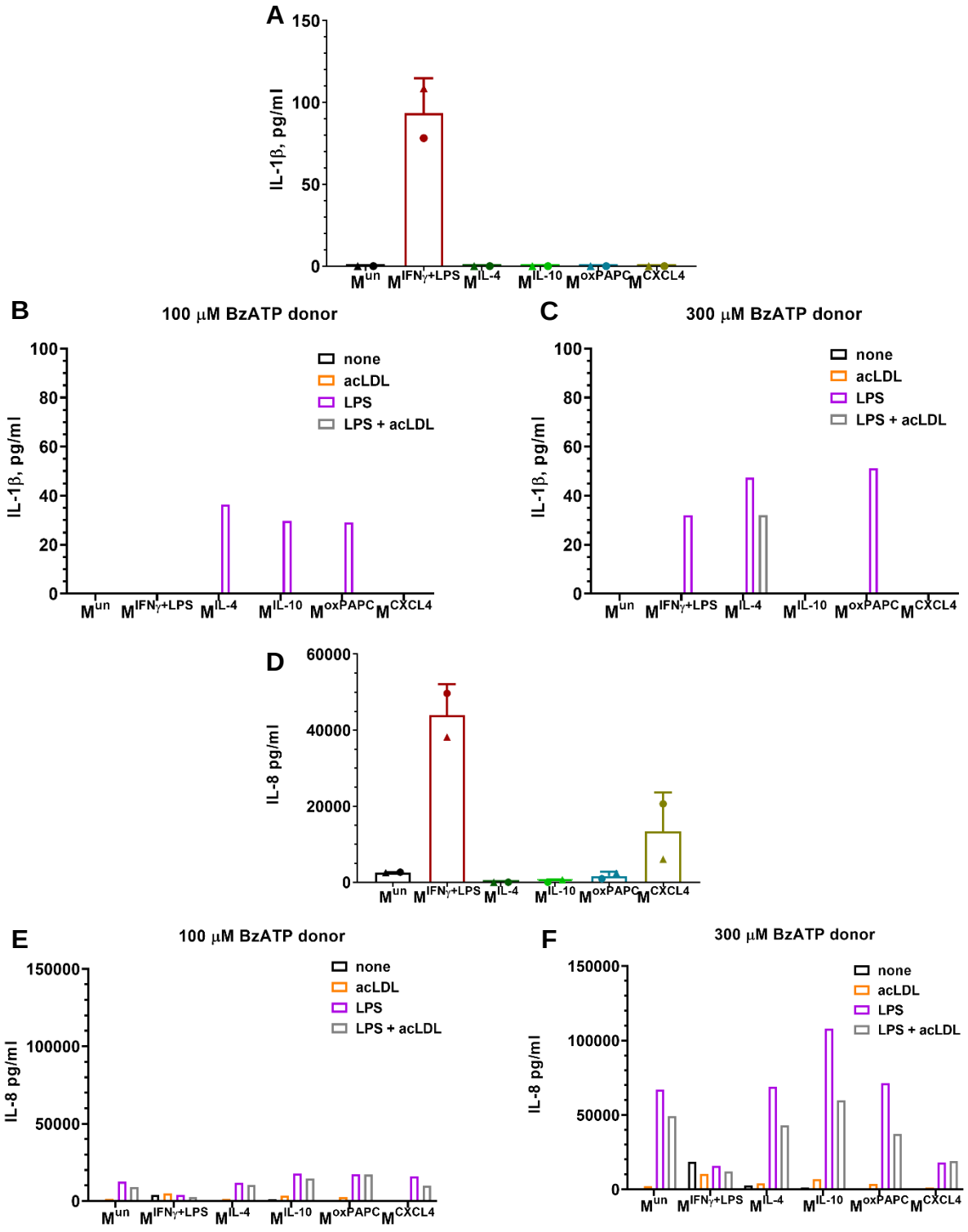

Figure 4.5.: MDM phenotype pro-inflammatory cytokine secretion.

Secretion of IL–1β in (**A**) post-polarisation and (**B** and **C**) secondary stimulation media for the indicated BzATP concentration donors. Secretion of IL–8 in (**D**) post-polarisation and (**E** and **F**) secondary stimulation media for the indicated BzATP concentration donors. (**A** and **D**) The circles and the triangles represent the 300 and 100 μM BzATP donor cell readings respectively. (**B**, **C**, **E** and **F**) LPS 1 ng/ml, acLDL 25 μg/ml.

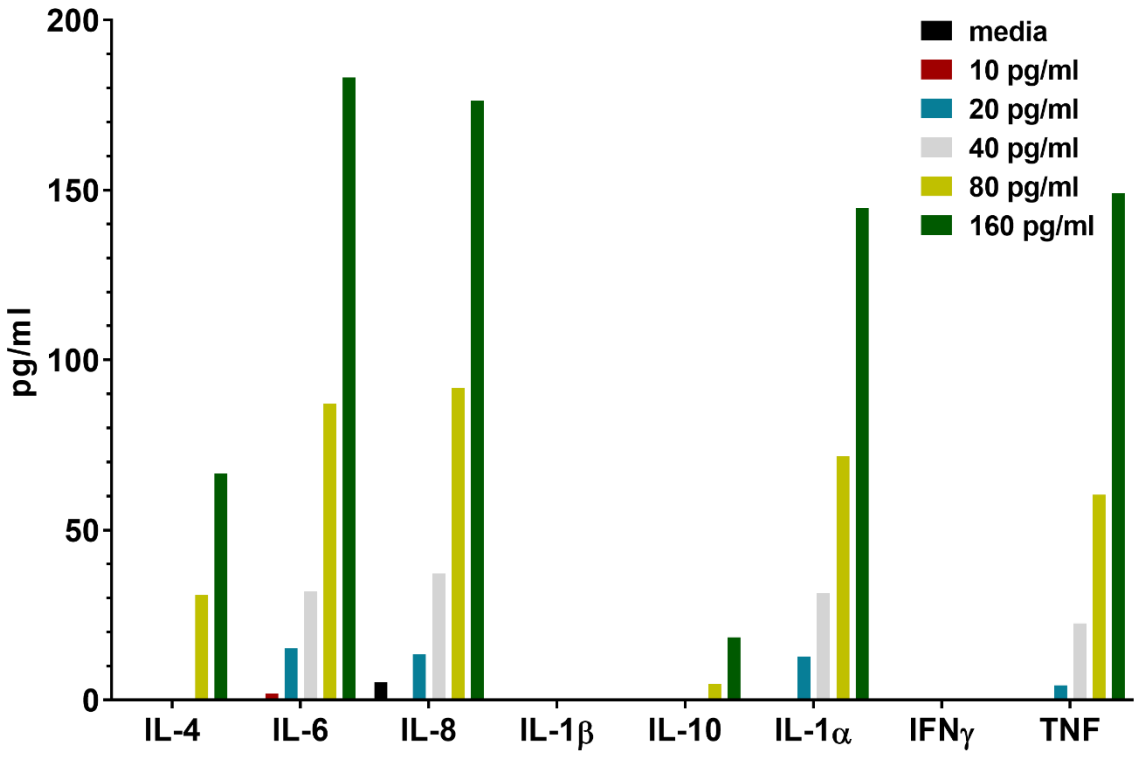

Figure 4.6.: CBA trial.

Average CBA readings of samples with known concentrations (legend) of the cell culture cytokines or ELISA standards (x axis labels). CBA – cytokine bead array, ELISA – enzyme–linked immunosorbent assay.

4.5. Discussion

As demonstrated in the published literature and observed here, pro-inflammatory macrophages use glycolysis to generate ATP and pyruvate, which instead of being channelled into the Krebs cycle is converted to lactic acid and protons (removed from the cell) (Verdeguer and Aouadi, 2017, Viola et al., 2019). M^{IL-4}, consistent with published research, showed markedly lower glycolytic flux likely due to relying more on such processes as FAO (Verdeguer and Aouadi, 2017, Viola et al., 2019). M^{oxPAPC} similar glycolytic flux to M^{IL-4}, which could have been the result of the dose, composition of and length of the oxidised phospholipid species (Serbulea et al., 2018b, Serbulea et al., 2018a). On average M^{IL-10} may have had intermediate glycolytic capacity, which along with a recent observation that IL–10 stimulation resets macrophage sensitivity to LPS (Gharib et al., 2019) may indicate that this cytokine is important in maintaining macrophage responsiveness to inflammatory stimuli or even changing their phenotype. However, this increase was not significant compared to M^{un} and it was recently observed that IL–10 dampens LPS–induced glycolysis in mouse macrophages (Ip et al., 2017, Minton, 2017), therefore, more research is needed to clarify the potential impact of IL–10 on macrophage glycolysis. Unfortunately, neither the data presented here nor in the Gleissner et al. publication (Gleissner et al., 2010) can give a clear explanation why M^{CXCL4} have an intermediate glycolytic capacity. Also, the M^{IL-4} increase in ECAR upon addition of oligomycin could indicate some spare glycolytic capacity, but its brief duration is difficult to interpret confidently. The complete lack of increase and even a slight decrease in ECAR for other phenotypes at this step was observed before in human macrophages (Penny et al., 2016) as glucose starvation for at least one hour depleted the intracellular stocks and upon introduction of excess glucose the cells may have used it to their maximal capacity. Assay media instead of the compound injections for the media–only wells may not have been ideal, but were also unlikely to skew the results, because each compound was diluted in the assay media before loading. More experimentation is required to further understand the metabolism of macrophage phenotypes, especially in revealing more about the internal processing of lipids in M^{oxPAPC}.

The results of preliminary experiments on IL–1β and IL–8 secretion presented here may show that upon polarisation pro-inflammatory macrophages could possibly secrete more IL–1β and IL–8 than other phenotypes, higher concentration of BzATP could have helped macrophages to release these cytokines and $M^{IFN\gamma+LPS}$ may have been desensitised to the secondary stimulation with LPS Similar results have previously been observed for pro-inflammatory cytokine secretion (Ward et al., 2010, da Silva et al., 2016) and for LPS desensitisation in mouse macrophages for expression of *Il6* and *Tnf* (O'Carroll et al., 2014), however, more repeats of these experiments are needed to validate these interpretations of preliminary experiments shown here. The most novel aspect of current work could be the observation that acLDL may have reduced IL–1β and IL–8 release when

it was included along with LPS in the secondary stimulation, but the experiments should be repeated more times to validate this interpretation. da Silva et al. previously reported decreased TNFα, IL–1β and IL–10 and increased IL–8 in pro-inflammatory foamy macrophages compared to unloaded cells (da Silva et al., 2016). The cell culture media and schedule used were different from the ones used here and the ELISA experiments in this thesis need to be repeated more times to draw any concrete conclusion, therefore, it is difficult to make any direct comparisons between the two datasets. Regardless, more research is required to better understand how polarisation and lipid loading alter the macrophage secretome.

5. CALHM6 in macrophages

5.1. Introduction

Calcium homeostasis modulator family member 6 (CALHM6, also known as FAM26F – family with sequence similarity member 26 F, C6orf187, INAM – IRF3–dependent natural killer cell–activating molecule) is a 2,407 bp protein–coding gene, located on 6q22.1 in the human genome. The gene has 3 exons separated by 2 introns and codes for several mRNA transcripts: isoform 1 (full–length, 1,127 bp, ENST00000368605.3), isoform 2 (missing exon 2, 546 bp, ENST00000368606.7) and "fragment" (540 bp, ENST00000368604.2) (**Figure 5.1.A**). Isoform 1 and 2 are predicted to yield proteins 34,458 and 16,490 Da respectively according to the main UniProt entry (Q5R3K3), while a separate "fragment" entry (Q5R3K2) indicates a computationally mapped potential polypeptide of 18,054 Da (**Figure 5.1.A**). Orthologous genes/proteins have been predicted in numerous organisms, including animal models such as: mouse, rat, rabbit and zebrafish (Malik et al., 2017). CALHM6 is predicted to have four transmembrane helices (similarly to the tetraspanin family, but without the key residues to belong to it) with a long intracellular C–terminal loop (119 out of 315 amino acids) and localised to the plasma membrane (Malik et al., 2017). The plasma membrane localisation has been shown in mouse CALHM6 expression vector viral infections of mouse bone marrow–derived dendritic cells (BMDCs), $DX5^+$ NK cells and the murine IL–3–dependent pro-B cell line Ba/F3 (Ebihara et al., 2010) (**Figure 5.1.A**). The protein is also likely to be phosphorylated on its only intracellular loop as well as the C terminus (Malik et al., 2017). Glycosylation at the extracellular N143 has been predicted (Malik et al., 2017) and confirmed in western blotting by another group performing cell lysate deglycosylation and using a custom anti-mouse antibody (Ebihara et al., 2010).

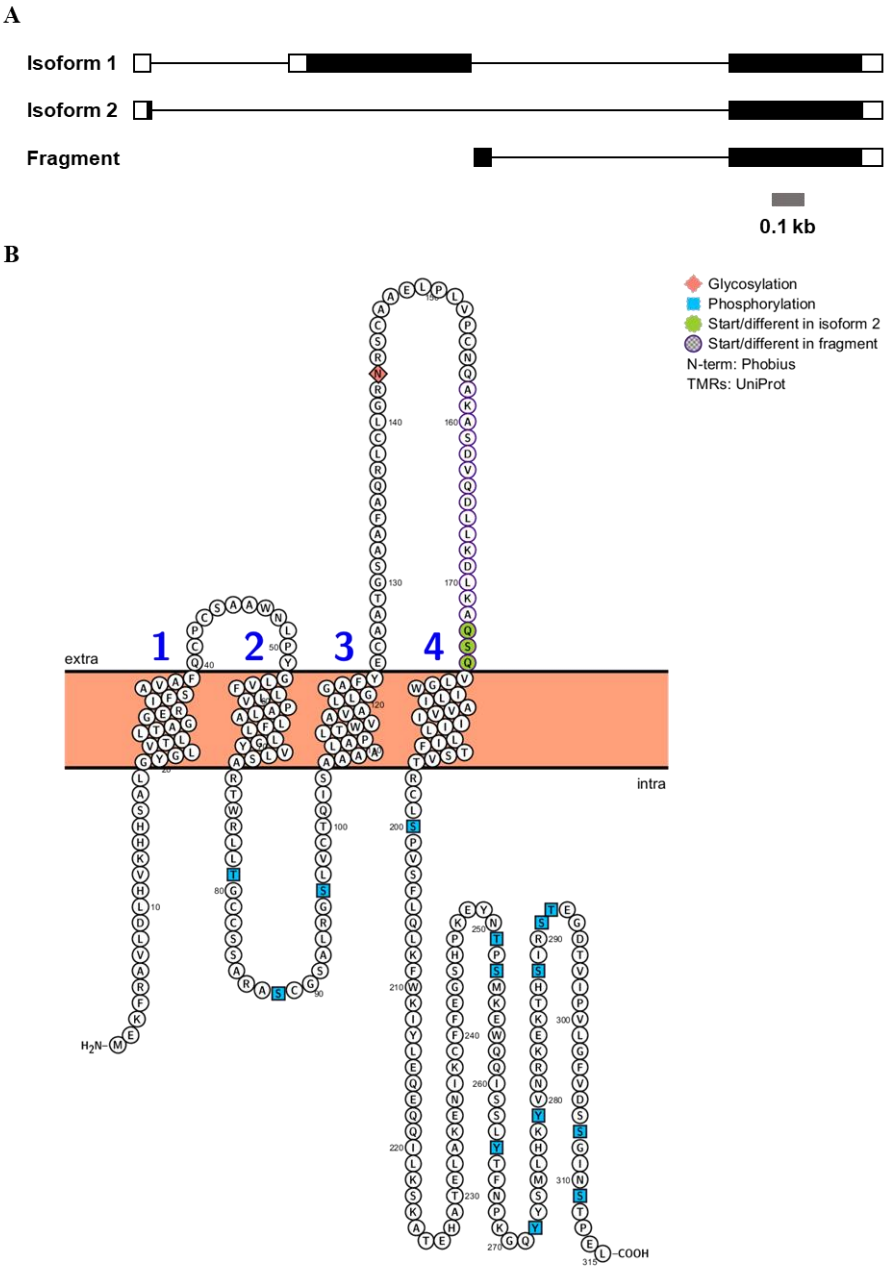

Figure 5.1.: CALHM6 transcripts and proteins.

(**A**) Schematic of the human CALHM6 transcripts: isoform 1 (1,127 bp [ENST00000368605.3], 34,458 Da peptide [Q5R3K3]), isoform 2 (546 bp [ENST00000368606.7], 16,490 Da peptide [Q5R3K3]) and fragment (540 bp [ENST00000368604.2], 18,054 Da peptide [Q5R3K2]). Lines indicate introns, bars exons (empty bars are untranslated regions and filled bars are translated regions). (**B**) Schematic of the predicted human CALHM6 structure and topology in a membrane; predicted post-translation modifications (Malik et al., 2017), the start/different amino acid regions for isoform 2 and fragment have been marked and are QSQ → MFP and AKASDVQDLLKDLKAQSQ → RWGRLGGAERPSFLRAAG respectively. Based on and data retrieved from (Malik et al., 2017), ENSEMBL and UniProt on 24 July, 2019, image of structure generated using Protter (Omasits et al., 2014).

Transcriptomic evidence suggests that *CALHM6*/*Calhm6* expression is up–regulated in human/animal disease and associated inflammation, these include: leprosy (Belone et al., 2015), in response to 5'—C—phosphate—G—3' (CpG) DNA via TNF in BMDMs (Caldwell et al., 2014), mouse alveolar macrophages following intranasal infection with *Streptococcus pneumoniae* or *Staphylococcus aureus* (Strehlitz, 2017), mouse DCs and NK cell co-culture with B16–F1 melanoma cell line induced mouse CALHM6 expression in the DCs via Dectin and IRF5, leading to NK activation for tumour cell killing (Chiba et al., 2014), in mouse neutrophils dependant on type II interferon upon *Streptococcus pneumoniae* infection in mice (Gomez et al., 2015), raised in primary cutaneous melanoma compared to skin/nevi (Ren et al., 2008), diethylstilbestrol–treated chicken oviducts (Song et al., 2011), porcine mesenteric lymph nodes to *Salmonella enterica* serovar Typhimurium (Wang et al., 2007) infant response within one day after vaccination with modified vaccinia Ankara 85A (MVA85A) against tuberculosis (Matsumiya et al., 2014), remote ischaemic conditioning (Nikkola et al., 2015), in a cryogenic mouse myocardial infarction model inflammatory (initial) stage (Walter et al., 2018).

CALHM6 expression can also be indicative of specific subtypes of certain diseases and could be a potential prognostic marker: amongst minimum of 20 discriminatory transcripts to separate inflammatory bowel disease and colorectal cancer biopsy samples (Galamb et al., 2008), amongst signature genes predictive of beneficial response to melanoma–associated antigen 3 specific cancer immunotherapy (Ulloa-Montoya et al., 2013), characteristic (among 37 genes in total) of sepsis caused by *Burkholderia pseudomallei* (Pankla et al., 2009), up–regulated in PBMCs of patients with advanced transplant coronary artery disease (Shahzad et al., 2010), quasimesenchymal subtype of pancreatic ductal adenocarcinoma with notably poorer survival prognosis (Collisson et al., 2011). It has also been associated with several single nucleotide polymorphisms (SNPs) and expression trait quantitative loci (eQTLs): monocyte–derived DCs stimulated with LPS or influenza, among 57 cis–reQTLs for direct LPS stimulation, indirect via type I interferon and direct influenza stimulation (Lee et al., 2014), ulcerative colitis SNP rs2858829 (Julia et al., 2014), steroid–sensitive nephrotic syndrome SNP rs2637678 (Dufek et al., 2019).

Interestingly, even though in most cases the basal expression of *CALHM6* is low, there are several instances of decreased expression: in rat airway epithelium following burn injury (Jacob et al., 2015), at 4 hours of rabbit PBMC stimulation with PMA and ionomycin (Jacquier et al., 2015), in ovarian cancer (Nikolova et al., 2009), in contracted aorta vs control and corrected aorta vs control (LaDisa et al., 2015), hypomethylated in cervical cancer (Farkas et al., 2013), decreased upon IFNγ blockade or just in mild/moderate systemic lupus erythematosus patients (Welcher et al., 2015),

suppressed activation by LPS using a synthetic compound that mimics acetylated histones (Nicodeme et al., 2010).

Expression in macrophages is likely to be controlled through inflammatory signalling pathways involving or closely associated to interferon, especially type II, and/or LPS signalling (**Figure 5.2.**). Increased *CALHM6* RNA expression has been observed only in IFNγ and/or LPS activated human macrophages (Xue et al., 2014), while raised protein expression was reported in $M^{IFN\gamma}$, but not M^{LPS} (Brown et al., 2010). Also, CALHM6 has recently been reported to be up–regulated in human $M^{IFN\gamma+LPS}$ cultured in 2 and 3D both at the mRNA and protein level (Court et al., 2019) as well as scRNA–seq on $CD45^{+}$ cells of murine atherosclerosis interferon gene cluster (Kim et al., 2018). Furthermore, *Calhm6* induction was observed to be dependent on TIR domain–containing molecule 1 (TICAM1)/IRF3 signalling in mouse DCs exposed to polyinosinic:polycytidylic acid (poly(I:C)) for cell–to–cell contact activation of NK cells (Ebihara et al., 2010), while upon stimulation with INFγ expression levels were largely abrogated in $Stat1^{-/-}$ compared wild–type mouse vascular smooth muscle cells in addition to the authors identifying a potential Stat1 binding site up–stream of the *Calhm6* gene (Chmielewski et al., 2014).

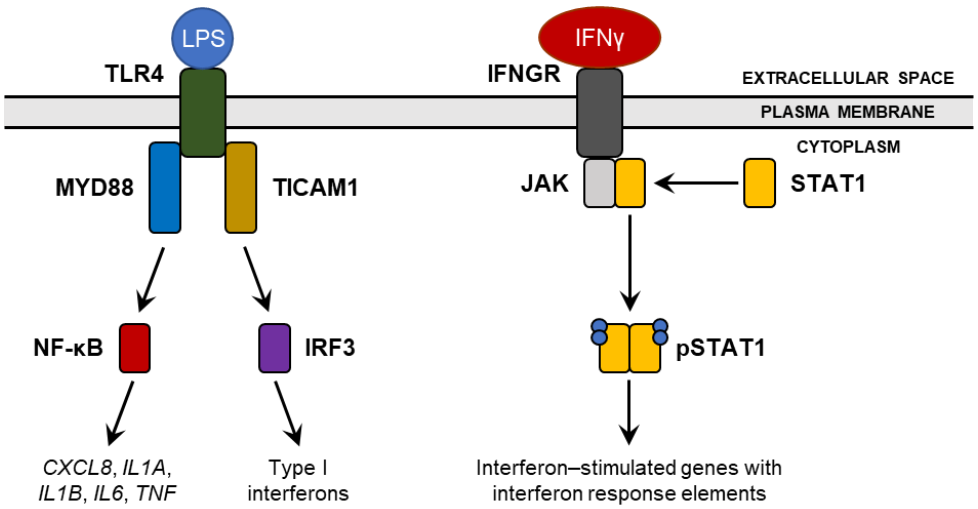

Figure 5.2.: TLR4 and IFNGR signalling.

LPS binding to TLR4 activates the canonical signalling pathway mediated via MYD88 and NF–κB as well as the non-canonical signalling pathway via TICAM1 and IRF3. The two pathways induce expression of different genes (examples shown at the end of each pathway. IFNγ binding to IFNGR recruits STAT1 to the receptor complex, where Janus kinase (JAK) phosphorylates STAT1, which is then able to dimerise and translocate to the nucleus to induce selected gene expression. CXCL8 – C-X-C motif chemokine ligand 8 (interleukin 8), IFNγ – interferon γ, IFNGR – interferon γ receptor, IL – interleukin, IRF3 – interferon response factor 3, JAK – Janus kinase, LPS – lipopolysaccharide, MYD88 – myeloid differentiation primary response protein 88, NF–κB – nuclear factor κ–light–chain–enhancer of activated B cells, (p)STAT1 – (phosphorylated) signal transducer and activator of transcription 1, TICAM1 – TIR domain–containing adapter molecule 1, TLR4 – Toll–like receptor 4, TNF – tumour necrosis factor. Adapted from (Diamond et al., 2015, Majoros et al., 2017, Michalska et al., 2018).

Little is known about the function of CALHM6. Protein sequence similarity to its other members of its family suggest involvement in calcium ion and other signalling molecule trafficking across membranes (Ma et al., 2018, Taruno et al., 2013, Romanov et al., 2018), however, this has not been confirmed experimentally. Recent work in mouse models indicated that mouse CALHM6 may participate in bridging innate and adaptive immune responses (Ebihara et al., 2010, Kasamatsu et al., 2014). In these reports NK cell activation by antigen presenting cells ($CD8\alpha^+$ conventional DCs or macrophages in particular) led to an increase in IFNγ and lowered tumour volume and metastasis rates of IFNγ–sensitive tumours, while these effects were abrogated in *Calhm6* whole–body knockout mice, their cells and upon use of an anti-NK antibody (Ebihara et al., 2010, Kasamatsu et al., 2014). However, further details of how CALHM6 may be involved in this process in any disease context are not known.

5.2. Hypothesis and aims

The following hypotheses and aims refer to the original research being submitted as part of the completion of this degree. Work that has been submitted before or is planned to be submitted in a different thesis has been acknowledged as such in the **Contributions** (**Section 5.3.**) for this chapter. Both original and previously submitted work are being included in the submission for publication with overall hypotheses and aims throughout the manuscript. The manuscript, as presented here, is currently being prepared for submission to a peer–reviewed journal as is still pending several experiments and analyses to be completed.

Hypothesis 1: CALHM6 is a novel gene and protein marker for pro-inflammatory macrophages.

Hypothesis 2: CALHM6 is involved in pro-inflammatory macrophage polarisation and function.

Aim 1: Confirm the specificity of CALHM6 up–regulation using both RNA and protein in IFNγ and/or LPS activated macrophages.

Aim 2: Test involvement of specific inflammatory pathways in CALHM6 expression up–regulation using knockdown models.

Aim 3: Explore the potential functions of CALHM6 by creating and utilising overexpression and knockdown models.

5.3. Contributions

My own contributions to the manuscript in this chapter are:

Human RNA extraction and qRT–PCR, except for the statin pre-treatment, immunocytochemistry/immunofluorescence, siRNA knockdowns, pY701 STAT1 western blot, generation and testing of CALHM6–3×FLAG THP–1s, data analysis and interpretation, manuscript writing.

The following people have also contributed to the manuscript and additional data presented in this chapter for completion of their degree and/or publication purposes:

Rehab Alqurashi (will be submitted as part of completion of PhD): co-immunoprecipitation and associated western blots, cell interaction assays, data analysis, manuscript writing (methods);

Klaudia Kocsy (will be submitted as part of completion of PhD): immunohistochemistry/immunofluorescence, immunohistochemistry staining for plaque section characterisation, statin pre-treatment macrophage culture and RNA extraction, qRT–PCR, data analysis and manuscript writing (methods);

Éva Hadadi (previously submitted work as part of completion of PhD): SILAC macrophage membrane proteomics, analysis, interpretation and manuscript writing (methods);

Radoslaw M Sobota: SILAC macrophage membrane proteomics and analysis and manuscript writing (methods);

Dilip Kumar: generation of CALHM6–3×FLAG THP–1s and manuscript writing (methods);

Laura Martínez Campesino (may be submitted as part of completion of PhD): BMDM culture, mouse RNA extraction, qRT–PCR, data analysis and manuscript writing (methods);

Bernett Lee: SILAC macrophage membrane proteomics analysis;

Michael Poidinger: SILAC macrophage membrane proteomics analysis;

Caroline Evans: co-immunoprecipitation sample mass spectrometry and analysis and manuscript writing (methods);

Jessica N Redgrave: histological carotid plaque section analysis and classification, conception and design;

S Kim Suvarna: histological carotid plaque section analysis and classification;

Mark J Dickman: conception and design;

Arshad Majid: conception and design;

Sheila E Francis: conception and design, data interpretation;

Siew Cheng Wong: conception and design, data interpretation, manuscript editing;

Endre Kiss–Tóth: conception and design, data interpretation, manuscript editing;

Heather L Wilson: co-immunoprecipitation, conception and design, data interpretation, manuscript writing.

5.4. Manuscript: Human pro-inflammatory macrophage CALHM6 regulates chemokine expression and macrophage–lymphocyte interaction

As mentioned in the **Hypotheses and aims** (**Section 5.2.**) for this chapter, the following manuscript is being prepared for submission to a peer–reviewed journal. The **Introduction** (**Section 5.4.2.**) of the manuscript provides additional context for the data introduced, while the **Results** and **Discussion** (**Sections 5.4.4.** and **5.4.5.** respectively) of this manuscript represent their respective sections that would be in place in a traditionally formatted thesis. The **Materials and methods** (**Chapter 2**) and the **References** (**Chapter 8**) of the thesis contains the **Materials and methods** and **References** respectively for this manuscript.

Human pro-inflammatory macrophage CALHM6 regulates chemokine expression and macrophage–lymphocyte interaction

Kajus Baidžajevas[a, b], Rehab Alqurashi[a], Klaudia Kocsy[a], Éva Hadadi[a, b, c], Radoslaw M Sobota[d], Dilip Kumar[b], Laura Martínez Campesino[a], Bernett Lee[b], Michael Poidinger[b], Caroline Evans[d], Jessica N Redgrave[e], S Kim Suvarna[a], Mark J Dickman[d], Arshad Majid[e], Sheila E Francis[a], Siew Cheng Wong[b], Endre Kiss–Tóth[a], Heather L Wilson[a, *].

a Department of Infection, Immunity & Cardiovascular Disease, University of Sheffield, Beech Hill Road, Sheffield, S10 2RX, UK

b Singapore Immunology Network (SIgN), Agency for Science, Technology and Research (A*STAR), Singapore

c Current address: INSERM U935, Villejuif, France

d Department of Chemical and Biological Engineering, The University of Sheffield, Mappin Street, Sheffield, S1 3JD, UK

e Sheffield Institute for Translational Neuroscience, University of Sheffield, 385a Glossop Road, Sheffield, S10 2HQ, UK

* Corresponding author: Heather L Wilson: Department of Infection, Immunity & Cardiovascular Disease, University of Sheffield, Beech Hill Road, Sheffield, S10 2RX, UK. Tel. + 44 114 215 9560. Email: H.L.Wilson@sheffield.ac.uk

Key words: atherosclerosis, inflammation, macrophages, FAM26F, CALHM6, INAM

5.4.1. Abstract

Background

Increased abundance of pro-inflammatory macrophages in atherosclerotic plaques is a risk factor for plaque rupture. The currently used markers to identify these cells have not been extensively tested for specificity, are not always up–regulated as transcripts and cell–surface protein and also cannot always be used in model organisms and humans. We sought to identify genes up–regulated in inflammatory macrophages to identify potential markers and functional changes in plaque inflammation.

Methods

Human MDMs and mouse BMDMs were polarised with interferon gamma, lipopolysaccharide, interleukin 4 and 10, oxidised phospholipid and chemokine C-X-C motif ligand 4 for 24 h. Gene expression was quantified by qRT–PCR, while protein expression was measured by membrane protein SILAC proteomics, immunocytochemistry, immunohistochemistry and western blotting. siRNA was used to knockdown selected genes. THP–1s were transfected to overexpress a 3×FLAG fusion protein for co-immunoprecipitation and cell interaction experiments.

Results

Calcium homeostasis modulator family member 6 (CALHM6) was the most highly uniquely up–regulated *in vitro* in both human and mouse primary macrophages activated with IFNγ(+LPS). CALHM6 expressing macrophages were also identified in human carotid artery atherosclerosis. siRNA knockdowns of *TICAM1* and *STAT1* resulted in lower induction of *CALHM6* upon activation with LPS or IFNγ respectively. siRNA knockdown of *CALHM6* reduced STAT1 phosphorylation and expression of *CCL5*, *CXCL8* and *CXCL11*. CALHM6–3×FLAG co-immunoprecipitated with linker for activation of T cells and overexpression of this construct resulted in a higher percentage of Jurkat cells attaching to THP–1s upon stimulation with IFNγ+LPS.

Conclusions

CALHM6 is a novel pro-inflammatory macrophage marker potentially expressed in a subset of human atherosclerotic plaque macrophages involved in regulating leukocyte recruitment and potentially activation. This finding provides us with a new understanding of immune cell activation in atherosclerotic plaques and mechanisms of inflammatory activation underlying plaque vulnerability.

5.4.2. Introduction

Patients with late–stage atherosclerosis are at increased risk of life–threatening ischaemia due to plaque rupture and resultant thrombosis (Yahagi et al., 2016). Leukocytes, such as pro-inflammatory macrophages, secrete MMPs, which breakdown collagen and other connective proteins, thin and weaken the protective cap of the atheroma (Huang et al., 2012, Newby, 2015, Orbe et al., 2003). Plaques with caps < 65 μm in thickness, notable macrophage and lymphocyte presence, rare or no SMCs and a necrotic core > 10% of plaque area, are classified as rupture–prone thin–cap fibroatheromas (Yahagi et al., 2016). In advanced plaques, macrophages positive for common pro-inflammatory markers tend to localise to specific regions of the plaque, such as the cap shoulders, which are particularly prone to mechanical stresses and therefore rupture (Stoger et al., 2012).

Identification and characterisation of plaque macrophages has been a major challenge in atherosclerosis research: early reports broadly classified macrophages into M1 and M2 pro- and anti-inflammatory phenotypes respectively, however, advancements in the field greatly expanded our understanding of macrophage heterogeneity (Murray et al., 2014). Also, recent reports on mouse atherosclerosis model single cell RNA–seq have challenged the concept of the *in vitro*–like M2 anti-inflammatory macrophage presence in plaques (Cochain et al., 2018, Kim et al., 2018). However, the use of phenotype or activation–specific markers is still common practice due to the speed, cost and convenience, especially in diagnostics and research involving patient samples. Characterisation of marker protein function may also aid in drug discovery and choice of treatment.

The current macrophage markers in use are constrained by a number of issues: (1) lack of thorough testing for specificity even in *in vitro* culture models, (2) limited choice of cell surface–expressed proteins as markers, (3) inconsistency across species, (4) expression increased only at the RNA or protein level. Therefore, it is difficult to precisely and confidently determine differentially activated macrophage presence in, and impact on, atherosclerotic plaque growth and rupture in human patients. We have therefore used a membrane proteomics approach to identify potential new macrophage phenotype markers.

We identified a new pro-inflammatory macrophage marker CALHM6 (also known as FAM26F – family with sequence similarity 26 member F or INAM), which is a tetraspanin–like protein predicted to function as a membrane pore for signalling molecules such as ATP and calcium ions (Malik et al., 2017). Expression of the *CALHM6* gene is up–regulated in several inflammatory disease contexts (Ebihara et al., 2010, Kasamatsu et al., 2014, Strehlitz, 2017). It has been shown to be induced by poly(I:C) via TLR3/TICAM1/IRF3 in mouse BMDCs and (NK) cells for cell–to–cell contact activation of the latter cells to produce IFNγ and induce tumour cell killing (Ebihara

et al., 2010). The same group later showed that mouse CD8α^{+} DCs and macrophages can up–regulate expression of CALHM6 upon poly(I:C) activation (Kasamatsu et al., 2014). Using a melanoma lung metastasis model they confirmed that CALHM6 is important in controlling tumour metastases (Kasamatsu et al., 2014). However, it has not been entirely confirmed that up–regulated CALHM6 gene and protein expression is specific to human pro-inflammatory macrophages as well as the signalling pathways involved in inducing expression. Also, further details of how CALHM6 may function to bridge innate and adaptive immunities have not been tested in human cells.

Here we show that CALHM6 is up–regulated specifically upon pro-inflammatory activation of human and mouse macrophages, and may be expressed in human carotid atherosclerotic plaque macrophages. We have also demonstrated involvement of TICAM1 and STAT1 signalling axes in CALHM6 induction as well as shown that it influences chemokine expression regulation. In addition, in our preliminary experiments we potentially observed CALHM6 co-immunoprecipitation with linker for activation of T–cells (LAT) and possibly increased THP–1/Jurkat cell interaction when overexpressed in the former. If validated through repeated experimentation these observations could suggest that human CALHM6 may be involved in linking innate to adaptive immunity and its potential upregulation in human plaques may provide us with a new insight into mechanisms underlying increased plaque vulnerability and disease progression.

5.4.3. Materials and methods

Detailed materials and methods for this manuscript are included in the **Materials and methods** (**Chapter 2**) of this thesis. In brief, PBMCs were isolated from whole blood donated by healthy adult donors and monocytes purified by CD14 positive magnetic selection. Monocytes were differentiated into MDMs over 7 days in M–CSF. On day 7, the media was replaced for 24 h with fresh complete media containing the following polarising agents: IFNγ; LPS; IL–4; IL–10; oxPAPC; CXCL4; or unpolarised as controls in each experiment. Mouse BMDMs, Jurkat cells and transfected THP–1 cells were also used. Gene expression was altered using siRNA and lentiviral plasmid transfections. Gene expression was measured by qRT–PCR, while protein expression was detected using SILAC membrane proteomics, co-immunoprecipitation, mass spectrometry, Western blotting, flow cytometry, immunocytochemistry and immunohistochemistry. Cell interactions were assessed using fluorescence labelling and microscopy. Replicate values (n) represent separate human donors or separate experiments on cell lines of different passages.

5.4.4. Results

5.4.4.1. CALHM6 expressing macrophages may be present in human atherosclerosis

In order to identify improved macrophage phenotype markers, we performed membrane SILAC proteomics on human *in vitro* polarised MDMs from two donors. The data showed that among proteins possibly uniquely up–regulated in $M^{IFN\gamma+LPS}$ a tetraspanin–like protein CALHM6 had the highest fold change (**Table 5.1.**), but the experiments should be repeated more times to validate these results. Interestingly, the expression of *CALHM6* was elevated in atherosclerotic tissue compared to adjacent macroscopically intact tissue in a previously published microarray dataset (Ayari and Bricca, 2013) (**Figure 5.3.A**). We were also able to identify $CD68^+$ macrophages that expressed CALHM6 in a section (n = 1) of carotid plaque taken from one patient, particularly the vulnerable shoulder region (**Figure 5.3.B–D**) and are currently in progress of performing the CD68/CALHM6/SMA (smooth muscle actin) staining in sections from more patients. Furthermore, Kim et al. observed that in their mouse atheroma single–cell RNA–seq macrophages in the interferon response cluster up–regulated expression of *Calhm6* (Kim et al., 2018). These data suggest that CALHM6 may be a potential marker for pro-inflammatory activation of macrophages in plaques, but more biological replicates are needed to support these interpretations.

Table 5.1.: Possibly unique up–regulation of proteins in $M^{IFN\gamma+LPS}$

SILAC membrane proteomics data were filtered for Wilcoxon signed–rank test $M^{IFN\gamma+LPS}$ $p < 0.05$. The data were further filtered by selecting only proteins with $M^{IFN\gamma+LPS}$ incorporation fold change > 1 in both donors (A and B) and ordered by average fold change for $M^{IFN\gamma+LPS}$. Proteins uniquely up–regulated in $M^{IFN\gamma+LPS}$ are highlighted.

No.	ID	Gene	$M^{IFN\gamma+LPS}$ p value	Fold change									
				$M^{IFN\gamma+LPS}$		M^{IL-4}		M^{IL-10}		M^{oxPAPC}		M^{CXCL4}	
				A	B	A	B	A	B	A	B	A	B
1	Q5R3K3	CALHM6	0.002	8.437	8.264								
2	P15309	ACPP	0.027	7.100	5.197		1.000		4.023	1.000	4.065	1.000	
3	P51452	DUSP3	0.047	3.204	5.484		3.175		0.687	4.076		2.775	0.764
4	P62829	RPL23	0.018	4.303	3.147					1.000		2.883	
5	B7Z779	TMEM106A	0.026	4.033	2.947	3.485	2.176					2.918	
6	Q92930	RAB8B	0.025	2.724	2.175		1.559		1.374	0.514	1.771	0.600	
7	Q6IQ22	RAB12	0.035	1.841	2.027	0.326	1.679	1.392	0.326	0.717	1.397	1.944	
8	O14879	IFIT3	0.002	1.877	1.746								
9	P18031	PTPN1	0.013	1.794	1.386					0.786		1.256	
10	P48735	IDH2	0.027	1.625	1.527	1.414	0.798	0.305	1.483	1.251	1.455	1.458	1.074
11	P32455	GBP1	0.027	1.554	1.597	1.338	0.864		0.223	0.776	1.068	1.333	
12	Q9BQE5	APOL2	0.025	1.675	1.372	0.948		0.907		1.177	1.161	1.094	
13	Q9NR31	SAR1A	0.050	1.728	1.171	1.504	0.777			0.230	0.230	0.989	1.148
14	Q03518	TAP1	0.037	1.515	1.331	0.210	1.122	0.364	0.548	1.270	1.007	1.101	1.389
15	Q9NQ34	TMEM9B	0.003	1.379	1.347								
16	P14902	IDO1	0.003	1.361	1.340								
17	Q12913	PTPRJ	0.027	1.343	1.253		1.205	0.966	0.670	0.777	1.034	1.005	
18	Q9P0S9	TMEM14C	0.016	1.410	1.145	2.697							
19	Q8WXG1	RSAD2	0.002	1.254	1.276								
20	Q96RQ9	IL4I1	0.007	1.390	1.083							1.020	
21	Q9H0D6	XRN2	0.019	1.265	1.187	1.002	0.987						
22	E9PC70	CD82	0.022	1.300	1.125		1.350			0.998			
23	Q07065	CKAP4	0.038	1.176	1.225	0.666	1.040	0.978	1.118	0.892	1.108	1.183	
24	Q9H3N1	TMX1	0.011	1.177	1.190	1.027	1.015	0.883	1.103	0.939	1.072	1.009	1.140
25	Q03405	PLAUR	0.025	1.141	1.129			0.902	0.914	0.873	1.109	0.946	
26	Q9GZP9	DERL2	0.039	1.137	1.092	0.955	0.923						
27	P04179	SOD2	0.037	1.085	1.142	0.516	1.052		1.051	0.646	0.894	0.903	0.946
28	O15243	LEPROT	0.003	1.138	1.054								
29	Q8TCU6	PREX1	0.033	1.160	1.018		0.965					0.887	

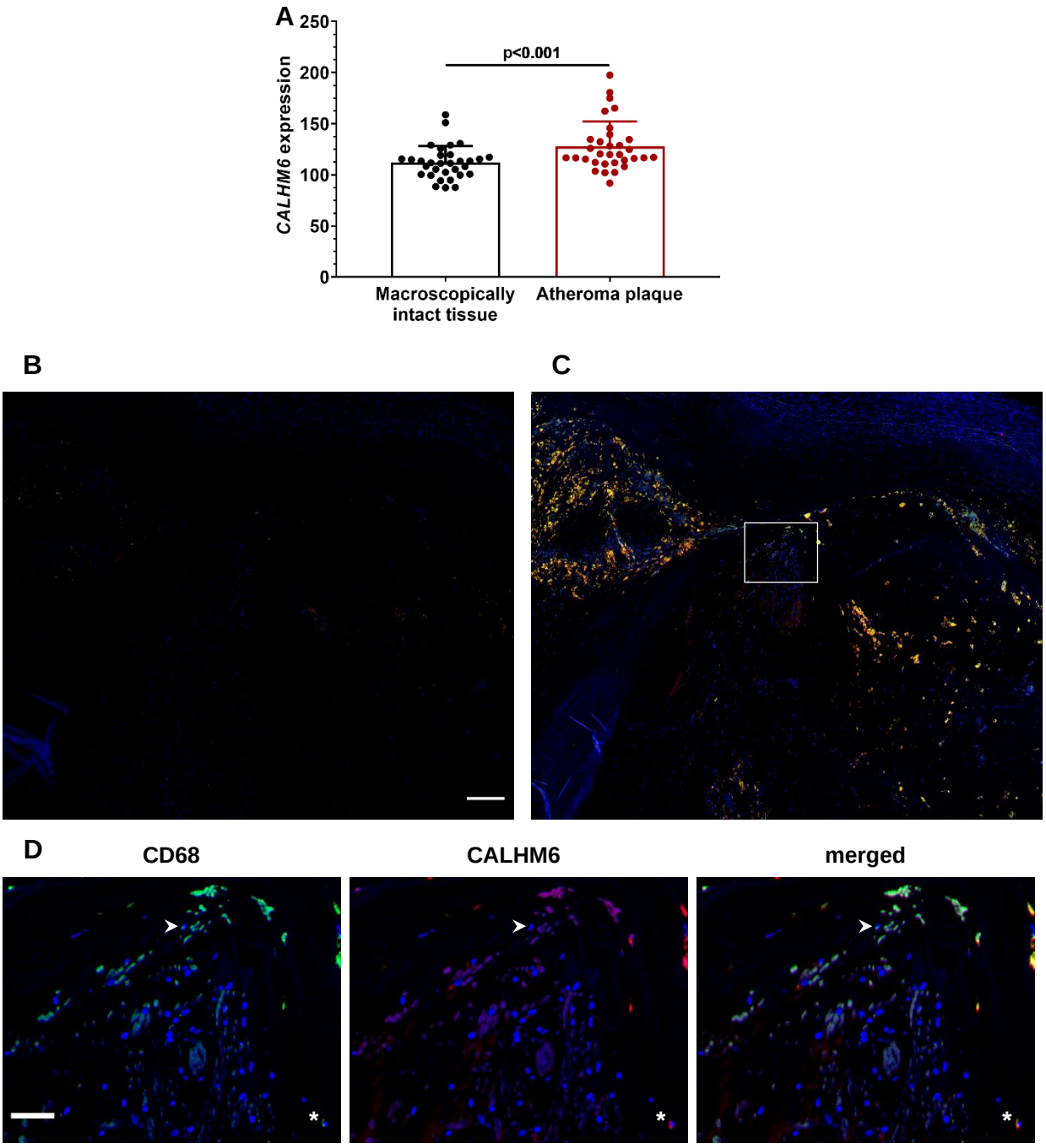

Figure 5.3.: Macrophages may express CALHM6 in human atherosclerosis.

(**A**) Quantification of GSE43292 data for gene expression in macroscopically normal adjacent and carotid plaque tissue; means ± SEMs, n = 32, paired two–tailed t–test. Immunohistochemistry/immunofluorescence staining of human carotid artery plaque section (n = 1) for (**B**) mouse (green) and rabbit (red) control IgG and also (**C**) CD68 (pan-macrophage marker, green) and CALHM6 (red) ($CD68^+CALHM6^+$ in yellow), cell nuclei stained with DAPI (blue), scale bar represents 200 µm for both images. (**D**) Enlarged white binding box in (**C**) arrow heads indicate $CD68^+CALHM6^-$ and asterisks indicate $CD68^+CALHM6^+$; scale bar represents 50 µm for all three images.

5.4.4.2. CALHM6 is up–regulated in IFNγ (and LPS) activated macrophages

The identification of CALHM6^{+} macrophages in a section from one human plaque and its possible up–regulation in human M$^{IFN\gamma+LPS}$ was further investigated *in vitro*. RNA–seq results from our previous study (see **Chapter 3**) showed unique up–regulation of *CALHM6* expression in human M$^{IFN\gamma+LPS}$ inflammatory macrophages, compared to all other macrophage phenotypes (**Figure 5.4.A**). In addition, human macrophage *in vitro* exposure to statins before and during polarisation with IFNγ+LPS did not have a significant effect on *CALHM6* expression (**Figure 5.5.**). Xue et al. in their transcriptomic study observed that both IFNγ and LPS separately induced *CALHM6* expression (Xue et al., 2014). We tested the level of *CALHM6* up–regulation by IFNγ and LPS treatment alone in our *in vitro* human macrophage model where we found that both IFNγ and LPS were capable of significantly inducing *CALHM6* expression (**Figure 5.4.B**).

Immunocytochemistry microscopy of macrophage phenotypes indicated that up–regulation of CALHM6 protein was unique to M$^{IFN\gamma+LPS}$ among our polarisation conditions (**Figure 5.4.C** and **Figure 5.6.**), supporting our observation in membrane SILAC proteomics. Interestingly, following separate treatment with IFNγ or LPS, only IFNγ significantly induced CALHM6 protein expression (**Figure 5.4.D** and **Figure 5.7.**).

In order to assess whether CALHM6 is specifically up–regulated in inflammatory macrophages in other mammalian species, mouse BMDMs were activated with IFNγ+LPS. This treatment significantly and uniquely up–regulated mouse macrophage *Calhm6* expression compared to other polarisation conditions (**Figure 5.4.E**). We concluded that CALHM6 was an *in vitro* human pro-inflammatory macrophage maker at both transcript and protein level that could potentially be used to assess human patient and mouse model atherosclerosis samples.

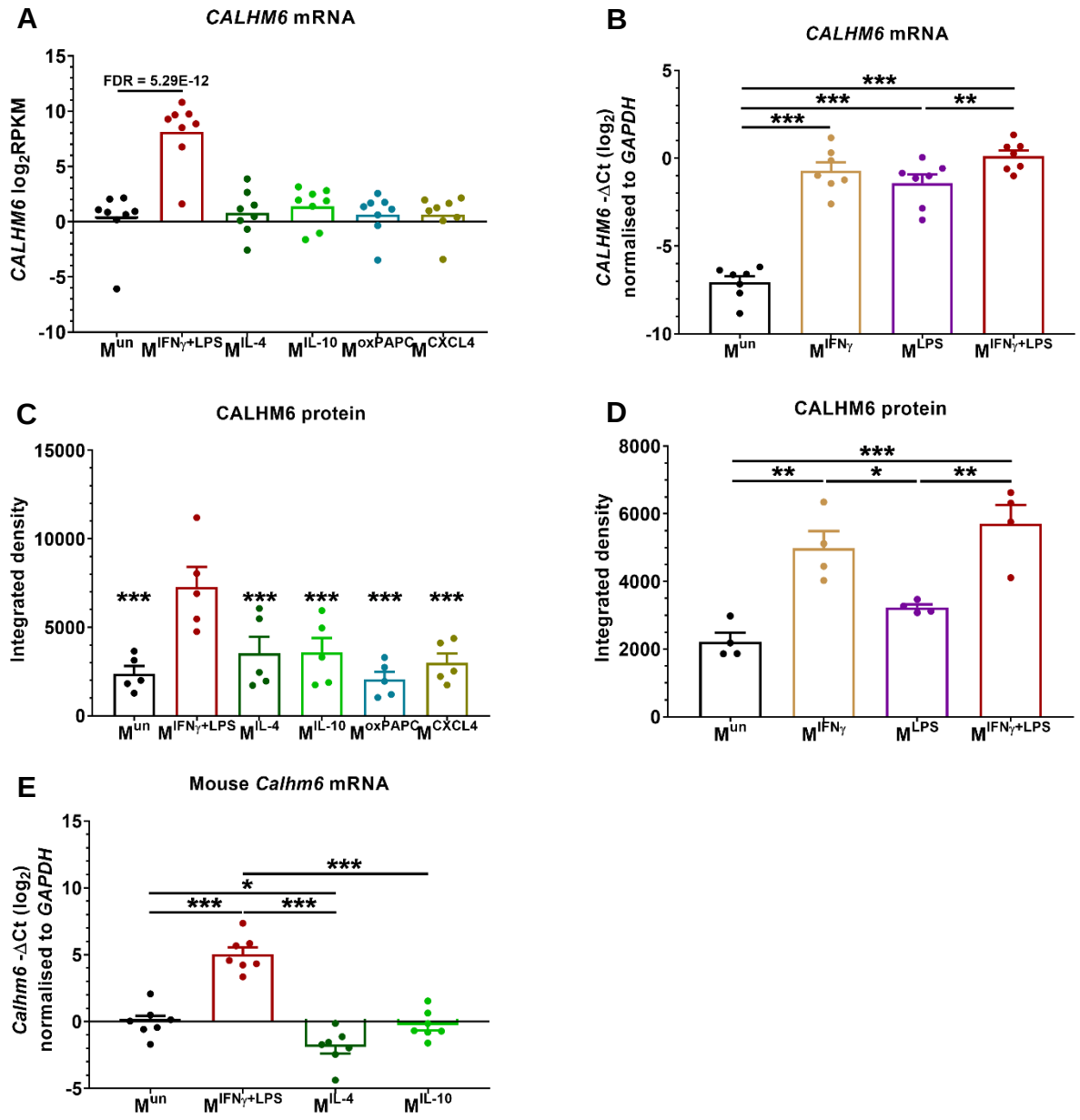

Figure 5.4.: CALHM6 is an *in vitro* marker for macrophages activated with IFNγ (and LPS). (**A**) RNA-seq quantification of *CALHM6* expression among MDM phenotypes compared to M^{un}; n = 8, mean of RPKM (reads per kilobase [of transcript per] million [mapped reads]) and FDR (false discovery rate, Benjamini and Hochberg method) shown. (**B**) qRT–PCR quantification of *CALHM6* gene expression upon stimulation with IFNγ and/or LPS; n = 7. Pooled quantification (10 images/condition, geometric means of integrated densities from each experiment shown as data points) of CALHM6 antibody staining (**C**) of MDM phenotypes (n = 5) and (**D**) of unpolarised, IFNγ and/or LPS–activated MDMs (n = 4). (**E**) qRT–PCR quantification of mouse BMDM *Calhm6* gene expression; n = 7. (**B – E**) Means ± SEMs, matched/repeated measures one–way ANOVA with Tukey's post test * $p < 0.05$, ** $p \leq 0.01$, *** $p \leq 0.001$, only significant comparisons are shown (for **C** M^{x} vs $M^{IFN\gamma+LPS}$).

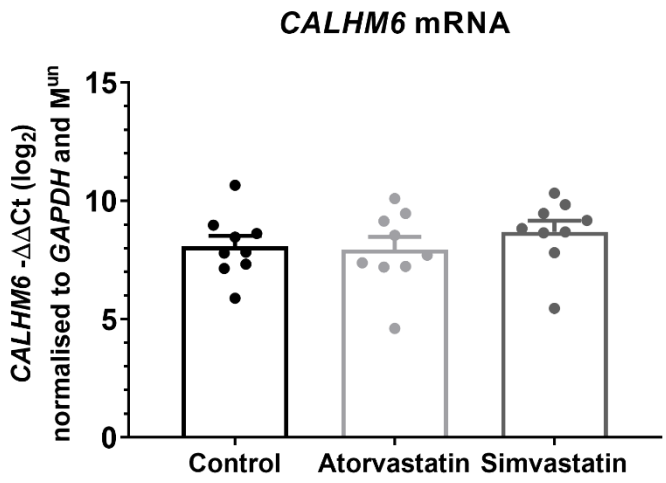

Figure 5.5.: Expression of *CALHM6* is not changed by atorvastatin or simvastatin.

qRT–PCR quantification of *CALHM6* expression in human MDMs pre-treated with 1µM atorvastatin or simvastatin 4 h before polarisation in fresh media containing both the statin and IFNγ+LPS. The data were normalised to *GAPDH* and M^{un} using the -ΔΔCt method and shown here in log_2; means ± SEMs, n = 9, matched/repeated measures one–way ANOVA with Dunnett's post test of atorvastatin or simvastatin vs control cells (no statin in the pre-treatment or the IFNγ+LPS polarisation), both comparisons were not significant.

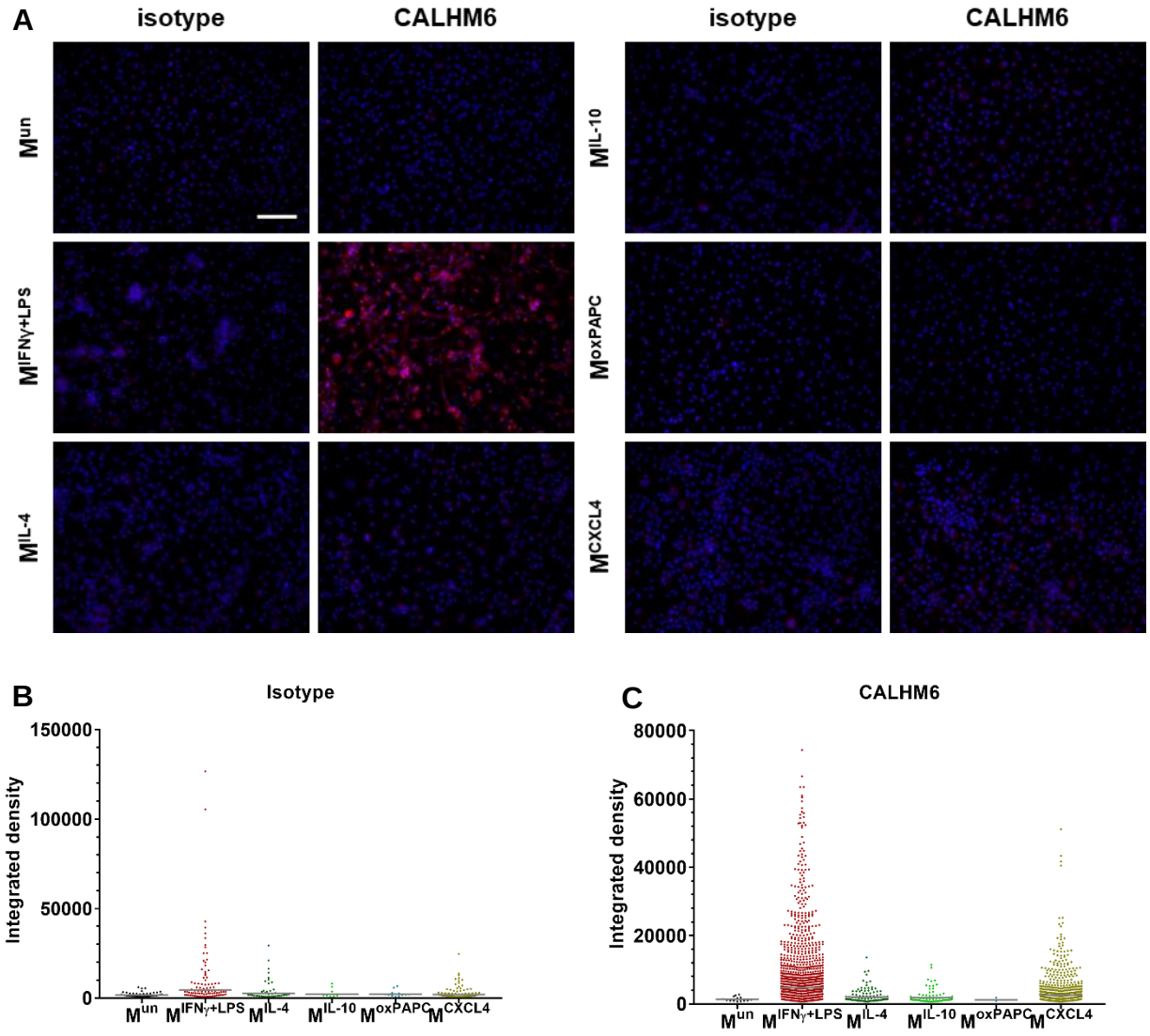

Figure 5.6.: Representative images and quantification of CALHM6 in MDM phenotypes.
(**A**) Representative images of one donor cell staining with DAPI (blue) or isotype/CALHM6 antibodies (red), scale bar represents 100 µm for all images. Quantification of (**B**) isotype and (**C**) CALHM6 antibody staining in the representative experiment shown; 10 images/condition, geometric means indicated.

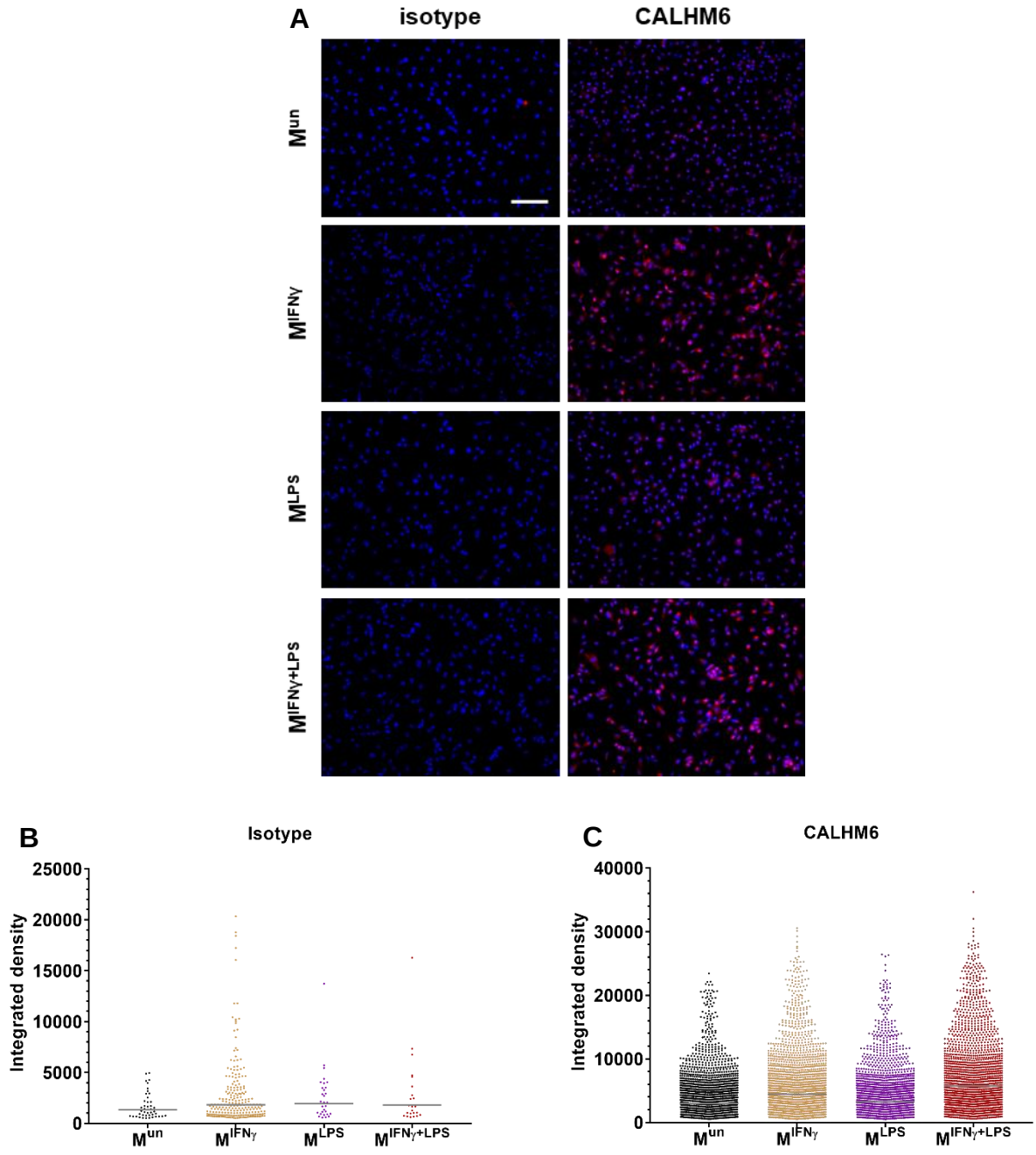

Figure 5.7.: Representative images and quantification of CALHM6 in MDMs activated with IFNγ and/or LPS.

(**A**) Representative images of one donor cell staining with DAPI (blue) or isotype/CALHM6 antibodies (red), scale bar represents 100 µm for all images. Quantification of (**B**) isotype and (**C**) CALHM6 antibody staining in the representative experiment shown; 10 images/condition, geometric means indicated.

5.4.4.3. CALHM6 is an IFNγ and non-canonical LPS response gene

Since identifying specific up–regulation of CALHM6 in pro-inflammatory macrophages we investigated which pathways were involved in activating transcription of the gene. Meanwhile, Ebihara et al. concluded that upon TLR3 stimulation with poly(I:C) mouse BMDCs and NK cells up–regulated *Calhm6* expression via the TLR3/TICAM1/IRF3 signalling axis (Ebihara et al., 2010).

We therefore investigated whether the IFNGR and TLR4 (major receptors for IFNγ and LPS, respectively (Diamond et al., 2015, Majoros et al., 2017, Michalska et al., 2018)) non-canonical signalling pathways induce *CALHM6* expression in our human macrophage model. Human MDMs were treated with siRNA targeting *MYD88* (myeloid differentiation primary response protein 88), *TICAM1* (canonical [NF–κB] and non-canonical TRL4 signalling pathway components respectively) or *STAT1* (downstream of IFNGR) followed by polarisation with IFNγ and/or LPS, knockdown confirmation (**Figure 5.8.A**) and assessment of the impact on CALHM6 induction (**Figure 5.8.A**). Analysis showed that reduced *MYD88* expression did not significantly affect *CALHM6* induction, while *TICAM1* and *STAT1* knockdown both significantly decreased *CALHM6* expression upon activation with LPS or IFNγ (**Figure 5.8.B**). These findings indicate that STAT1 and non-canonical TLR4 signalling are involved in induction of *CALHM6*.

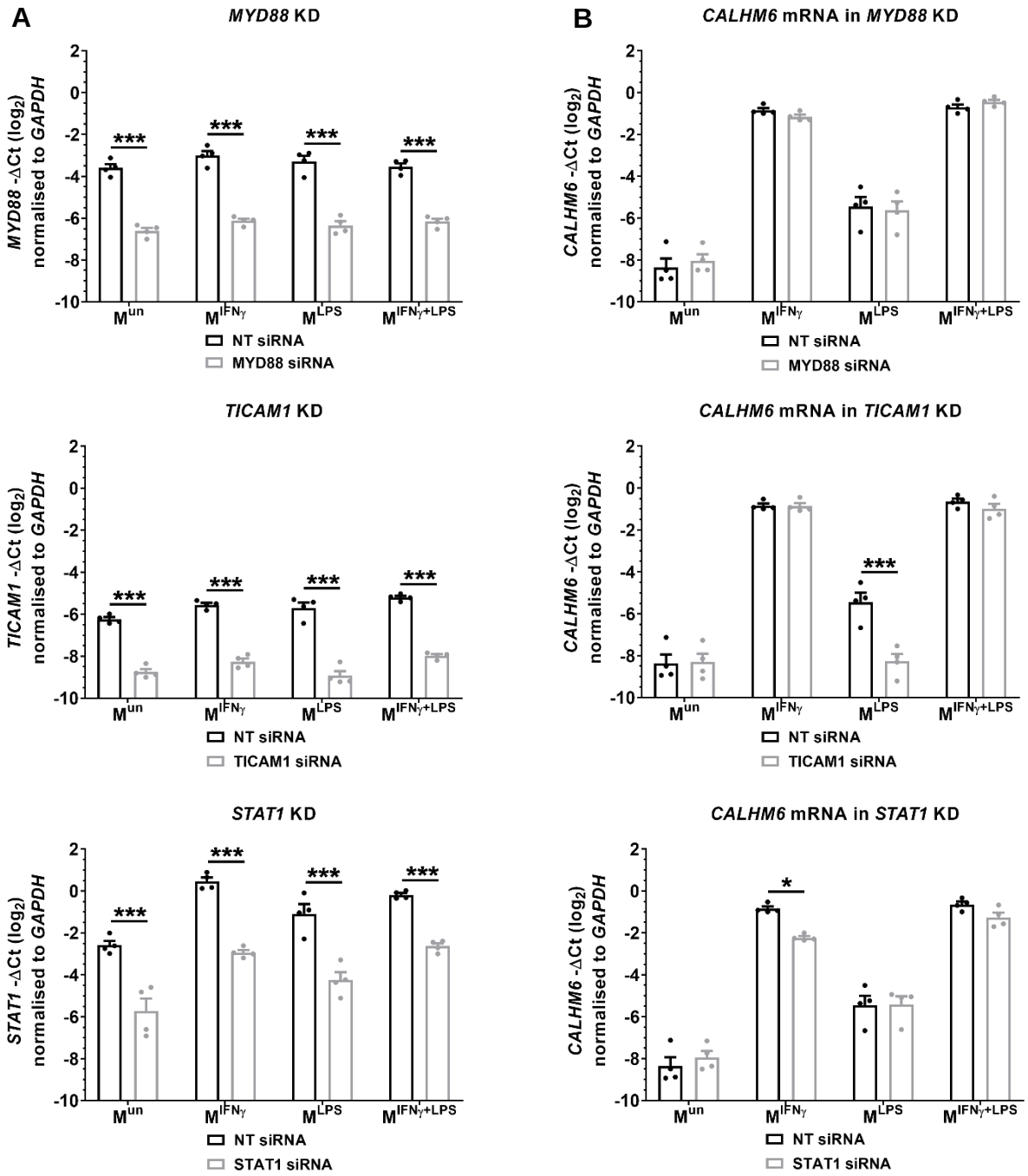

Figure 5.8.: Induction of *CALHM6* gene expression is dependent on *STAT1* and *TICAM1*.
(**A**) qRT–PCR quantification of *MYD88*, *TICAM1* and *STAT1* gene siRNA knockdowns in differentially activated human MDMs. (**B**) qRT–PCR quantification of *CALHM6* gene expression in siRNA knockdowns of *MYD88*, *TICAM1* and *STAT1* in differentially activated human MDMs. The data were normalised to *GAPDH* using the -ΔCt method and shown here in $\log_2$; NT – non-targeting siRNA, n = 4, means ± SEMs, matched/repeated measures two–way ANOVA with Sidak's post test; * $p \leq 0.05$ *** $p \leq 0.001$ compared to NT siRNA of the same polarisation.

5.4.4.4. CALHM6 may regulate STAT1 phosphorylation and chemokine expression

Our findings suggested that induction of CALHM6 is associated with IFNγ signalling. We also wished to determine if CALHM6 itself regulated IFNγ signalling pathways, in a potential regulatory feedback mechanism. IFNγ–induced signalling is relayed via STAT1, the activity of which in inducing transcription of target genes depends on its phosphorylation: Y701 phosphorylation is required for STAT1 to dimerise, translocate from the cytoplasm to the nucleus and bind DNA to initiate target gene transcription (Ramana et al., 2002). We speculated that CALHM6 regulates STAT1 phosphorylation. We inhibited *CALHM6* expression using siRNA, activated the cells with 20 ng/ml IFNγ for 24 h and measured gene expression by qRT–PCR and protein expression by western blotting. We were able to consistently knockdown *CALHM6* gene expression in our model (95.81 ± 0.73% SEM knockdown efficiency, **Figure 5.9.A**). In a preliminary trial experiment (n = 1) *CALHM6* knockdown resulted in a decreased Y701 phosphorylated STAT1 signal compared to non-targeting control siRNA treatment (**Figure 5.9.B** and **C**). This suggests that CALHM6 could be able to affect STAT1 activity, but confirmation of this is needed by repeating the experiment more times, which is currently in progress.

A previous report indicated that CALHM6 is involved in NK cell activation via cell–to–cell contact by $CD8\alpha^+$ conventional DCs or macrophages, involving IFNγ and leading to reduced volume and metastases of IFNγ–sensitive tumours in mice (Ebihara et al., 2010, Kasamatsu et al., 2014). We therefore tested if CALHM6 is involved in regulating the expression of chemokines, which are known chemoattractants and activators of lymphocytes and in many cases are known to be regulated by IFNγ/IFNGR/STAT1. We observed in human MDM that *CALHM6* siRNA knockdown leads to significantly reduced expression of *CCL5*, *CXCL8* and *CXCL11* (**Figure 5.9.D**, **E** and **G**), while *CXCL9* expression was not statistically significantly altered (**Figure 5.9.F**).

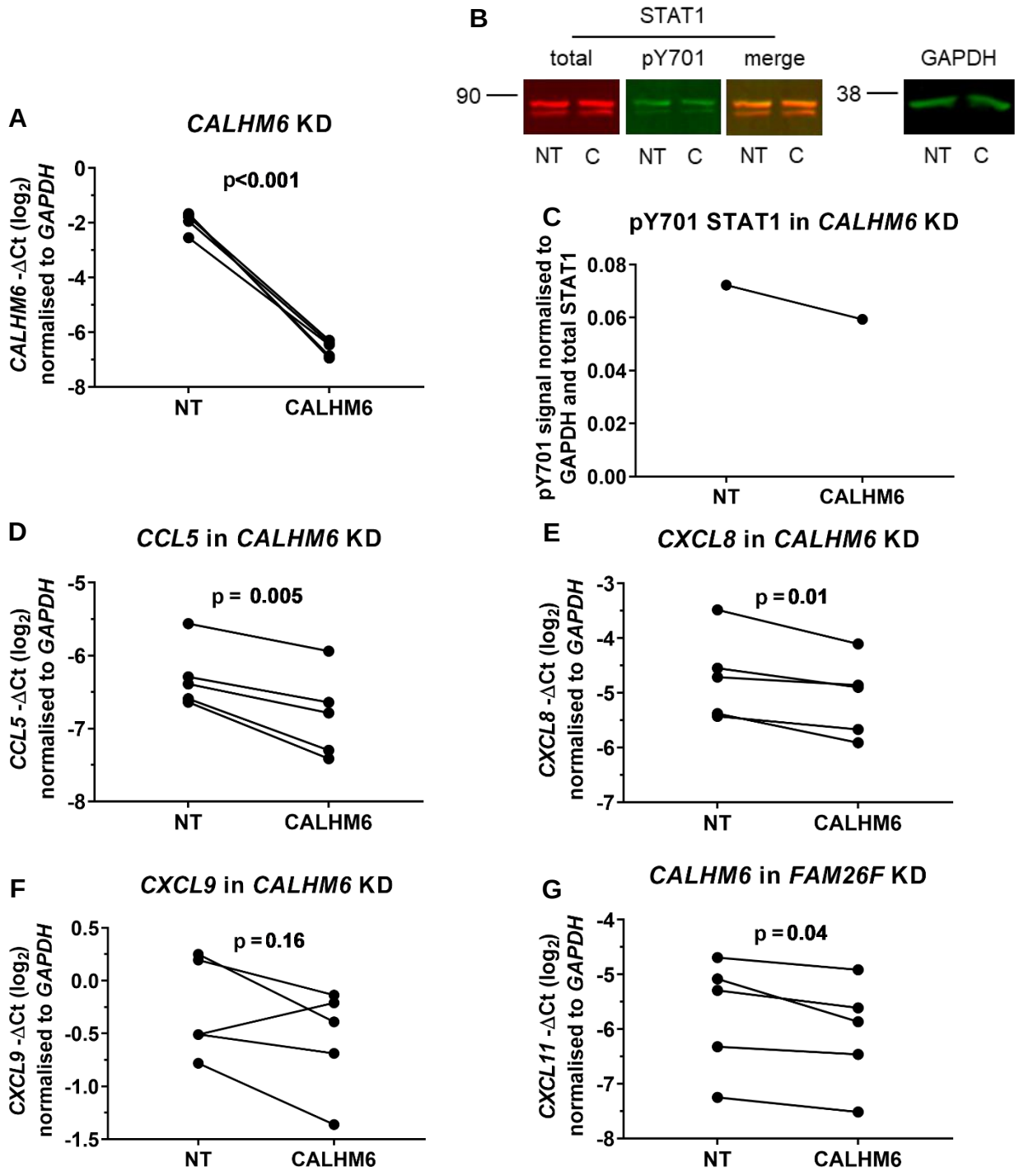

Figure 5.9.: *CALHM6* knockdown may attenuate STAT1 phosphorylation and chemokine expression.

(continued on the next page)

Figure 5.9.: *CALHM6* knockdown may attenuate STAT1 phosphorylation and chemokine expression (continued).

(**A**) qRT–PCR quantification of *CALHM6* gene expression in cells treated with non-targeting (NT) or *CALHM6* siRNA, followed by activation with IFNγ. (**B**) Western blot for phosphorylated Y701 and total STAT1, GAPDH; NT – non-targeting siRNA, C – CALHM6 siRNA, numbers indicate molecular weight standards in kDa. (**C**) Quantification of fluorescence of phosphorylated Y701 STAT1 normalised to GAPDH and total STAT1 (n = 1). (**D**–**G**) qRT–PCR quantification of gene expression in cells treated with non-targeting (NT) or *CALHM6* siRNA, followed by activation with IFNγ. (**A** and **D**–**G**) The data were normalised to *GAPDH* using the -ΔCt method and shown here in $\log_2$; n = 5, lines connect samples from the same donor, paired two–tailed t test.

5.4.4.5. CALHM6 may interact with LAT in pro-inflammatory THP–1 macrophages and promote macrophage–T cell interactions

In order to gain insight into the mechanism of activation of CALHM6, we sought to identify CALHM6 protein–protein interaction partners. We created a CALHM6–3×FLAG stably expressing THP–1 cell line (**Figure 5.10.**) for use in co–immunoprecipitation. Anti-FLAG beads were used on control ("empty" vector) and CALHM6–3×FLAG IFNγ+LPS THP–1 lysates to precipitate CALHM6 and interacting proteins in two separate experiments (**Figure 5.11.A**). We identified peptides of 25 human proteins unique to CALHM6–3×FLAG samples that were shared between the two experiments (**Table 5.2.**). Out of these proteins some were of particular interest due to their function and cellular localisation: dermcidin (DCD) among its other functions displays anti-microbial activity (Schittek et al., 2001) and LAT is an adapter protein involved in lymphocyte activation (Fuller and Zhang, 2009, Sommers et al., 2004). We were able to find interaction of LAT, but not DCD with CALHM6–3×FLAG in one additional co–immunoprecipitation involving samples of our THP–1s co-cultured with Jurkat cells (**Figure 5.11.B** and **C**) and are currently testing the co–immunoprecipitation elutions from experiments with only THP–1s to further test the presence of LAT.

Since LAT is involved in lymphocyte activation (Fuller and Zhang, 2009, Sommers et al., 2004), and because mouse CALHM6 has been implicated in DC/macrophage to NK cell interactions (Ebihara et al., 2010, Kasamatsu et al., 2014), we wished to determine whether the CALHM6/LAT expression influences macrophage–lymphocyte binding. We therefore co-cultured fluorescently labelled human T-cells with macrophages, with or without overexpression or knock down of CALHM6. In a trial experiment (n = 1) we applied PHK-labelled differentiated Jurkat T cells to differentiated and IFNγ+LPS polarised THP–1 cells overexpressing CALHM6–3×FLAG construct (or "empty" control THP-1s). The interaction between THP-1 and Jurkat cells was assessed using fluorescence microscopy and analysed by quantifying cells under contact (**Figure 5.11.D**). In this one experiment a higher proportion of Jurkat cells interacted with THP–1s overexpressing CALHM6–3×FLAG compared to "empty" control THP-1 cells (**Figure 5.11.E**). These preliminary data may indicate that CALHM6 may function in human macrophage and lymphocyte cell lineage interaction due to its probable association with proteins known to be involved in the process as well as increased proportion of lymphocyte–like cells attaching to CALHM6 overexpressing macrophage–like cells upon pro-inflammatory activation, however, the experiments presented here should be repeated more times support such interpretations.

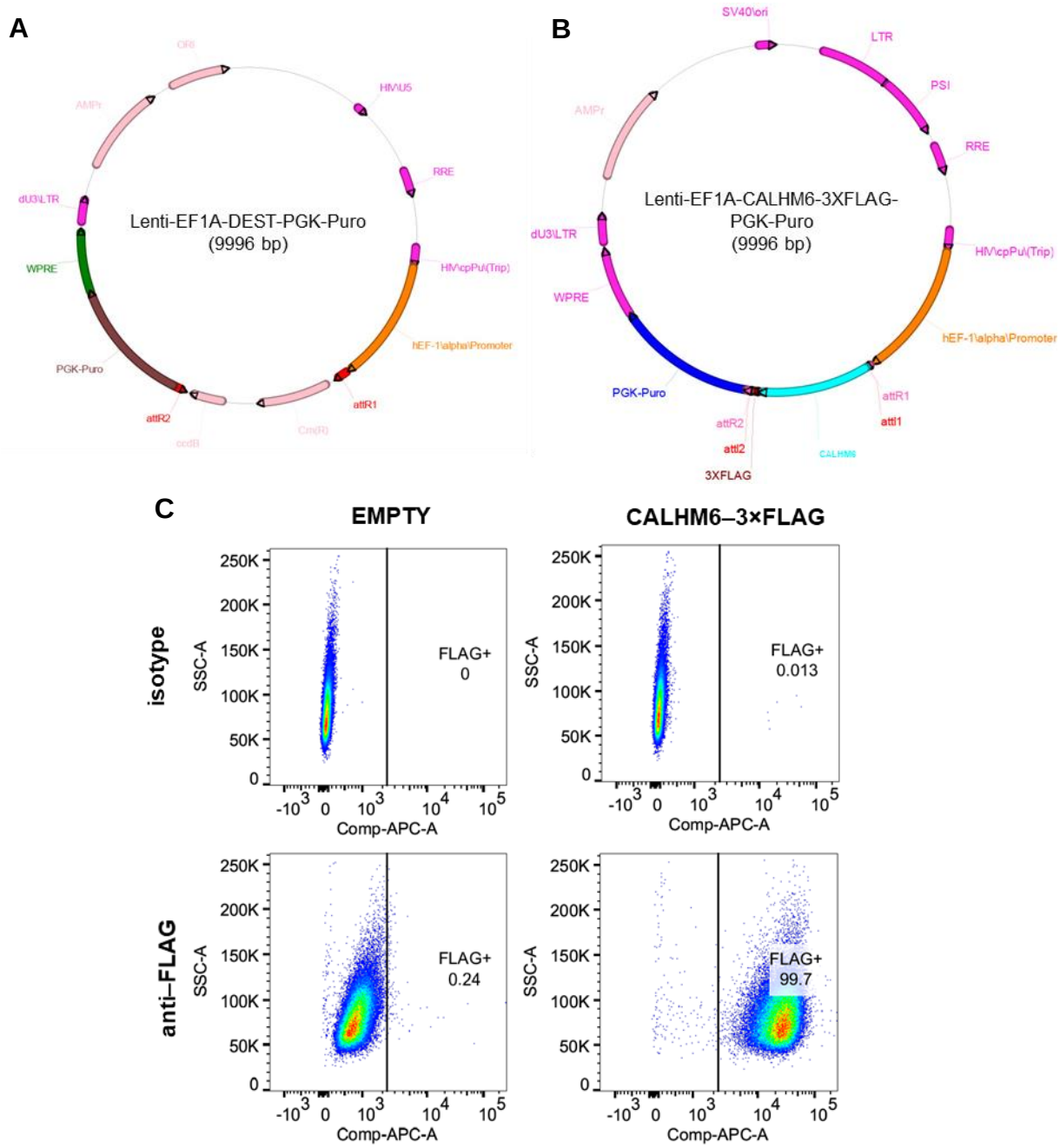

Figure 5.10.: CALHM6–3×FLAG expression construct.

Maps of (**A**) control (“empty”) and (**B**) CALHM6–3×FLAG plasmids transfected into monocytic THP–1s; CALHM6 shown in light blue. (**C**) Flow cytometry testing for FLAG in monocytic THP–1s.

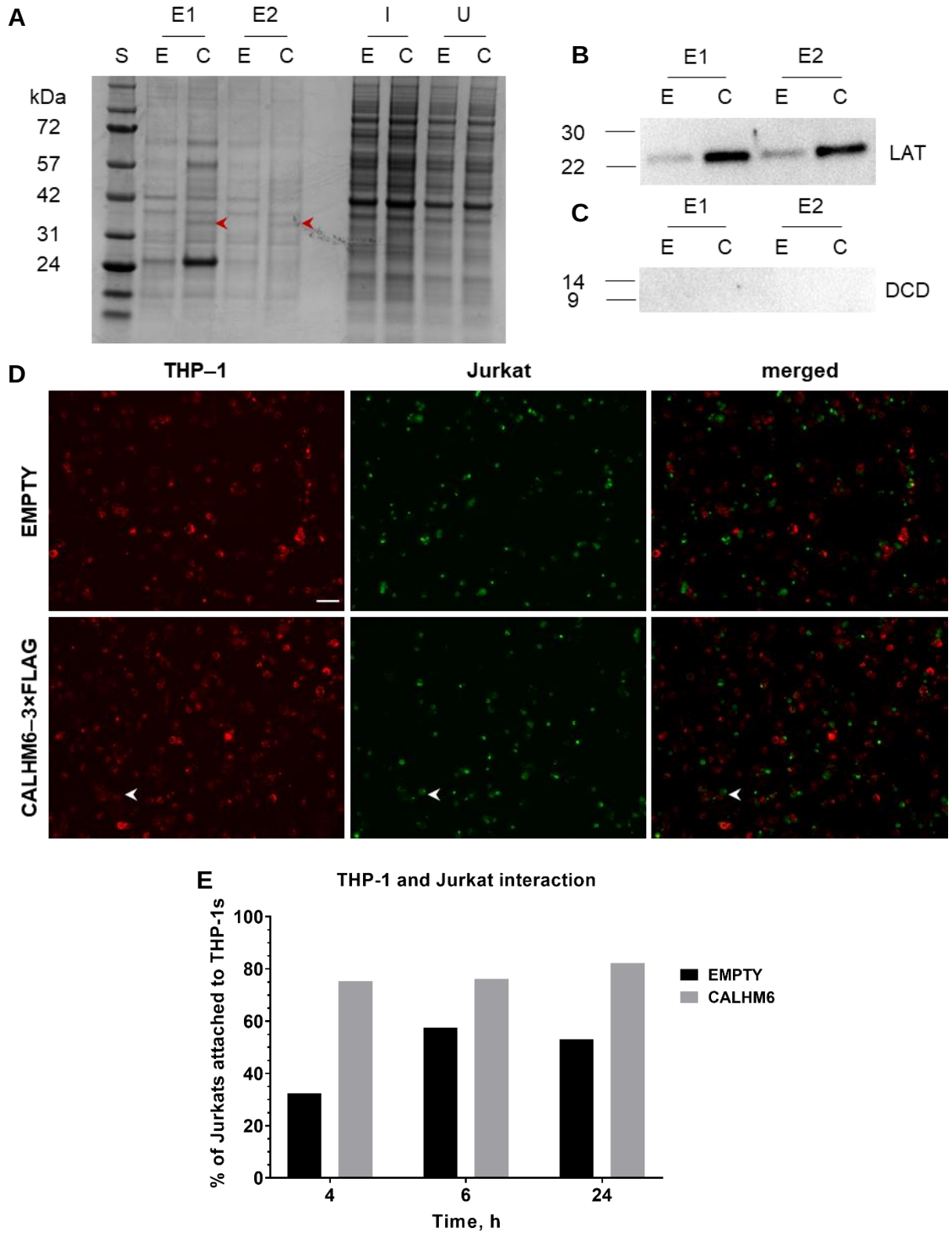

Figure 5.11.: CALHM6 may regulate macrophage interaction with lymphocytes.

(continued on the next page)

Figure 5.11.: CALHM6 may regulate macrophage interaction with lymphocytes (continued). (**A**) Representative Coomassie Blue staining of CALHM6–3×FLAG co-immunoprecipitation; E1 – bound sample elution 1, E2 – bound sample elution 2, I – input sample lysate, U – unbound sample lysate, E – "empty" vector control THP–1s, C – CALHM6–3×FLAG THP–1s, S – molecular weight standards; arrow heads indicate predicted CALHM6–3×FLAG protein molecular weight (~37.3 kDa). Western blots of co-immunoprecipitation elutions of THP–1 and Jurkat co-culture samples for (**B**) LAT (linker for activation of T cells, predicted molecular weight ~24.8 – 28.6 kDa) and (**C**) DCD (dermicidin, predicted molecular weight ~8.3 – 12.4 kDa); numbers indicate molecular weight standards in kDa, n = 1. (**D**) Representative images of THP–1 (red) and Jurkat (green) co-culture, scale bar represents 50 µm for all images, arrow heads indicate THP–1 and Jurkat interaction, EMPTY – THP–1 "empty" vector control cells. (**E**) Quantification of percentage of Jurkat cells attached to THP–1 cells at 4, 6 and 24 h of co-culture; means of 2 – 4 fields of view, n = 1.

Table 5.2.: Proteins detected only in CALHM6–3×FLAG samples in both co-immunoprecipitation experiments.

UniProt IDs and names are listed for the proteins, peptides of which were detected only in CALHM6–3×FLAG samples in both experiments.

	Identifiers	Proteins
1	sp|P49748|ACADV_HUMAN; tr|G3V1M7|G3V1M7_HUMAN	Acyl-CoA dehydrogenase very long chain
2	sp|Q0VD83|APOBR_HUMAN	Apolipoprotein B receptor
3	sp|Q9BT09|CNPY3_HUMAN	Canopy FGF signaling regulator 3
4	tr|J3QKQ4|J3QKQ4_HUMAN; sp|Q9UGN4|CLM8_HUMAN	CD300a
5	sp|P81605|DCD_HUMAN	Dermcidin
6	sp|P49411|EFTU_HUMAN	Elongation factor Tu, mitochondrial
7	sp|P30040|ERP29_HUMAN; tr|F8VY02|F8VY02_HUMAN	Endoplasmic reticulum protein 29
8	tr|H0YDT8|H0YDT8_HUMAN; sp|Q9NPA0|EMC7_HUMAN	ER membrane protein complex subunit 7
9	tr|D6RBH1|D6RBH1_HUMAN; tr|D6RDX1|D6RDX1_HUMAN; tr|D6RBV2|D6RBV2_HUMAN; sp|Q12907|LMAN2_HUMAN	Lectin, mannose binding 2
10	tr|A0A1W2PQT7|A0A1W2PQT7_HUMAN; sp|O43561|LAT_HUMAN	Linker for Activation of T cells
11	sp|P29966|MARCS_HUMAN	Myristoylated alanine rich protein kinase C substrate
12	sp|P30044|PRDX5_HUMAN	Peroxiredoxin 5
13	sp|Q9UHV9|PFD2_HUMAN	Prefoldin subunit 2
14	tr|F8VR77|F8VR77_HUMAN; sp|Q9UQ80|PA2G4_HUMAN	Proliferation-associated 2G4
15	tr|A0A087WVV1|A0A087WVV1_HUMAN; sp|P49721|PSB2_HUMAN	Proteasome subunit beta 2
16	sp|P13667|PDIA4_HUMAN	Protein disulfide isomerase family A member 4
17	sp|P78527|PRKDC_HUMAN	Protein kinase, DNA-activated, catalytic subunit
18	sp|P61020|RAB5B_HUMAN	RAB5B, member RAS oncogene family
19	sp|P49792|RBP2_HUMAN	RAN binding protein 2

Table 5.2. (continued).

	Identifiers	Proteins
20	tr|J3KRE2|J3KRE2_HUMAN; tr|J3KTF8|J3KTF8_HUMAN; sp|P52565|GDIR1_HUMAN; tr|J3QQX2|J3QQX2_HUMAN	Rho GDP-dissociation inhibitor 1
21	sp|O14828|SCAM3_HUMAN	Secretory Carrier Membrane Protein 3
22	tr|A0A0C4DFV9|A0A0C4DFV9_HUMAN; sp|Q01105|SET_HUMAN; tr|A0A087X027|A0A087X027_HUMAN; sp|P0DME0|SETLP_HUMAN	SET nuclear proto-oncogene
23	sp|P08240|SRPRA_HUMAN	SRP receptor subunit alpha
24	sp|Q9Y320|TMX2_HUMAN	Thioredoxin related transmembrane protein 2
25	sp|O60763|USO1_HUMAN	USO1 vesicle transport factor

5.4.5. Discussion

Pro-inflammatory macrophages are an integral part of chronic inflammatory disease progression: in atherosclerosis such cells have long been associated with elevated plaque instability and therefore risk of severe complications (Stoger et al., 2012). Numerous marker transcripts and proteins have been used to identify pro-inflammatory macrophages in pathologies (Chinetti-Gbaguidi et al., 2015), but without thorough validation even *in vitro* for polarisation specificity, up–regulation at transcript and protein level and use across species.

We have identified a novel human pro-inflammatory macrophage marker CALHM6, increased expression of which was specific to $M^{IFN\gamma+LPS}$ at both transcript and protein level as shown in RNA–seq (n = 8, expression differences between M^{x} and M^{un} confirmed by qRT–PCR using parallel samples for other selected genes in **Figure 3.4.**) and in part supported by qRT–PCR on separate samples (n = 7, **Figure 5.4.B**) as well as shown by immunocytochemistry (n = 5). These findings are in agreement with previously published human macrophage transcriptomes (Xue et al., 2014) and proteomics for $M^{IFN\gamma}$ (Brown et al., 2010). We also showed that mouse $M^{IFN\gamma+LPS}$ increased expression of *Calhm6* compared to M^{un}, while M^{IL-4} and M^{IL-10} did not. In addition, in their mouse atheroma live $CD45^{+}$ single cell RNA–seq study Kim et al. observed that cells with higher expression of *Calhm6* also displayed increased expression of interferon–stimulated genes (Kim et al., 2018). We were able to identify $CD68^{+}$/$CALHM6^{+}$ cells in one section of human carotid artery atherosclerosis (currently performing further biological replicates to validate interpretation) and show that human macrophage *in vitro* exposure to simvastatin or atorvastatin did not significantly alter *CALHM6* expression. We therefore propose that with additional human atheroma section staining and *in vitro* experiments, such as assessing the influence of modified lipoprotein loading to macrophage *CALHM6* gene and protein expression, CALHM6 could be used as a new marker across mouse model and human atherosclerosis to characterise macrophages.

Similarly to published literature on mouse smooth muscle cells (Chmielewski et al., 2014), we concluded that STAT1 was involved in regulating *CALHM6* expression upon human macrophage stimulation with IFNγ as well as showed that TICAM1 participated in *CALHM6* induction upon LPS challenge. Involvement of murine TICAM1 in induction of *Calhm6* gene expression in DCs and macrophages stimulated with poly(I:C) has been shown before (Ebihara et al., 2010, Kasamatsu et al., 2014). However, following stimulation with poly(I:C) mouse *Ifnar1* (part of the IFNα/β receptor) splenocytes failed to up–regulate expression of *Calhm6* (levels similar to unstimulated), while *Ticam1* or *Irf3* (downstream of *Ticam1*) knockout splenocytes up–regulated *Calhm6* expression to a similar or lower level, respectively (Kasamatsu et al., 2014). Further studies are needed to elucidate if potential involvement of type I IFN signalling in CALHM6

induction (especially *in vivo*) is shared among myeloid cells and different activating molecules or is specific to stimulation with double–stranded RNA and its mimics. Interestingly, in one trial experiment CALHM6 knockdown using siRNA resulted in a lower proportion of STAT1 phosphorylated at Y701, indicating that CALHM6 may be involved in a feedback loop that regulates phosphorylation and therefore transcriptional activity of STAT1, but more repeats and at shorter (15 – 60 min) IFNγ stimulations are needed to confirm this.

Furthermore, we observed significantly lower expression of *CCL5*, *CXCL8* and *CXCL11* in our *CALHM6* siRNA knockdown human macrophages. All three genes encode chemokines, which function in leukocyte recruitment, and *CXCL11* in particular is an IFNγ–inducible gene (Griffith et al., 2014, Tokunaga et al., 2018). Regulation of these and other leukocyte attractants could be an additional mechanism of CALHM6 bridging innate and adaptive immunities to the previously shown mouse antigen presenting cell–to–cell activation of NK cells to control IFNγ–sensitive tumours (Ebihara et al., 2010, Kasamatsu et al., 2014). Also, in our experiments on macrophage–like IFNγ+LPS CALHM6–3×FLAG THP–1s, CALHM6 co-precipitated with LAT (n = 2) (involved in T cell activation (Fuller and Zhang, 2009, Sommers et al., 2004)) and we are currently performing confirmatory experiments (also involving Jurkat cells as a T cell model) to support these results, but the co-immunoprecipitation and spectrometry need to be repeated more times. We also used both THP–1s and Jurkats in another trial experiment to show that increased CALHM6 expression in THP–1 macrophages resulted in a higher percentage of Jurkat cells attaching to them compared to the "empty" vector control THP–1 cells. These findings potentially build upon the reports published by Ebihara et al. and Kasamatsu et al. (Ebihara et al., 2010, Kasamatsu et al., 2014) by showing that similarly to mouse cells CALHM6 may also be involved in regulating human myeloid and lymphocyte cell interactions.

Our data support the notion that CALHM6 could be used in a panel of markers for detection of pro-inflammatory macrophages in research and diagnostics of cardiovascular disease. Future studies should focus on identifying the function of CALHM6, particularly in the potential interplay between innate and adaptive immunities in chronic inflammatory diseases as well as acute infections, which have been proposed as a risk factor contributing to late stage atheroma destabilisation. Following this CALHM6 could be exploited as a new drug target in limiting or enhancing leukocyte recruitment and activation.

5.4.6. Funding, acknowledgements, author contributions and conflict of interest

Funding

This work was supported by: the Biomedical Research Council (BMRC), Agency for Science, Technology and Research (A*STAR) Research Attachment Programme to HLW, EKT and SCW to support EH and KB; the Royal Embassy of Saudi Arabia, Cultural Bureau to support RA; the University of Sheffield and the NIHR Sheffield Biomedical Research Centre (BRC) / NIHR Sheffield Clinical Research Facility (CRF) to SEF, EKT and JNR to support KK; BL is part of the SIgN Immunomonitoring platform (supported by a BMRC IAF 311006 grant, BMRC transition funds #H16/99/b0/011, BMRC IAF-PP H1901a0024 grant and NRF SIS NRF2017_SISFP09 grant); LMC was funded by a Marie Sklodowska Curie ITN (721532) award from the European Union.

Acknowledgements

We thank Fiona J Wright and Jonathan Kilby for technical support.

Author contributions:

Conception and design: HLW, EKT, SCW, SEF, JNR, MJD, AM. Performed experiments: KB, RA, KK, ÉH, HLW, RMS, DK, LMC, CE. Experimental analysis: KB, RA, KK, ÉH, RMS, BL, MP, LMC, SKS, JNR, CE. Interpretation: KB, ÉH, HLW, EKT, SCW, SEF. Wrote manuscript: HLW, KB, ÉH (methods), RA (methods), CE (methods), KK (methods), DK (methods), LMC (methods), RM (methods). Edited manuscript: EKT, SCW.

Conflict of interest

No conflicts of interest.

5.4.7. References

References for this manuscript are included in the **References** (**Chapter 8**) for the entire thesis.

6. Bioinformatics on CALHM6 and its family

6.1. Introduction

Previous publications and data presented here indicate that CALHM6 is involved in the pro-inflammatory immune response (see **Chapter 5** for discussion and references). It is grouped into a family along with 5 other proteins all with similarity in containing a calcium homeostasis modulator domain: CALHM1 is the best studied member of the family and is known to function in neuronal excitability due to Ca^{2+} changes (Romanov et al., 2018) and oligomerised with CALHM3 in taste perception as calcium ion concentration and voltage–gated pore for ATP coming from specialised mitochondria in type II taste cells to be channelled towards neurons (Ma et al., 2018, Taruno et al., 2013). The molecular function of the other proteins in the family has been inferred from experiments using human and mouse CALHM1 (Ma et al., 2018, Taruno et al., 2013, Romanov et al., 2018). At present, there is little/no experimental evidence that CALHM6 has the same molecular, cellular and tissue function. The experimental models used and the data shown here do not conclusively indicate whether CALHM6 functions similarly to CALHM1. However, bioinformatics approaches can and have been used to initially steer experimental work. Here *in silico* observations by (Malik et al., 2017) were taken and expanded upon using the human macrophage phenotype RNA–seq (**Chapter 5**) and publicly available data, with the aim to gain further insight into the potential functions of CALHM6.

6.2. Hypothesis and aims

The following hypotheses and aims refer to the original research being submitted as part of the completion of this degree. Work that has been performed by others is acknowledged as such in the **Contributions** (**Section 6.3.**) for this chapter.

Hypothesis: Properties and functions of CALHM6 can be predicted by analysing available data on it and the rest of the CALHM family.

Aim 1: Survey the *CALHM* gene expression in healthy human tissues, the macrophage phenotype RNA–seq used in **Chapter 3** as well as monocyte subsets.

Aim 2: Analyse the *CALHM6* isoform expression data in the macrophage phenotype RNA–seq used in **Chapter 3**.

Aim 3: Align the CALHM protein sequences.

6.3. Contributions

My own contributions to the data in this chapter are:

Published transcriptomics data retrieval and analysis, protein sequence alignment, data analysis and interpretation.

The following people have also contributed to the data presented in this chapter:

Bernett Lee: published transcriptomics data retrieval and analysis, RNA–seq analysis including isoform expression.

6.4. Results

6.4.1. *CALHM* family

Most of the *CALHM* family genes are not highly expressed in healthy human tissue (**Table 6.1.**), except for *CALHM2*, which had the most widespread expression pattern among tissues together with a higher magnitude than the other *CALHM* genes. Conversely, *CALHM4* and *5* had a more specific expression pattern: highest expression in the placenta with *CALHM5* also being abundant in the fat. Interestingly, *CALHM6* expression showed considerable tissue specificity towards components of, or areas with, high prevalence of immune cells. The highest expression of *CALHM6* was observed in the spleen, appendix, lymph node and the bone marrow.

The macrophage phenotype RNA–seq offer further insight into *CALHM* gene regulation in the immune system (**Table 6.2.**). 3 out of 6 member transcripts were detected, of which *CALHM2* showed the highest expression levels in most phenotypes. Also, different polarisation conditions had the least impact on the expression of this gene. *CALHM1* had the lowest expression, especially in $M^{IFN\gamma+LPS}$. Stimulation of macrophages with IFNγ and LPS specifically resulted in a large increase of *CALHM6* transcript abundance, reaching much higher levels than those of other *CALHM* member genes.

6.4.2. *CALHM6* isoforms

Additional analysis for *CALHM6* isoform (**Figure 6.1.A**) abundance showed that upon activation with IFNγ and LPS isoform 1 (ENST00000368605.2, full–length transcript) was the most abundant isoform, followed by the fragment (ENST00000368604.2, does not have the 5' untranslated region), while isoform 2 (ENST00000368606.7, excludes exon 2) was not detected in most samples (**Figure 6.1.B**). Relative percentages of each isoform did not appear to change significantly among phenotypes (**Figure 6.1.C**), which suggests that there was little preferential expression of any isoform in any phenotype.

6.4.3. *CALHM6* gene regulation

In their transcriptomic data Xue et al. observed that *CALHM6* gene expression was selectively significantly up–regulated in macrophages stimulated with IFNγ and/or standard/ultra–pure (s/up) LPS as well as down–regulated in the TPP stimulation (TNF + prostaglandin E2 + Pam3CSK4 [mimic of acetylated bacterial lipopolypeptide N-term]) (Xue et al., 2014). Further to the macrophage data, monocyte subsets have been shown to differentially express *CALHM6*. Data published by Wong et al. show that resting monocyte subset *CALHM6* transcript levels were higher in intermediate ($CD14^{++}CD16^{+}$) and non-classical ($CD14^{+}CD16^{++}$) than classical ($CD14^{++}CD16^{-}$) monocytes (**Figure 6.2.**) (Wong et al., 2011), which are in line with observations that surface CD16–positive monocyte subsets expand in pro-inflammatory disease and aging (Ong et al., 2018).

Table 6.1.: *CALHM* gene family expression in normal human tissues.

Data (Fagerberg et al., 2014) available on NCBI were downloaded on 30 July, 2018 and converted to $\log_2$, – indicates values below the limit of detection in the original data that were left blank prior to conversion to log to exclude $\log_2(0)$, RPKM – reads per kilobase per million mapped.

Gene / Tissue	*CALHM1*	*CALHM2*	*CALHM3*	*CALHM4*	*CALHM5*	*CALHM6*
adrenal	-7.281	2.257	-6.31	–	-1.318	0.401
appendix	-3.911	2.558	–	–	-0.279	3.632
bone marrow	-9.764	-0.446	-7.882	–	-7.256	2.248
brain	-0.593	1.257	-5.083	–	-2.582	-0.971
colon	-6.601	1.911	-7.171	-11.389	-0.897	1.333
duodenum	-4.073	1.454	-3.932	–	-1.644	1.316
endometrium	-6.98	3.744	-6.012	–	-0.245	-1.326
esophagus	-8.138	1.744	–	-9.937	-0.331	-0.624
fat	-8.43	3.142	-6.601	-5.487	1.151	-0.531
gall bladder	-6.078	3.511	–	–	0.214	0.496
heart	-8.739	2.081	-8.11	-6.04	0.014	-1.269
kidney	-13.742	1.029	–	-5.436	0.333	-0.713
liver	–	-0.456	–	–	-2.857	0.496
lung	-6.853	2.905	–	-8.4	0.287	0.926
lymph node	-4.861	2.48	-7.865	–	-0.932	3.322
ovary	-5.48	4.307	-6.573	-7.366	-1.889	-0.554
pancreas	–	-1.276	-4.692	–	-5.179	-4.177
placenta	-7.067	2.687	-3.961	2.128	1.496	1.163
prostate	-5.93	2.365	-7.447	-10.177	-0.771	-0.739
salivary gland	-6.937	0.379	–	–	-4.19	-1.083
skin	–	1.202	–	–	-2.523	-2.474
small intestine	-8.715	1.373	-6.56	–	-1.276	1.465
spleen	-4.474	3.597	-5.93	-10.126	0.07	4.812
stomach	-5.174	1.305	-5.054	–	-1.994	0.678
testis	-4.526	2.703	-2.373	-4.396	-0.699	1.098
thyroid	-6.939	1.373	–	-7.042	-0.819	-2.017
urinary bladder	-5.059	3.293	-6.615	-9.078	0.275	0.978

$\log_2$RPKM	-15	-10	-5	5

Table 6.2.: Expression of *CALHM* family genes in the macrophage RNA–seq data.

CALHM3, *CALHM4* and *CALHM5* transcripts were not detected, data shown here are in $\log_2$, RPKM – reads per kilobase per million mapped.

Donor	M^{un}	$M^{INF\gamma+LPS}$	M^{IL-4}	M^{IL-10}	M^{oxPAPC}	M^{CXCL4}
	CALHM1					
A	0.109	-3.378	0.864	1.401	-3.65	1.293
B	-1.663	-7.445	-1.283	0.174	-1.54	-1.045
C	0.707	-7.445	0.671	-1.029	-3.026	-0.491
D	0.442	-7.445	0.365	-2.519	0.46	-1.183
E	0.598	-3.046	-0.199	-1.588	-1.846	-0.477
F	0.923	-3.059	-1.482	-0.433	-0.854	0.079
G	-0.785	-1.729	-0.627	-1.214	-7.445	-1.153
H	0.05	-7.445	-0.996	-2.124	-7.445	-0.531
	CALHM2					
A	6.074	4.115	5.177	5.584	6.138	5.625
B	6.046	4.468	4.848	5.531	5.33	5.599
C	6.207	4.151	5.329	5.402	5.611	5.475
D	6.158	4.381	5.802	5.789	5.83	5.798
E	5.925	4.418	5.194	5.779	5.663	5.861
F	5.907	4.679	5.368	5.536	5.505	5.862
G	6.184	4.649	5.469	5.685	5.947	5.975
H	5.913	4.202	5.159	5.507	5.686	5.897
	CALHM6					
A	0.172	8.855	0.468	1.384	0.611	0.979
B	0.633	9.654	1.499	1.949	1.122	0.391
C	0.926	8.51	0.099	-1.624	-3.482	1.262
D	2.043	10.794	3.868	3.147	1.685	-3.41
E	-6.091	9.282	1.155	1.874	1.741	1.951
F	2.14	9.737	2.645	-1.045	2.556	2.143
G	0.85	1.605	-0.684	2.8	1.348	1.66
H	1.074	6.759	-2.584	2.493	-0.359	0.079

$\log_2$RPKM	-12	-6	6	12

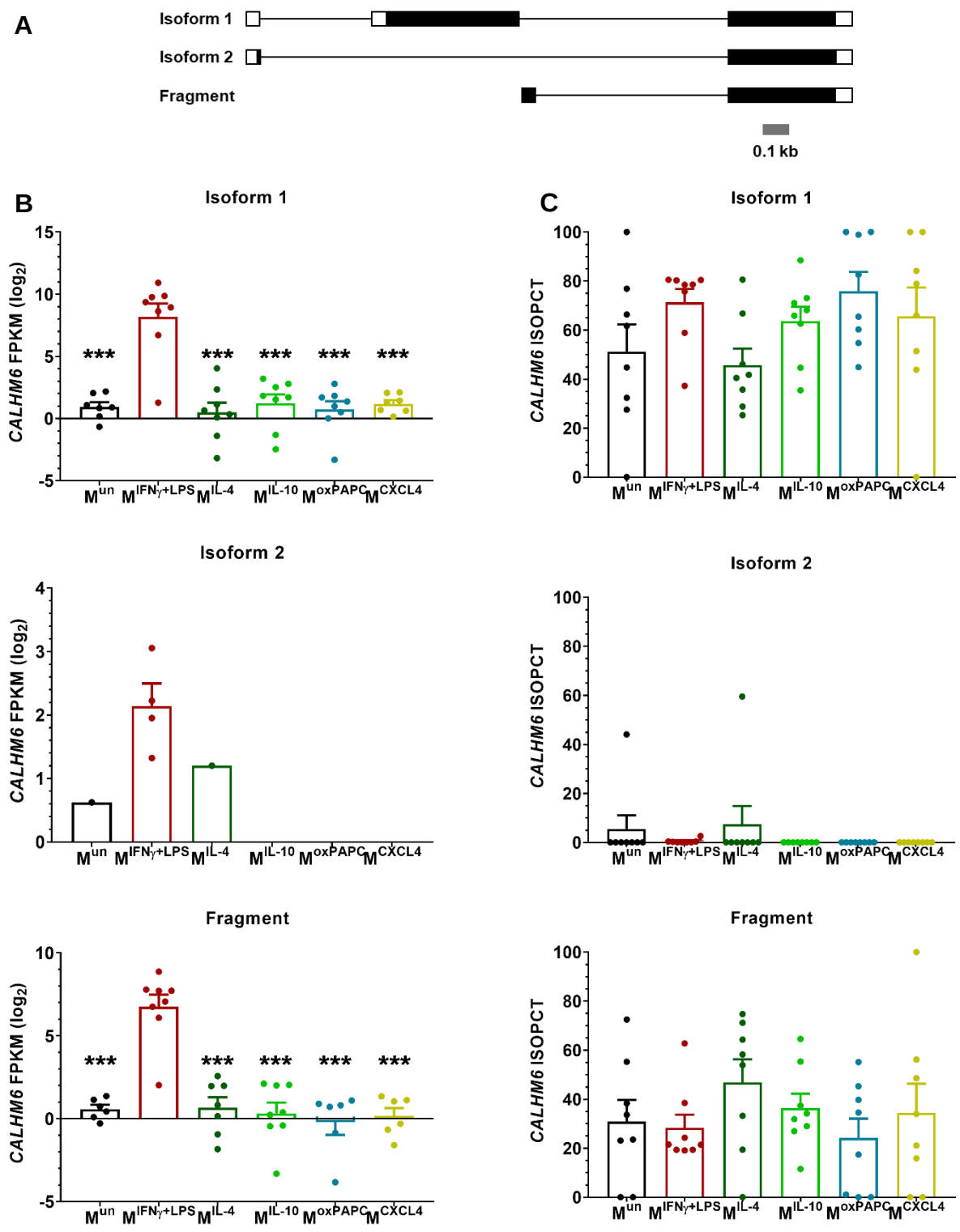

Figure 6.1.: *CALHM6* isoform expression in human macrophage phenotypes (continued on the next page).

Figure 6.1.: *CALHM6* isoform expression in human macrophage phenotypes (continued).
(**A**) ENSEMBL schematics of the human *CALHM6* transcripts; coloured bars indicate translated, empty ones untranslated regions, based on ENSEMBL on 24 July, 2019. (**B**) Relative expression levels of each isoform in human macrophage phenotypes; FPKM – fragments per kilobase million mapped, ordinary one–way ANOVA. (**C**) Percentage of each isoform among the counted *CALHM6* transcripts (ISOPCT) in each phenotype; matched sample/repeated measures one–way ANOVA. (**B** and **C**) Means ± SEMs, n = 1 – 8, ANOVA tests with Tukey's test for all conditions vs all other conditions, *** $p \leq 0.001$ compared to $M^{IFN\gamma+LPS}$ (all other comparisons were not significant).

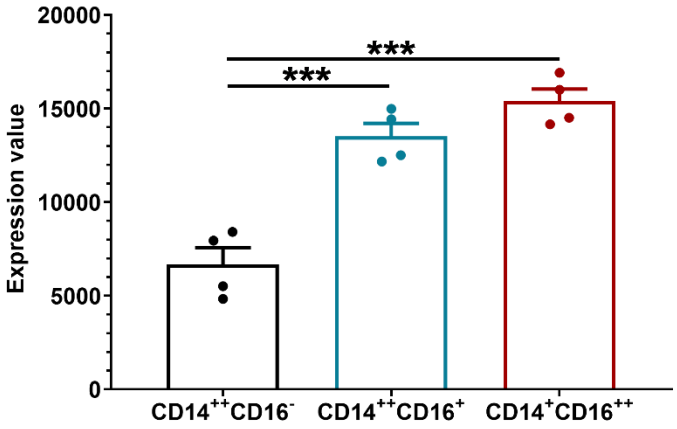

Figure 6.2.: Human monocyte subset expression of *CALHM6*.

Microarray data were acquired from (Wong et al., 2011) as described in **Materials and methods**. $CD14^{++}CD16^{-}$ – classical monocytes, $CD14^{++}CD16^{+}$ – intermediate monocytes, $CD14^{+}CD16^{++}$ – non-classical monocytes; n = 4, means ± SEMs, matched/repeated measures one–way ANOVA with Tukey's post test, *** $p \leq 0.001$.

6.4.4. CALHM6 protein N–terminus and loop regions differ from other CALHM members in charged residue abundance and identity

The 6 current family members are similar in their overall sequence and topology as indicated by their amino acid sequence alignment and predicted locations of transmembrane helices (**Figure 6.3.A**). Interestingly, after alignment two clusters of sequence similarity can still be identified: (1) CALHM1 – 3 and (2) CALHM5 and 6 with CALHM4 on its own between the two clusters (**Figure 6.3.B**). In particular, CALHM6 has the highest number of basic residues (6) in its N–terminus (3 – 4 more than the other proteins), but no charged residues in the first loop (40 – 51 residues, 45 – 57 consensus sequence), no positively charged (same as CALHM5) and only arginine (R) for negatively charged residues in the second loop (73 – 103 residues, 78 – 114 consensus sequence) (**Figure 6.4.**). Also, loop 3 of CALHM6 appears to contain slightly less charged residues than the other proteins (125 – 175 residues, 135 – 195 consensus sequence).

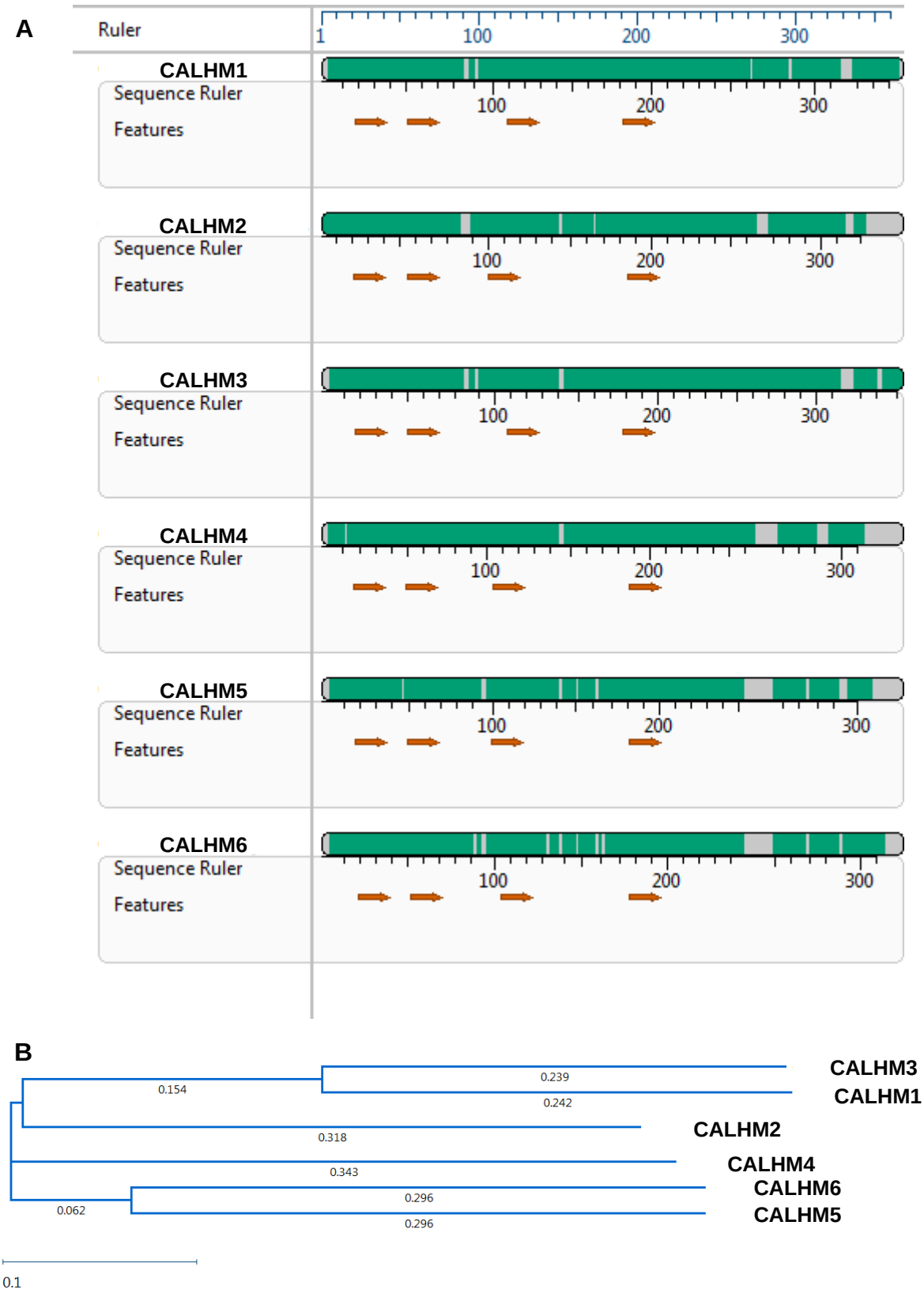

Figure 6.3.: Human CALHM protein sequence alignment.

(**A**) Overview of alignment, green areas – continuous sequence, grey areas – breaks in sequences, arrows – predicted transmembrane regions (21 amino acids each). (**B**) Protein sequence similarity clustering tree; numbers indicate relative distances among protein sequence similarities. Protein sequences were downloaded from UniProt on 29 May, 2019.

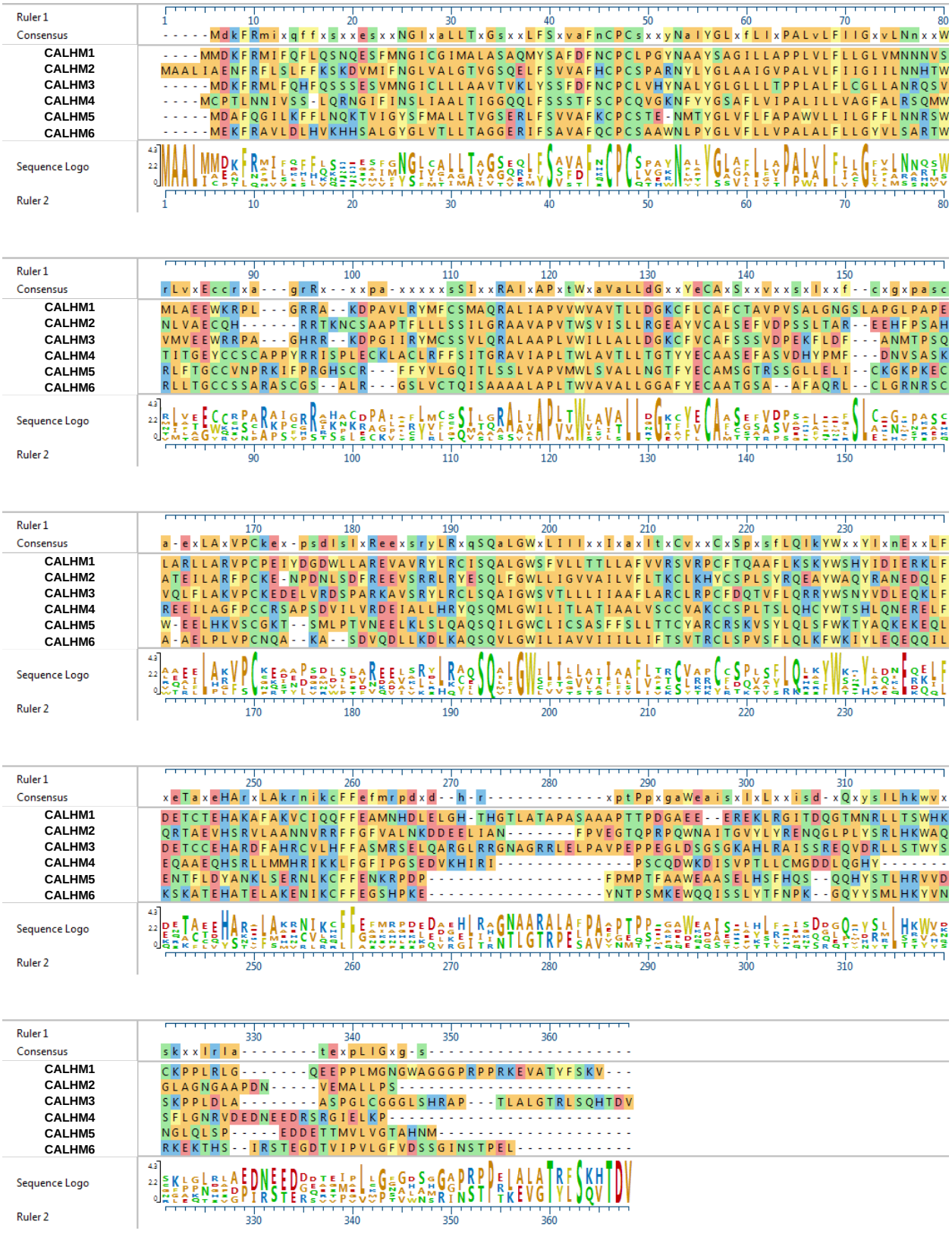

Figure 6.4.: Detailed alignment of the human CALHM protein sequences.

Both rulers indicate the numbering of the consensus sequence, while the sequence logo shows the predominant side chain(s) at each position. Colour scheme used to indicate different types of amino acid sidechains: yellow – aromatic, red – negatively charged, blue – positively charged, non-polar – orange and polar – green. Protein sequences were downloaded from UniProt on 29 May, 2019.

6.5. Discussion

All members of the CALHM family are similar in their amino acid sequence and predicted topology, which, as suggested before, may mean that all of these proteins perform the same or similar molecular functions. However, the data shown here indicate tissue–specific expression of some of the genes. In particular, *CALHM6* had the highest level of expression in tissues involved in regulating and/or with high presence of the immune system. Furthermore, *CALHM6* was expressed more in monocyte subsets with CD16 cell–surface protein (intermediate and non-classical) and upon pro-inflammatory stimulation became the most abundant CALHM family member transcribed in macrophages. Expansion of $CD16^{+}$ monocyte subsets has been associated with aging and pro-inflammatory conditions (Ong et al., 2018), which is in agreement with macrophage CALHM6 being up–regulated upon pro-inflammatory stimulation. Also, despite the overall amino acid sequence of the CALHM6 protein being similar to those of the other family members, the non-transmembrane parts of CALHM6 have numerous differences, particularly in the composition of charged residues. This observation may be indicative of differences in ligand and/or other protein interactions in the immune system, which could be explored in further studies.

7. Discussion

7.1. Summary

Macrophage function is important to the progression of atherosclerosis (Chinetti-Gbaguidi et al., 2015). The work presented in this thesis shows the changes in macrophage transcriptome and protein expression upon polarisation in connection with down–stream macrophage phenotype function, including lipid handling and glycolysis. CALHM6 could potentially be used to identify macrophages and further characterise their properties, particularly in IFNγ–related increase in immune cell recruitment, plaque instability and risk of rupture. As discussed in **Chapters 3** and **4** the findings of these studies are largely in agreement with previously published literature, while also adding to existing explanations and providing new insights into the properties and potential functions of multiple human macrophage phenotypes, beyond the most commonly studied ones. **Chapter 5** builds upon previously published work (mainly in mouse models) with the use of human donor MDMs to assess CALHM6 expression, in various *in vitro* culture models for macrophage polarisation, other stimulations and decreased expression of signalling pathway components. Data from preliminary experiments in **Chapter 5** also suggest that CALHM6 may be important for STAT1 phosphorylation and interactions between macrophages and lymphocytes, however, these results require further validation to draw conclusions. Data in **Chapter 6** provide with possible insights how to further develop part of research on CALHM6 and its importance in immune responses.

7.2. Limitations

The primary limitation of the work presented in this thesis is that the majority of the experiments were carried out *in vitro* using cell monolayer models in carefully controlled culture conditions. These models fail to replicate the three–dimensional space macrophages are situated *in vivo* and also do not fully account for macrophage interactions with their surrounding environment: cytokines, lipids, bacterial products, viral products, danger–associated molecular patterns, fluid flow and other cells of the body (Cochain and Zernecke, 2017).

In addition, some of the experiments shown here need to be repeated to validate their interpretation before the data are considered for the purposes of publication and/or directing future research. In the case of SILAC membrane and co-immunoprecipitation proteomics (both performed on cells from two different donors or cells lines of two different passages), their results have been or are in progress of being supported by using immunocytochemistry and western blotting respectively, but the proteomics experiments should still be repeated more times to strengthen their interpretation.

Another major limitation of the work presented in this thesis is that macrophage phenotype mRNA and protein expression, glycolysis were assessed only before lipid loading. Lipid loading may have induced significant changes in gene and protein expression (beyond the observed lack of influence on pro-inflammatory cytokine secretion) that could potentially functionally separate macrophage phenotypes from their derived foam cells. Furthermore, in the work included in this thesis others and I (cytokine secretion experiments) used acLDL, which is not found in the body, but used instead of atherogenic oxLDL: both lipoproteins bind MSR1, MARCO, CD36 and SCARB1, but acLDL does not bind COLEC12, OLR1, CXCL16, while oxLDL does not bind STAB1 and 2 (Pluddemann et al., 2007, Goyal et al., 2012). These differences may result in differential lipid loading and macrophage responses to lipoprotein loading, especially considering that it was previously shown in published literature (Xue et al., 2014) and reported here that macrophage polarisation with IFNγ+LPS increases *OLR1* gene expression. Therefore, further confirmation of conclusions drawn from experiments performed with acLDL using oxLDL would increase the validity and value of findings in the context of atherosclerosis. Furthermore, proteins involved in lipid handling were assessed only for their cell–surface expression, but not their modifications or activity, which may have differed from expression and allowed to better explain some of the differences observed in macrophage lipid handling.

In addition, the co-immunoprecipitation and macrophage/T cell interactions were modelled using THP–1s and Jurkats using CALHM6 tagged with 3×FLAG. Use of cell lines allowed substantially easier acquisition of the large number of cells required for co-immunoprecipitation experiments, however, experiments carried out using cell lines should be validated using primary cells isolated

from human donors, especially considering that THP–1s have been shown to differ from MDMs (Tedesco et al., 2018). The 3×FLAG tag was used to aid in protein detection and precipitation, but it was not demonstrated here that this tag did not affect protein folding, shape, localisation, interactions with other proteins and other important properties of CALHM6. In addition, here the THP–1s were treated with lentivirus to overexpresses the tagged CALHM6 and selected for using puromycin, both of which (lentivirus and puromycin) may have affected both the control "empty" plasmid (no CALHM6 construct) and CALHM6–3×FLAG THP–1s.

7.3. Future work

As mentioned, macrophage phenotype RNA and selected protein expression were measured only before lipid loading to then relate them to down–stream lipid handling. A further systematic characterisation of macrophage phenotype transcriptome and proteome with and without lipid loading may reveal more transcriptomic and proteomic differences among the phenotypes, especially when comparing cells that were exposed to modified lipoprotein to those that were not. The modified lipid of choice would preferably be oxLDL due to its presence in human atherosclerosis. Additionally, functional assays, such as foam cell formation, assessment of lipid handling, glycolysis and cytokine secretion could be repeated for all phenotypes to increase the number of biological repeats where needed and also by including incubation with oxLDL to further increase the relevance and value of these experiments to the study of atherosclerosis. As elaborated in the Discussion of **Chapter 3** (**Section 3.4.5.**) MDM sorting for the CXCL4 receptor CXCR3 before polarisation with CXCL4 could also reveal more about M^{CXCL4} lipid handling.

Further probing into the energy pathways of human macrophage phenotypes may reveal more about their dependency on different metabolites and energy use. Assessments of mitochondrial stress/activity, glutamine oxidation and fatty acid oxidation may expand upon and help to explain differences among macrophage phenotypes, including foam cell formation and lipid handling.

Research on CALHM6 is still in its early stages and a lot of beneficial advancements could be made by studying this gene/protein. The *in vitro* work presented here largely focussed on confirmation of CALHM6 induction specificity and pathways. However, the published literature and the preliminary *in vitro* data presented in this thesis suggest that CALHM6 could potentially be involved in regulating STAT1 signalling and interactions between innate and adaptive immune cells. Also, it would be interesting to perform similar experiments focussing on TICAM1.

Multiple experiments should be carried out to validate these predictions. Experiments, such as western blots, are required to confirm presence of LAT in the CALHM6–3×FLAG THP–1 co-immunoprecipitations' mass spectrometry data. Also, pull–downs replacing the lysates of at least one of the cell lines with those of the corresponding human donor cells as well as LAT knockdown and blocking with siRNA and antibodies respectively would be useful to further test the predictions. The cell interaction assays should be repeated more times in the current cell line culture model and could also be carried out by replacing at least some cell lines with human donor cells to prove that increased CALHM6 expression in macrophages can lead to increased interaction with lymphocytes. In addition, macrophages of more donors should be treated with siRNA to knockdown expression of *CALHM6* and subsequently treated with IFNγ for up to 1 h and assessed

for phosphorylated Y701 and total STAT1 to test the prediction from preliminary data that CALHM6 affects STAT1.

More work could also be done to see if CALHM6 is a membrane–spanning pore that is sensitive to voltage and Ca^{2+} concentrations similarly to other members of its family. It could also be beneficial for immunological research to see if the differences in the loop regions of CALHM6 in comparison to other CALHM family members are reflected in the preferred ligands and/or functional characteristics of these proteins.

Published reports identified potential roles of mouse CALHM6 in tumour control (Ebihara et al., 2010, Kasamatsu et al., 2014). In those experiments immune cell stimulation with poly(I:C) was key in down–stream activation of NK to produce IFNγ against tumours sensitive to the cytokine. Increased *Calhm6* expression in alveolar macrophages has been observed upon respiratory infections with bacteria such as *Streptococcus pneumoniae* (Strehlitz, 2017). Research on simian immunodeficiency virus has shown that levels of CALHM6 before infection could be used for prognosis of acute and post-acute infection stages (Javed et al., 2016) and also *CALHM6* siRNA knockdown in human macrophages reduced the expression of *CCL5* and other chemokines (**Chapter 3**). Therefore, it may be of interest to use the *CALHM6* siRNA knockdown model for *in vitro* infection experiments to see if *CALHM6* has roles in pathogen uptake, replication control and killing (currently in early planning stages). In addition, whole–body *Calhm6* knock out mice and zebrafish are available and could also be used to test the importance of the gene using *in vivo* infection models.

CALHM6 could be involved in regulating cytokine expression as evidenced by the siRNA knockdown model in human macrophages, however, it is not known if the same could be said about glycolysis or other metabolic pathways. Experiments such as the Seahorse glycostress and mitostress assays (or any other assay for measuring glycolytic flux and mitochondrial function in macrophages) could be used on *CALHM6* siRNA knockdown macrophages to test the influence of this gene on cellular metabolism. The wider transcriptomic influence of *CALHM6* knockdown/knockout in macrophages or animal models surveyed by use of technologies such as RNA–seq may also reveal more potential functions of *CALHM6*.

It is also not known if, given its association with inflammatory responses, CALHM6 has roles in atherosclerotic plaque development, progression and stability. CD68 and CALHM6 staining should be repeated along with that for SMA using sections of plaques from more patients to confirm $CALHM6^{+}$ macrophage presence in human atherosclerosis as well as exclude any SMCs. These experiments could provide with data on $CALHM6^{+}$ macrophage abundance and localisation

at different stages and risk of rupture of the atherosclerotic plaque. Furthermore, it could be checked *in vitro* by DAPI/BODIPY/anti-CALHM6 antibody fluorescent staining if CALHM6 expression is different in modified lipoprotein–loaded from unloaded cells. The *CALHM6* siRNA knockdown model could be used in foam cell formation (using oxLDL) and other functional lipid handling assays to elaborate on these findings. Also, *Calhm6* knockout mice could be used to set up *in vivo* experiments to test the importance of this gene/protein in the development of atherosclerosis and plaque vulnerability. Furthermore, it has been suggested that pathogen burden and interaction with the host immune system, which can also vary in its responsiveness, may contribute to atherosclerosis development (Epstein et al., 2009). It would be interesting to combine the infection and atherosclerosis animal models to test if and how CALHM6 may be involved in modulating the likelihood of adverse cardiovascular events upon infection. Development of monoclonal antibodies against CALHM6 (currently in early testing) may aid research as well as evaluation of both disease and treatment. Ultimately, with further research CALHM6 may become a drug target in controlling leukocyte recruitment and activation to reduce the risk of atherosclerotic plaque rupture as well as to treat other chronic inflammatory diseases and acute infections.

8. References

If the page numbers are unavailable, article number or a similar identifier is given.

AYARI, H. & BRICCA, G. 2013. Identification of two genes potentially associated in iron-heme homeostasis in human carotid plaque using microarray analysis. *Journal of Biosciences,* 38**,** 311-315.

BELONE, A. D. F. F., ROSA, P. S., TROMBONE, A. P. F., FACHIN, L. R. V., GUIDELLA, C. C., URA, S., BARRETO, J. A., PINILLA, M. G., DE CARVALHO, A. F., CARRARO, D. M., SOARES, F. A. & SOARES, C. T. 2015. Genome-wide screening of mRNA expression in leprosy patients. *Frontiers in Genetics,* 6**,** 334.

BENJAMINI, Y. & HOCHBERG, Y. 1995. Controlling the false discovery rate - a practical and powerful approach to multiple testing. *Journal of the Royal Statistical Society Series B-Statistical Methodology,* 57**,** 289-300.

BERG, K. E., LJUNGCRANTZ, I., ANDERSSON, L., BRYNGELSSON, C., HEDBLAD, B., FREDRIKSON, G. N., NILSSON, J. & BJORKBACKA, H. 2012. Elevated $CD14^{++}CD16^{-}$ monocytes predict cardiovascular events. *Circulation: Cardiovascular Genetics,* 5**,** 122-131.

BIGLEY, V., HANIFFA, M., DOULATOV, S., WANG, X.-N., DICKINSON, R., MCGOVERN, N., JARDINE, L., PAGAN, S., DIMMICK, I., CHUA, I., WALLIS, J., LORDAN, J., MORGAN, C., KUMARARATNE, D. S., DOFFINGER, R., VAN DER BURG, M., VAN DONGEN, J., CANT, A., DICK, J. E., HAMBLETON, S. & COLLIN, M. 2011. The human syndrome of dendritic cell, monocyte, B and NK lymphoid deficiency. *Journal of Experimental Medicine,* 208**,** 227-234.

BORIES, G. F. P. & LEITINGER, N. 2017. Macrophage metabolism in atherosclerosis. *Febs Letters,* 591**,** 3042-3060.

BOYLE, J. J., JOHNS, M., KAMPFER, T., NGUYEN, A. T., GAME, L., SCHAER, D. J., MASON, J. C. & HASKARD, D. O. 2012. Activating transcription factor 1 directs Mhem atheroprotective macrophages through coordinated iron handling and foam cell protection. *Circulation Research,* 110**,** 20-33.

BREWER, H. B. 2004. High-density lipoproteins: A new potential therapeutic target for the prevention of cardiovascular disease. *Arteriosclerosis Thrombosis and Vascular Biology,* 24**,** 387-391.

BROWN, J. N., WALLET, M. A., KRASTINS, B., SARRACINO, D. & GOODENOW, M. M. 2010. Proteome bioprofiles distinguish between M1 priming and activation states in human macrophages. *Journal of Leukocyte Biology,* 87**,** 655-662.

BROWN, M. S., HO, Y. K. & GOLDSTEIN, J. L. 1980. The cholesteryl ester cycle in macrophage foam cells - continual hydrolysis and re-esterification of cytoplasmic cholesteryl esters. *Journal of Biological Chemistry,* 255**,** 9344-9352.

CALDWELL, A. B., CHENG, Z., VARGAS, J. D., BIRNBAUM, H. A. & HOFFMANN, A. 2014. Network dynamics determine the autocrine and paracrine signaling functions of TNF. *Genes & Development,* 28**,** 2120-2133.

CHAWLA, A., BOISVERT, W. A., LEE, C. H., LAFFITTE, B. A., BARAK, Y., JOSEPH, S. B., LIAO, D., NAGY, L., EDWARDS, P. A., CURTISS, L. K., EVANS, R. M. & TONTONOZ, P. 2001. A PPAR gamma-LXR-ABCA1 pathway in macrophages is involved in cholesterol efflux and atherogenesis. *Molecular Cell,* 7**,** 161-171.

CHIBA, S., IKUSHIMA, H., UEKI, H., YANAI, H., KIMURA, Y., HANGAI, S., NISHIO, J., NEGISHI, H., TAMURA, T., SAIJO, S., IWAKURA, Y. & TANIGUCHI, T. 2014. Recognition of tumor cells by Dectin-1 orchestrates innate immune cells for anti-tumor responses. *Elife,* 3.

CHINETTI-GBAGUIDI, G., COLIN, S. & STAELS, B. 2015. Macrophage subsets in atherosclerosis. *Nature Reviews Cardiology,* 12**,** 10-17.

CHISTIAKOV, D. A., BOBRYSHEV, Y. V., NIKIFOROV, N. G., ELIZOVA, N. V., SOBENIN, I. A. & OREKHOV, A. N. 2015. Macrophage phenotypic plasticity in atherosclerosis: The associated features and the peculiarities of the expression of inflammatory genes. *International Journal of Cardiology,* 184**,** 436-445.

CHISTIAKOV, D. A., BOBRYSHEV, Y. V. & OREKHOV, A. N. 2016. Macrophage-mediated cholesterol handling in atherosclerosis. *Journal of Cellular and Molecular Medicine,* 20**,** 17-28.

CHMIELEWSKI, S., OLEJNIK, A., SIKORSKI, K., PELISEK, J., BLASZCZYK, K., AOQUI, C., NOWICKA, H., ZERNECKE, A., HEEMANN, U., WESOLY, J., BAUMANN, M. & BLUYSSEN, H. A. R. 2014. STAT1-dependent signal integration between IFN gamma and TLR4 in vascular cells reflect pro-atherogenic responses in human atherosclerosis. *Plos One,* 9**,** e113318.

COCHAIN, C., VAFADARNEJAD, E., ARAMPATZI, P., PELISEK, J., WINKELS, H., LEY, K., WOLF, D., SALIBA, A. E. & ZERNECKE, A. 2018. Single-cell RNA-seq reveals the transcriptional landscape and heterogeneity of aortic macrophages in murine atherosclerosis. *Circulation Research,* 122**,** 1661-1674.

COCHAIN, C. & ZERNECKE, A. 2017. Macrophages in vascular inflammation and atherosclerosis. *Pflugers Archiv-European Journal of Physiology,* 469**,** 485-499.

COILLARD, A. & SEGURA, E. 2019. In vivo differentiation of human monocytes. *Frontiers in Immunology,* 10**,** 1907.

COLLISSON, E. A., SADANANDAM, A., OLSON, P., GIBB, W. J., TRUITT, M., GU, S., COOC, J., WEINKLE, J., KIM, G. E., JAKKULA, L., FEILER, H. S., KO, A. H., OLSHEN, A. B., DANENBERG, K. L., TEMPERO, M. A., SPELLMAN, P. T., HANAHAN, D. & GRAY, J. W. 2011. Subtypes of pancreatic ductal adenocarcinoma and their differing responses to therapy. *Nature Medicine,* 17**,** 500-503.

COURT, M., MALIER, M. & MILLET, A. 2019. 3D type I collagen environment leads up to a reassessment of the classification of human macrophage polarizations. *Biomaterials,* 208**,** 98-109.

CROS, J., CAGNARD, N., WOOLLARD, K., PATEY, N., ZHANG, S.-Y., SENECHAL, B., PUEL, A., BISWAS, S. K., MOSHOUS, D., PICARD, C., JAIS, J.-P., D'CRUZ, D., CASANOVA, J.-L., TROUILLET, C. & GEISSMANN, F. 2010. Human $CD14^{dim}$ monocytes patrol and sense nucleic acids and viruses via TLR7 and TLR8 receptors. *Immunity,* 33**,** 375-386.

DA SILVA, R. F., LAPPALAINEN, J., LEE-RUECKERT, M. & KOVANEN, P. T. 2016. Conversion of human M-CSF macrophages into foam cells reduces their proinflammatory responses to classical M1-polarizing activation. *Atherosclerosis,* 248**,** 170-178.

DE GAETANO, M., CREAN, D., BARRY, M. & BELTON, O. 2016. M1-and M2-type macrophage responses are predictive of adverse outcomes in human atherosclerosis. *Frontiers in Immunology,* 7**,** 275.

DERLINDATI, E., DEI CAS, A., MONTANINI, B., SPIGONI, V., CURELLA, V., ALDIGERI, R., ARDIGO, D., ZAVARONI, I. & BONADONNA, R. C. 2015. Transcriptomic analysis of human polarized macrophages: more than one role of alternative activation? *Plos One,* 10**,** e0119751.

DIAMOND, C. E., KHAMENEH, H. J., BROUGH, D. & MORTELLARO, A. 2015. Novel perspectives on non-canonical inflammasome activation. *Immunotargets and Therapy,* 4**,** 131-140.

DICKINSON, R. E., MILNE, P., JARDINE, L., ZANDI, S., SWIERCZEK, S. I., MCGOVERN, N., COOKSON, S., FEROZEPURWALLA, Z., LANGRIDGE, A., PAGAN, S., GENNERY, A., HEISKANEN-KOSMA, T., HAMALAINEN, S., SEPPANEN, M., HELBERT, M., THOLOULI, E., GAMBINERI, E., REYKDAL, S., GOTTFREDSSON, M., THAVENTHIRAN, J. E., MORRIS, E., HIRSCHFIELD, G., RICHTER, A. G., JOLLES, S., BACON, C. M., HAMBLETON, S., HANIFFA, M., BRYCESON, Y.,

ALLEN, C., PRCHAL, J. T., DICK, J. E., BIGLEY, V. & COLLIN, M. 2014. The evolution of cellular deficiency in GATA2 mutation. *Blood,* 123**,** 863-874.

DINARELLO, C. A. 2007. Historical insights into cytokines. *European Journal of Immunology,* 37**,** S34-S45.

DISKIN, C. & PALSSON-MCDERMOTT, E. M. 2018. Metabolic modulation in macrophage effector function. *Frontiers in Immunology,* 9**,** 270.

DOBASHI, K., AIHARA, M., ARAKI, T., SHIMIZU, Y., UTSUGI, M., IIZUKA, K., MURATA, Y., HAMURO, J., NAKAZAWA, T. & MORI, M. 2001. Regulation of LPS induced IL-12 production by IFN-gamma and IL-4 through intracellular glutathione status in human alveolar macrophages. *Clinical and Experimental Immunology,* 124**,** 290-296.

DOBIN, A., DAVIS, C. A., SCHLESINGER, F., DRENKOW, J., ZALESKI, C., JHA, S., BATUT, P., CHAISSON, M. & GINGERAS, T. R. 2013. STAR: ultrafast universal RNA-seq aligner. *Bioinformatics,* 29**,** 15-21.

DUFEK, S., CHESHIRE, C., LEVINE, A. P., TROMPETER, R. S., ISSLER, N., STUBBS, M., MOZERE, M., GUPTA, S., KLOOTWIJK, E., PATEL, V., HOTHI, D., WATERS, A., WEBB, H., TULLUS, K., JENKINS, L., GODINHO, L., LEVTCHENKO, E., WETZELS, J., KNOERS, N., TEENINGA, N., NAUTA, J., SHALABY, M., ELDESOKY, S., KARI, J. A., THALGAHAGODA, S., RANAWAKA, R., ABEYAGUNAWARDENA, A., ADEYEMO, A., KRISTIANSEN, M., GBADEGESIN, R., WEBB, N. J., GALE, D. P., STANESCU, H. C., KLETA, R. & BOCKENHAUER, D. 2019. Genetic identification of two novel loci associated with steroid-sensitive nephrotic syndrome. *Journal of the American Society of Nephrology : JASN,* 30**,** 1375-1384.

EBIHARA, T., AZUMA, M., OSHIUMI, H., KASAMATSU, J., IWABUCHI, K., MATSUMOTO, K., SAITO, H., TANIGUCHI, T., MATSUMOTO, M. & SEYA, T. 2010. Identification of a polyI:C-inducible membrane protein that participates in dendritic cell-mediated natural killer cell activation. *Journal of Experimental Medicine,* 207**,** 2675-2687.

EPSTEIN, S. E., ZHU, J., NAJAFI, A. H. & BURNETT, M. S. 2009. Insights Into the Role of Infection in Atherogenesis and in Plaque Rupture. *Circulation,* 119**,** 3133-U160.

ERBEL, C., TYKA, M., HELMES, C. M., AKHAVANPOOR, M., RUPP, G., DOMSCHKE, G., LINDEN, F., WOLF, A., DOESCH, A., LASITSCHKA, F., KATUS, H. A. & GLEISSNER, C. A. 2015. CXCL4-induced plaque macrophages can be specifically identified by co-expression of MMP7(+)S100A8(+) in vitro and in vivo. *Innate Immunity,* 21**,** 255-265.

FAGERBERG, L., HALLSTROM, B. M., OKSVOLD, P., KAMPF, C., DJUREINOVIC, D., ODEBERG, J., HABUKA, M., TAHMASEBPOOR, S., DANIELSSON, A., EDLUND, K., ASPLUND, A., SJOSTEDT, E., LUNDBERG, E., SZIGYARTO, C. A.-K., SKOGS, M., TAKANEN, J. O., BERLING, H., TEGEL, H., MULDER, J., NILSSON, P., SCHWENK, J. M., LINDSKOG, C., DANIELSSON, F., MARDINOGLU, A., SIVERTSSON, A., VON FEILITZEN, K., FORSBERG, M., ZWAHLEN, M., OLSSON, I., NAVANI, S., HUSS, M., NIELSEN, J., PONTEN, F. & UHLEN, M. 2014. Analysis of the human tissue-specific expression by genome-wide integration of transcriptomics and antibody-based proteomics. *Molecular & Cellular Proteomics,* 13**,** 397-406.

FARKAS, S. A., MILUTIN-GASPEROV, N., GRCE, M. & NILSSON, T. K. 2013. Genome-wide DNA methylation assay reveals novel candidate biomarker genes in cervical cancer. *Epigenetics,* 8**,** 1213-1225.

FASANO, T., PISCIOTTA, L., BOCCHI, L., GUARDAMAGNA, O., ASSANDRO, P., RABACCHI, C., ZANONI, P., FILOCAMO, M., BERTOLINI, S. & CALANDRA, S. 2012. Lysosomal lipase deficiency: Molecular characterization of eleven patients with Wolman or cholesteryl ester storage disease. *Molecular Genetics and Metabolism,* 105**,** 450-456.

FERNANDEZ, D. M., RAHMAN, A. H., FERNANDEZ, N. F., CHUDNOVSKIY, A., AMIR, E.-A. D., AMADORI, L., KHAN, N. S., WONG, C. K., SHAMAILOVA, R., HILL, C.

A., WANG, Z., REMARK, R., LI, J. R., PINA, C., FARIES, C., AWAD, A. J., MOSS, N., BJORKEGREN, J. L. M., KIM-SCHULZE, S., GNJATIC, S., MA'AYAN, A., MOCCO, J., FARIES, P., MERAD, M. & GIANNARELLI, C. 2019. Single-cell immune landscape of human atherosclerotic plaques. *Nature Medicine,* 25**,** 1576-1588.

FERRO, C. J., MARK, P. B., KANBAY, M., SARAFIDIS, P., HEINE, G. H., ROSSIGNOL, P., MASSY, Z. A., MALLAMACI, F., VALDIVIELSO, J. M., MALYSZKO, J., VERHAAR, M. C., EKART, R., VANHOLDER, R., LONDON, G., ORTIZ, A. & ZOCCALI, C. 2018. Lipid management in patients with chronic kidney disease. *Nature Reviews Nephrology,* 14**,** 727-749.

FINN, A. V., NAKANO, M., POLAVARAPU, R., KARMALI, V., SAEED, O., ZHAO, X., YAZDANI, S., OTSUKA, F., DAVIS, T., HABIB, A., NARULA, J., KOLODGIE, F. D. & VIRMANI, R. 2012. Hemoglobin directs macrophage differentiation and prevents foam cell formation in human atherosclerotic plaques. *Journal of the American College of Cardiology,* 59**,** 166-177.

FROSTEGARD, J. 2013. Immunity, atherosclerosis and cardiovascular disease. *BMC Medicine,* 11**,** 117.

FULLER, D. M. & ZHANG, W. 2009. Regulation of lymphocyte development and activation by the LAT family of adapter proteins. *Immunological Reviews,* 232**,** 72-83.

GALAMB, O., SIPOS, F., SOLYMOSI, N., SPISAK, S., KRENACS, T., TOTH, K., TULASSAY, Z. & MOLNAR, B. 2008. Diagnostic mRNA expression patterns of inflamed, benign, and malignant colorectal biopsy specimen and their correlation with peripheral blood results. *Cancer Epidemiology Biomarkers & Prevention,* 17**,** 2835-2845.

GARGIULO, S., GRAMANZINI, M. & MANCINI, M. 2016. Molecular imaging of vulnerable atherosclerotic plaques in animal models. *International Journal of Molecular Sciences,* 17**,** 1511.

GENG, Y. J. & HANSSON, G. K. 1992. Interferon-gamma inhibits scavenger receptor expression and foam cell-formation in human monocyte-derived macrophages. *Journal of Clinical Investigation,* 89**,** 1322-1330.

GERIC, I., TYURINA, Y. Y., KRYSKO, O., KRYSKO, D. V., DE SCHRYVER, E., KAGAN, V. E., VAN VELDHOVEN, P. P., BAES, M. & VERHEIJDEN, S. 2018. Lipid homeostasis and inflammatory activation are disturbed in classically activated macrophages with peroxisomal -oxidation deficiency. *Immunology,* 153**,** 342-356.

GHARIB, S. A., MCMAHAN, R. S., EDDY, W. E., LONG, M. E., PARKS, W. C., AITKEN, M. L. & MANICONE, A. M. 2019. Transcriptional and functional diversity of human macrophage repolarization. *Journal of Allergy and Clinical Immunology,* 143**,** 1536-1548.

GHOSH, J., GUHA, R., DAS, S. & ROY, S. 2014. Liposomal cholesterol delivery activates the macrophage innate immune arm to facilitate intracellular *Leishmania donovani* killing. *Infection and Immunity,* 82**,** 607-617.

GHOSH, S. 2011. Macrophage cholesterol homeostasis and metabolic diseases: critical role of cholesteryl ester mobilization. *Expert Review of Cardiovascular Therapy,* 9**,** 329-40.

GHOSH, S., ZHAO, B., BIE, J. H. & SONG, J. M. 2010. Macrophage cholesteryl ester mobilization and atherosclerosis. *Vascular Pharmacology,* 52**,** 1-10.

GINHOUX, F., SCHULTZE, J. L., MURRAY, P. J., OCHANDO, J. & BISWAS, S. K. 2016. New insights into the multidimensional concept of macrophage ontogeny, activation and function. *Nature Immunology,* 17**,** 34-40.

GLEISSNER, C. A. 2012. Macrophage phenotype modulation by CXCL4 in atherosclerosis. *Frontiers in Physiology,* 3.

GLEISSNER, C. A., SHAKED, I., LITTLE, K. M. & LEY, K. 2010. CXC chemokine ligand 4 induces a unique transcriptome in monocyte-derived macrophages. *Journal of Immunology,* 184**,** 4810-4818.

GOMEZ, J. C., YAMADA, M., MARTIN, J. R., DANG, H., BRICKEY, W. J., BERGMEIER, W., DINAUER, M. C. & DOERSCHUK, C. M. 2015. Mechanisms of interferon-gamma

production by neutrophils and its function during *Streptococcus pneumoniae* pneumonia. *American Journal of Respiratory Cell and Molecular Biology,* 52**,** 349-364.

GOODMAN, B. E. 2010. Insights into digestion and absorption of major nutrients in humans. *Advances in Physiology Education,* 34**,** 44-53.

GORDON, S. & MARTINEZ, F. O. 2010. Alternative activation of macrophages: mechanism and functions. *Immunity,* 32**,** 593-604.

GOUGH, P. J., GREAVES, D. R. & GORDON, S. 1998. A naturally occurring isoform of the human macrophage scavenger receptor (SR-A) gene generated by alternative splicing blocks modified LDL uptake. *Journal of Lipid Research,* 39**,** 531-543.

GOYAL, T., MITRA, S., KHAIDAKOV, M., WANG, X. W., SINGLA, S., DING, Z. F., LIU, S. J. & MEHTA, J. L. 2012. Current concepts of the role of oxidized LDL receptors in atherosclerosis. *Current Atherosclerosis Reports,* 14**,** 150-159.

GRIFFITH, J. W., SOKOL, C. L. & LUSTER, A. D. 2014. Chemokines and chemokine receptors: positioning cells for host defense and immunity. *Annual Review of Immunology, Vol 32,* 32**,** 659-702.

GRUTZ, G. 2005. New insights into the molecular mechanism of interieukin-10-mediated immunosuppression. *Journal of Leukocyte Biology,* 77**,** 3-15.

GUO, L., AKAHORI, H., HARARI, E., SMITH, S. L., POLAVARAPU, R., KARMALI, V., OTSUKA, F., GANNON, R. L., BRAUMANN, R. E., DICKINSON, M. H., GUPTA, A., JENKINS, A. L., LIPINSKI, M. J., KIM, J., CHHOUR, P., DE VRIES, P. S., JINNOUCHI, H., KUTYS, R., MORI, H., KUTYNA, M. D., TORII, S., SAKAMOTO, A., CHOI, C. U., CHENG, Q., GROVE, M. L., SAWAN, M. A., ZHANG, Y., CAO, Y. H., KOLODGIE, F. D., CORMODE, D. P., ARKING, D. E., BOERWINKLE, E., MORRISON, A. C., ERDMANN, J., SOTOODEHNIA, N., VIRMANI, R. & FINN, A. V. 2018. CD163(+) macrophages promote angiogenesis and vascular permeability accompanied by inflammation in atherosclerosis. *Journal of Clinical Investigation,* 128**,** 1106-1124.

HADADI, É. 2015. *Contribution of macrophage phenotypes and their precursors in inflammatory function and the development of cardiovascular disease.* University of Sheffield.

HAN, X., KITAMOTO, S., LIAN, Q. & BOISVERT, W. A. 2009. Interleukin-10 facilitates both cholesterol uptake and efflux in macrophages. *Journal of Biological Chemistry,* 284**,** 32950-32958.

HEALY, L. M., PERRON, G., WON, S. Y., RAO, V. T. S., GUIOT, M. C., MOORE, C., BAR-OR, A. & ANTEL, J. P. 2018. Differential transcriptional response profiles in human myeloid cell populations. *Clinical Immunology,* 189**,** 63-74.

HEINE, G. H., ULRICH, C., SEIBERT, E., SEILER, S., MARELL, J., REICHART, B., KRAUSE, M., SCHLITT, A., KOEHLER, H. & GIRNDT, M. 2008. $CD14^{++}CD16^{+}$ monocytes but not total monocyte numbers predict cardiovascular events in dialysis patients. *Kidney International,* 73**,** 622-629.

HOPFNER, F., JACOB, M., ULRICH, C., RUSS, M., SIMM, A., SILBER, R. E., GIRNDT, M., NOUTSIAS, M., WERDAN, K. & SCHLITT, A. 2019. Subgroups of monocytes predict cardiovascular events in patients with coronary heart disease. The PHAMOS trial (Prospective Halle Monocytes Study). *Hellenic Journal of Cardiology,* 60**,** 311-321.

HUANG, S. C.-C., EVERTS, B., IVANOVA, Y., O'SULLIVAN, D., NASCIMENTO, M., SMITH, A. M., BEATTY, W., LOVE-GREGORY, L., LAM, W. Y., O'NEIL, C. M., YAN, C., DU, H., ABUMRAD, N. A., URBAN, J. F., JR., ARTYOMOV, M. N., PEARCE, E. L. & PEARCE, E. J. 2014. Cell-intrinsic lysosomal lipolysis is essential for alternative activation of macrophages. *Nature Immunology,* 15**,** 846-855.

HUANG, W.-C., SALA-NEWBY, G. B., SUSANA, A., JOHNSON, J. L. & NEWBY, A. C. 2012. Classical macrophage activation up-regulates several matrix metalloproteinases through mitogen activated protein kinases and nuclear factor-kappa B. *Plos One,* 7**,** e42507.

HUBNER, N. C., REN, S. & MANN, M. 2008. Peptide separation with immobilized pI strips is an attractive alternative to in-gel protein digestion for proteome analysis. *Proteomics,* 8**,** 4862-4872.

IDZKOWSKA, E., ELJASZEWICZ, A., MIKLASZ, P., MUSIAL, W. J., TYCINSKA, A. M. & MONIUSZKO, M. 2015. The role of different monocyte subsets in the pathogenesis of atherosclerosis and acute coronary syndromes. *Scandinavian Journal of Immunology,* 82**,** 163-173.

IGARASHI, M., OSUGA, J.-I., UOZAKI, H., SEKIYA, M., NAGASHIMA, S., TAKAHASHI, M., TAKASE, S., TAKANASHI, M., LI, Y., OHTA, K., KUMAGAI, M., NISHI, M., HOSOKAWA, M., FLEDELIUS, C., JACOBSEN, P., YAGYU, H., FUKAYAMA, M., NAGAI, R., KADOWAKI, T., OHASHI, K. & ISHIBASHI, S. 2010. The critical role of neutral cholesterol ester hydrolase 1 in cholesterol removal from human macrophages. *Circulation Research,* 107**,** 1387-1395.

IP, W. K. E., HOSHI, N., SHOUVAL, D. S., SNAPPER, S. & MEDZHITOV, R. 2017. Anti-inflammatory effect of IL-10 mediated by metabolic reprogramming of macrophages. *Science,* 356**,** 513-519.

JACOB, S., ZHU, Y., KRAFT, R., COTTO, C., CARMICAL, J. R., WOOD, T. G., ENKHBAATAR, P., HERNDON, D. N., HAWKINS, H. K. & COX, R. A. 2015. Physiologic and molecular changes in the tracheal epithelium of rats following burn injury. *International Journal of Burns and Trauma,* 5**,** 36-45.

JACQUIER, V., ESTELLE, J., SCHMALTZ-PANNEAU, B., LECARDONNEL, J., MOROLDO, M., LEMONNIER, G., TURNER-MAIER, J., DURANTHON, V., OSWALD, I. P., GIDENNE, T. & ROGEL-GAILLARD, C. 2015. Genome-wide immunity studies in the rabbit: transcriptome variations in peripheral blood mononuclear cells after in vitro stimulation by LPS or PMA-ionomycin. *BMC Genomics,* 16**,** 26.

JAVED, A., LEUCHTE, N., SALINAS, G., OPITZ, L., STAHL-HENNIG, C., SOPPER, S. & SAUERMANN, U. 2016. Pre-infection transcript levels of FAM26F in peripheral blood mononuclear cells inform about overall plasma viral load in acute and post-acute phase after simian immunodeficiency virus infection. *Journal of General Virology,* 97**,** 3400-3412.

JULIA, A., DOMENECH, E., CHAPARROM, M., GARCIA-SANCHEZ, V., GOMOLLON, F., PANES, J., MANOSA, M., BARREIRO-DE ACOSTA, M., GUTIERREZ, A., GARCIA-PLANELLA, E., AGUAS, M., MUNOZ, F., ESTEVE, M., MENDOZA, J. L., VERA, M., MARQUEZ, L., TORTOSA, R., LOPEZ-LASANTA, M., ALONSO, A., GELPI, J. L., GARCIA-MONTERO, A. C., BERTRANPETIT, J., ABSHER, D., MYERS, R. M., GISBERT, J. P. & MARSAL, S. 2014. A genome-wide association study identifies a novel locus at 6q22.1 associated with ulcerative colitis. *Human Molecular Genetics,* 23**,** 6927-6934.

KADL, A., MEHER, A. K., SHARMA, P. R., LEE, M. Y., DORAN, A. C., JOHNSTONE, S. R., ELLIOTT, M. R., GRUBER, F., HAN, J., CHEN, W. S., KENSLER, T., RAVICHANDRAN, K. S., ISAKSON, B. E., WAMHOFF, B. R. & LEITINGER, N. 2010. Identification of a novel macrophage phenotype that develops in response to atherogenic phospholipids via Nrf2. *Circulation Research,* 107**,** 737-746.

KAPELLOS, T. S., BONAGURO, L., GEMUEND, I., REUSCH, N., SAGLAM, A., HINKLEY, E. R. & SCHULTZE, J. L. 2019. Human monocyte subsets and phenotypes in major chronic inflammatory diseases. *Frontiers in Immunology,* 10**,** 2035.

KASAMATSU, J., AZUMA, M., OSHIUMI, H., MORIOKA, Y., OKABE, M., EBIHARA, T., MATSUMOTO, M. & SEYA, T. 2014. INAM plays a critical role in IFN-gamma production by NK cells interacting with polyinosinic-polycytidylic acid-stimulated accessory cells. *Journal of Immunology,* 193**,** 5199-5207.

KAVURMA, M. M., RAYNER, K. J. & KARUNAKARAN, D. 2017. The walking dead: macrophage inflammation and death in atherosclerosis. *Current Opinion in Lipidology,* 28**,** 91-98.

KHALLOU-LASCHET, J., VARTHAMAN, A., FORNASA, G., COMPAIN, C., GASTON, A.-T., CLEMENT, M., DUSSIOT, M., LEVILLAIN, O., GRAFF-DUBOIS, S., NICOLETTI, A. & CALIGIURI, G. 2010. Macrophage plasticity in experimental atherosclerosis. *Plos One,* 5**,** e8852.

KIM, K., SHIM, D., LEE, J. S., ZAITSEV, K., WILLIAMS, J. W., KIM, K. W., JANG, M. Y., JANG, H. S., YUN, T. J., LEE, S. H., YOON, W. K., PRAT, A., SEIDAH, N. G., CHOI, J., LEE, S. P., YOON, S. H., NAM, J. W., SEONG, J. K., OH, G. T., RANDOLPH, G. J., ARTYOMOV, M. N., CHEONG, C. & CHOI, J. H. 2018. Transcriptome analysis reveals nonfoamy rather than foamy plaque macrophages are proinflammatory in atherosclerotic murine models. *Circulation Research,* 123**,** 1127-1142.

KUNAU, W. H., DOMMES, V. & SCHULZ, H. 1995. beta-oxidation of fatty acids in mitochondria, peroxisomes, and bacteria: A century of continued progress. *Progress in Lipid Research,* 34**,** 267-342.

KUNJATHOOR, V. V., FEBBRAIO, M., PODREZ, E. A., MOORE, K. J., ANDERSSON, L., KOEHN, S., RHEE, J. S., SILVERSTEIN, R., HOFF, H. F. & FREEMAN, M. W. 2002. Scavenger receptors class A-I/II and CD36 are the principal receptors responsible for the uptake of modified low density lipoprotein leading to lipid loading in macrophages. *Journal of Biological Chemistry,* 277**,** 49982-49988.

KWAN, B. C. H., KRONENBERG, F., BEDDHU, S. & CHEUNG, A. K. 2007. Lipoprotein metabolism and lipid management in chronic kidney disease. *Journal of the American Society of Nephrology,* 18**,** 1246-1261.

LADISA, J. F., JR., BOZDAG, S., OLSON, J., RAMCHANDRAN, R., KERSTEN, J. R. & EDDINGER, T. J. 2015. Gene expression in experimental aortic coarctation and repair: candidate genes for therapeutic intervention? *Plos One,* 10**,** e0133356.

LEE, M. N., YE, C., VILLANI, A.-C., RAJ, T., LI, W., EISENHAURE, T. M., IMBOYWA, S. H., CHIPENDO, P. I., RAN, F. A., SLOWIKOWSKI, K., WARD, L. D., RADDASSI, K., MCCABE, C., LEE, M. H., FROHLICH, I. Y., HAFLER, D. A., KELLIS, M., RAYCHAUDHURI, S., ZHANG, F., STRANGER, B. E., BENOIST, C. O., DE JAGER, P. L., REGEV, A. & HACOHEN, N. 2014. Common genetic variants modulate pathogen-sensing responses in human dendritic cells. *Science,* 343**,** 1246980.

LIAO, Y., SMYTH, G. K. & SHI, W. 2014. featureCounts: an efficient general purpose program for assigning sequence reads to genomic features. *Bioinformatics,* 30**,** 923-930.

LIBBY, P., RIDKER, P. M. & HANSSON, G. K. 2011. Progress and challenges in translating the biology of atherosclerosis. *Nature,* 473**,** 317-325.

LIM, S. C., TAJIKA, M., SHIMURA, M., CAREY, K. T., STROUD, D. A., MURAYAMA, K., OHTAKE, A. & MCKENZIE, M. 2018. Loss of the mitochondrial fatty acid beta-oxidation protein medium-chain acyl-coenzyme A dehydrogenase disrupts oxidative phosphorylation protein complex stability and function. *Scientific Reports,* 8**,** 153.

LIN, J. D., NISHI, H., POLES, J., NIU, X., MCCAULEY, C., RAHMAN, K., BROWN, E. J., YEUNG, S. T., VOZHILLA, N., WEINSTOCK, A., RAMSEY, S. A., FISHER, E. A. & LOKE, P. 2019. Single-cell analysis of fate-mapped macrophages reveals heterogeneity, including stem-like properties, during atherosclerosis progression and regression. *JCI Insight,* 4**,** e124574.

LOW, H., ANH, H. & SVIRIDOV, D. 2012. Cholesterol efflux assay. *Jove-Journal of Visualized Experiments***,** e3810.

MA, X. J., SUN, J. W., PAPASAVVAS, E., RIEMANN, H., ROBERTSON, S., MARSHALL, J., BAILER, R. T., MOORE, A., DONNELLY, R. P., TRINCHIERI, G. & MONTANER, L. J. 2000. Inhibition of IL-12 production in human monocyte-derived macrophages by TNF. *Journal of Immunology,* 164**,** 1722-1729.

MA, Z., TARUNO, A., OHMOTO, M., JYOTAKI, M., LIM, J. C., MIYAZAKI, H., NIISATO, N., MARUNAKA, Y., LEE, R. J., HOFF, H., PAYNE, R., DEMURO, A., PARKER, I., MITCHELL, C. H., HENAO-MEJIA, J., TANIS, J. E., MATSUMOTO, I., TORDOFF, M. G. & FOSKETT, J. K. 2018. CALHM3 is essential for rapid ion channel-mediated purinergic neurotransmission of GPCR-mediated tastes. *Neuron,* 98**,** 547-561.

MAJOROS, A., PLATANITIS, E., KERNBAUER-HOELZL, E., ROSEBROCK, F., MUELLER, M. & DECKER, T. 2017. Canonical and non-canonical aspects of JAK-STAT signaling: lessons from interferons for cytokine responses. *Frontiers in Immunology,* 8**,** 29.

MALIK, U., JAVED, A., ALI, A. & ASGHAR, K. 2017. Structural and functional annotation of human FAM26F: A multifaceted protein having a critical role in the immune system. *Gene,* 597**,** 66-75.

MARTINEZ, F. O., GORDON, S., LOCATI, M. & MANTOVANI, A. 2006. Transcriptional profiling of the human monocyte-to-macrophage differentiation and polarization: New molecules and patterns of gene expression. *Journal of Immunology,* 177**,** 7303-7311.

MATSUMIYA, M., HARRIS, S. A., SATTI, I., STOCKDALE, L., TANNER, R., O'SHEA, M. K., TAMERIS, M., MAHOMED, H., HATHERILL, M., SCRIBA, T. J., HANEKOM, W. A., MCSHANE, H. & FLETCHER, H. A. 2014. Inflammatory and myeloid-associated gene expression before and one day after infant vaccination with MVA85A correlates with induction of a T cell response. *BMC Infectious Diseases,* 14**,** 314.

MICHALSKA, A., BLASZCZYK, K., WESOLY, J. & BLUYSSEN, H. A. R. 2018. A positive feedback amplifier circuit that regulates interferon (IFN)-stimulated gene expression and controls type I and type II IFN responses. *Frontiers in Immunology,* 9**,** 1135.

MINTON, K. 2017. IL-10 targets macrophage metabolism. *Nature Reviews Immunology,* 17**,** 345.

MOORE, K. J., SHEEDY, F. J. & FISHER, E. A. 2013. Macrophages in atherosclerosis: a dynamic balance. *Nature Reviews Immunology,* 13**,** 709-721.

MOSS, J. W. E. & RAMJI, D. P. 2016. Cytokines: roles in atherosclerosis disease progression and potential therapeutic targets. *Future Medicinal Chemistry,* 8**,** 1317-1330.

MUELLER, A., MEISER, A., MCDONAGH, E. M., FOX, J. M., PETIT, S. J., XANTHOU, G., WILLIAMS, T. J. & PEASE, J. E. 2008. CXCL4-induced migration of activated T lymphocytes is mediated by the chemokine receptor CXCR3. *Journal of Leukocyte Biology,* 83**,** 875-882.

MURRAY, P. J. 2017. Macrophage polarization. *Annual Review of Physiology,* 79**,** 541-566.

MURRAY, P. J., ALLEN, J. E., BISWAS, S. K., FISHER, E. A., GILROY, D. W., GOERDT, S., GORDON, S., HAMILTON, J. A., IVASHKIV, L. B., LAWRENCE, T., LOCATI, M., MANTOVANI, A., MARTINEZ, F. O., MEGE, J. L., MOSSER, D. M., NATOLI, G., SAEIJ, J. P., SCHULTZE, J. L., SHIREY, K. A., SICA, A., SUTTLES, J., UDALOVA, I., VAN GINDERACHTER, J. A., VOGEL, S. N. & WYNN, T. A. 2014. Macrophage activation and polarization: nomenclature and experimental guidelines. *Immunity,* 41**,** 14-20.

NASCIMENTO, B. R., BRANT, L. C. C., MORAES, D. N. & RIBEIRO, A. L. P. 2014. Global health and cardiovascular disease. *Heart,* 100**,** 1743-1749.

NEWBY, A. C. 2015. Metalloproteinases promote plaque rupture and myocardial infarction: A persuasive concept waiting for clinical translation. *Matrix Biology,* 44-46**,** 157-166.

NEWBY, A. C. 2016. Metalloproteinase production from macrophages - a perfect storm leading to atherosclerotic plaque rupture and myocardial infarction. *Experimental Physiology,* 101**,** 1327-1337.

NICODEME, E., JEFFREY, K. L., SCHAEFER, U., BEINKE, S., DEWELL, S., CHUNG, C.-W., CHANDWANI, R., MARAZZI, I., WILSON, P., COSTE, H., WHITE, J., KIRILOVSKY, J., RICE, C. M., LORA, J. M., PRINJHA, R. K., LEE, K. & TARAKHOVSKY, A. 2010. Suppression of inflammation by a synthetic histone mimic. *Nature,* 468**,** 1119-1123.

NIH. 2019. *Atherosclerosis* [Online]. https://www.nhlbi.nih.gov/health-topics/atherosclerosis. [Accessed 13 September, 2019].
NIKKOLA, E., LAIWALLA, A., KO, A., ALVAREZ, M., CONNOLLY, M., OOI, Y. C., HSU, W., BUI, A., PAJUKANTA, P. & GONZALEZ, N. R. 2015. Remote ischemic conditioning alters methylation and expression of cell cycle genes in aneurysmal subarachnoid hemorrhage. *Stroke,* 46**,** 2445-2451.
NIKOLOVA, D. N., DOGANOV, N., DIMITROV, R., ANGELOV, K., LOW, S.-K., DIMOVA, I., TONCHEVA, D., NAKAMURA, Y. & ZEMBUTSU, H. 2009. Genome-wide gene expression profiles of ovarian carcinoma: identification of molecular targets for the treatment of ovarian carcinoma. *Molecular Medicine Reports,* 2**,** 365-384.
NOFER, J. R. & REMALEY, A. T. 2005. Tangier disease: still more questions than answers. *Cellular and Molecular Life Sciences,* 62**,** 2150-2160.
NOZAKI, S., KASHIWAGI, H., YAMASHITA, S., NAKAGAWA, T., KOSTNER, B., TOMIYAMA, Y., NAKATA, A., ISHIGAMI, M., MIYAGAWA, J. I., KAMEDATAKEMURA, K., KURATA, Y. & MATSUZAWA, Y. 1995. Reduced uptake of oxidized low-density lipoproteins in monocyte-derived macrophages from CD36-deficient subjects. *Journal of Clinical Investigation,* 96**,** 1859-1865.
O'CARROLL, C., FAGAN, A., SHANAHAN, F. & CARMODY, R. J. 2014. Identification of a unique hybrid macrophage-polarization state following recovery from lipopolysaccharide tolerance. *Journal of Immunology,* 192**,** 427-436.
OMASITS, U., AHRENS, C. H., MUELLER, S. & WOLLSCHEID, B. 2014. Protter: interactive protein feature visualization and integration with experimental proteomic data. *Bioinformatics,* 30**,** 884-886.
ONG, S. M., HADADI, E., DANG, T. M., YEAP, W. H., TAN, C. T. Y., NG, T. P., LARBI, A. & WONG, S. C. 2018. The pro-inflammatory phenotype of the human non-classical monocyte subset is attributed to senescence. *Cell Death & Disease,* 9**,** 266.
OPPI, S., LUSCHER, T. F. & STEIN, S. 2019. Mouse models for atherosclerosis research-which is my line? *Frontiers in Cardiovascular Medicine,* 6**,** 46.
ORBE, J., FERNANDEZ, L., RODRIGUEZ, J. A., RABAGO, G., BELZUNCE, M., MONASTERIO, A., RONCAL, C. & PARAMO, J. A. 2003. Different expression of MMPs/TIMP-1 in human atherosclerotic lesions. Relation to plaque features and vascular bed. *Atherosclerosis,* 170**,** 269-276.
PANKLA, R., BUDDHISA, S., BERRY, M., BLANKENSHIP, D. M., BANCROFT, G. J., BANCHEREAU, J., LERTMEMONGKOLCHAI, G. & CHAUSSABEL, D. 2009. Genomic transcriptional profiling identifies a candidate blood biomarker signature for the diagnosis of septicemic melioidosis. *Genome Biology,* 10**,** R127.
PANOUSIS, C. G. & ZUCKERMAN, S. H. 2000a. Interferon-gamma induces downregulation of Tangier disease gene (ATP-binding-cassette transporter 1) in macrophage-derived foam cells. *Arteriosclerosis Thrombosis and Vascular Biology,* 20**,** 1565-1571.
PANOUSIS, C. G. & ZUCKERMAN, S. H. 2000b. Regulation of cholesterol distribution in macrophage-derived foam cells by interferon-gamma. *Journal of Lipid Research,* 41**,** 75-83.
PARK, Y. M. 2014. CD36, a scavenger receptor implicated in atherosclerosis. *Experimental and Molecular Medicine,* 46**,** e99.
PARKER, B. L., PALMISANO, G., EDWARDS, A. V. G., WHITE, M. Y., ENGHOLM-KELLER, K., LEE, A., SCOTT, N. E., KOLARICH, D., HAMBLY, B. D., PACKER, N. H., LARSEN, M. R. & CORDWELL, S. J. 2011. Quantitative N-linked glycoproteomics of myocardial ischemia and reperfusion injury reveals early remodeling in the extracellular environment. *Molecular & Cellular Proteomics,* 10**,** M110.006833.
PENNY, H. L., SIEOW, J. L., ADRIANI, G., YEAP, W. H., EE, P. S. C., SAN LUIS, B., LEE, B., LEE, T., MAK, S. Y., HO, Y. S., LAM, K. P., ONG, C. K., HUANG, R. Y. J., GINHOUX, F., ROTZSCHKE, O., KAMM, R. D. & WONG, S. C. 2016. Warburg

metabolism in tumor-conditioned macrophages promotes metastasis in human pancreatic ductal adenocarcinoma. *Oncoimmunology,* 5**,** e1191731.

PICELLI, S., FARIDANI, O. R., BJORKLUND, A. K., WINBERG, G., SAGASSER, S. & SANDBERG, R. 2014. Full-length RNA-seq from single cells using Smart-seq2. *Nature Protocols,* 9**,** 171-181.

PLUDDEMANN, A., NEYEN, C. & GORDON, S. 2007. Macrophage scavenger receptors and host-derived ligands. *Methods,* 43**,** 207-217.

POWER, C. P., WANG, J. H., MANNING, B., KELL, M. R., AHERNE, N. F., WU, Q. D. & REDMOND, H. P. 2004. Bacterial lipoprotein delays apoptosis in human neutrophils through inhibition of caspase-3 activity: regulatory roles for CD14 and TLR-2. *Journal of Immunology,* 173**,** 5229-5237.

PROTO, J. D., DORAN, A. C., GUSAROVA, G., YURDAGUL, A., SOZEN, E., SUBRAMANIAN, M., ISLAM, M. N., RYMOND, C. C., DU, J., HOOK, J., KURIAKOSE, G., BHATTACHARYA, J. & TABAS, I. 2018. Regulatory T cells promote macrophage efferocytosis during inflammation resolution. *Immunity,* 49**,** 666-677.

QUE, X., HUNG, M.-Y., YEANG, C., GONEN, A., PROHASKA, T. A., SUN, X., DIEHL, C., MAATTA, A., GADDIS, D. E., BOWDEN, K., PATTISON, J., MACDONALD, J. G., YLA-HERTTUALA, S., MELLON, P. L., HEDRICK, C. C., LEY, K., MILLER, Y. I., GLASS, C. K., PETERSON, K. L., BINDER, C. J., TSIMIKAS, S. & WITZTUM, J. L. 2018. Oxidized phospholipids are proinflammatory and proatherogenic in hypercholesterolaemic mice. *Nature,* 558**,** 301-306.

RAMANA, C. V., GIL, M. P., SCHREIBER, R. D. & STARK, G. R. 2002. Stat1-dependent and -independent pathways in IFN-gamma-dependent signaling. *Trends in Immunology,* 23**,** 96-101.

RAMASAMY, I. 2014. Recent advances in physiological lipoprotein metabolism. *Clinical Chemistry and Laboratory Medicine,* 52**,** 1695-1727.

RAMJI, D. P. & DAVIES, T. S. 2015. Cytokines in atherosclerosis: Key players in all stages of disease and promising therapeutic targets. *Cytokine & Growth Factor Reviews,* 26**,** 673-685.

RAPPSILBER, J., ISHIHAMA, Y. & MANN, M. 2003. Stop and go extraction tips for matrix-assisted laser desorption/ionization, nanoelectrospray, and LC/MS sample pretreatment in proteomics. *Analytical Chemistry,* 75**,** 663-670.

REMMERIE, A. & SCOTT, C. L. 2018. Macrophages and lipid metabolism. *Cellular Immunology,* 330**,** 27-42.

REN, S., LIU, S., HOWELL, P., JR., XI, Y., ENKEMANN, S. A., JU, J. & RIKER, A. I. 2008. The impact of genomics in understanding human melanoma progression and metastasis. *Cancer control: Journal of the Moffitt Cancer Center,* 15**,** 202-215.

ROBINSON, M. D., MCCARTHY, D. J. & SMYTH, G. K. 2010. edgeR: a Bioconductor package for differential expression analysis of digital gene expression data. *Bioinformatics,* 26**,** 139-140.

ROGACEV, K. S., CREMERS, B., ZAWADA, A. M., SEILER, S., BINDER, N., EGE, P., GROSSE-DUNKER, G., HEISEL, I., HORNOF, F., JEKEN, J., REBLING, N. M., ULRICH, C., SCHELLER, B., BOEHM, M., FLISER, D. & HEINE, G. H. 2012. CD14++CD16+ monocytes independently predict cardiovascular events. *Journal of the American College of Cardiology,* 60**,** 1512-1520.

ROGACEV, K. S., ZAWADA, A. M., HUNDSDORFER, J., ACHENBACH, M., HELD, G., FLISER, D. & HEINE, G. H. 2015. Immunosuppression and monocyte subsets. *Nephrology Dialysis Transplantation,* 30**,** 143-153.

ROMANOV, R. A., LASHER, R. S., HIGH, B., SAVIDGE, L. E., LAWSON, A., ROGACHEVSKAJA, O. A., ZHAO, H., ROGACHEVSKY, V. V., BYSTROVA, M. F., CHURBANOV, G. D., ADAMEYKO, I., HARKANY, T., YANG, R., KIDD, G. J., MARAMBAUD, P., KINNAMON, J. C., KOLESNIKOV, S. S. & FINGER, T. E. 2018.

Chemical synapses without synaptic vesicles: Purinergic neurotransmission through a CALHM1 channel-mitochondrial signaling complex. *Science Signaling,* 11**,** eaao1815.

RUDEL, L. L., LEE, R. G. & COCKMAN, T. L. 2001. Acyl coenzyme A : cholesterol acyltransferase types 1 and 2: structure and function in atherosclerosis. *Current Opinion in Lipidology,* 12**,** 121-127.

SANKARANARAYANAN, S., KELLNER-WEIBEL, G., DE LA LLERA-MOYA, M., PHILLIPS, M. C., ASZTALOS, B. F., BITTMAN, R. & ROTHBLAT, G. H. 2011. A sensitive assay for ABCA1-mediated cholesterol efflux using BODIPY-cholesterol. *Journal of Lipid Research,* 52**,** 2332-2340.

SARVARI, A. K., DOAN-XUAN, Q. M., BACSO, Z., CSOMOS, I., BALAJTHY, Z. & FESUS, L. 2015. Interaction of differentiated human adipocytes with macrophages leads to trogocytosis and selective IL-6 secretion. *Cell Death & Disease,* 6**,** e1613.

SCHITTEK, B., HIPFEL, R., SAUER, B., BAUER, J., KALBACHER, H., STEVANOVIC, S., SCHIRLE, M., SCHROEDER, K., BLIN, N., MEIER, F., RASSNER, G. & GARBE, C. 2001. Dermcidin: a novel human antibiotic peptide secreted by sweat glands. *Nature Immunology,* 2**,** 1133-1137.

SCHLITT, A., HEINE, G. H., BLANKENBERG, S., ESPINOLA-KLEIN, C., DOPHEIDE, J. F., BICKEL, C., LACKNER, K. J., IZ, M., MEYER, J., DARIUS, H. & RUPPRECHT, H. J. 2004. CD14+CD16+ monocytes in coronary artery disease and their relationship to serum TNF-alpha levels. *Thrombosis and Haemostasis,* 92**,** 419-424.

SERBULEA, V., UPCHURCH, C. M., AHERN, K. W., BORIES, G., VOIGT, P., DEWEESE, D. E., MAHER, A. K., HARRIS, T. E. & LEITINGER, N. 2018a. Macrophages sensing oxidized DAMPs reprogram their metabolism to support redox homeostasis and inflammation through a TLR2-Syk-ceramide dependent mechanism. *Molecular Metabolism,* 7**,** 23-34.

SERBULEA, V., UPCHURCH, C. M., SCHAPPE, M. S., VOIGT, P., DEWEESE, D. E., DESAI, B. N., MEHER, A. K. & LEITINGER, N. 2018b. Macrophage phenotype and bioenergetics are controlled by oxidized phospholipids identified in lean and obese adipose tissue. *Proceedings of the National Academy of Sciences of the United States of America,* 115**,** E6254-E6263.

SHAHZAD, K., CADEIRAS, M., MEMON, S., ZEEBERG, B., KLINGLER, T., SINHA, A., TABAK, E. G., UNNIACHAN, S. & DENG, M. C. 2010. Gene expression signatures of peripheral blood mononuclear cells during the early post-transplant period in patients developing cardiac allograft vasculopathy. *Journal of transplantation,* 2010**,** 719696.

SHERIFF, S., DU, H. & GRABOWSKI, G. A. 1995. Characterization of lysosomal acid lipase by site-directed mutagenesis and heterologous expression. *Journal of Biological Chemistry,* 270**,** 27766-27772.

SICA, A., ERRENI, M., ALLAVENA, P. & PORTA, C. 2015. Macrophage polarization in pathology. *Cellular and Molecular Life Sciences,* 72**,** 4111-4126.

SOMMERS, C. L., SAMELSON, L. E. & LOVE, P. E. 2004. LAT: a T lymphocyte adapter protein that couples the antigen receptor to downstream signaling pathways. *Bioessays,* 26**,** 61-67.

SONG, G., SEO, H. W., CHOI, J. W., RENGARAJ, D., KIM, T. M., LEE, B. R., KIM, Y. M., YUN, T. W., JEONG, J.-W. & HAN, J. Y. 2011. Discovery of candidate genes and pathways regulating oviduct development in chickens. *Biology of Reproduction,* 85**,** 306-314.

SORCI-THOMAS, M. G. & THOMAS, M. J. 2016. Microdomains, inflammation, and atherosclerosis. *Circulation Research,* 118**,** 679-691.

STEFFENSEN, L. B., MORTENSEN, M. B., KJOLBY, M., HAGENSEN, M. K., OXVIG, C. & BENTZON, J. F. 2015. Disturbed laminar blood flow vastly augments lipoprotein retention in the artery wall: a key mechanism distinguishing susceptible from resistant sites. *Arteriosclerosis Thrombosis and Vascular Biology,* 35**,** 1928-1935.

STOGER, J. L., GIJBELS, M. J. J., VAN DER VELDEN, S., MANCA, M., VAN DER LOOS, C. M., BIESSEN, E. A. L., DAEMEN, M. J. A. P., LUTGENS, E. & DE WINTHER, M. P. J. 2012. Distribution of macrophage polarization markers in human atherosclerosis. *Atherosclerosis,* 225**,** 461-468.

STREHLITZ, A. 2017. *Identification of biomarker signatures for the discrimination of pneumococcal pneumonia from staphylococcal pneumonia.* Technical University of Braunschweig.

TABAS, I. 2002. Consequences of cellular cholesterol accumulation: basic concepts and physiological implications. *Journal of Clinical Investigation,* 110**,** 905-911.

TABAS, I. & BORNFELDT, K. E. 2016. Macrophage phenotype and function in different stages of atherosclerosis. *Circulation Research,* 118**,** 653-667.

TARIQUE, A. A., LOGAN, J., THOMAS, E., HOLT, P. G., SLY, P. D. & FANTINO, E. 2015. Phenotypic, functional, and plasticity features of classical and alternatively activated human macrophages. *American Journal of Respiratory Cell and Molecular Biology,* 53**,** 676-688.

TARUNO, A., VINGTDEUX, V., OHMOTO, M., MA, Z., DVORYANCHIKOV, G., LI, A., ADRIEN, L., ZHAO, H., LEUNG, S., ABERNETHY, M., KOPPEL, J., DAVIES, P., CIVAN, M. M., CHAUDHARI, N., MATSUMOTO, I., HELLEKANT, G., TORDOFF, M. G., MARAMBAUD, P. & FOSKETT, J. K. 2013. CALHM1 ion channel mediates purinergic neurotransmission of sweet, bitter and umami tastes. *Nature,* 495**,** 223-226.

TEDESCO, S., DE MAJO, F., KIM, J., TRENTI, A., TREVISI, L., FADINI, G. P., BOLEGO, C., ZANDSTRA, P. W., CIGNARELLA, A. & VITIELLO, L. 2018. Convenience versus biological significance: are PMA-differentiated THP-1 cells a reliable substitute for blood-derived macrophages when studying *in vitro* polarization? *Frontiers in Pharmacology,* 9**,** 71.

THORNTON, S., TAN, R., SPROLES, A., DO, T., SCHICK, J., GROM, A. A., DELAY, M. & SCHULERT, G. S. 2019. A multiparameter flow cytometry analysis panel to assess CD163 mRNA and protein in monocyte and macrophage populations in hyperinflammatory diseases. *Journal of Immunology,* 202**,** 1635-1643.

TOKUNAGA, R., ZHANG, W., NASEEM, M., PUCCINI, A., BERGER, M. D., SONI, S., MCSKANE, M., BABA, H. & LENZ, H.-J. 2018. CXCL9, CXCL10, CXCL11/CXCR3 axis for immune activation - a target for novel cancer therapy. *Cancer Treatment Reviews,* 63**,** 40-47.

ULLOA-MONTOYA, F., LOUAHED, J., DIZIER, B., GRUSELLE, O., SPIESSENS, B., LEHMANN, F. F., SUCIU, S., KRUIT, W. H. J., EGGERMONT, A. M. M., VANSTEENKISTE, J. & BRICHARD, V. G. 2013. Predictive gene signature in MAGE-A3 antigen-specific cancer immunotherapy. *Journal of Clinical Oncology,* 31**,** 2388-2395.

VAN DEN BOSSCHE, J., BAARDMAN, J., OTTO, N. A., VAN DER VELDEN, S., NEELE, A. E., VAN DEN BERG, S. M., LUQUE-MARTIN, R., CHEN, H. J., BOSHUIZEN, M. C. S., AHMED, M., HOEKSEMA, M. A., DE VOS, A. F. & DE WINTHER, M. P. J. 2016. Mitochondrial dysfunction prevents repolarization of inflammatory macrophages. *Cell Reports,* 17**,** 684-696.

VAN DEN MAAGDENBERG, A. M. J. M., HOFKER, M. H., KRIMPENFORT, P. J. A., DEBRUIJN, I., VANVLIJMEN, B., VANDERBOOM, H., HAVEKES, L. M. & FRANTS, R. R. 1993. Transgenic mice carrying the apolipoprotein-e3-Leiden gene exhibit hyperlipoproteinemia. *Journal of Biological Chemistry,* 268**,** 10540-10545.

VAN TITS, L. J. H., STIENSTRA, R., VAN LENT, P. L., NETEA, M. G., JOOSTEN, L. A. B. & STALENHOEF, A. F. H. 2011. Oxidized LDL enhances pro-inflammatory responses of alternatively activated M2 macrophages: A crucial role for Kruppel-like factor 2. *Atherosclerosis,* 214**,** 345-349.

VARGAS-ALARCON, G., POSADAS-ROMERO, C., VILLARREAL-MOLINA, T., ALVAREZ-LEON, E., ANGELES, J., VALLEJO, M., POSADAS-SANCHEZ, R.,

CARDOSO, G., MEDINA-URRUTIA, A. & KIMURA-HAYAMA, E. 2013. Single nucleotide polymorphisms within LIPA (lysosomal acid lipase A) gene are associated with susceptibility to premature coronary artery disease. A replication in the genetic of atherosclerotic disease (GEA) Mexican study. *Plos One,* 8**,** e74703.

VATS, D., MUKUNDAN, L., ODEGAARD, J. I., ZHANG, L., SMITH, K. L., MOREL, C. R., GREAVES, D. R., MURRAY, P. J. & CHAWLA, A. 2006. Oxidative metabolism and PGC-1 beta attenuate macrophage-mediated inflammation. *Cell Metabolism,* 4**,** 13-24.

VERDEGUER, F. & AOUADI, M. 2017. Macrophage heterogeneity and energy metabolism. *Experimental Cell Research,* 360**,** 35-40.

VESELI, B. E., PERROTTA, P., DE MEYER, G. R. A., ROTH, L., VAN DER DONCKT, C., MARTINET, W. & DE MEYER, G. R. Y. 2017. Animal models of atherosclerosis. *European Journal of Pharmacology,* 816**,** 3-13.

VINJE, T., WIEROD, L., LEREN, T. P. & STROM, T. B. 2018. Prevalence of cholesteryl ester storage disease among hypercholesterolemic subjects and functional characterization of mutations in the lysosomal acid lipase gene. *Molecular Genetics and Metabolism,* 123**,** 169-176.

VIOLA, A., MUNARI, F., SANCHEZ-RODRIGUEZ, R., SCOLARO, T. & CASTEGNA, A. 2019. The metabolic signature of macrophage responses. *Frontiers in Immunology,* 10**,** 1462.

WALTER, W., ALONSO-HERRANZ, L., TRAPPETTI, V., CRESPO, I., IBBERSON, M., CEDENILLA, M., KARASZEWSKA, A., NUNEZ, V., XENARIOS, I., ARROYO, A. G., SANCHEZ-CABO, F. & RICOTE, M. 2018. Deciphering the dynamic transcriptional and post-transcriptional networks of macrophages in the healthy heart and after myocardial injury. *Cell Reports,* 23**,** 622-636.

WANDERS, R. J. A., RUITER, J. P. N., IJLST, L., WATERHAM, H. R. & HOUTEN, S. M. 2010. The enzymology of mitochondrial fatty acid beta-oxidation and its application to follow-up analysis of positive neonatal screening results. *Journal of Inherited Metabolic Disease,* 33**,** 479-494.

WANG, X. Q., PANOUSIS, C. G., ALFARO, M. L., EVANS, G. F. & ZUCKERMAN, S. H. 2002. Interferon-gamma-mediated downregulation of cholesterol efflux and ABC1 expression is by the Stat1 pathway. *Arteriosclerosis Thrombosis and Vascular Biology,* 22**,** E5-E9.

WANG, Y., QU, L., UTHE, J. J., BEARSON, S. M. D., KUHAR, D., LUNNEY, J. K., COUTURE, O. P., NETTLETON, D., DEKKERS, J. C. M. & TUGGLE, C. K. 2007. Global transcriptional response of porcine mesenteric lymph nodes to *Salmonella enterica* serovar Typhimurium. *Genomics,* 90**,** 72-84.

WARD, J. R., WEST, P. W., ARIAANS, M. P., PARKER, L. C., FRANCIS, S. E., CROSSMAN, D. C., SABROE, I. & WILSON, H. L. 2010. Temporal interleukin-1 beta secretion from primary human peripheral blood monocytes by P2X7-independent and P2X7-dependent mechanisms. *Journal of Biological Chemistry,* 285**,** 23145-23156.

WARNER, G. J., STOUDT, G., BAMBERGER, M., JOHNSON, W. J. & ROTHBLAT, G. H. 1995. Cell toxicity induced by inhibition of acyl-coenzyme A-cholesterol acyltransferase and accumulation of unesterified cholesterol. *Journal of Biological Chemistry,* 270**,** 5772-5778.

WELCHER, A. A., BOEDIGHEIMER, M., KIVITZ, A. J., AMOURA, Z., BUYON, J., RUDINSKAYA, A., LATINIS, K., CHIU, K., OLINER, K. S., DAMORE, M. A., ARNOLD, G. E., SOHN, W., CHIRMULE, N., GOYAL, L., BANFIELD, C. & CHUNG, J. B. 2015. Blockade of interferon-gamma normalizes interferon-regulated gene expression and serum CXCL10 levels in patients with systemic lupus erythematosus. *Arthritis & Rheumatology,* 67**,** 2713-2722.

WHO. 2018. *Global health estimates 2016: deaths by cause, age, sex, by country and by region, 2000-2016* [Online].

https://www.who.int/healthinfo/global_burden_disease/estimates/en/: World Health Organisation. [Accessed 2018].
WINKELS, H., EHINGER, E., VASSALLO, M., BUSCHER, K., DINH, H. Q., KOBIYAMA, K., HAMERS, A. A. J., COCHAIN, C., VAFADARNEJAD, E., SALIBA, A. E., ZERNECKE, A., PRAMOD, A. B., GHOSH, A. K., MICHEL, N. A., HOPPE, N., HILGENDORF, I., ZIRLIK, A., HEDRICK, C. C., LEY, K. & WOLF, D. 2018. Atlas of the immune cell repertoire in mouse atherosclerosis defined by single-cell RNA-sequencing and mass cytometry. *Circulation Research,* 122**,** 1675-1688.
WONG, K. L., TAI, J. J.-Y., WONG, W.-C., HAN, H., SEM, X., YEAP, W.-H., KOURILSKY, P. & WONG, S.-C. 2011. Gene expression profiling reveals the defining features of the classical, intermediate, and nonclassical human monocyte subsets. *Blood,* 118**,** E15-E30.
WYNN, T. A. & VANNELLA, K. M. 2016. Macrophages in tissue repair, regeneration, and fibrosis. *Immunity,* 44**,** 450-462.
XUE, J., SCHMIDT, S. V., SANDER, J., DRAFFEHN, A., KREBS, W., QUESTER, I., DE NARDO, D., GOHEL, T. D., EMDE, M., SCHMIDLEITHNER, L., GANESAN, H., NINO-CASTRO, A., MALLMANN, M. R., LABZIN, L., THEIS, H., KRAUT, M., BEYER, M., LATZ, E., FREEMAN, T. C., ULAS, T. & SCHULTZE, J. L. 2014. Transcriptome-based network analysis reveals a spectrum model of human macrophage activation. *Immunity,* 40**,** 274-288.
YAHAGI, K., KOLODGIE, F. D., OTSUKA, F., FINN, A. V., DAVIS, H. R., JONER, M. & VIRMANI, R. 2016. Pathophysiology of native coronary, vein graft, and in-stent atherosclerosis. *Nature Reviews Cardiology,* 13**,** 79-98.
YANG, L., YANG, J. B., CHEN, J., YU, G. Y., ZHOU, P., LEI, L., WANG, Z. Z., CHANG, C. C. Y., YANG, X. Y., CHANG, T. Y. & LI, B. L. 2004. Enhancement of human ACAT1 gene expression to promote the macrophage-derived foam cell formation by dexamethasone. *Cell Research,* 14**,** 315-323.
ZAWADA, A. M., ROGACEV, K. S., ROTTER, B., WINTER, P., MARELL, R.-R., FLISER, D. & HEINE, G. H. 2011. SuperSAGE evidence for CD14(++)CD16(+) monocytes as a third monocyte subset. *Blood,* 118**,** E50-E61.
ZHAO, B., SONG, J., CHOW, W. N., CLAIR, R. W. S., RUDEL, L. L. & GHOSH, S. 2007a. Macrophage-specific transgenic expression of cholesteryl ester hydrolase significantly reduces atherosclerosis and lesion necrosis in Ldlr(-)/(-) mice. *Journal of Clinical Investigation,* 117**,** 2983-2992.
ZHAO, B., SONG, J., ST CLAIR, R. W. & GHOSH, S. 2007b. Stable overexpression of human macrophage cholesteryl ester hydrolase results in enhanced free cholesterol efflux from human THP1 macrophages. *American Journal of Physiology-Cell Physiology,* 292**,** C405-C412.

9. Abbreviations

2-DG – 2-deoxyglucose

ABCA1 – ATP binding cassette subfamily A member 1

ABCG1 – ATP binding cassette subfamily G member 1

acLDL – acetylated low density lipoprotein

ANOVA – analysis of variance

Apo – apoliprotein

ATF1 – activating transcription factor 1

ATP – adenosine triphosphate

BMDC – bone marrow–derived dendritic cell

BMDM – bone marrow–derived macrophage

BSA – bovine serum albumin

BzATP – 2′(3′)-O-(4-Benzoylbenzoyl)adenosine triphosphate triethylammonium salt

CALHM – calcium homeostasis modulartor family (member), also known as FAM26 – family with sequence similarity (member)

CBA – cytometric bead array

CCL – C–C motif chemokine ligand

CCR – C–C chemokine receptor

CD – cluster of differentiation

cDNA – complimentary DNA

CETP – cholesteryl ester transfer protein

CITE–seq – cellular indexing of transcriptomes and epitopes by sequencing

CoA – coenzyme A

CpG – 5'—C—phosphate—G—3'

CVD – cardiovascular disease

CX3CR1 – CX3C receptor 1

CXCL – C-X-C motif chemokine ligand

CyTOF – cytometry by time of flight

DAPI – 4′,6-diamidino-2-phenylindole

DC – dendritic cell

DCD – dermicidin

DEG – differentially expressed gene

DMEM – Dulbecco's modified eagle media

DNA – deoxyribonucleic acid

ECAR – extracellular acidification rate

ECL – enhanced chemiluminescence

EDTA – ethylenediaminetetraacetic acid

ELISA – enzyme–linked immunosorbent assay

eQTL – expression trait quantitative locus

ER – endoplasmic reticulum

ETC – electron transport chain

$FADH_2$ – flavin adenine dinucleotide

FAM26 – family with sequence similarity (member), also known as calcium homeostasis modulator family (member)

FAO – fatty acid oxidation

FBS – foetal bovine serum

FC – fold change

FDR – false discovery rate

FPKM – fragments per kilobase million mapped

GAPDH – glyceraldehyde-3-phosphate dehydrogenase

GM–CSF – granulocyte–macrophage colony stimulating factor

HDL – high density lipoprotein

HIF1A – hypoxia inducible factor subunit alpha

HLA – human leukocyte antigen

HMOX1 – haeme oxygenase 1

ICC/IF – immunocytochemistry coupled with immunofluorescence

IFN – interferon

IFNGR – interferon gamma receptor

IL – interleukin

IL10R – interleukin 10 receptor

IL13RA – interleukin 13 receptor α chain

IL4RA – interleukin 4 receptor α chain

ILDL – intermediate density lipoprotein

INAM – IRF3–dependent natural killer cell–activating molecule, another name given to CALHM6 (previously known as FAM26F)

IPA – Ingenuity pathway analysis

IRF – interferon regulatory factor

ISOPCT – isoform percentage

JAK – Janus kinase

Jurkat

LAT – linker for activation of T cells

LC MS/MS – liquid chromatography with mass spectrometry

LCAT – lecithin–cholesterol acyltransferase

LDH – lactate dehydrogenase

LDL – low density lipoprotein

LDLR – low density lipoprotein receptor

LE – late endosome

LIPA – lipase A, lysosomal acid type

LIPE – lipase E, hormone sensitive type

LPS – lipopolysaccharide

LRP1 – low density lipoprotein receptor related protein 1

LXRA – liver X receptor alpha renamed to NR1H3 (nuclear receptor subfamily 1 group H member 3)

LXRβ – liver X receptor beta renamed to NR1H2 (nuclear receptor subfamily 1 group H member 2)

MARCO – macrophage receptor with collagenous structure

M–CSF – macrophage colony stimulating factor

MDM – monocyte–derived macrophage

MGLL – monoglyceride lipase

MMP – matrix metalloproteinase

MRC1 – mannose receptor C-type 1

MSR1 – macrophage scavenger receptor 1

MVA85A – modified vaccinia Ankara 85A

MYD88 – myeloid differentiation primary response protein 88

NADH – nicotinamide adenine dinucleotide

NCEH1 – neutral cholesterol ester hydrolase 1

NFE2L2 – nuclear factor, erythroid 2 like 2

NF–κB – nuclear factor κ–light–chain–enhancer of activated B cells

NK – natural killer

NOS2 – nitric oxide synthase 2

NP40 – Nonidet™ P40

NR1H3 (LXRA) – nuclear receptor subfamily 1 group H member 3 (liver X receptor alpha)

NR1H2 (LXRB) – nuclear receptor subfamily 1 group H member 2 (liver X receptor beta)

OCR – oxygen consumption rate

ORO – Oil–Red–O

oxLDL – oxidised low density lipoprotein

oxPAPC – oxidised phospholipid: 1-palmitoyl-2-arachidonyl-sn-glycero-3-phosphorylcholine

PBMC – peripheral blood mononuclear cell

PBS – phosphate–buffered saline

PBSE – phosphate–buffered saline containing 2 mM ethylenediaminetetraacetic acid

PCA – principal component analysis

PCR – polymerase chain reaction

PCSK9 – proprotein convertase subtilisin/kexin type 9

PDHX – pyruvate dehydrogenase complex component X

pFAO – peroxisomal fatty acid oxidation

PMA – phorbol myristate acetate

PNPLA4 – phospholipase domain containing 4

poly(I:C) – polyinosinic:polycytidylic acid

PPAR – peroxisome proliferator activated receptor

pSTAT1 – phosphorylated signal transducer and activator of transcription 1

PVDF polyvinylidene difluoride

qRT–PCR – quantitative real–time polymerase chain reaction

rh – recombinant human

RIN – RNA integrity number

RIPA – radioimmunoprecipitation

RNA – ribonucleic acid

RNA–seq – ribonucleic acid sequencing

RPKM – reads per kilobase per million mapped

RP-LC – reverse phase liquid chromatography

RPMI – Roswell Park Memorial Institute

RXR – retinoid X receptor

S100A8 – S100 calcium binding protein A8

SCARB1 – scavenger receptor class B member 1

SEM – standard error of the mean

SILAC – stable isotope labelling with amino acids in cell culture

siRNA – small interfering RNA

SMA – smooth muscle actin

SMC – smooth muscle cell

SNP – single nucleotide polymorphism

SOAT1 – sterol O-acyltransferase

SRXN1 – sulfiredoxin 1

STAT1 – signal transducer and activator of transcription 1

TBST – Tris buffered saline with 0.1% (v/v) Tween 20

TCA – tricarboxylic acid (Kreb's) cycle

TICAM1 – TIR domain–containing molecule 1

TLR – Toll–like receptor

TNF – tumour necrosis factor

TREM2 – triggering receptor expressed on myeloid cells 2

TXNRD1 – thioredoxin reductase 1

VEGFA – vascular endothelial growth factor A

VLDL – very low density lipoprotein